**ISTANBUL TECHNICAL UNIVERSITY ★ GRADUATE SCHOOL OF SCIENCE ENGINEERING AND TECHNOLOGY**

# DESIGN OF A FLOATING PIPE BREAKWATER - WAVE ENERGY CONVERTER HYBRID SYSTEM

**Ph.D. THESIS**

**Mehmet Adil AKGUL**

**Department of Coastal Sciences and Engineering**

**Coastal Sciences and Engineering Programme**

**APRIL 2014**

**ISTANBUL TECHNICAL UNIVERSITY ★ GRADUATE SCHOOL OF SCIENCE ENGINEERING AND TECHNOLOGY**

# DESIGN OF A FLOATING PIPE BREAKWATER - WAVE ENERGY CONVERTER HYBRID SYSTEM

**Ph.D. THESIS**

**Mehmet Adil AKGUL**
**(517072007)**

**Department of Coastal Sciences and Engineering**

**Coastal Sciences and Engineering Programme**

**Thesis Advisor: Prof. Dr. M. Sedat KABDASLI**

**APRIL 2014**

**İSTANBUL TEKNİK ÜNİVERSİTESİ ★ FEN BİLİMLERİ ENSTİTÜSÜ**

# BORU TİPİ YÜZER DALGAKIRAN - DALGA ENERJİSİ DÖNÜŞTÜRÜCÜ ÇOK AMAÇLI SİSTEM TASARIMI

**DOKTORA TEZİ**

**Mehmet Adil AKGÜL**
**(517072007)**

**Kıyı Bilimleri ve Mühendisliği Anabilim Dalı**

**Kıyı Mühendisliği Programı**

**Tez Danışmanı: Prof. Dr. M. Sedat KABDAŞLI**

**NİSAN 2014**

**M. Adil AKGÜL**, a **Ph.D.** student of ITU **Graduate School of Science, Engineering and Technology** student ID **517072007**, successfully defended the **dissertation** entitled "**DESIGN OF A FLOATING PIPE BREAKWATER - WAVE ENERGY CONVERTER HYBRID SYSTEM**" which he prepared after fulfilling the requirements specified in the associated legislations, before the jury whose signatures are below.

| | | |
|---|---|---|
| **Thesis Advisor :** | **Prof. Dr. M. Sedat KABDAŞLI**<br>İstanbul Technical University | ..... |
| **Jury Members :** | **Prof. Dr. Şevket ÇOKGÖR**<br>Istanbul Technical University | ..... |
| | **Prof. Dr. Emel İRTEM**<br>Balikesir University | ..... |
| | **Prof. Dr. Necati AĞIRALİOĞLU**<br>Istanbul Technical University | ..... |
| | **Prof. Dr. Hayrullah AĞAÇÇIOĞLU**<br>Yıldız Technical University | ..... |

**Date of Submission : 27 February 2014**
**Date of Defense : 30 April 2014**

***To my parents,***

## FOREWORD

A fairly new topic in coastal an marine engineering has arisen as the design and implementation of multipurpose structures. In this study, an attempt has been conducted to evaluate a hybrid consisting of two very special types of marine structures, floating breakwaters and wave energy converters. For this purpose, existing literature has been inspected, possible combinations have been recommended and the combination of an overtopping type wave energy converter with a floating breakwater has been studied by carrying out physical model tests.

Being executed under a vast number of hindering conditions ranging from equipment inavailability to time limit and health problems, and spanning a very wide range of literature, looking back, I can state that the thesis stage was a different but joyful period in my life by dealing with many unknowns and actu items still discussed by the experts in the field.

Being my supervisor since the start of my graduate studies, I kindly would like to present my sincere thanks to Prof. Dr. M. S. Kabdasli for his expertise, guidance, efforts and fatherly friendship. This study, having initiated a new field of research in my academic life, is only just a start for some promising progress. I also appreciate the patience and support of my parents during all the busy time I was studying on this work.

I express my graditude is to Prof. Atilla Incecik for his invitation, advices and support during the study. For their encouragement and support, I also would like to thank to Prof. Dr. Ilhan Avci, Prof. Dr. Sevket Cokgor, Prof. Dr. Bihrat Onoz and Prof. Dr. Hafzullah Aksoy. Overcoming the difficulties in laboratory for three months during the model tests could not be succeeded by the very precious help of the laboratory staff, especially Mr. Yasar Aktas. I also thank to my colleagues and the members of the Coastal and Marine Hydrodynamics Research Group for their presence.

February 2014

M. Adil AKGÜL
MSc. Coastal Engineer

**TABLE OF CONTENTS**

**Page**

## ABBREVIATIONS

| | |
|---|---|
| **2D** | **:** Two dimensional |
| **3D** | **:** Three dimensional |
| **App** | **:** Appendix |
| **FPBW** | **:** Floating pipe breakwater |
| **FTB** | **:** Floating tire breakwater |
| **MWL** | **:** Mean water level |
| **PTO** | **:** Power take-off unit |
| **RANS** | **:** Reynolds averaged Navier-Stokes |
| **RMS** | **:** Root mean square |
| **SG** | **:** Strain gauge |
| **TRL** | **:** Technical readiness level |
| **US** | **:** Ultrasonic sensor |
| **VOF** | **:** Volume of fluid |
| **WD** | **:** Wave dragon |
| **WEC** | **:** Wave energy converter |
| **WG** | **:** Wave gauge |

**LIST OF TABLES**

**Page**

**LIST OF FIGURES**

**Page**

## LIST OF SYMBOLS

**a** : Horizontal particle acceleration
**$A_B$** : Base area
**$A_Q$** : Cross section area of the overtopping volume
**$b_c$** : Width of channel
**B** : Structure beam
**$B_c$** : Structure crest width
**c** : Wave celerity, wave travel speed
**$c_g$** : Group velocity
**$c_h$** : Wave celerity at depth h
**$C_D$** : Energy dissipation coefficient
**$C_R$** : Reflection coefficient
**$C_T$** : Transmission coefficient
**$d_s$** : Submerged depth (draft) of cylinder
**$d_\delta$** : Corrected draft
**D** : Cylinder diameter
**$E_D$** : Dissipated wave energy
**$E_I$** : Incident wave energy
**$E_K$** : Total kinetic energy in one wavelength
**$\bar{E}_K$** : Average kinetic wave energy in one square meter surface area
**$E_P$** : Total potential energy in one wavelength
**$E_{P0}$** : Total potential energy with respect to MWL for one wavelength
**$E_{PT}$** : Total potential energy with respect to sea bottom for one wavelength
**$\bar{E}_P$** : Average potential wave energy in one square meter surface area
**$E_R$** : Reflected wave energy
**$E_T$** : Transmitted wave energy
**f** : Frequency
**F** : Freeboard
**$F_R$** : Dimensionless freeboard
**$F_\delta$** : Corrected freeboard
**g** : Gravitational acceleration
**h** : Water depth
**H** : Wave height
**$H_D$** : Dissipated wave height
**$H_I$** : Incident wave height
**$H_{m0}$** : Zero momenth wave height
**$H_R$** : Reflected wave height
**$H_{rms}$** : Root-mean-square wave height
**$H_s$** : Significant wave height
**$H_T$** : Transmitted wave height
**I** : Moment of inertia
**k** : Wave number

$k_S$ : Stiffness coefficient
**KC** : Keulegan-Carpenter number
**l** : Length
**L** : Wavelength
$L_h$ : Wavelength at depth h
$L_0$ : Deepwater wavelength
$L_{m0}$ : Deepwater zero-momenth wavelength
**m** : Mass or sea bottom slope
**n** : Wave coefficient
**N** : Number of measurements in one wave period
$N_{RE}$ : Reynolds number
$p_D$ : Dynamic pressure
**P** : Power
$\overline{P}$ : Time-averaged power
$P_K$ : Mean power component caused by kinetic energy
$P_P$ : Mean power component caused by potential energy
$q_{1m}$ : Discharge rate per 1m width
**Q** : Discharge
$Q_{1W}$ : Overtopping volume for one wave cycle
$Q_A$ : Dimensionless overtopping rate acc. to volume of immersed object
$Q_V$ : Dimensionless discharge rate acquired acc. to wave crest volume
$Q_W$ : Dimensionless discharge rate acquired by weir analogy
**r** : Radius of the cylinder
**R** : Runup height
$R_0$ : Dimensionless freeboard
$R_D$ : Corrected dimensionless freeboard
$R_M$ : Multiple correlation coefficient
$R_{u\%2}$ : Runup exceeded by 2% of the total number of the incident waves
$R_{umax}$ : Maximum runup height
$S_c$ : Shortage in crest height
$s_0$ : Deepwater wave steepness
$s_h$ : Wave steepness at depth h
$s_{m0}$ : Wave steepness for the mean period of the deepwater spectrum
$s_{p0}$ : Wave steepness for the peak period of the deepwater spectrum
**t** : Time
$t_{ci}$ : Pass time of the i-th crest
$t_{fn}$ : End of the optimum sampling duration for nth wave probe
$t_{fS}$ : End of the optimum sampling duration for the structure
$t_{ij}$ : Wave travel duration between objects i and j
$t_{in}$ : Initiation of the optimum sampling duration for nth wave probe
$t_{iS}$ : Initiation of the optimum sampling duration for the structure
$t_n$ : Optimum sampling duration for a wave probe
$t_S$ : Optimum sampling duration for the structure
$t_{ti}$ : Pass time of the i-th trough
**T** : Wave period
$T_I$ : Incident wave period
$T_R$ : Reflected wave period
$T_T$ : Transmitted wave period
$T_m$ : Mean wave period
$T_{m0}$ : Mean wave period of the deepwater spectrum

$\mathbf{u}$ : Horizontal water particle velocity
$\mathbf{v}$ : Total water particle velocity
$\bar{\mathbf{v}}$ : Mean propagation velocity
$\mathbf{v_c}$ : Crest propagation velocity
$\mathbf{v_G}$ : Centroid propagation velocity
$\mathbf{v_t}$ : Trough propagation velocity
$\mathbf{V}$ : Volume
$\mathbf{V_{1m}}$ : Cumulative discharge volume per unit width
$\mathbf{w}$ : Vertical water particle velocity
$\mathbf{W}$ : Weight
$\mathbf{x}$ : Distance in horizontal
$\mathbf{x_G}$ : Horizontal coordinate of the centroid of a body
$\mathbf{x_{ij}}$ : Distance between the i-th and j-th item
$\mathbf{z}$ : Distance in vertical
$\mathbf{z_0}$ : Mean water level at calm condition
$\bar{\mathbf{z}}_{\boldsymbol{\eta}}$ : Average mean water level under wave attack
$\mathbf{z_G}$ : Vertical coordinate of the centroid of a body
$\mathbf{z_{ci}}$ : Elevation of the ith crest
$\mathbf{z_{ti}}$ : Elevation of the ith trough
$\boldsymbol{\alpha}$ : Slope angle
$\boldsymbol{\delta_p}$ : Rise in MWL due to wave interaction; partial setup
$\boldsymbol{\varepsilon_{a0}}$ : Mean absolute error
$\boldsymbol{\varepsilon_{r0}}$ : Mean relative error
$\boldsymbol{\xi}$ : Iribarren number
$\boldsymbol{\xi_{m0}}$ : Iribarren number calculated for the mean wave steepness of the deepwater spectra
$\boldsymbol{\gamma}$ : Specific weight or correction coefficient
$\boldsymbol{\gamma_b}$ : Berm correction factor
$\boldsymbol{\gamma_r}$ : Surface roughness correction factor
$\boldsymbol{\gamma_h}$ : Shallow foreshore correction factor
$\boldsymbol{\gamma_\beta}$ : Wave angle correction factor
$\boldsymbol{\eta}$ : Water surface elevation
$\boldsymbol{\nu}$ : Kinematic viscosity
$\boldsymbol{\rho}$ : Unit mass
$\boldsymbol{\varphi}$ : Overtopping volume curve slope angle
$\boldsymbol{\omega}$ : Angular frequency
$\boldsymbol{\Delta t_c}$ : Crest travel duration
$\boldsymbol{\Delta t_t}$ : Trough travel duration
$\boldsymbol{\lambda_a}$ : Correction factor for small freeboard values
$\boldsymbol{\lambda_d}$ : Correction factor for limited draft
$\boldsymbol{\lambda s}$ : Correction factor for slope angle

**DESIGN OF A FLOATING BREAKWATER-WAVE ENERGY CONVERTER HYBRID SYSTEM**

## SUMMARY


Increase in global population and life quality has lead to a significant increase in the personal energy consumption during the last decades. Coupled with the diminishing of conventional fossil-based energy sources and environmental problems caused due to their consumption, also boosted by some strategical and logistical conflicts in their supply, many developed countries have shifted to renewable energy sources such as wind, solar and marine energies. Ocean wave energy comprises a challenging field of study in the renewable energy era.

Today, triggered by the increasing number of offshore structures serving to many different purposes, an attempt to improve efficiency and productivity is to combine multiple functions at a single offshore structure, leading to the so-called multi-use offshore structures.

In this study, the hybrid of a floating breakwater and a wave energy converter device has been inspected by adopting physical modelling techniques. A horizontal pipe breakwater has been chosen as the basis of the system, whereas the wave energy converter has been assumed as an overtopping type device with a hydrokinetic power take-off unit. The study is focused on the hydraulic efficiency of the overtopping device and the efficiency of the floating breakwater system.

For the assessment of the wave energy converter, physical model tests have been carried out to evaluate the overtopping performance of the system. A total of seven different immersion depths have been tested under regular waves. It has been found out that the relative freeboard and the wave steepness are fundamental predominant parameters with the effect of relative freeboard diminishing for its small values and the effect of wave steepness decreases with increasing freeboard levels. Furthermore, it has been concluded that the partial setup taking place in front of the cylinder due to partial reflection drastically affects the overtopping rates.

For emergent configurations, following equation has been evaluated:

$$\frac{Q_{1m}}{\sqrt{gH_{rms}^3}} = 0.059exp\left(-3.45\frac{F_d}{H_{rms}} + 0.31s_h\right) \quad \textbf{(1)}$$

By introducing a new dimensionless discharge defined as the ratio of the overtopping volume per wave to the cross section area of the cylinder, Eq. 2 has been evaluated, yielding a better correlation result:

$$\frac{Q_{1m}T}{0.25\pi D^2} = 0.441exp\left(-4.542\frac{F_d}{H_{rms}} + 1.166s_h\right) \quad \textbf{(2)}$$

For submerged configurations, Eq. (2) and Eq. (3) has been evaluated:

$$Q_{1m} = 4.809\ln(s_h) - 21.250;\ \text{D=125mm} \quad \textbf{(3)}$$

$$Q_{1m} = 4.415 \ln(s_h) - 20.870; \text{ D=160mm} \quad \textbf{(4)}$$

Based on the coupled assessment of existing data on floating pipe breakwaters and the overtopping rates, a submergence ratio of F/D=0.12 has been chosen to evaluate the hydraulic efficiency of the system.

The propagation of the overtopping volumes have been studied by using their time vs elevation data measured at two consecutive stations. An energy budget has been introduced, consisting of a potential and a kinetic component. It has been shown that propagation velocities do not significantly differ between the crest and the trough of the overtopping volume. Thus, an equal distribution of propagation velocity has been assumed, over which, the spatial distribution of the overtopping volumes have been evaluated. A correction has been introduced for the average propagation velocity by taking the propagation velocity of the overtopping volumes centroid into account, which is smaller than the crest and trough velocities because of the dispersing and hence reshaping volume. By omitting all vertical velocities, the potential and kinetic energy contained in the overtopping volume have been evaluated. The hydraulic efficiency, defined as the ratio of the mean power introduced at each overtopping volume to the incident wave power has been calculated and its variation with various governing parameters has been assessed. It has been found out that an exponential relationship can be written between the hydraulic efficiency and the volumetric overtopping rate, given by Eq. (5):

$$\chi_T = 0.0289 exp(9.776 Q_V) \quad \textbf{(5)}$$

It has been found out that the hydraulic efficiency of the system varies between 9%-50%, and it increases for steep waves.

In order to assess the performance of the floating breakwater unit, a study carried out by Akgul and Kabdasli (2008) has been expanded into a new system consisting of three circular cylinders stiffly connected to each other by transverse elements. The effect of pipe spacing has been studied by three different configurations. Based on regular wave tests composed of 30 wave series for each configuration, it has been found out that the interaction between the cylinders decreases significantly as the distance between the axis of the cylinders increases. The variation of transmission coefficients with governing parameters has been studied, concluding that the dominant parameter in wave transmission is the wavelength. An exponential relationship has been recommended for the prediction of wave transmission, given by Eq. (6):

$$C_T = 1.506 exp\left(9.24 s_h - 4.647 \frac{B}{L_h}\right) \quad \textbf{(6)}$$

It has been found out that the floating breakwater system performs as an acceptable wave attenuator for mild wave environments with transmission coefficients ranging between 0.20-0.45, and as a moderate wave attenuator for medium-to high wave conditions, where the transmission increases to 40%-70% of the incident wave.

Mooring forces for both fore- and aft mooring lines have been inspected. Initial theoretical studies clearly indicate that under the tested waves inertial forces are dominant with KC values ranging between 0.85 and 3.20. It has been found out that snap loads do not exert for the tested case.

The assessment of the hybrid system has been made under the assumption that the effect of structure motions do not act on overtopping performance. It has been found out that the efficiency of both systems increase in case of steeper waves, which falls well together with the general application of floating breakwater systems. In other words, expected applications of such a system most probably shall take place in sheltered regions and against fetch-limited waves, which usually become steeper than open sea waves. As another outcome, it has been found out that the overtopping performance increases parallel to the decrease in wave transmission, stating that the performance curves for both components of the hybrid system show similar trends.

**BORU TİPİ YÜZER DALGAKIRAN - DALGA ENERJİSİ DÖNÜŞTÜRÜCÜ ÇOK AMAÇLI SİSTEM TASARIMI**

## ÖZET


Küresel nüfus ve yaşam kalitesinde görülen artış, son yıllarda kişi başına düşen enerji tüketiminde önemli bir artışa yol açmıştır. Konvansiyonel fosil bazlı yakıt rezervlerinin azalması ve bu yakıtların tüketiminden kaynaklanan çevre kirliliği, söz konusu kaynakların temininde karşılaşılan lojistik ve stratejik sıkıntılarla birleşerek pek çok ülkenin enerji politikalarını rüzgar enerjisi, güneş enerjisi ve deniz kökenli enerjiler gibi yenilenebilir enerji kaynakları üzerine çevirmesine yol açmıştır. Bu kapsamda deniz dalgalarından enerji elde edilmesi, günümüz yenilenebilir enerji çağında özellikle ilgi çeken alanlardan biri haline gelmiştir.

Günümüzde, pek çok farklı amaca hizmet veren açık deniz yapılarının sayılarında görülen artış, bu sistemlerin randımanını ve üretkenliğini arttırmak amacı ile farklı amaçların tek bir platformda toplanması yaklaşımını doğurmuştur. "Çok amaçlı açık deniz platformları" olarak adlandırılan bu yapılara yönelik tasarım ve geliştirme çalışmaları günümüzde revaçta olan bir araştırma konusudur.

Bu çalışmada, bir yüzer dalgakıran yapısı ve bir dalga enerjisi dönüştürücü sistemden oluşacak çok amaçlı bir melez yapının tasarımı fiziksel modelleme teknikleri kullanılarak incelenmiştir. Sistemin temeli, boru tipi bir yüzer dalgakırandan mürekkep olup dalga enerjisi dönüştürücü sistem için aşma prensibi ile çalışacak, hidrokinetik enerji dönüştürücü ile teçhiz edilmiş bir sistem öngörülmüştür. Çalışma, ağırlıklı olarak aşma sisteminin hidrolik verimi ve yüzer dalgakıranın performansına odaklanmaktadır.

Dalga enerjisi dönüştürücü sistemin değerlendirilmesi için,fiziksel model çalışması gerçekleştirilerek dairesel silindir üzerinden dalga aşması modellenmiş ve aşma debileri incelenmiştir. Testler toplam yedi farklı konfigürasyon ve altı farklı batmışlık oranı üzerinden düzenli dalgalar ile gerçekleştirilmişlerdir. Yapı fribord yüksekliği ve dalga dikliğinin dalga aşma debilerini belirleyen baskın parametreler olduğu tespit edilmiştir. Fribord yüksekliğinin etkisi, fribord yüksekliği azaldıkça ortadan kalkmakta, dalga dikliğinin etkisi ise artan fribord yüksekliğine bağlı olarak azalmaktadır. Silindir önünde kısmi yansıma nedeniyle husule gelen ortalama su seviyesindeki kabarmanın aşma debilerinin miktarını önemli ölçüde etkidiği belirlenmiştir.

Kısmi batık silindir için aşağıdaki denklem regresyon analizi ile elde edilmiştir:

$$\frac{Q_{1m}}{\sqrt{gH_{rms}^3}} = 0.059exp\left(-3.45\frac{F_d}{H_{rms}} + 0.31s_h\right) \quad \textbf{(1)}$$

Dk. (1)'in uygulamasında veride görülen saçılım üzerine, dalga başına aşan debinin silindir kesit alanına oranı olarak yeni bir boyutsuz debi ifadesi tanımlanmıştır. Bu ifade kullanılarak gerçekleştirilen regresyon analizi ile aşma debilerinin tayini için

Dk. (2) elde edilmiş olup bu denklemin uyumluluğunun daha iyi olduğu gözlemlenmiştir:

$$\frac{Q_{1m}T}{0.25\pi D^2} = 0.441exp\left(-4.542\frac{F_d}{H_{rms}} + 1.166s_h\right) \quad \textbf{(2)}$$

Batık silindir durumu için Dk. (3) ve Dk. (4) elde edilmiştir:

$$Q_{1m} = 4.809\ln(s_h) - 21.250;\ \text{D=125mm} \quad \textbf{(3)}$$

$$Q_{1m} = 4.415\ln(s_h) - 20.870;\ \text{D=160mm} \quad \textbf{(4)}$$

Aşma debileri ve yüzer dalgakıranın ortak değerlendirmesinden, F/D = 0.12 batıklık oranı uygun aşma debileri ve hidrolik verim için melez sistemin tasarımında baz alınmış ve enerji ve güç hesapları bu konfigürasyon için gerçekleştirilmiştir.

Silindir arkasına kurulan iki istasyon üzerinden alınan zaman-seviye eğrileri kullanılarak aşan su hacminin ilerlemesi incelenmiştir. Su kütlesinin potansiyel ve kinetik enerjilerini dikkate alan bir enerji bütçesi tanımlanmış ve hesaplanmıştır. Su kütlesinin kret ve çukurundaki ilerleme hızlarının yakın mertebelerde olduğu ölçümlerde ortaya konulmuştur. Bu husus dikkate alınarak tüm kütlenin eşit bir hız ile ilerlediği kabul edilmiş ve üniform yatay hız dağılımı kabulü yapılarak aşan su hacminin uzaysal dağılımı elde edilmiştir. Ortalama ilerleme hızı için, su kütlesinin dispersiyon etkisinde şekil değiştirmesi nedeniyle, ağırlık merkezlerinin koordinatları ve deplasmanları hesaplanarak bir düzeltme gerçekleştirilmiş; kinetik enerji bileşeni kret ve çukur ilerleme hızlarından daha düşük olan ağırlık merkezinin ilerleme hızı üzerinden ifade edilmişlerdir. Düşey hız bileşenleri ihmal edilerek, tek bir dalga altında aşan su hacmi için kinetik ve potansiyel enerji değerleri hesaplanmıştır. Hidrolik verim, aşan su hacminin zamansal ortalama gücünün yapıya etkiyen dalganın gücüne oranı cinsinden tanımlanmıştır. Hidrolik verim değerleri hesaplanarak hakim parametrelere göre değişimleri incelenmiştir. Yapılan denemelerde, hidrolik verim ile hacimsel boyutsuz debi arasında üstel bir bağıntı yazılabileceği görülmüştür. Hidrolik verim bağıntısı Dk. (5) ile verilmiştir:

$$\chi_T = 0.0289exp(9.776Q_V) \quad \textbf{(5)}$$

Hidrolik verimin, dalga özelliklerine göre %9 ila %50 arasında değiştiği gözlemlenmiş olup söz konusu parametrenin dalga dikliğine paralel olarak artış gösterdiği belirlenmiştir.

Yüzer dalgakıran ünitesinin performansının saptanması amacıyla, Akgül ve Kabdaşlı (2008) tarafından incelenmiş olan bir sistem baz alınarak, önceki sistemde uygulanan birbirinden bağımsız hareket edebilen üç silindir yaklaşımı değiştirilmiştir. Bu çalışmada incelenen sistemde silindirler rijit bir şekilde birbirlerine bağlı olup silindirler arasında boşluk bırakılmıştır. Boşluk oranının dalga geçişine etkisinin araştırılması amacıyla üç farklı konfigürasyon düzenli dalgalar altında 30 farklı dalga serisi ile test edilmiştir. Sonuçlar, silindir ara mesafesinin artışına paralel olarak dalga geçişinin de arttığını göstermektedir. Dalga geçişinin hakim parametreler ile değişimi incelenmiştir. Genel olarak, baskın parametrenin yapı genişliğiinin dalga boyuna oranı olarak tanımlanan rölatif genişlik olduğu ortaya konmuştur. Bu durum, yüzer dalgakıranların genel performans özellikleri ile de örtüşmektedir.

Dalga geçiş katsayılarının elde edilmesi için regresyon analizi uygulanarak ampirik bağıntılar elde edilmiştir. Bu denklemler, dalga geçişini dalga dikliği ve rölatif genişliğin veya rölatif dalga yüksekliği ile rölatif genişliğin bir fonksiyonu olarak tanımlamaktadırlar. Birinci durum için Dk. (6) türetilmiştir:

$$C_T = 1.506exp\left(9.24s_h - 4.647\frac{B}{L_h}\right) \quad \textbf{(6)}$$

Sonuçların incelenmesi, önerilen yüzer dalgakıran sisteminin hafif dalga koşullarında tatminkar bir dalga sönümleyici olarak performans verdiğini göstermektedir. Bu koşullar için dalga geçişi %20 ila %45 oran aralığındadır. Orta sert ve sert dalga koşullarında ise dalga geçişi %40 ila %70 oranları arasında kalmakta olup sistemin orta derecede bir dalga sönümleyici olarak çalıştığını göstermektedir.

Yüzer dalgakıran ünitesinde husule gelen bağlama kuvvetleri ön ve arka bağlama halatları için ayrı ayrı incelenmiştir. Hesaplanan Keulegan-Carpenter sayıları 0.85 ila 3.20 arasında değişmekte olup Reynolds sayıları 105 mertebelerindedir. Bu açılardan ele alındığında atalet kuvvetleri yapı üzerinde baskın durumdadır. Bağlama kuvvetlerinin azami değerleri 200 N mertebelerinde ölçülmüş olup yüksek yansıma yaratan birkaç dalga dışında ani germe kuvvetleri gözlemlenmemiştir.

Melez sistemin değerlendirmesi, yapı deplasmanlarının aşma performansını etkilemediği kabulü ile gerçekleştirilmiştir. Her iki sistemin etkinliğinin de dalga dikliğine paralel olarak artış gösterdiği tespit edilmiştir. Bu açıdan ele alındığında, yüzer dalgakıran sistemlerinin genel olarak uygulandığı korunmuş ve/veya feç sınırlı bölgelerde oluşacak dalgaların da yüksek dalga dikliklerine sahip olacakları dikkate alınırsa, melez sistemin söz konusu bölgelerde mikro ölçekte bir dalga enerjisi dönüştürücü olarak uygulanabileceği ortaya çıkmaktadır. Elde edilen diğer bir sonuç, geçiş katsayılarında gözlemlenen düşüşe paralel olarak sistemin hidrolik veriminde görülen artmadır. Buna bağlı olarak, melez sistemi oluşturan yüzer dalgakıran ve aşma tipi dalga enerjisi dönüştürücü sistemlere ait performans eğrilerinin benzer trende sahip oldukları görülmekte, bu durum da eşleştirmenin uyumunu ortaya koymaktadır.

# 1. INTRODUCTION

Though mankind are land-living organisms, their relations with the sea date back almost to the existence of civilization. While the sea should be seen as the boundary of the living area for the human at the dawn of civilization, the need of crossing rivers and seas in order to provide territory and resources has lead to the development of marine and coastal engineering during the centuries. Being assessed as an obstruction to be crossed and as a source of food during ancient times, rivers and oceans have evolved to initial paths of transportation in the following centuries, leading to the foundation of many coastal cities, most of which are still in existence. The importance of waterways and oceans boosted further due to the evolution of nations and kingdoms, bringing them further the feature of being international routes of trade. Based on the developments mentioned above, the fields of marine and coastal engineering have been evolved in order to protect mankind from the dangers of sea and to ease the harnessing of sea resources.

While all the benefits of oceans and waterways counted above are still valid, further features have been added by means of harnessing natural sources in the ocean environment. Oil can be mentioned as the most important milestone here, which forced engineers and scientists to the design of comprehensive offshore structures such as drilling rigs and mooring and storage units. However, increase in environmentalist countermeasures and limited amount of fossil-based energy sources diverted the attention to more ecological energy sources such as wind, solar and marine energy. Marine energy, consisting mainly of wave, tidal and current energy forms, is mandatorily harnessed in the oceans, whereas harnessing wind energy with ocean-based platforms has been found more feasible, steady and environmental-friendly during last decades. Thus, design and development of offshore structures in order to utilise renewable energy has become a primary field of research and investment during the last decades.

It is well known that in many cases a limited volume of an offshore structure can be utilised in order to serve to its certain purpose, indicating that an important volume of

the structure is free. Based on this fact, designing multi-purpose offshore structures in order to keep a larger volume of the structure in use and hence reduce costs has become a field of study during recent years.

Supporting the aim mentioned above, this study is an attempt to create a multi-purpose offshore structure to act both as a wave energy converter and as a floating breakwater unit.

### 1.1 Purpose and Structure of Thesis

The fundamental aim in this thesis is the design of a floating hybrid structure, which should function both as a wave energy converter device and also as a floating breakwater.

Following the introduction, Chapter 2 provides the user with the literature review, starting with floating breakwaters. Section 2.2 is based on providing brief information about wave energy and wave energy converters. At the last part of the literature review, Subchapter 2.3 provides the user with a comprehensive information about wave overtopping, on which the designed wave energy converter system is based.

A summary of the literature review presented in Chapter 2 with focus on the hybrid system design and some fundamentals on preliminary dimensioning are given in Chapter 3.

The physical model studies carried out for the thesis are given in Chapter 4. Following a brief introduction, the subchapters explain the tests made for wave overtopping measurements and floating breakwater performance, respectively.

Evaluation of the test results and development and recommendations of formulae for the prediction of the physical properties measured during the tests are given in Chapter 5.

Chapter 6 combines the results from Chapter 5 in order to make the dimensioning of the hybrid system, and presents an assessment of efficiency for the hybrid system.

## 1.2 Restrictions and Limitations

Primary assessment and object maintained throughout the thesis is the applicability of the hybrid system. Thus, a subject kept on utmost importance is the quantification of wave overtopping over a cylinder and the hydraulic efficiency. In order to maintain an acceptable content and put some limits for further research, the study has been limited to two-dimensional performance for all tests. As a consequence, the effect of oblique wave attack has been disregarded. In a similar way, the effect of limited water depth has also been omitted due to the fact that the device has been developed for deployment in either deep water or the transition zone.

A second limitation has been brought by simplifying the type of mooring system. In general, it can be stated that mooring optimization for an offshore structure is made based on the properties of the incident wave climate and structural necessities. Thus, moorings used for the floating breakwater tests are kept as simple vertical cable elements bearing ignorable stiffness in the horizontal direction. For this case, the motion allowance of the structure is expected to be maximum and hence the wave transmission.

The development of a PTO unit, on the other hand, is a field of study for both mechanical and electronical engineers and researchers, so the subject has been kept on hydraulic efficiency.

In short, the purpose of the thesis is to bring answers to following action items:

i. Efficiency of a circular cylinder as an overtopping ramp for a wave energy converter: The subject is to evaluate the mean overtopping rates and evaluate functions for their prediction with respect to the cylinders immersion depth and incident wave properties.

ii. Estimating the hydraulic efficiency: Focus is kept on evaluating a method to predict captured wave power in a progressing overtopping volume, and the variation of efficiency with respect to incident wave properties.

iii. Efficiency of a proposed floating breakwater unit: Primary target is the wave attenuation performance, whereas the mooring forces also have been inspected.

iv. Coupled assessment of both systems: Assessment of efficiency with respect to various governing parameters. Predicting factors affecting the performance of the hybrid unable to be retrieved from individual tests.

# 2. LITERATURE REVIEW

Existing studies and their outcomes related to the concept of this thesis are summarized in this section. Subchapter 2.1 summarizes the development and recent status of floating breakwaters. Ocean wave energy and wave energy converters are treated in Subchapter 2.2. Subchapter 2.3 deals with wave overtopping, its governing parameters and related scientific output.

## 2.1 Floating Breakwaters

### 2.1.1 Historical development, features and drawbacks

Initial ideas and attempts on using floating elements as breakwaters dates back to the second half of the 19th century. However, these structures have been criticised by many experts by means of safety and reliability (Shield, 1910). The best known application of floating breakwaters has been laid down during the Normandy Landings in 1944 at the end of the Second World War, where a rapid-installable military port had to be constructed at the coast of Normandy, France, in order to provide logistics and ensure the safety of the landing. The port has been protected by submerged caissons and cruciform-shaped floating breakwaters called Bombardons (Carr, 1951). This application of floating breakwaters has proven that the functionality and performance of these structures is satisfying as long as the design wave conditions are not exceeded. Indeed, a storm encountered between 19th and 23rd of June caused severe damage to the harbour, pointing out that besides functionality, the structural integrity of a floating breakwater can also be ruined under extreme events (Carr, 1951).

Following the war, floating breakwaters have been studied by military engineers further due to their strategic benefits for the incomparable speed of construction and mobility. At the same time, other features of these structures such as rearrangeability, applicability for temporary installations and environmental benefits has caught the attention of other marine commercials such as marinas and fisheries. Since floating

breakwaters permit water exchange between the offshore side and the sheltered zone, they have minimum effect on local current patterns and hence do not hinder flushing in the sheltered zone. Unlike conventional breakwater structures, the feature of maintaining water quality in the port basin increases the interest to these structures as environmental friendly coastal protection elements. Furthermore, in contrast to conventional breakwaters, construction costs of floating breakwaters are less affected by water depth and poor foundation conditions (McCartney, 1985), making them an economical -even maybe unique- solution in these cases.

Though floating breakwaters feature many important benefits as mentioned above, they also have their restrictions. An important drawback on the application of floating breakwaters is the frequency-based limitation of the structures performance. A parameter defining the structures performance is given as the relative width of the structure, which is the ratio of the structures beam B to the incident wavelength L. Gaythwaite (2004) states that floating breakwaters become ineffective for relative width values smaller than 0.2, whereas their wave attenuation performance increases significantly for B/L values larger than 0.5. Consequently, the application range for floating breakwaters is limited due to limitations in structural construction, and based on existing examples, this limit can be given as wave periods up to 4-5 seconds (Gaythwaite, 2004). However, improvements in science and technology seem to increase structure sizes and hence range of applicability, as it has become evident at the construction of Monaco Quay Port. The structure mentioned here is a concrete caisson designed to act both as a quay and as a breakwater. With a length of 352 meters and a beam of 28 meters plus two 8 meter long anti-roll fins (de Wit and Hovhanessian, 2008), the structure has been designed to attenuate 2.5 m high storm waves.

Another shortcome of floating breakwaters excluding the limited range of applicability can be stated as the requirement of periodical inspections and maintenance. Since the system is highly dynamic, fatigue inspections, especially on module connectors and mooring elements should be performed periodically. Floats, on the other hand, are prone to marine growth and impact-based damage. Consequently, management costs of floating breakwaters are fairly higher than conventional breakwaters.

### 2.1.2 Functioning principles and assessment of performance

A floating breakwater can also be considered as a special form of offshore structures, designed to attenuate waves. Regarding wave-structure interaction, there are three important phenomena which can be counted as the transmission, reflection and dissipation of incident waves. Wave transmission here is the primary parameter regarding the design.

Paths of wave transmission through a floating body are shown in Figure 2.1. The most important component here can be counted as the free transmission, taking place between the sea bottom and the bottom of the structure. A second method of transmission can be counted as transmission through wave overtopping, which, in general, is much smaller than free transmission. The third method of wave transmission is dynamic transmission, where waves are generated at the sheltered side of the breakwater because of the wavemaker-like motions of the structure.

Reflected wave trains also consist of two parts, which can be defined as the diffracted waves from the surface of the floats and the radiated waves due to the structures motion. Wave dissipation, on the other hand, takes place along the boundaries of the structure, mainly due to formation of turbulence.

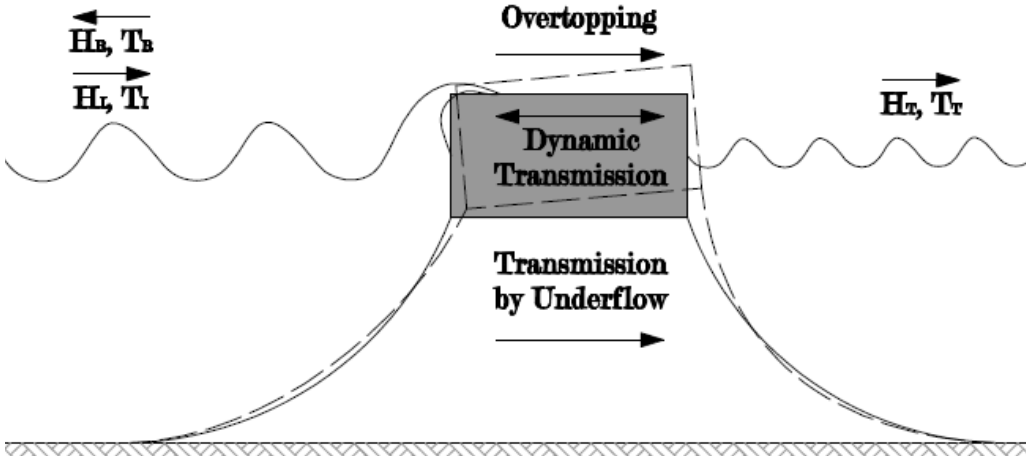


**Figure 2.1 :** Wave interaction with a floating breakwater.

To assess the performance of the structure, let us review the problem from the point of energy. When a wave with an energy $E_I$ strikes the structure, part of its energy $E_R$ is reflected back to the sea, composing reflected waves. Waves crossing to the sheltered side of the structure comprise the transmitted waves, which carry the transmitted wave energy $E_T$ shoreward. Energy dissipation, i.e. conversion of energy

to sound and heat due to generation of turbulence in the vicinity of the structure, forms the third energy component. $E_D$. If we take the conservation of energy into account, we can write:

$$E_I = E_T + E_R + E_D \tag{2.1}$$

For a further simplification, let us consider the case of regular waves, where the wave energy amount per unit surface area is defined according to linear wave theory as:

$$E = \frac{1}{8}\rho g H^2 \tag{2.2}$$

If we assume no changes in the period of the reflected and transmitted waves, we can rewrite Eq. 2.1 in terms of wave heights. If we denote $H_I$, $H_T$ and $H_R$ as the incident, transmitted and reflected wave heights, respectively, and assume a fictituous wave height $H_D$ related to energy dissipation, we can rewrite Eq. 2.1 as

$$H_I^2 = H_T^2 + H_R^2 + H_D^2 \tag{2.3}$$

Now let us introduce the definitions for the transmission, reflection and dissipation coefficients $C_T$, $C_R$ and $C_D$. These coefficients are given as the ratios of the mentioned wave height to the incident wave height:

$$C_T = \frac{H_T}{H_I};\ C_R = \frac{H_R}{H_I};\ C_D = \frac{H_D}{H_I} \tag{2.4}$$

Now, by using Eq. 2.1 and Eq. 2.4, we can write

$$C_T^2 + C_R^2 + C_D^2 = 1 \tag{2.5}$$

Since it is impractical to calculate $C_D$, it is usually solved out once the values of $C_T$ and $C_R$ are calculated:

$$C_D = \sqrt{1 - C_T^2 - C_R^2} \tag{2.6}$$

Another method for calculating the transmission, reflection and dissipation coefficients can be applied if the spectral energy density diagrams for the incident,

reflected and transmitted waves are known. In this case, the coefficients are given as cumulative numbers, containing the contribution of each frequency in the wave trains, so this method is also applicable to random seas:

$$C_T = \sqrt{\frac{E_T}{E_I}};\ C_R = \sqrt{\frac{E_R}{E_I}}; C_D = \sqrt{\frac{E_D}{E_I}} \tag{2.7}$$

In general, wave transmission past a floating breakwater can be defined as the function of incident wave properties, structure size, structure mass and inertia, stiffness of the mooring system and the physical properties of seawater (Oliver et al., 1994):

$$C_T = f\left[\left(\frac{h}{L},\frac{H}{L}\right),\left(\frac{B}{L},\frac{d}{h}\right),\left(\frac{m}{\rho B d},\frac{I}{mB^2}\right),\left(\frac{z_G}{d},\frac{kB}{mg}\right),\left(\theta,\frac{B\sqrt{gh}}{\nu}\right)\right] \tag{2.8}$$

In Eq. 2.8, *h, H* and *L* are the water depth, wavelength and the wave height, respectively. This group in the first clusters defines the incident wave properties. The second group of parameters indicate the geometrical size of the structure, where *B* counts for the structure width in wave propagation direction and *d* is the height of the structure. The third clustered group contains the structures mass properties with *m*, $\rho$ and *I* denoting the structures mass, density and inertia, respectively. The fourth clustered group defines the effect of mooring lines, where $z_G$ is the structures center of mass, *k* is the total stiffness of the mooring lines and *g* is the gravitational acceleration. The last clustered group of terms are a measure of viscosity, where $\theta$ is the viscosity of the fluid and the second term is an expression for the Reynolds number.

As seen from Eq. 2.8, there is a vast number of parameters acting on the performance of a floating breakwater unit. As a consequence, in many cases, research remains limited to assess the effect of some of these parameters. In almost all cases the first tests are limited to inspect the effects of structure size, water depth and incident wave properties. Improvement and the so-called "tuning" of the mooring system is carried out in the second step, coupled together with the mass and inertial properties of the structure. The vast number of governing parameters also restricts the existence of a general transmission formula, where all the parameters affecting the performance are considered. Thus, all studies on floating breakwaters are limited to some extent.

### 2.1.3 Types

Many different types of floating breakwaters have been developed, tested and applied during the second half of the 20th century. Most of these structures did not propagate past the physical model stage. A comprehensive review regarding older studies has been presented by Hales (1981). McCartney (1985) summarized the important types of floating breakwaters which have found prototype and field applications, and summarized their benefits and drawbacks together with design charts. A more recent classification has been made by Oliver et al. (1994), where the dominant functioning principle of the breakwater has been considered as the primary classification parameter, leading to two main groups, which are called reflective and dissipative systems, respectively. However, many other floating breakwater models have been developed since the publication date of Oliver et al.'s work. So, while keeping both the reflective and dissipative systems as primary classes, we shall introduce here a third main group called hybrid systems, which are designed by incorporating both reflective and dissipative mechanisms together, or by coupled working of multiple bodies.

#### 2.1.3.1 Reflective systems

Reflective floating breakwaters mainly comprise of a large prismatic box, sufficiently large to generate diffraction and hence reflection. The simplest type of reflective systems can be counted as the simple rectangular box type floating breakwater (Carver, 1979). In the literature, these structures are also called box-type or pontoon-type floating breakwaters. It can be stated here that most of the box type FBW's are built on rectangular floats or by using old barges, but there are also studies for different cross sections such as circular or a T-shaped structure.

Since the performance of the structure is related to its inertia, an attempt to increase inertia and hence the radii of gyration in order to reduce structure motions without increasing the total mass has lead to the development of double pontoon-type floating breakwaters, which are composed of two solid boxed connected to each other by rigid elements. A second feature of double pontoon systems is the energy dissipation due to turbulence generation in the gap between the pontoons, which also helps to reduce the transmitted wave heights.

Double pontoon type floating breakwaters have been studied by many scientists. Ofuya (1968) researched a double pontoon structure consisting of two ballasted pontoons spaced apart with a distance equal to the pontoon width and assessed the effects of changing mass and hence the draft of the structure (Hales, 1981). Results, as expected, indicate that increasing the mass of the structure leads to a higher draft and hence reduce wave transmission. Davidson (1971) studied a slightly different double pontoon breakwater, called catamaran type due to its much smaller pontoon widths. The structure, tested both for chained and piled moorings, has been developed for the small boat basin in Oak Harbor, Washington. Alaskan breakwater is another different form of double pontoon breakwaters with transverse members thicker in section, where the shape of the structure resembles a ladder in plan (Carver, 1979).

A different model, called the A-Frame floating breakwater, has been developed by Brebner and Ofuya (1968). The structure consists of a vertical thin plate connected to two circular cylinder floats with thin metal members, resembling an "A" in cross section view.

Another group of reflective structures have their dominant direction in vertical. Leach et al. (1985), recommended a hinged floating breakwater, which consists of a vertical plate mounted to the sea bottom, strained by inclined mooring lined attached to its top. The performance of the structure has been assessed both theoretically and experimentally. Williams et al. (1991) studied the performance of a similar structure, consisting of a buoyancy chamber at the MWL and a flexible beam extending from the MWL down until the sea bottom. Based on the numerical model they developed and verified with physical model tests, their results indicate that wave attenuation performance of such a structure increases with increasing stiffness.

There are also studies on submerged structures to act as floating breakwaters. Evans and Linton (1991) studied the case of a submerged plate and a submerged cylinder as wave attenuation devices to be used at port entrances by using the potential theory and the assumption that the structures frequency is "tuned" to neutralize the dominant wave frequency. A similar study has been carried out by Williams and McDougal (1996) for a rectangular submerged floating breakwater moored by vertical linear elastic springs.

A different and interesting design of interest is the RIBS (Rapidly Installed Breakwater System) floating breakwater (Briggs et al., 2002) developed for naval operations. The system consists of a V-shaped body in plan, with vertical planes extending down the MWL, composed of a foldable membrane. RIBS units are deployed head-on to the incident waves, providing shelter in the V-shaped shadow zone for ship operations. The concept is still being developed by numerical and physical model tests and prototype trials.

#### 2.1.3.2 Dissipative systems

The functioning principle of a dissipative floating breakwater is mainly based on viscousity effects and turbulence generation. A vast number of dissipative floating breakwaters have been based on the idea of utilising scrap vehicle tires. For this purpose, a porous and flexible structure from scrap vehicle tires is built at the still water level, which tend to reduce the vertical motion of water particles and generate a vast amount of energy dissipation due to flow through the porous structure (Oliver et al., 1994).

Many different types of floating tire breakwaters (FTB) have been developed during the 70's and 80's. Some good known examples can be counted as the Goodyear, Wavemaze and Waveguard models (Hales, 1981). Based on physical model studies, Harms (1979) pointed out that the reflection coefficient is small for FTB's and most of the energy becomes dissipated due to drag forces. He also calibrated and recommended an empirical equation for the estimation of transmission coefficients in case of Goodyear and Waveguard FTB models by adopting an exponential decay curve as a function of structure size, structure porousity, wavelength and a drag coefficient.

There are also studies about flexible membrane type structures as floating wave barriers. Williams (1996) conducted a theoretical investigation about a floating membrane breakwater by using 2D linear potential theory and boundary element methods. The breakwater consists of a vertical membrane structure providing a gap at its bottom, stationed with a buoy at the top and a ballast weight at the bottom and moored by elastic mooring lines. Lo (1998) studied the attenuation performance of a double membrane system, consisting of two elastic membranes extending from MWL to the sea bottom. The structure is similar to the one studied by Williams

(1996), but no gap is present between the bottom line of the structure and the sea bottom.

#### 2.1.3.3 Hybrid systems

Hybrid systems can be counted as more complex types of floating breakwaters, where both of the reflection and dissipation mechanisms are coupled together to increase the structures wave attenuation performance.

Some typical examples for hybrid floating breakwaters are recommended and tested with physical models by Chen and Wiegel (1970). These structures consist of multiple pontoon systems, where the gap between the pontoons is closed at the bottom with a porous plate and skirts are added to the structure.

A typical example for the hybrid systems can be given as the Y-frame breakwater researched by Mani (1991), developed by attaching vertical pipe segments to the bottom of a trapezoidal float in order to provide a narrower structure. This floating breakwater model later has been evaluated to the so-called cage floating breakwater to act both as a fish farm structure and a floating breakwater unit, where two of the Y-frame breakwater units are combined as a catamaran pontoon to form a floating breakwater unit (Murali and Mani, 1997).

Another hybrid system has been recommened by Kee and Kim (1997), who carried out a theoretical study verified by physical model tests to inspect the efficiency of a system consisting of a buoy and a membrane spanned between the buoy and the sea bottom, supported with cable type mooring elements at the top. The study points out that while the membrane can increase the efficiency of such a structure significantly, the size and submergence of the buoy predominates for success in a wider frequency band.

As a multiple structure hybrid, double pontoon system consisting of two pontoons independently connected to the sea bottom by linear elastic mooring lines has been inspected by Williams et al. (2000), pointing out that the spacing, draft and width of the pontoons are dominating parameters in wave transmission whereas excess buoyancy has a smaller effect.

### 2.1.4 Analytical and numerical works on floating breakwaters

Since the number of parameters acting on the performance of a floating breakwater is fairly high, development of simple analytical formulae to estimate the performance of floating breakwaters is not possible. In many cases, it is recommended to start with some analytical formulae developed for a fixed structure of simple geometry.

Some of the most known and applied practical formulations have been developed by Carr (1951), Macagno (1953) and Stiassnie (1982).

Carr (1951) developed a simple formula for the prediction of wave transmission past a fixed rectangular floating breakwater in shallow water:

$$C_T = \left( \sqrt{1 + \left( \left( \frac{\pi B}{L} \right) \left( 1 + \frac{d}{h-d} \right) \right)^2} \right)^{-1} \quad \textbf{(2.9)}$$

The work of Macagno (1953) is based on the transmission coefficient for a rectangular body with a defined draft d and width B, fixed at a water depth h:

$$C_T = \left( \sqrt{1 + \left( \frac{\pi B \sinh\left( 2\pi \frac{h}{L} \right)}{L \cosh\left( 2\pi \frac{(h-d)}{L} \right)} \right)^2} \right)^{-1} \quad \textbf{(2.9)}$$

Further analytical works are carried out by Stiassnie (1982) and Drimer et al. (1992), but results necessitate solutions of multiple cumbersome equations lacking simplicity. Stiassnie (1982) developed a simple mathematical model for the case of a thin vertical plate with a limited draft imitating the floating breakwater by using linear potential theory. Drimer et al. (1992) have developed an analytical solution for a box type floating breakwater by using two-dimensional linear potential theory with some simplifications. While the results achieved are consistent with some numerical verifications, they are still far from simplicity for practical applications. As an output of the study, the authors point out that increasing mooring line stiffnesses increases performance but also increases the wave forces, which even may exceed the forces on a fixed structure. Williams and McDougal (1996) used 2D potential theory to form an analytical solution to the wave transmission and motion responses of a submerged rectangular floating breakwater.

An initial numerical model recommended to analyze floating breakwater systems can be shown as the studies of and the study of Adee et al. (1976). Yamamoto et al. (1980), critisizing Adee et al.'s solution because of its deep water limitation and poor representation of mooring line stiffnesses, developed a more advanced model for the calculation of wave transmission, reflection and structure motions. The achieved solution, verified with regular wave tests in a small wave flume, is for the 2D case, where all the body motion, wave transformation and mooring forces are solved simultaneously by using Green's identity formula for a given potential function. It has been reported that the method is applicable for any cross section and for any bottom topography, even suitable for cases of multiple bodies by introducing some modifications to the boundary conditions. A further expansion supported by large scale physical model tests has shown that the response of the structure to irregular waves is essentially the same to regular waves (Yamamoto et al., 1981). Conseqently, it has been argued that both regular or irregular waves can be used to predict floating breakwater responses in a physical model study. The authors further point out that the model fails if flow separation along the boundary of the structure predominates (Yamamoto et al., 1981).

Fugazza and Natale (1988) carried out a study on floating breakwaters, where they point out the error caused by separating the problem into its diffraction and radiation components and solving them independently. They recommended some corrections to count the effect of nonlinear interaction between diffraction and radiation by using the principle of energy conservation.

Stating that second order wave drift forces cannot be simulated by linear frequency domain analysis models, a time domain based numerical model has been developed by Headland and Vallianos (1990). The model has been reported to be able to include both wave drift forces and nonlinear mooring line characteristics.

By pointing out that uncoupling the hydrodynamic analysis and the mooring analysis leads to errors, Isaacson and Bhat (1996) developed an iterative model using the wave drift force as the primary force dictating the quasi-steady equilibrium of the breakwater, which is incorporated into mooring line forces.

Williams and Abul-Azm (1997) researched the behavior of a catamaran type floating breakwater, consisting of two pontoons stiffly connected to each other. By using a

boundary element method and two-dimensional potential flow theory during the study, they assessed the effects of various parameters on wave transmission and wave reflection.

Williams et al. (2000) inspected the case of two floating pontoon breakwaters moored individually to the bottom via elastic mooring lines under small displacemensts assumption by using linear potential theory . Lee and Cho (2002), based on their numerical and experimental study, inspected the effect of mean wave drift on the mooring line tensions and transmission performance of a pontoon floating breakwater, stating that mean wave drift has an important effect especially on the offshore mooring line tension.

Stating that applying potential flow theory has its drawbacks in the modeling of large scale motions, Rahman et al. (2006) applied a VOF model for the structure containing three materials, the solid representing the body, the fluid and air. The model uses a combined solution of the continuity equation, Navier-Stokes equation and advection equation, validated with physical model tests.

Loukogeorgaki and Angelides (2005), adopting the iterative algorithm given by Isaacson and Bhat (1996), developed a three-dimensional numerical solution for a pontoon type floating breakwater in frequency domain. Diamantoulaki and Angelides (2010) inspected the case of a floating breakwater array consisting of a number of modules connected to each other by hinges. Based on a 3D study with regular waves in frequency domain, they point out that wave direction affects the performance of the structure with transmission decreasing with increasing wave angle. Furthermore, the pontoon-length to wavelength ratio becomes insignificant in case of very low and very high frequencies.

### 2.1.5 Recent studies on floating breakwaters

With the developments in computers and computational fluid mechanics, a vast number of studies on floating breakwaters carried out during the last decade deal with the numerical modeling of the structure. At the same time, there are also new breakwater models under development, together with the attempts of increasing the performance of existing types. In such studies, physical modeling is used frequently. Besides studies based on numerical and physical modeling of the subject, there are

also some studies dealing with points of particular interest such as the measurement of forces on the module interconnection elements.

Koftis and Pinos (2006) conducted a both experimental and numerical study on the effect of wave overtopping over a floating breakwater structure. A small wave flume has been used for the tests where a rectangular fixed body with different freeboard values set as main configurations represents the breakwater. The model study has been coupled with a RANS-based numerical model utilizing a VOF method to capture the surface interaction. Their result indicate that wave overtopping starts after a threshold dimensionless freeboard value of F/H = 0.78 and induces secondary waves at the sheltered zone of the structure, which interact with the transmitted waves. They also point out that in case of a zero-freeboard structure, an increase in draft leads to increase in overtopping and hence higher transmission coefficients. It is pointed out that in case of overtopping, higher order frequencies are more evident in the transmitted waves.

Another important field of study of particular interest in floating breakwater design is the measurement of module connector forces. A physical model study conducted by Peňa et al. (2011) also focuses on mooring forces and module connector forces, where different floating breakwater bodies composed of different pontoon-type structures are tested in 2D and 3D regular waves. The output of the study indicates that oblique wave attack has its major effect on module connector forces.

### 2.1.6 Floating pipe breakwaters

A different group of floating breakwaters can be defined as floating pipe breakwaters. The idea of using circular elements as floating breakwaters has two prominent origins: The use of logs as protection elements, and benefiction of commercial pipes as floating breakwaters. Though not as popular as conventional floating breakwater types, interest into design of such scructures is still evident, where the primary focus is the introduction of pipeline industry into floating breakwater construction in order to reduce construction costs.

Initial works on wave transmission past circular cylinders date back to the studies of Ursell (1950). The first attempt of utilizing circular cylinders as floating breakwaters dates back to the study of Jackson (1964), where the aim was using tree logs in a two row series forming a pontoon to protect a small boat basin in Juneau, Alaska. The

mooring system on this example consisted of vertical piles. In order to develop an efficient system, physical model tests have been carried out on the so called twin log floating breakwaters. The effects of angle of attack, log diameter and log spacing are inspected. The results indicated that wave tranmission is primarily governed by the wave period and the effect of pipe spacing can be counted as negligible. However, it can also be stated that the tested range of waves is fairly small, consisting only of three wave periods.

Following Jackson, Ofuya (1968) conducted laboratory tests on a twin pipe floating breakwater model, consisting of two circular cylinders connected to each other by rigid members. Ofuya inspected the effect of relative submergence of the pipes by changing their masses and the effect of cylinder spacing.

Mays et al. (1999) conducted a numerical study about the 3D wave attenuation performance of submerged, tautly moored, rigid horizontal circular cylinders. A single-cylinder and a dual cylinder combination have been analyzed for both normal and oblique waves. Plaut et al. (2000) studied the snap loads for a semi-submerged circular cylinder moored with taut mooring lines, where snap loads exist under large amplitude waves. Sundar et al. (2005) studied the forces on the cylinder body and the mooring forces on a submerged open moored cylinder by physical model tests. Regarding the effect of oblique wave attack, their results indicate that the horizontal force acting on the cylinder decrease with increasing angle of attack, which is opposite for the case of vertical force. Both forces decrease with increasing depth of submergence.

Sundar et al. (2003) studied another variant of FPBWs, where the structure consisted of multiple pipes of equal diameter, placed in an horizontal array with gaps provided between the pipes with spacings equal to the pipe diameter. Based on physical model tests, effect of structure size and submergence have been assessed by using three models with different pipe diameters and masses. While their outcome states that the depth of submergence is not significant for the variation of the transmission coefficients, this should be assessed more due to changing mass on each configuration. They further state that the gaps between the pipes induce turbulence, and waves with high steepness values decompose into their smaller harmonics during the transmission process.

A slightly different system has been researched by Hedge et al. (2007), where a raft-like structure has been constructed from pipe elements, which are arranged in three layers forming a grid. The alignment of the central layer pipes is parallel to the wave propagation direction, whereas the pipes on the outer layers are aligned parallel to the wave crests. The performance of the structure has been assessed by conducting 2D physical model tests, and results are compared with the mathematical model developed by Harms (1979). Mooring forces for this type of FPBW have been assessed later by Hedge et al. (2008), given as nondimensional diagrams as a function of relative width.

Ozeren et al. (2008) conducted physical model tests on the performance of a single horizontal pipe and twin- and triple pipes to act as a wave attenuator. They tested a variety of models with three types of moorings; fixed, pile-guided and cable-moored, respectively. The effect of structures submergence ratio has been assessed during the tests. An outcome for the fixed single cylinder is that the optimum ratio of submergence is recommended as d/D = 0.7. It has been stated that a fully submerged cylinder loses its efficiency due to initiation of transmission through overtopping, while reduction of relative submergence increases the transmission area below the structure. For a pile-restrained cylinder, by which the depth of submergence ratio is adjusted by changing the weight of the structure, best performance has been achieved again at the ratio of submergence d/D = 0.7. On the other hand, the cable-moored system has its best performance at the fully submerged configuration, which, however, should also result as a consequence of the increase in the excess buoyancy of the cylinder, acting as a restoring force. These results validate the results achieved during the tests made by Akgul (2008) for the optimization of the breakwaters submergence ratio.

Further results achieved by Ozeren et al. (2008) indicate that replacing a single pipe with a bundle of pipes of an equivalent size does not affect the performance, however, it might be a more economical solution when it comes to any field application, mainly due to ease of transport. Regarding a two-pipe combination, they state that installation of a second pipe with a smaller diameter in the onshore side reduces the transmission of steep waves, which decompose into higher harmonics upon striking the first cylinder. Ozeren et al (2011), in a further study, inspected various arrangements of cylindrical floating breakwaters with different mooring

arrangements. Having also investigated configurations with multiple pipes bound together, they point out that a bundle of pipes of smaller diameters has the same effect with a singular pipe of equivalent outer diameter.

Akgul and Kabdasli (2012) inspected the wave attenuation properties of a floating pipe breakwater, consisting of three pipes connected with taut lines to the seafloor and to each other. While the performance of the system seemed satisfying, motions of the pipes relative to each other represented a risk of internal collision.

## 2.2 Wave Energy and Wave Energy Conversion

### 2.2.1 Introduction

Growing global population, improvements in technology, increase in global trade and production and advances in personal life quality are leading to a continuous increase in the global energy demand. With the growing global caution on environmental protection, usage of conventional fossil-based energy sources and its consequences on global pollution has started to be highly anticipated. Besides this, limited reserves of these resources are seen as a threat to the national energy politics by many countries. As a consequence, alternative energy sources have been started to be researched. While being highly productive and efficient, nuclear energy has its own risks of meltdown and radiative pollution as observed in the cases of Chernobyl and Fukushima nuclear power plants. These threats triggered and boosted the research on environmental friendly energy sources.

Primary sources of natural energy can be counted as solar energy, wind energy, marine energy, hydraulic energy and biomass energy. Global potential of these renewable energy forms are given in Table 2.1 (Ozdamar, 2000).

As seen in Table 2.1, marine energy, following solar and wind energies, has the largest global natural potential in renewable energies. Though this might seems to reduce its importance, marine energy has its unique features. First of all, it is known that the amount of marine energy stored in unit area is 10-15 times of the amount which can be stored by solar and wind energies (Saglam et al., 2005). This feature indicates that a marine energy converter should occupy much less space in contrast to a wind or solar energy converter of equivalent capacity, being more cost- and space-

effective. Furthermore, the seasonal variation of the marine energy follows the trend of the seasonal public energy demand (Drew et al., 2009).

**Table 2.1 :** Global natural potential of renewable energy sources (Ozdamar, 2000).

| Energy Source | Global Annual Natural Potential [x10 kWh] |
|---|---|
| Solar | 1.524.240.000 |
| Wind | 30.844.000 |
| Marine | 7.621.000 |
| Hydraulic | 46.000 |
| Biomass | 1.524.000 |

### 2.2.2 About wave energy

#### 2.2.2.1 On ocean waves

Wave motion observed in the ocean environment is formed under different driving forces such as the Coriolis force, moon attraction and wind-generated shear forces. A diagram showing the energy distribution of ocean waves according to their frequency and sources of disturbance and restoration is given by Kinsman (1965), shown in Figure 2.2. It can be seen from Figure 2.2 that the largest portion of ocean energy is stored in gravity waves, which are built due to the shear forces acting on the ocean surface, caused by wind action. Wind generated ocean waves, during their development and in their fully developed status, usually have period values remaining between 1 sec and 30 seconds (Kabdasli, 1992). Waves with larger periods, called inragravity waves, exist in case when the wind is ceased and the existing storm waves start to disperse and decay. Ultragravity waves, which are waves with periods smaller than 1 sec are observed mainly at the initial stage of a developing sea. Thus, by the term wave energy converter we shall consider devices, which are designed to produce electricity from gravity waves, which have a period range varying between 1 sec and 30 sec.

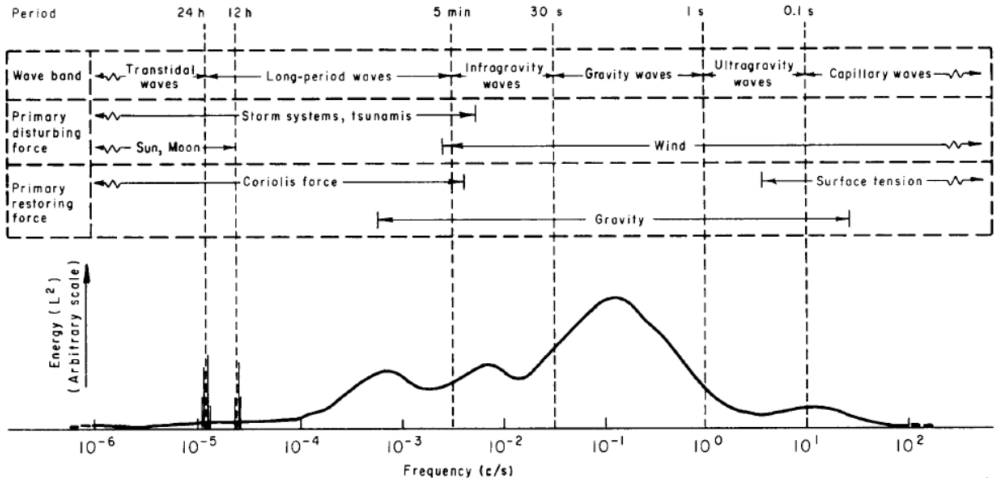


**Figure 2.2 :** Distribution of ocean surface wave energy classified according to frequency band, type of wave and driving force (Kinsman, 1965).

### 2.2.2.2 Derivation of wave energy and wave power

Energy carried in a wave train consists of two components, potential energy and kinetic energy, respectively. Potential energy arises due to deformation of free water surface and existence of wave crests, where particles are at a higher elevation level compared to the case of still water. Kinetic energy, on the other hand, is caused by the motion of the water particles during wave progression (Dean and Dalrymple, 1991). Derivation of wave energy components and wave energy flux for regular waves is given in the following.

**Potential energy**

As known, the potential energy $E_P$ carried by a body with respect to a reference level can be calculated as the product of the bodies weight W (which itself is the product of the bodies mass m and the gravitational acceleration g) and the elevation of its center of gravity $z_G$ from the reference level:

$$E_P = mgz_G \tag{2.11}$$

In order to apply Eq. 2.11 to waves, let us take a wave profile into account (Figure 2.3). Assuming the reference level as the sea bottom, let us take an inifinitesmal fluid column of differential width *dx* into account. Let the instantaneous water surface elevation be defined by a function $\eta(x,t)$. In order to calculate the potential energy $E_P$ under a single wave, we are going to use an integration along the x-axis for the sum of the infinitesmal columns under the wave. The mass *dm* of such a column can be written as:

$$dm = \rho(h+\eta)dx \tag{2.12}$$

The center of gravity of the water column $z_G$ can be typed as

$$z_G = \frac{h+\eta}{2} \tag{2.13}$$

By using Eq. 2.12 and 2.13, we can calculate the potential energy $dE_{PT}$ of the water column as

$$dE_{PT} = dmgz_P = \rho g(h+\eta)\left(\frac{h+\eta}{2}\right)dx \tag{2.14}$$

Simplifying Eq. 2.14 yields

$$dE_{PT} = \frac{1}{2}\rho g(h^2+\eta^2+2\eta h)dx \tag{2.15}$$

Now, in order to calculate the total potential energy under the wave, let us integrate Eq. 2.15 along the *x* axis for one wave length *L*:

$$E_{PT} = \int_x^{x+L} \frac{\rho g}{2}(h^2+\eta^2+2\eta h)\,dx \tag{2.16}$$

Eq. 2.16 can be used for any free surface function $\eta(x,t)$. Let us assume linear wave theory valid, where the free surface equation is given as

$$\eta(x,t) = \frac{H}{2}\cos(\mathrm{kx}-\omega\mathrm{t}) \tag{2.17}$$

If we substitute Eq. 2.17 into Eq. 2.16, we get

$$E_{PT} = \frac{\rho g}{2}\int_x^{x+L}\left(\begin{array}{c} h^2+\left(\frac{H}{2}\cos(kx-\omega t)\right)^2 \\ +2hcos(kx-\omega t)\end{array}\right)dx \tag{2.18}$$

Simplifying and evaluating the integral gives

$$E_{PT} = \frac{\rho g L}{2}\left(h^2+\frac{H^2}{8}\right) \tag{2.19}$$

The value of $E_{PT}$ calculated by Eq. 2.19 represents the total potential energy carried by a sine wave with respect to the sea bottom reference level. To calculate the potential energy induced by wave existence only, we have to subtract the still water potential energy, which can be calculated as

$$E_{P0} = \int_{x}^{x+L} (\rho g h)\left(\frac{h}{2}\right) dx \tag{2.20}$$

Evaluating the integral and simplifying yields

$$E_{P0} = \rho g L \frac{h^2}{2} \tag{2.21}$$

Thus, the potential energy caused by waves can be calculated as

$$E_P = E_{PT} - E_{P0} = \frac{1}{16}\rho g H^2 L \tag{2.22}$$

In case we are interested into the length-averaged potential energy $\bar{E}_P$ in a wave, we simply divide Eq. 2.22 to the wavelength *L*:

$$\bar{E}_P = \frac{1}{16}\rho g H^2 \tag{2.23}$$

**Kinetic energy**

In order to calculate the total kinetic energy under a single wave, let us consider an infinitesmal body with a mass of *dm*, a lenght of *dx* and a height of *dz* in the wave domain. If the velocity of the particle *v* is known, then the kinetic energy of the body can be written as

$$dE_K = \frac{1}{2} dm v_m^2 \tag{2.24}$$

Considering wave mechanics, the total velocity of a water particle $v_m$ is usually given in its horizontal and vertical components, which can be used to calculate the bodies resultant velocity. Retyping the velocity term and substituting *dm* with *ρdzdx* gives

$$dE_K = \frac{1}{2}\rho dx dz (u^2 + w^2) \tag{2.25}$$

In order to calculate the total kinetic energy under a wave, Eq. 2.25 should be integrated along the water depth in vertical and one wavelength in horizontal:

$$E_K = \int_x^{x+L} \int_{-h}^{\eta} \frac{1}{2}\rho(u^2 + w^2)dzdx \tag{2.26}$$

Eq. 2._ can be used for any wave theory. Let us apply linear wave theory in order to evaluate it further, where the horizontal and vertical particle velocities *u* and *w* are given by

$$\begin{aligned} u &= \frac{gHk}{2\omega}\frac{\cosh\big(k(z+h)\big)}{\sinh(kh)}\cos(kx-\omega t) \\ w &= \frac{\omega H}{2}\frac{\sinh\big(k(z+h)\big)}{\sinh(kh)}\sin(kx-\omega t) \end{aligned} \tag{2.27}$$

By substituting Eq. 2.27 into Eq. 2.26, we get

$$E_K = \psi \int_x^{x+L} \int_{-h}^{\eta} \begin{bmatrix} \cosh^2\big(\mathrm{k(z+h)}\big)\cos^2(\mathrm{kx-\omega t}) \\ +\sinh^2\big(\mathrm{k(z+h)}\big)\sin^2(\mathrm{kx-\omega t}) \end{bmatrix} dzdx \tag{2.28a}$$

where

$$\psi = \frac{\rho}{2}\left(\frac{gHk}{2\omega}\frac{1}{\cosh(kh)}\right)^2 \tag{2.28b}$$

Following the evaluation of the integrals and some simplifications we can write Eq. 2.28 as

$$E_K = \frac{1}{16}\rho g H^2 L \tag{2.29}$$

Just to remind, it should be noted that both Eq. 2.22 and 2.29 have been derived for a horizontal area spanning one wavelength parallel to the wave propagation direction and having a unit width. Similar to the modification carried out in Eq. 2.23, the average kinetic energy per unit surface area can also be calculated by dividing Eq. 2.29 to the wavelength, which yields

$$\bar{E}_K = \frac{1}{16}\rho g H^2 \tag{2.30}$$

The total energy contained under a progressive wave hence can be written as

$$E = E_P + E_K = \frac{1}{8}\rho g H^2 L \tag{2.31}$$

Similarly, for the unit surface area, the total wave energy can be given as

$$\bar{E} = \frac{1}{8}\rho g H^2 \tag{2.32}$$

**Wave energy flux (Wave power)**

As known from general physics, power is defined as the rate of work done in unit time. Applying this principle to water waves, we can define wave power or wave energy flux as a measure of energy transfer in the direction of wave propagation (Dean and Dalrymple, 1991).

Let us consider a vertical section in the wave medium. Here, for any depth z, we can define the instantaneous work (i.e. power) as the product of dynamic pressure $p_D$ and particle velocity $u$. For this case, if we try to evaluate the total wave energy flux carried out at an instant over a vertical plane, we can write

$$P = \int_{-h}^{\eta} p_D u dz \tag{2.33}$$

In order to reach a time averaged value, we have to use Eq. 2.33 and average it for the wave period:

$$\bar{P} = \frac{1}{T}\int_{t}^{t+T}\int_{-h}^{\eta} p_D u dz dt \tag{2.34}$$

The expression of dynamic pressure for linear wave theory is given as

$$p_D = -\rho g z + \rho g \frac{H}{2}\frac{\cosh\left(k(z+h)\right)}{\cosh\left(kh\right)}\cos\left(kx - \omega t\right) \tag{2.35}$$

By substituting Eq. 2.35 and Eq. 2.27 for the horizontal velocity component $u$ into Eq. 2.34, we get

$$\bar{P} = \frac{1}{T}\int_{t}^{t+T}\int_{-h}^{\eta}\left[\rho g\eta\frac{\cosh\big(k(z+h)\big)}{\cosh(kh)}\right] \left[\frac{gHk}{2\omega}\frac{\cosh\,(k(z+h))}{\cosh\,(kh)}\cos\,(kx-\omega t)\right]dzdt \tag{2.36}$$

Integrating Eq. 2.36 up to the MWL leads to:

$$\bar{P} = \frac{1}{T}\int_{t}^{t+T}\int_{-h}^{0}\rho g\omega\eta^2\frac{cosh^2(k(h+z))}{\cosh(kh)\sinh\,(kh)}dzdt \tag{2.37}$$

Evaluating the integral yields

$$\bar{P} = \frac{\rho g\omega}{4k}\left(\frac{H}{2}\right)^2\frac{2kh+\sinh(2kh)}{\sinh(2kh)} \tag{2.38}$$

Eq. 2. 38 can also be written in a more familiar form as

$$\bar{P} = \left(\frac{1}{8}\rho gH^2\right)\left(\frac{\omega}{k}\right)\left[\frac{1}{2}\left(1+\frac{2kh}{\sinh(2kh)}\right)\right] \tag{2.39}$$

The first term in the clusters had been calculated as the mean wave energy $\bar{E}$ per unit surface area in the previous section. The second term in clusters is equal to the wave celerity *c*, i.e. the travel speed of a wave. The product of the celerity with the third term in clusters is called group velocity $c_g$, and defines the energy transmission speed. Using the definitions and conversions given here, the mean power of a wave can be expressed as

$$\bar{P} = \bar{E}c_g = \bar{E}cn \tag{2.40}$$

where

$$n = \frac{c_g}{c} = \frac{1}{2}\left(1+\frac{2kh}{\sinh(2kh)}\right) \tag{2.41}$$

Applications of Eq. 2.40 and 2.41 to represent the wave power in irregular sea states is also carried out by introducing the properties of the inspected wave spectra. However, since regular waves have been treated during this study, the mentioned expansion shall not be explained here.

### 2.2.3 Purpose and historical development

It has been reported that the first patent on utilising wave energy has been acquired in 1799 (Cruz, 2008). However, the increase in interest on wave energy has started in 1970's due to the occurrence of the oil crisis. As a response Salter (1974) developed a device called "Salter's Duck" in Edinburgh University, UK to extract energy from ocean waves. The device consists of a teardrop shaped body mounted to a shaft parallel to the free surface. While its efficiency has been shown in a range reaching up 90% in some cases, it has been reported that the resultant forces on the shaft are very large (Mynett et al., 1979) and introducing further degrees of freedom reduces the efficiency. Another device consisting of a moored submerged horizontal circular cylinder oscillating with incident waves has been studied by Evans et al. (1979). Called the Bristol Cylinder, the device utilizes the motions of the cylinder under the wave excitation forces to generate electricity. Competing other non fossil-fuel based energy sources such as nuclear plants, solar plants and wind plants, the ocean wave energy has become an important field of interest, mainly due to its benefits mentioned in Chapter 2.3.1. The boost in research on wave energy devices did happen during the last two decades, where many different wave energy converters with different mechanisms have been developed.

It is well known that there is a vast number of different models still being developed in different TRL stages. A fairly recent list on the global development of WEC's identifies 147 different systems designed and improved by different countries and companies (Losada et al., 2013). In order to remain focused on the main object, only some fundamentals are given based on the classification of WECs, followed by an introduction to the existing overtopping type WECs.

### 2.2.4 Classification of wave energy converters

For the classification of WEC systems, different features of the structures are considered.

According to the depth of installation, WEC systems are classified into three groups called coastal, nearshore and offshore devices. Coastal devices are installed into very shallow depths or onto shore protection structures such as the SSG Slot Cone Generator or LIMPET WEC systems. Nearshore structures are constructed at shallow to intermediate water depths up to 15-20 meters, providing easy access from the

shore in case of maintenance and repairs. Offshore structures, on the other hand, are deployed in much deeper waters; while access to these structures may becomes problematic in case of rough weather, they feature the capture of wave energy before wave trains lose energy due to wave-sea bottom interaction and wave breaking.

Based on their alignment with respect to the incident waves, WEC systems are separated into three subcategories called attenuators, point absorbers and terminators, respectively. If the structure is aligned with its characteristic dimension parallel to the wave direction propagation, the structure is called an attenuator, with a typical example of the PELAMIS WEC. Terminator type systems have their characteristic dimension aligned perpendicular to the wave propagation direction, a typical example can be given as the Wave Dragon WEC. Point absorbers, on the other hand, have no major dimensions with respect to the wave length; they absorb wave energy on a relatively small area.

### 2.2.5 WECs working with overtopping principle

The design of a WEC using overtopping principle is based on the attempt of storing the incident overtopped water mass at a level higher than the MWL and hence creating a static head to drive the turbines. The systems explained below -excluding the Wave Plane WEC- utilize this method to produce electricity. The first example of overtopping type WEC's is given as the TapChan, followed by the Wave Dragon as an extension to offshore. Both these structures use a single reservoir to accumulate water. A different approach in enhancing the efficiency of overtopping type WEC's is the installation of multilevel reservoirs, enabling storage of water in different elevations and hence leading to an increase in the potential energy stored. Some applications of the multilevel approach can be counted as the SSG Slot Cone Generator and the Power Pyramid WEC, explained below.

Different types of overtopping type WEC's have been proposed for offshore and onshore installations. Most of the structures mentioned below have reached large scale model testing level and/or deployment in open sea.

#### 2.2.5.1 TapCHAN

TapCHAN is an abbreviation for "Tapered Channel". The system is an onshore device consisting of a reservoir, a low-head turbine PTO equipped with Kaplan

turbines and a tapering channel extending offshore (Thorpe, 1999). Waves approaching the structure enter the channel and they are amplified on their propagation along the tapering section of the channel. Near the reservoir, the amplified waves spill into the reservoir over the walls of the channel, increasing the water level in the reservoir, and the head difference drives the turbines discharging water back to the ocean (Hagerman, 1992).

A TapCHAN WEC has been installed in Toftestallen, Norway in 1985. The expected capacity of the system had been estimated as 350 kW, which, more or less has been achieved during its operation (Thorpe, 1999). Having operated for some years, the structure was subject to severe damage during a maintenance and improvement taken place in 2009, where a major storm hit the structure and lead to major destruction. As far as it is known, the project is currently standby due to lack of finance.

#### 2.2.5.2 Wave Dragon

Invented by Erik Friis-Madsen, the Wave Dragon WEC is being developed by Wave Dragon ApS from Denmark (Url-1). The device (Figure 2.3) is a slack moored offshore type WEC, consisting of an overtopping ramp, a reservoir and low head Kaplan turbines. The single point mooring enables the device to align itself perpendicular to the incident wave direction. To enhance the overtopping rates, the device has been equipped with special designed parabolic guide walls, focusing incident waves to the overtopping ramp. The device contains a major volume of floats with open bottom, which enable the adjustment of freeboard and reduce structural motions and hull forces (Kofoed et al, 2006).

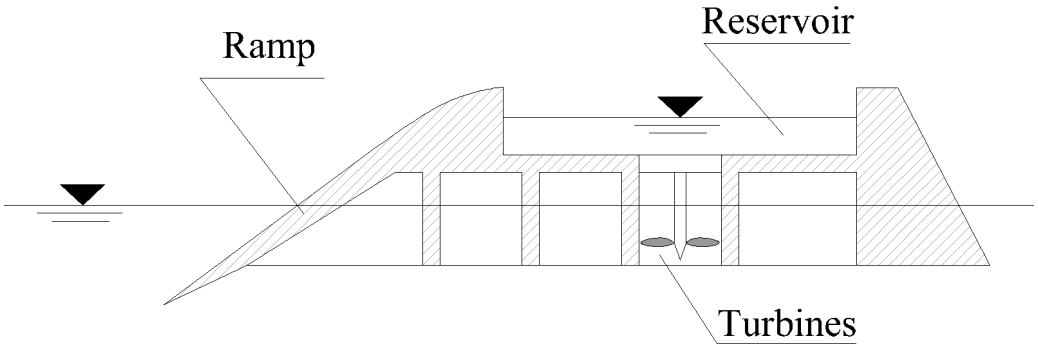


**Figure 2.3 :** Wave Dragon WEC (Kofoed, 2002).

A fair amount of research has been carried out for the development of Wave Dragon WEC. Recent works are also based on the 1:4.5 scaled prototype of the structure,

deployed in 2003 at Nissum Bredning, Denmark (Kofoed et al., 2006), being the worlds first offshore wave energy converter connected to a grid system. Based on the studies on the prototype device, it has been reported that the operating head for the turbines vary significantly and frequently, leading to a frequent need of regulation for the turbines. The annual efficiency of the device has been reported as 12%, necessitating an optimization to improve efficiency.

#### 2.2.5.3 Seawave Slot Cone Generator

Seawave Slot Cone Generator is a multi-level wave energy converter device designed to be deployed on coastal installations. The principle of this device is to gain the potential energy directly at the highest possible runup elevations before letting the water mass accumulate in a reservoir at a lower elevation.

#### 2.2.5.4 Power Pyramid WEC

Power Pyramid is another overtopping type WEC utilizing multilevel reservoir approach. In fact, it can be stated that Power Pyramid is the offshore adaptation of the Seawave Slot Cone Generator mentioned above.

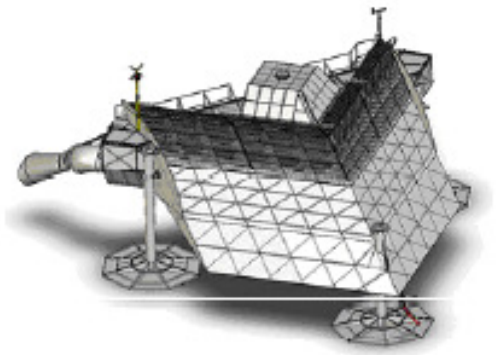

**Figure 2.4 :** WavePlane WEC (Url-2).

#### 2.2.5.5 Wave Plane

A quite different WEC utilizing overtopping principle is the Wave Plane WEC invented by Erik Skaarup, founder of WavePlane Electric A/S from Denmark (Url-2). A different method has been used in the PTO of the Wave Plane WEC, where the overtopped water is turned into a rotating mass in a pipe, driving the turbines (Figure 2.4). It has been stated that the primary aim of the device is to use the kinetic energy of the incident waves. However, information about this WEC and its current status is sparse. It is noted that a full-scale prototype has been deployed off the west coast of

Denmark in 2009, but it has been reported as grounded due to the failure of its mooring lines (Url-2).

## 2.3 Wave Overtopping

### 2.3.1 Definitions

In general, wave overtopping can be defined as the propagation of a fraction of a water wave along the crest (deck) of a coastal (marine) structure towards its sheltered zone.

Reviewing the literature, different types of wave overtopping can be classified based on the intensity and strength of the flow. Simple and less harmful types of overtopping can be counted as spray and splash. Spray can be defined as the carriage of water particles over the structure by wind or similar effects, forming the lightest type of overtopping. Splash occurs when waves break in front of the structure and fractions of broken waves travel over the structure. The most severe type of overtopping is called as the green water overtopping, where an entire mass of water exceeds the structures freeboard level and runs along the crest of the structure. Based on its severity, most studies existing in the literature deal with green water overtopping. Spray and splash, on the other hand, are rarely researched due to their smaller importance and also due to limitations in the physical modeling of these processes.

Wave overtopping is an important field of study in both coastal and marine engineering sciences. In coastal engineering, estimation and inhibition/reduction of wave overtopping is a problem to be dealt with in order to provide safety and functionability of coastal protection structures and to protect sheltered zones from flooding. In marine engineering, waves overtopping a ships deck can lead to stability problems, it is also considered as a risk for the crew and deck equipment on board. A more recent field to assess wave overtopping has come forth due to its application on some wave energy converter systems.

### 2.3.2 Governing parameters

The parameters controlling the amount of wave overtopping can be classified into three different categories, which can be counted as the characteristics of incident

waves, the geometrical properties of the structure considered and the physical properties of the structure considered. A general sketch showing the parameters acting on wave overtopping for a coastal structure is given in Figure 2.5.

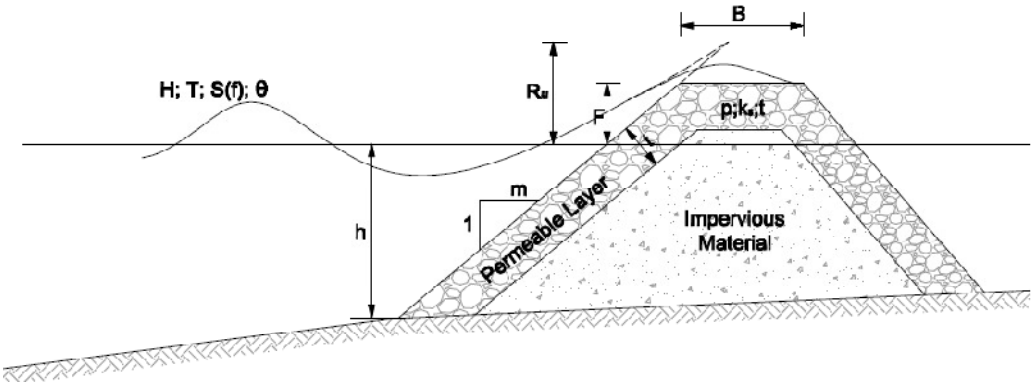


**Figure 2.5 :** Parameters governing wave overtopping.

The characteristics of incident waves include the wave height H, wave period T, wave steepness $s_h$, the wave approach angle θ and for the case of irregular waves, the spectral properties of the wave, to be given under a wave spectra function S(f). If we take the transition zone or the case of shallow water into account, then the water depth h and sea bottom slope tanβ can also be included in this group, since they affect both individual and spectral properties of waves reaching the toe of the structure through the shoaling and breaking processes.

The geometrical properties of the structure are also of major importance. Since the shape of a coastal or marine structure can vary significantly according to its type and function, only one important parameter can be generalized here, which is the freeboard height (or the crest level) F of the structure. For any case, overtopping can take place if and only if the runup height at the boundary of the structure exceeds the freeboard of the structure, making the freeboard height a very important parameter.

Since overtopping process is highly related to the runup height of incident waves on the structure, the geometry of the offshore side has a major role in the amount of overtopping, because it describes the solid boundary directing the water particles on wave interaction. In case of structures with planar offshore slopes, a second important parameter is known as the slope angle tanα, which, coupled with the incident wave properties, dictates the type of breaking and the amount of runup. In addition to the offshore geometry, the existence of a berm in front of the structure

and the type, shape and dimensions of the crest also have effects on overtopping rates.

By the term physical properties, we point out two items, the texture of the structure and the dynamic and/or kinematic status of the structure. By the term texture of the structure, porousity and surface roughness are mentioned. These parameters are usually assessed separately from the geometry of the structure, since they increase turbulent dissipation and hence reduce the energy of the waves running up the structure. On the other hand, if the structure is in motion, due to waves or being driven by any other force, the interaction becomes quite complex due to continuously varying freeboard and radiation waves based on the structures motion.

Having conducted a dimensional analysis, Weggel (1976) identifies the non-dimensional parameters controlling wave overtopping for sloped coastal structures as

$$f\left(\frac{Q^2}{gH^3};\frac{H}{gT^2};\frac{F}{H};\frac{R}{H};\frac{H}{h};\alpha;\frac{H^2}{\nu T}\right)=0 \qquad \textbf{(2.42)}$$

In Eq. 2.42, the first term represents a dimensionless discharge, explained in detail below. Following terms define the wave steepness, the third term is the relative freeboard height, relative runup height, relative water depth at the toe of the structure, structure slope angle and a Reynolds number, respectively.

Weggel further states that the Reynolds number in overtopping studies is a measure of scale effects because of the gravity-dominated nature of the flow, and the relative runup term may be omitted if a relationship between relative freeboard and wave runup can be written. Competent with this statement, in almost all studies related to the measurement of overtopping rates, two main parameters emerge as the dimensionless discharge and the dimensionless freeboard, with the rest of the parameters depending on the structure geometry and incident wave properties.

Reviewing the literature, there are two fundamental approaches for the derivation of a dimensionless discharge parameter. The first has been defined by Saville and Caldwell (1953) as the ratio of the overtopping water volume per one wave to the mass of water volume remaining above the MWL in a sinusoidal wave, which yields:

$$Q_V=\frac{q_{1m}T}{HL} \qquad \textbf{(2.43)}$$

Another definition for dimensionless discharge, and the most frequently used one comes from the adoption of the weir formula, written as:

$$Q_W = \frac{q_{1m}}{\sqrt{gH^3}} \tag{2.44}$$

The derivation of Eq. 2.44 is first given in Kikkawa et al.'s study (1968).

The dimensionless freeboard, on the other hand, has been defined as the ratio of the structures freeboard to the incident wave height in almost all studies.

### 2.3.3 Empirical models for the prediction of overtopping rates

Initial studies on wave overtopping are observed as the studies of Saville and Caldwell (1953), Grantham (1953), Sibul (1955) and Saville (1955). The study of Saville (1955) consists of physical model studies with regular waves on smooth and riprap-covered structures with different geometries. The output of these studies are given as dimensional diagrams showing the relationship between the overtopping rates and the freeboard of the structure for each particular incident wave properties, clearly indicating the major effect of freeboard as a governing parameter in wave overtopping.

An initial attempt to compare overtopping discharges with various parameters has been made by Paape (1960). The study consists of physical model tests on single-sloped seawall models, where the slope and the crest level of the structure have been changed to inspect their effect on overtopping. Paape is the first one to make a non-dimensional expression for the freeboard of the structure, which is called today the relative freeboard, and is given as the ratio of the freeboard height to the incident wave height (s. Table 2.4): Furthermore, he inspected the variation of overtopping rate with the wave steepness and slope angle and for the latter he found out that for slopes flatter than tanα = 1/3, the overtopping rate is proportional to the 3/2$^{nd}$ power of the tangent of the structure slope.

Tsuruta and Goda (1968) conducted irregular wave tests in a wave tank for vertical and rubble mound structures to inspect the effect of wave irregularity on overtopping. They point out that in case of irregular waves, wave overtopping volumes can be achieved by taking a linear sum of individual waves.

**Table 2.2 :** Equations for the estimation of overtopping rates.

| Developer | General Form | Expression for $q_{1m}$ | Expression for $F_R$ | Eq. No. |
|---|---|---|---|---|
| Saville and Caldwell (1953) | N/A | $\frac{q_{1m}T}{HL}$ | $\frac{F}{H}$ | **(2.45)** |
| Sibul (1955) | N/A | $\frac{q_{1m}T}{H^2}$ | $\frac{F}{H}$ | **(2.46)** |
| Paape (1960) | N/A | $\frac{q_{1m}T}{HL}$ | $\frac{F}{H(\tan \propto)^{3/2}}$ | **(2.47)** |
| Weggel (1976) | $Q = aexp(-btanhF_R)$ | $\frac{q_{1m}^2}{gH_0^3}$ | $\frac{F}{T\sqrt{gH}}$ | **(2.48)** |
| Owen (1980) | $Q = aexp(-bF_R)$ | $\frac{q_{1m}}{gH_sT_{m0}}$ | $\frac{F}{H_s}\sqrt{\frac{s_{m0}}{2\pi}}\frac{1}{\gamma}$ | **(2.49)** |
| Ahrens and Heimbaugh (1988) | $Q = aexp(-bF_R)$ | $\frac{q_{1m}}{\sqrt{gH_s^3}}$ | $\frac{F}{\left(H_s^2L_{p0}\right)^{1/3}}$ | **(2.50)** |
| Bradbury et al. (1988) | $Q = aF_R^{-b}$ | $\frac{q_{1m}}{gH_sT_{m0}}$ | $\left(\frac{F}{H_s}\right)^2\sqrt{\frac{s_{m0}}{2\pi}}$ | **(2.51)** |
| Aminti and Franco (1988) | $Q = aF_R^{-b}$ | $\frac{q_{1m}}{gH_sT_{m0}}$ | $\left(\frac{F}{H_s}\right)^2\sqrt{\frac{s_{m0}}{2\pi}}$ | **(2.52)** |
| Sawaragi et al. (1988) | $Q = aF_R^{-b}$ | $\frac{q_{1m}}{\sqrt{gH_s^3}}$ | $\frac{F}{H}$ | **(2.53)** |
| Pedersen and Burcharth (1992) | $Q = aF_R^{b}$ | $\frac{q_{1m}T_{m0}}{L_{m0}^2}$ | $\frac{H_s}{F}$ | **(2.54)** |
| de Waal and van der Meer (1992) | $Q = aexp(bF_R)$ | $\frac{q_{1m}}{\sqrt{gH_s^3}}$ | $\frac{S}{H_s}$ | **(2.55)** |
| Juhl and Sloth (1994) | $Q = aexp(-bF_R)$ | $\frac{q_{1m}}{\sqrt{gH_s^3}}\frac{1}{\gamma_\beta}$ | $\frac{2F + 0.35B_c}{H_s}$ | **(2.56)** |
| van der Meer and Janssen (1994) | $Q = aexp(-bF_R)$ | $\frac{q_{1m}}{\sqrt{gH_s^3}}\sqrt{\frac{s_{p0}}{\tan \propto}}$ | $\frac{F}{H_s}\frac{\sqrt{s_{p0}}}{\tan \propto}\frac{1}{\gamma}$ | **(2.57a)** |

**Table 2.2 (continued):** Equations for the estimation of overtopping rates.

| Developer | General Form | Expression for $q_{1m}$ | Expression for $F_R$ | Eq. No. |
|---|---|---|---|---|
| van der Meer and Janssen (1994) | $Q = aexp(-bF_R)$ | $\frac{q_{1m}}{\sqrt{gH_s^3}}$ | $\frac{F}{H_s}\frac{1}{\gamma}$ | **(2.57b)** |
| Franco et al. (1994) | $Q = aexp(-bF_R)$ | $\frac{q_{1m}}{\sqrt{gH_s^3}}$ | $\frac{F}{H_s}\frac{1}{\gamma}$ | **(2.58)** |
| Pedersen (1996) | $Q = F_R$ | $\frac{q_{1m}T_{m0}}{L_{m0}^2}$ | $c_1\frac{H_s^5 \tan \propto}{F^3 c_2 c_3}$ | **(2.59)** |
| Hedges and Reis (1997) | $Q = a(1 - F_R)^b$ | $\frac{q_{1m}}{\sqrt{gR_{umax}^3}}$ | $\frac{F}{R_{umax}}$ | **(2.60)** |
| Hebsgaard et al. (1998) | $Q = aexp(-bF_R)$ | $\frac{q_{1m}}{\ln(s_{p0})\sqrt{gH_s^3}}$ | $\frac{R_c^*}{H_s}\frac{1}{\gamma}$ | **(2.61)** |
| Schüttrumpf et al. (2001) | $Q = aexp(-bF_R)$ | $\frac{q_{1m}}{\sqrt{2gH_s^3}}$ | $\frac{F}{1.5\xi_{m0}H_s}$ | **(2.62)** |

Tsuruta and Goda (1968) also state that the wave steepness does not have a major effect on wave overtopping for the tested configurations unless swell-like waves are considered.

Nagai and Takada (1972) inspected wave runup and overtopping for the case of non-breaking waves. In their paper, they also relate wave runup to the type of wave breaking. By adopting second-order approximation to the standing wave theory, they recommended formulae for wave runup and overtopping. They also investigated the effects of slope angle and wave steepness on overtopping rates.

The first attempt to develop nondimensional terms to express wave overtopping has been conducted by Weggel (1976). By applying a dimensional analysis on the governing parameters, Weggel developed nondimensional terms and formulae to quantify wave overtopping. He further recommended a method for the prediction of overtopping rates, based on an exponential model. Ahrens (1977) developed a method to incorporate the case of irregular waves into Weggel's (1976) equation. Owen (1980), based on an extensive physical model dataset on seawalls of different geometries, recommended an exponential formula for the estimation of overtopping

rates, where he modified the relative freeboard parameter by introducing the wave steepness and a breaker depth factor.

Ahrens and Heimbaugh (1988) conducted physical model tests on 13 seawall and revetment models with different geometries, focused on wave overtopping. Their output shows that an exponential relationship exists between the overtopping rate and the relative freeboard defined by Eq. 2.50. Based on these parameters, three different models have been recommended, which have slightly varying components in the exponentiation brackets.

Based on the dimensionless parameters of Owen (1980), Bradbury et al. (1988) conducted physical model tests and recommended overtopping formulae (Eq. 2.51) for rubble mound breakwaters with a 1:2 sloped offshore side and different crest arrangements. Aminti and Franco (1988) tested rock, cube and tetrapod armoured mound breakwaters with different armour crest berm widths and offshore slopes varying between 1:1.33 and 1:2.0, they evaluated coefficients for the configurations tested by adopting the model of Owen (Eq. 2.49). Sawaragi et al. (1988) pointed out the significance of the wave setup in front of the structure on overtopping rates.

Goda (1985) summarized the Japanese experience on prediction of overtopping rates for vertical and composite structures in his work. He prepared diagrams to estimate overtopping rates, most of which use the weir approach for the definition of dimensionless discharge.

Another important study has been performed by de Waal and van der Meer (1992), where a total of 360 tests have been carried out in 2D and 3D wave tanks. The focus on this study was wave runup and effect of some parameters such as existence of a berm, oblique wave attack, structure roughness and effect of shallow water on runup height, for which, correction factors have been introduced to the runup equations. Furthermore, the runup equation has been based on the Iribarren number, defined by Battjes (1974) in order to distinguish different types of wave breaking; given by

$$\xi = \frac{\tan \alpha}{\sqrt{s_0}} \qquad \textbf{(2.63)}$$

By taking the relationship between runup height and wave overtopping into account, de Waal and van der Meer (1992) introduced a new term for the relative freeboard, which they called "shortage in crest height", defined as

$$S = \frac{F - R_{u\%2}}{H_s} \quad \textbf{(2.64)}$$

Here, $R_{u\%2}$ is defined as the value of wave runup which is exceeded by 2% of the number of incident waves. This type of formulation implicitly contains the correction factors of wave approach angle, existence of a berm, roughness effect and shallow water effect, since they are directly used for the calculation of the runup height.

Pedersen and Burcharth (1992) carried out physical model studies on rubble mound breakwaters with a 1:1.5 front slope, covered with a number of different crown walls. Keeping the main focus on the wave forces on crown walls, they also measured overtopping rates during the tests and recommended equations (Eq. 2.54).

Juhl and Sloth (1994), based on physical model studies conducted on a 1:2 sloped conventional rubble mound breakwater, researched the effect of oblique wave attack on wave overtopping over a conventional 1:2 sloped rubble mound breakwater by physical model tests. They point out that while no major reduction in overtopping rates are observed up to an angle of approach of 20°, a decrease starts this point on, and for higher approach angles up to 50° the reduction coefficient drops down until 0.1. Another study item in the tests is the effect of crest width, introduced as a linear component of the relative freeboard parameter into the overtopping model (Eq. 2.56).

Franco et al. (1994) conducted physical model tests on vertical and composite structures with different crown wall geometries, investigating both overtopping rates and individual overtopping volumes under irregular waves. They applied a 3-parameter Weibull distribution for the probabilistic distribution of overtopping volumes, and recommended an exponential relationship for the prediction of overtopping rates.

Van der Meer and Janssen (1994), based on the results of the study of de Waal and van der Meer and the addition of further tests and some existing datasets, recommended a two-part equation for the prediction of overtopping rates (Eq. 2.57). They point out that the breaker parameter becomes significant in case of breaking waves, but can be omitted for the case of nonbreaking waves. Furthermore, the

effects of a berm, angle of attack, slope roughness and limited water depth have been added to the equation as reduction parameters.

Hebsgaard et al. (1998) proposed a slightly modified overtopping formula (Eq. 2.61) in an exponential form, where the effect of wave steepness has been introduced by its logarithmical value. Compatible with their previous study (Juhl and Sloth, 1994), they recommended the use of a modified dimensionless freeboard parameter R*, which includes a revision based on the crest width, angle of attack and surface roughness.

In order to bring a solution to the particular problem where the coast is protected by any submerged or low crested structure far from the shoreline, Lorenzo et al. (2000) studied the effect of bi-model wave spectra on overtopping rates. They developed an equivalent breaker parameter based on the properties of the peak wave heights and periods and introduced this modified breaker parameter into the equation recommended by van der Meer and Janssen (1994).

The case of low and zero freeboard has been inspected in the study of Schüttrumpf (2001). For this particular case, it has been stated that the overtopping rate can be expressed as a function of the dimensionless freeboard expressed according to the weir equation and the Iribarren number. The diagrams achieved for this case indicate that for values of Iribarren number larger than 4, the dimensionless discharge remains constant. Another study inspecting overtopping rates for zero freeboard vertical structures has been carried out by Smid (2001), indicating that the weir-type dimensionless discharge leads to a constant mean overtopping rate value with significant scattering.

In order to provide engineers with guidelines for prediction of overtopping rates, some manuals have been written by coastal authorities. The Shore Protection Manual (1984), followed by the Coastal Engineering Manual (2003) comprise the US guidelines, while in Europe, TAW (2002) can be considered as a continuously upgrading manual. The importance of the topic, coupled with the green water effect due to global warming has lead to the commissioning of the CLASH EU Project (Url-3), where a major database of relevant overtopping measurements carried out both in laboratory and prototype scala have been collected and assessed by the corporation of an international research team with further works carried out for many

special cases. Based on CLASH Project, full scale measurements have been carried out on some shore protection structures (De Rouck et al., 2003; Franco et al., 2003; Geeraerts et al, 2003). Kortenhaus et al. (2003) investigated the efficiency of recurving walls against wave overtopping and recommended a correction factor to introduce the effect of recurved wall section. Pearson et al. (2004) recommended a refinement and a decision chart for the procedure to be applied to predict overtopping rates by taking the structure geometry and sea bottom profile into account.

A manual related to the prediction of wave overtopping and related quantities, EurOtop (2007), has been prepared as the outcome of this project. EurOtop, differing from the previous works summarizing the overtopping works as per the type of structure, initiated a general categorization of the structure type according to the slope structure, leading to three categories, smooth slopes, rough slopes and vertical or very steep slopes.

Today, there is still a number of papers for the improvement of equations on overtopping rate estimation. Van der Meer et al. (2014) point out that the overtopping rates can be estimated by a Weibull-type formula as recommended by Battjes (1974), leading to a better prediction for the range $0<F/H_{m0}<0.8$.

### 2.3.4 Propagation of overtopped water mass

Overtopping flow height and flow velocities have become a relatively recent field of study. There are two important works conducted on this topic; the study of Schüttrumpf (2001) and the study of van Gent (2002). Schüttrumpf (2001) investigated the overtopping-induced flow at the fore slope, crest and the back slope of a levee structure with emphasis kept on flow velocities and layer thicknesses. Both studies are still in use, however, they have been based on the achievement of maximum flow velocities during overtopping events.

### 2.3.5 Analytical and numerical modelling studies

One of the initial studies on analytical modelling of wave overtopping has been carried out by Shi-Igai and Kono (1970). Kobayashi and Wurjanto (1989), evaluating the run-up model developed by Kobayashi et al. (1987), developed a numerical model for the prediction of regular wave overtopping over a impermeable sloping structure by using the nonlinear shallow water equations in a finite difference

method. Their results, compared with the test data of Saville (1955) indicate that the predictions are satisfying, but more detailed laboratory measurements are needed to achieve more realistic results. The model, in a later study (Kobayashi and Raichle, 1994), has been evaluated further to accomodate irregular waves and multiple friction coefficients for different pavements.

Umeyama (1993) used the partial standing wave theory to develop an analytical work for the prediction of wave overtopping on vertical structures. By using a perturbation method to evolve the kinematics of a third-order standing wave, they defined the surface displacements for the case of wave overtopping. By using a time-dependent form of the modified weir equation, and introducing the conservation of energy, they developed a model to predict the mean overtopping rates. Compared with physical model test results, model results are reported to be in good agreement for low crest levels with accuracy decreasing with increasing crest level. The work has been expanded further by introducing the nonlinear two-dimensional standing wave theory equations (Umeyama, 1994).

Dodd (1998) developed a numerical model based on the application of nonlinear shallow water equations into a finite volume model. Verified with physical model tests carried out by other researchers, he points out that the benefit of such a model is that no shore-tracking algorithms have to be developed in contrast to finite difference models.

Tuan and Oumeraci (2010) developed a numerical model based on nonlinear shallow water equations to predict the behavior of wave overtopping on dikes. They point out that a conventional NLSW model underpredicts mean overtopping rates for violent breaking waves, and introduced a roller term for improvement.

### 2.3.6 Overtopping for wave energy converters

Application of wave overtopping on wave energy converters is a fairly recent field of research. In general, it can be stated that an important part of the existing studies are focused on fixed structures, which are based on the utilisation of coastal shore protection structures. Studies dealing with wave overtopping on floating structures are much less in number, most of which have been conducted during the development of the Wave Dragon wave energy converter.

A major part on the overtopping related research for the Wave Dragon WEC has been conducted by Kofoed (2002). During his thesis, Kofoed researched the effect of different slope geometries which can be summarized as linear, convex and concave slopes and some of their combinations. Special attention has been kept on the effect of freeboard of the structure on overtopping rates. While Kofoed used the equation developed by van der Meer and Janssen (1994) for his wave overtopping model, he introduced a correction parameter $\lambda_d$ for the limited freeboard effect, which has been calculated as a ratio of the time averaged energy flux along the draft of the structure to its total value between the sea floor and the mean water level:

$$\lambda_d = \frac{\int_{-d}^{0} p^{+} u dz}{\int_{-h}^{0} p^{+} u dz} \tag{2.65}$$

By using linear wave theory, Eq. 2.65 can be written as

$$\lambda_d = 1 - \frac{\sinh\left(2kd\left(1-\frac{d}{h}\right)\right) + 2\mathrm{kd}\left(1-\frac{\mathrm{d}}{\mathrm{h}}\right)}{\sinh(2kd) + 2kd} \tag{2.66}$$

Two more parameters have been introduced further in Kofoed's study (2002) to the overtopping equation. The first parameter $\lambda_\alpha$ is included to add the effect of the slope angle of the ramp, given as

$$\lambda_\alpha = \cos^3(\alpha - 30°) \tag{2.67}$$

The second parameter, $\lambda_s$, adds the effect of a limited freeboard. It has been defined by Eq. 2.68 as the result of a best-fit curve:

$$\lambda_s = \begin{cases} 0.4 \sin\left(\frac{2\pi}{3} F_R\right), & F_R < 0.75 \\ 1, & F_R \geq 0.75 \end{cases} \tag{2.68}$$

By introducing the terms $\lambda_d$, $\lambda_s$ and $\lambda_\alpha$ defined above into the equation of van der Meer and Janssen (1994), following equation has been recommended for the prediction of overtopping rates over an inclined slope with limited draft:

$$\frac{q_{1m}}{\lambda_d \lambda_s \lambda_\alpha \sqrt{g H_s^3}} = 0.2 exp\left(-2.6 \frac{R_C}{H_s} \frac{1}{\gamma_b \gamma_r \gamma_h \gamma_\beta}\right) \quad \textbf{(2.69)}$$

In Eq. 2.69, $\gamma_b$ is a correction parameter for the existence of a berm, $\gamma_r$ is the surface roughness correction parameter, $\gamma_h$ is the shallow water correction parameter and $\gamma_\beta$ is the correction parameter for the angle of wave attack. For a structure located in deepwater with a smooth runup surface subject to head-on waves, all these coefficients take the value of 1.

# 3. SYNTHESIS AND MOTIVATION

In this section, we shall focus on the similarities and common features of floating breakwaters and floating wave energy conversion devices, and plot out the outline of the study, which shall be followed throughout the rest of the work.

## 3.1 Combining Both Structures

Design and implementation of multipurpose offshore structures comprise a recent field of study in coastal and marine engineering. Besides some national and international projects focused on design and optimization of such platforms such as the MERMAID project (Url-4) and the TROPOS project (Url-5), there are several researchers supporting multifunctionality.

Martinelli et al. (2009) point out that combining breakwaters and wave energy converters can be assessed as an attempt to improve the total efficiency of the designed system.

Another study on utilizing floating WEC systems as floating breakwaters has been carried out by Ruol et al. (2010), where the DEXA WEC system has been inspected through physical model studies as a wave attenuation system. According to the results, showing a total transmission coefficients varying between 0.6-0.9, Ruol et al. argue that arranged on grid installations, DEXA WECs can be used as floating breakwater elements. From the authors point of view, however, the given transmission coefficients are fairly high, showing the need in improving the structure as a breakwater. Here it should be mentioned that DEXA is a highly mobile system under wave attack, i.e. it has its own drawback by generating radiation waves.

Let us assess the combination of a wave energy converter and a floating breakwater at the same platform. By using the literature review given in Chapter 2, we can point out some principles for the hybrid design of a WEC and FBW system. These principles are listed below.

### 3.1.1 Alignment and functionality

In general, wave transmission is not a criteria to be considered in the design of wave energy converters. An exception is the case where the WEC systems are installed as farms allocated over pre-planned grids, reduction of wave transmission tends to reduce the efficiency of the WEC units in the lee of the offshore row. From the viewpoint of floating breakwater design, the opposite can be said, i.e. wave transmission is the subject to be minimized. Thus, we can conclude that an efficient and successful design of a hybrid system should be based on a terminator type WEC coupled with any floating breakwater unit.

### 3.1.2 Structure motions

For many types of WECs, free motion of the WEC unit under incident waves does not represent a problem; even for cases where electricity is generated by wave induced motions of the body, it is a desired feature. This feature is slightly different in the case of a floating breakwater. Especially in case of reflective structures, structural motions lead to generation of radiation waves, which increase wave transmission and reflection. Furthermore, extreme motions of the system lead to overloading on moorings and module connectors. Thus, the combination of a reflective floating breakwater and a WEC should be designed by keeping focused on smallest possible structural motions under wave attack.

In case of dissipative floating breakwater systems, the motions of the structure are fairly larger and they do not lead to significant amounts of radiated waves. Thus, the motion on flexible floating breakwaters can be used as a driving force for the PTO unit of any WEC to be combined with.

### 3.1.3 Site selection

One of the most important limitations is the limited range of functionality as stated in Chapter 2.2. It is well known that floating breakwaters are efficient only in mild to medium wave climates. The hybrid system accordingly should be designed to be an effective WEC in case of storm waves which do not exceed the functional limits of the floating breakwater unit. These limits are given as 1.0-1.5m in wave height and 4-6 s as wave period (Gaythwaite, 2004), but examples exceeding these limitations

are in use today, and it is believed that improvements in science and technology and advances in construction materials and methods shall increase these limits further in.

Based on the limitation of the wave climate mentioned above, relatively sheltered regions should be considered during the process of site selection. A feature of the selected site should be its wave climate, which at its best should be as steady as possible. Taking these aspects into account, it can be stated that the most suitable locations for the installation of such structures can be defined as fetch-limited sites, where wave growth under a given wind cannot exceed a certain level.

### 3.2 Possible Combinations

Possible combinations for the buildup of a wave energy converter-floating breakwater hybrid have been inspected in Akgul and Kabdasli's study (Akgul and Kabdasli, 2013). A summary of the studies output is given below.

#### 3.2.1 OWC type WEC and reflective floating breakwater

The mentioned system consists of a floating box with OWC chambers attached to the incident wave direction. A preliminary sketch for the mentioned system is given in Figure 3.1. The geometry and mass distribution of the system may be adjusted to optimize the structures hydraulic stability, where additional pontoons may be installed between the OWC chambers to counterbalance the shifted centre of gravity.

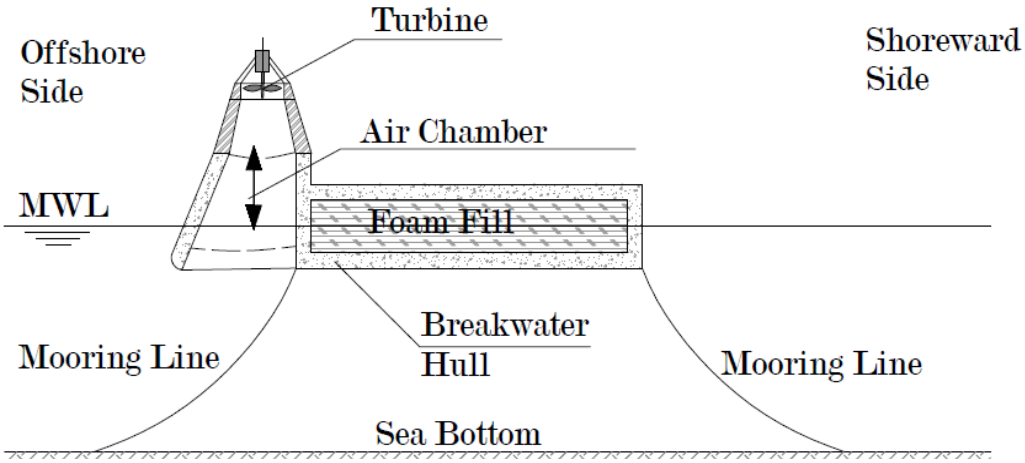


**Figure 3.1 :** Representative sketch for an OWC type WEC & FBW hybrid.

The design of such a system may be extended further by adding a crown wall to the region between the OWC chambers in order to reduce splash and overtopping over the deck of the structure, thus, enabling pedestrian access to the structure as a walkway.

### 3.2.2 Overtopping type WEC and reflective floating breakwater

In the case of an overtopping type WEC and a reflective FBW, one may change the geometry of the offshore wall of the structure in order to create a ramp for the waves approaching the structure. Energy conversion can take place in a reservoir located at the middle of the floats by using low head turbines. A sample drawing of the mentioned system is shown in Figure 3.2.

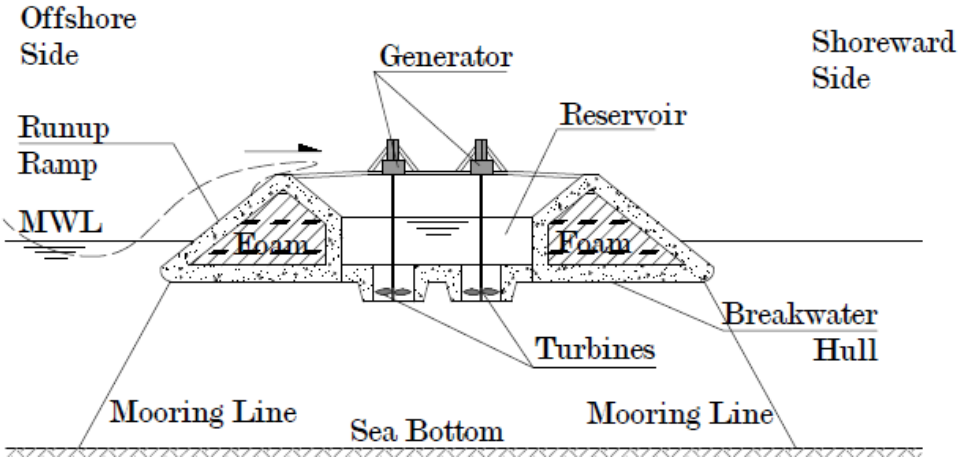


**Figure 3.2 :** Sample sketch for an overtopping type WEC & FBW hybrid.

In contrast to the combination with an OWC based WEC, an overtopping-based system is expected to have some drawbacks such as the excess weight of the structure caused by the water level in the reservoir. Furthermore, the system should have a relatively low freeboard to benefit from efficient amounts of overtopping. Under these circumstances, pedestrian access to such a structure might be risky, or it should be enabled by introducing a promenade deck located at a higher elevation.

### 3.2.3 Attenuator type WEC and dissipative floating breakwater

It might also be possible to combine a dissipative floating breakwater with a WEC system. While an option may be the usage of point absorbers bound to floats of relatively small size, a more simplified system may be achieved by combining a

flexible structure extending along the water surface with a PTO unit, which shall use the relative motion between the modules to generate electricity. Such a system may be thought as an expansion of the PELAMIS WEC to a two-dimensional field-type energy harvesting area. A representative sketch of the proposed system is shown in Figure 3.3.

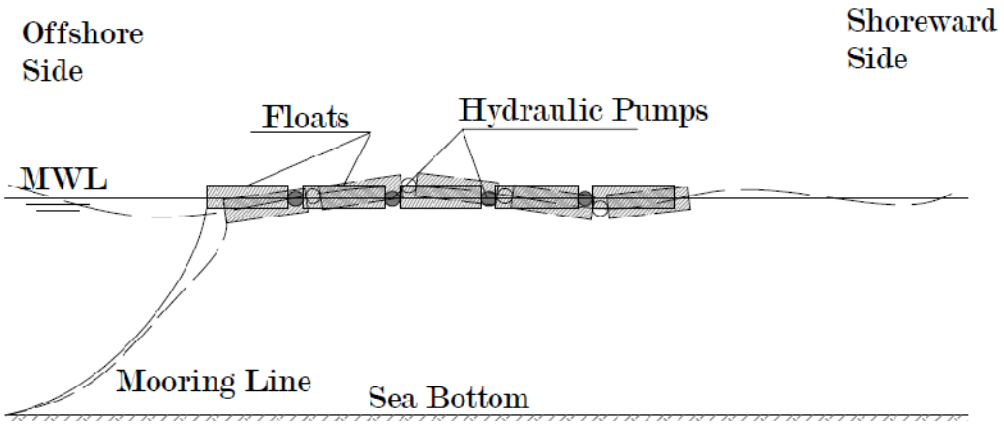


**Figure 3.3 :** Sample sketch for a surface mat type WEC & FBW hybrid.

The feasibility of the system sketched in Figure 3.3, however, is questionable due to the low performance levels of mat-type FBWs and their large occupation area. Drawbacks of dissipative FBW systems are discussed in detail in Chapter 2.2. Furthermore, independent of the design, the arrangement of the hydraulic pumps on such a system can be found complex, opposing the concept of simplicity.

## 3.3 Conceptual Design

### 3.3.1 On the system studied

While there are some alternatives applicable for the hybrid system design as stated in Chapter 3.2, we shall particularly focus on a system utilizing wave overtopping for energy extraction during this thesis.

Since a major object in this study -as mentioned in Chapter 1- was the design of a simple system, OWC-type WECs are kept out of scope due to the complex air and water interaction in the turbine chambers. Combination of an attenuator type WEC and a dissipative FBW, on the other hand, seems not feasible mainly due to the reasons mentioned in Chapter 2.2 and is not easily applicable in laboratory tests, both due to the enormous size of the structure.

As a consequence, focus is kept on the design of an overtopping type WEC and reflective FBW hybrid, which itself contains many opposing and questionable factors as stated below.

### 3.3.2 Design factors

One of the most important problems is the amount of overtopped water volume and its sufficiency to drive low head turbines. As mentioned in Chapter 2.4, the most critical factor dictating overtopping rates is the freeboard of the structure. Combined with the geometry of the offshore wall and incident wave properties, overtopping has been deeply studied in the advance of this work.

A second factor is the existence of a reservoir, which shall introduce additional weight to the structure caused by the mass of water in the reservoir. Thus, the structure should own a fair amount of excess buoyancy to accomodate the mass of water to be stored in the reservoir, whereas it also has to retain its stability under this top-heavy loading.

The third factor is the retention of structure motions at an acceptable level such that it should not reduce the overtopping capture efficiency and also should not introduce radiation waves to the shoreward side.

### 3.3.3 Pre-dimensioning

Considering the factors stated above, the fundamental system has been evolved. Based on the attempt of utilizing commercial pipeline industry for the construction, the breakwater has been decided to be composed of circular cylinder elements. Based on the literature review made in Chapter 2.7, concerning a floating pipe breakwater, where the pipes are horizontally installed, an optimum depth of submergence has been recommended as $d_s/D = 0.70$. Furthermore, substituting a single pipe with a bundle of multiple pipes of an equivalent cumulative diameter does have negligible effect on wave transmission. A single pipe of the submergence mentioned above does lead to inclusion of secondary waves in its wake, caused by the reformation of the overtopping water volume as waves, so installation of a second pipe has been found useful. Thus, the conceptual model has been selected to be composed of least three cylinders. Since there are varying comments on the effect of pipe spacing to

wave transmission, pipe spacing has been chosen as a parameter to be inspected during the design process.

In order to provide the system with some excess buoyancy to overcome the weight of the water in the reservoir, a taut-moored system has been chosen. The draft of the system is to be adjusted by taking the overtopping rates and wave transmission features of the structure into account, for which, an initial relative value between 0.70-0.80 is estimated to keep the PTO and walkways at a safe level.

The restriction of motion for the structure is another problem. In order to bring a solution, a TLP-type taut mooring is planned, which seemingly provides the best solution. However, the design and arrangement of mooring lines is primarily related to the properties of the wave climate. So it has been decided to keep it as simple as possible and out of the scope of this study. Vertical mooring lines are used during the tests, which, for TLP-type mooring, should give the maximum displacements.

A third question rises due to the mechanics of the system. In case of a reservoir application, most of the kinetic energy of the incident waves is dissipated, which is a direct measure in reduction of efficiency. It is thought that a PTO unit, able to use the overtopped water bore in motion without using a stilling basin (i.e. reservoir), can simplify the system significantly. The applicability of such a system has also been considered during the design, which limits the minimum value of the freeboard to a level, where transmitted waves do not flow back into the turbine outlet.

### 3.4 Flowchart of the Work

In order to design the structure, the start is given by inspecting the most unknown part, which is based on the estimation of overtopping rates over a circular cylinder. To assess the topic, physical model studies are carried out in a wave flume for 2D conditions. To simplify the problem, a fixed cylinder and regular waves have been used.

In the next part, a taut-moored floating breakwater consisting of three horizontal pipes has been researched for its wave attenuation capacity. Particular interest has been paid on the spacing of the pipes.

The final part consists of uniting both systems, where first the optimal functional range is estimated. In the next part, the floatation of the FBW unit is inspected to provide safety under irregular wave environments.

# 4. EXPERIMENTAL STUDY

## 4.1 Introduction

This section summarizes the physical model studies performed during this thesis. In general, the tests have been carried out under three categories, which can be counted as the quantification of wave overtopping over a near-surface fixed horizontal circular cylinder, the performance of a trimaran floating pipe breakwater and the performance of the wave energy converter-floating breakwater hybrid system. Details and contents corresponding to each category are given in detail in the forthcoming subchapters.

## 4.2 Wave Overtopping Over a Near-Surface Fixed Horizontal Circular Cylinder

As mentioned in Chapter 3, the first part of the study is based on the quantification of wave overtopping rates over a circular cylinder. This introductive study is important for the assessment of the systems feasibility, and it shall give an answer to the question whether a circular cylinder can be used directly as an overtopping ramp or not. In order to answer these questions, a fixed circular cylinder has been installed into a wave flume and overtopping rates are measured with the main variables chosen as the submergence ratio of the cylinder and incident wave parameters.

### 4.2.1 Model setup

#### 4.2.1.1 Wave flume

In order to carry out the tests, a wave flume in the Hydraulics Laboratory of Civil Engineering Faculty, Istanbul Technical University has been utilised. The wave flume is 24.00 m long, 0.98 m wide and 1.00 m deep (Figure 4.1). Equipped with a paddle type wave generator driven by an electro-hydraulic servo motor controlled via PC, both regular and irregular wave trains can be generated in the wave flume.

**Figure 4.1 :** Top view of the wave flume, hydraulic ram of the wave paddle and the hydroelectric power unit used during the tests.

A 1:7 sloped rubble mound dissipator has been constructed at the end of the flume to minimize wave reflection from the shoreward end. A brick dissipator is present at the back side of the paddle to reduce wave agitation on this side (Figure 4.2).

#### 4.2.1.2 Overtopping model

The model used for the overtopping measurements consists of three elements, a circular cylinder, a rectangular duct and a collector tank, respectively. The horizontal cylinder, forming the main overtopping surface is constructed by using a PVC pipe segment. In order to cover a wider wave range, two pipes with diameters of 125 mm and 160 mm have been prepared.

A jig has been constructed from thin steel members to mount the model and the overtopping measurement equipment. The jig has been mounted to the top rails of the wave flume, fastened by bolts and clamps to avoid displacement. It consists of two parts, an outer frame and an inner frame, respectively. The outer frame is affixed to the top of the wave flume, whereas the inner frame, carrying the model and the overtopping tank, is allowed to move vertically in the outer frame. Thus, the depth of the cylinder can be adjusted without changing the water level. The connection between the outer and inner frames has been supplied by eight M16 bolts.

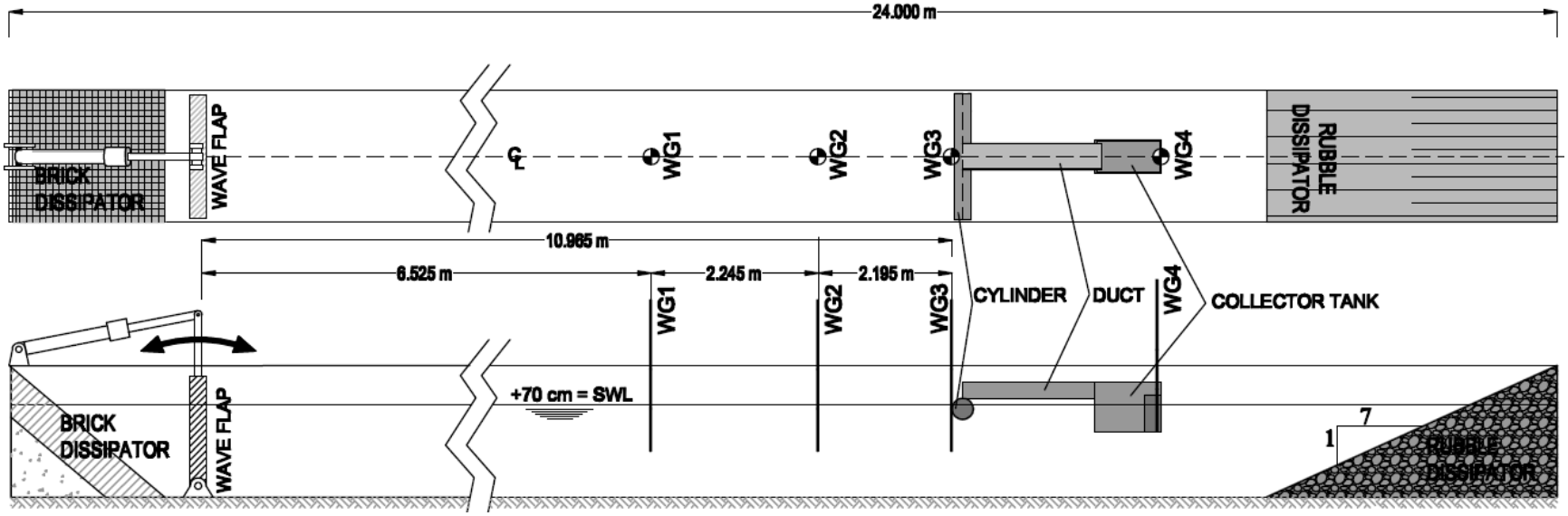


**Figure 4.2 :** Plan and profile view of the wave flume.

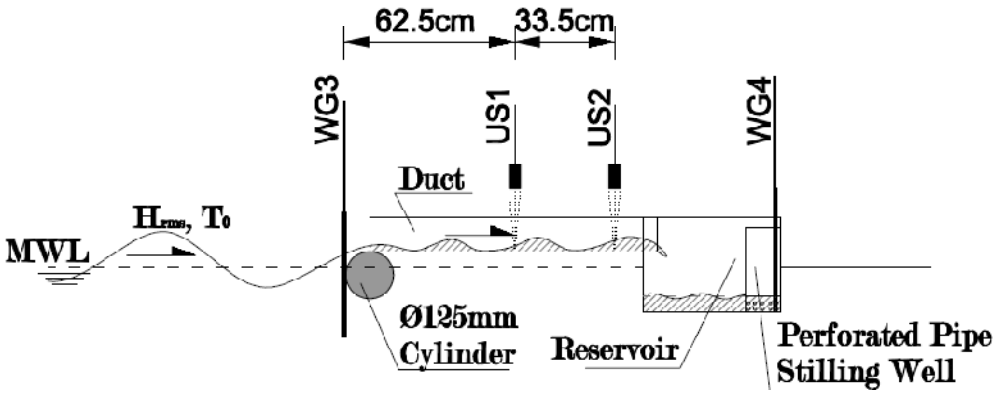


**Figure 4.3 :** Profile view of the overtopping model and instrumentation.

The test cylinder has been mounted at the offshore side of the inner frame, fastened by some timber and steel submembers running along the interior of the cylinder to provide additional structural strength.

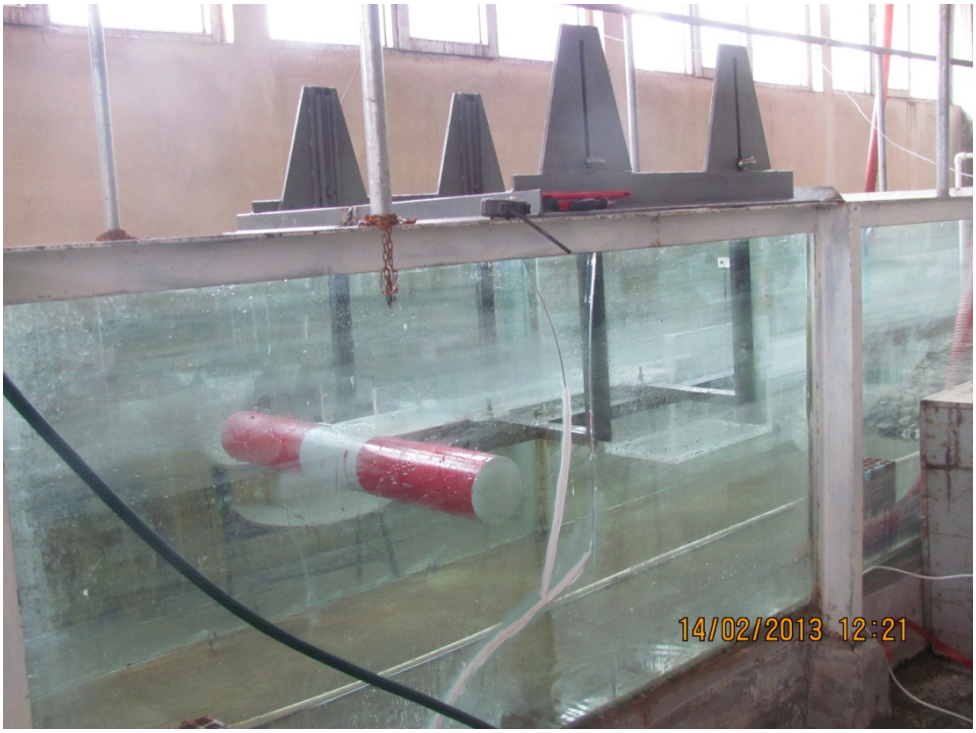


**Figure 4.4 :** Model shown in the channel fixed at the mounting frames.

A 20 cm wide, 100 cm long and 13 cm high plexiglass duct with a rectangular cross section has been mounted to the steel frame at the shoreward side of the test cylinder, located symmetrical along the centreline of the wave flume. The duct has outward-tapered fore edges at the offshore side to minimize scattering on wave interaction, and it is connected to the test cylinder by a watertight silicone seal. The duct is

followed by a collecting reservoir made of 1cm thick plexiglass with a base plate of 23 cm x 47 cm internal dimensions and a height of 22.5 cm, allowing a collection volume of 24.3 liters. At the back side of the reservoir, a perforated PVC pipe with 75 mm diameter has been vertically installed to act as a stilling well for the elevation gauge (Figure 4.3- Figure 4.4). A remote operating removable micro pump has been prepared to make the reservoir empty at the start of each test.

### 4.2.2 Instrumentation

In order to measure water surface elevations, three resistance type wave gauges have been installed to the offshore side of the test structure. The maximum and minimum voltage measurements on the wave gauges are +10 and -10 VDC, adjusted over an eight-channel wave monitor manufactured by HR Wallingford. Data has been acquired over an A/D converter card manufactured by Native Instruments.

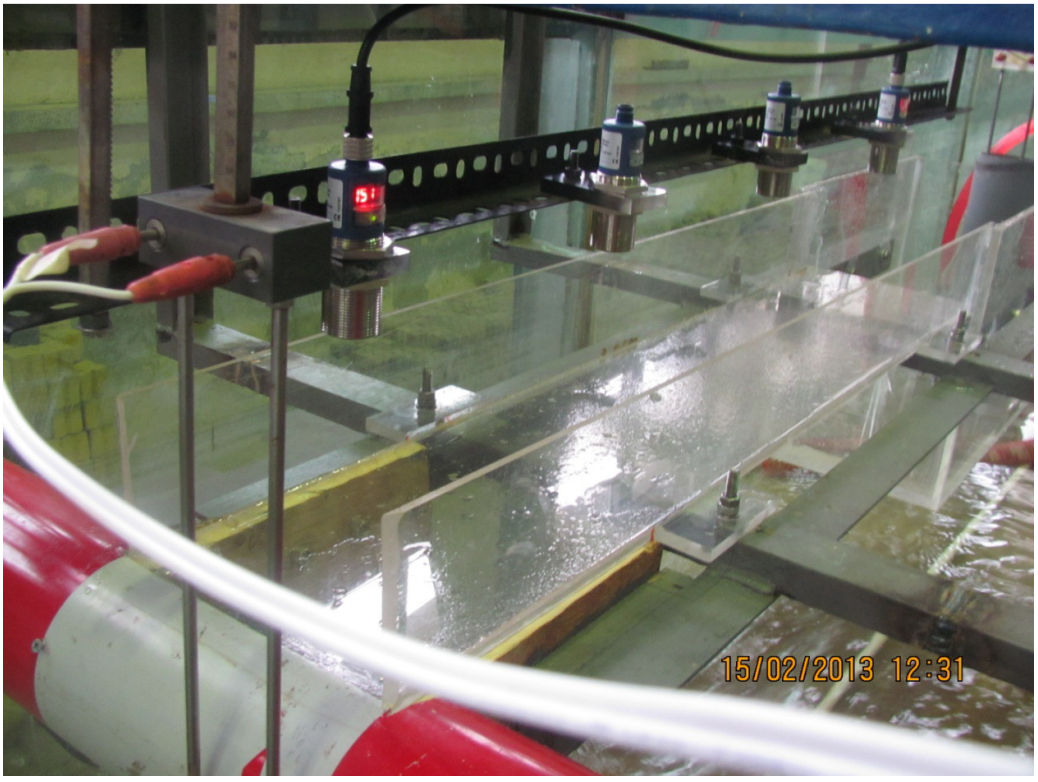


**Figure 4.5 :** A close-up view of the ultrasonic sensor installation.

In order to inspect the overtopping volume, two acoustic pre-calibrated elevation sensors, US1 and US2 have been mounted over the duct with spacings of 56cm and 89.5cm from the axis of the cylinder. A close-up view of the system is shown in

Figure 4.5. Both devices have been connected to a TestLab 2010 data logger, connected to a second PC.

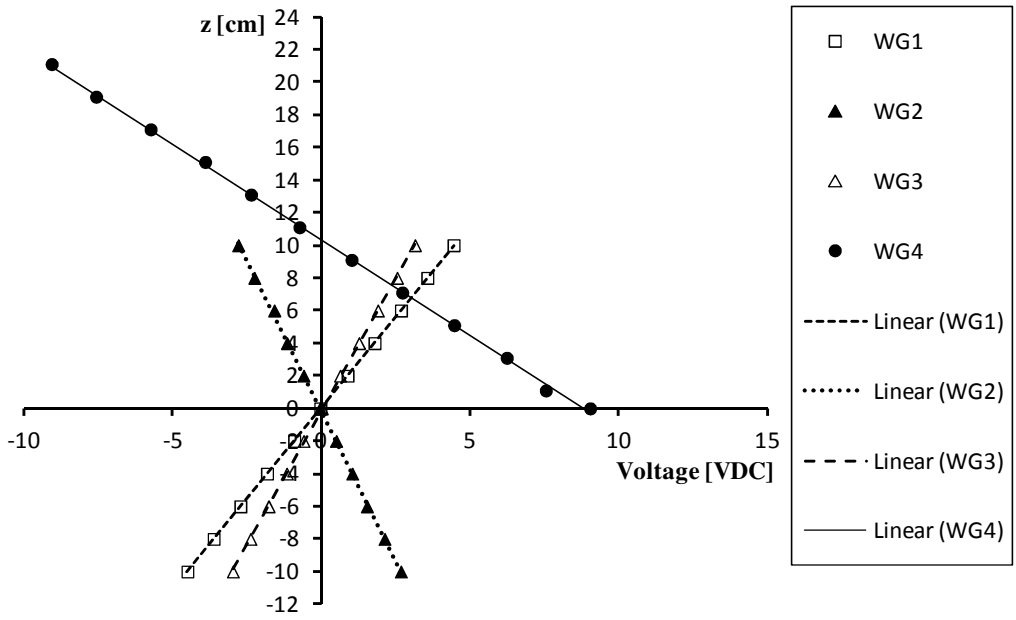


**Figure 4.6 :** Calibration curves for the wave gauges.

A fourth wave gauge has been installed into the collector tank to measure the elevation of the collected overtopping water volume. This gauge has been calibrated in such a way that it displays a -9 VDC voltage output in case of blank reservoir and +9 VDC for the case of full reservoir. The calibration equations of the wave gauges yield a linear relationship between the measured VDC value and the water surface elevation, written as

$$y = mx + c \qquad \textbf{(4.1)}$$

The curves achieved for the first configuration are shown in Figure 4.6 as an example. The values m and c of the calibration curves, together with their correlation coefficients are given in Table 4.1.

**Table 4.1 :** Calibration equations and $R^2$ values for the wave gauges.

| Probe No. | m | c | $R^2$ |
|---|---|---|---|
| WG1 | 2.2272 | 0.0699 | 1.0000 |
| WG2 | -3.6825 | -0.2169 | 0.9996 |
| WG3 | 3.2607 | -0.1556 | 0.9998 |
| WG4 | -1.1751 | 10.326 | 0.9998 |

### 4.2.3 Test matrix and test procedure

Tests have been carried out for 7 different configurations with particular emphasis based on the freeboard height of the cylinder. The first six configurations are made with the 125 mm diameter cylinder with freeboard heights varying between 2.5 mm and 62.5 mm. The cylinder with 160 mm diameter has been used in Configuration 7 to assess the effect of cylinder size and draft. The tested configurations with the variations at the freeboard and draft of the cylinder and their relative and absolute values are summarized in Table 4.2.

**Table 4.2 :** Configurations used in the overtopping tests.

| Configuration No. | D [mm] | F [mm] | $d_s$ [mm] | F/D [-] | $d_s$/D [-] |
|---|---|---|---|---|---|
| 1 | 125 | 2.5 | 122.5 | 0.02 | 0.98 |
| 2 | 125 | 15.0 | 110.0 | 0.12 | 0.88 |
| 3 | 125 | 25.0 | 100.0 | 0.20 | 0.80 |
| 4 | 125 | 37.5 | 87.5 | 0.30 | 0.70 |
| 5 | 125 | 50.0 | 75.0 | 0.40 | 0.60 |
| 6 | 125 | 62.5 | 62.5 | 0.50 | 0.50 |
| 7 | 160 | 3.0 | 157.0 | 0.02 | 0.98 |

Since the wave flume does not contain an active wave absorber, it has not been found logical to use irregular waves due to the very short test durations which should limit the total number of waves between 20-30. Consequently, regular waves have been selected for the tests. Another important reason for the selection of regular waves is to eliminate the statistical manipulations to be conducted on the results of irregular wave series. It is also known that use of regular waves is helpful to understand the physical process taking place during the tests.

A total of 30 different regular wave series are selected and tested under each configuration. Before the installation of the model, the waves have been tested in the blank channel to retriveve information on their characteristics. Characteristic values of the wave series summarized from these pilot tests are presented in Appendix A. The range of waves can be given by Eq. 4.2:

$$5.69cm \leq H_{rms} \leq 14.88cm$$
$$0.86s \leq T_m \leq 1.50s \qquad \textbf{(4.2)}$$

The calibration of the wave gauges has been re-checked between each configuration to ensure the reliability of the data. Measurement of water surface elevations has

been initiated before the start of each wave series and terminated after the end of the series has been met. A frequency of 25 Hz has been used for the wave gauge data, whereas the ultrasonic sensors are used at a sampling rate of 250 Hz.

### 4.2.4 Data analysis

#### 4.2.4.1 Wave characteristics

**Evaluation of water surface elevation time series**

In the evaluation of the wave properties, the first action to be taken is to convert the measured volt values to the actual water surface elevation values by using the calibration equations obtained for each wave probe. A typical water surface elevation-time series diagram is given in Figure 4.9. In the same figure, the typical sections of the time series are also shown. As usual, the first couple of waves do not reach the expected wave height due to spreading to the lee side, and the expected wave heights start to take place in the following. Thus, these couple of waves best should be excluded during the analysis process.

A typical view of the regular waves generated in the wave flume during the tests is given in Figure 4.7. Figure 4.8 shows the data acquisition station with the personal computers and A/D cards.


**Figure 4.7 :** A view of the wave flume during regular wave tests.


**Figure 4.8 :** Data acquisition station.

**Estimation of optimum sampling intervals for data evaluation**

Since the wave flume does not contain an active wave absorber at the wave paddle, the maximum duration of any test cannot exceed a total permissible test duration $t_{max}$ for any particular wave series. In order to give a better description for the total permissible test duration, let us check Figure 4.9, where wave generation in a flume without an active absorber on the wave paddle is scetched over a real water surface elevation-time series.

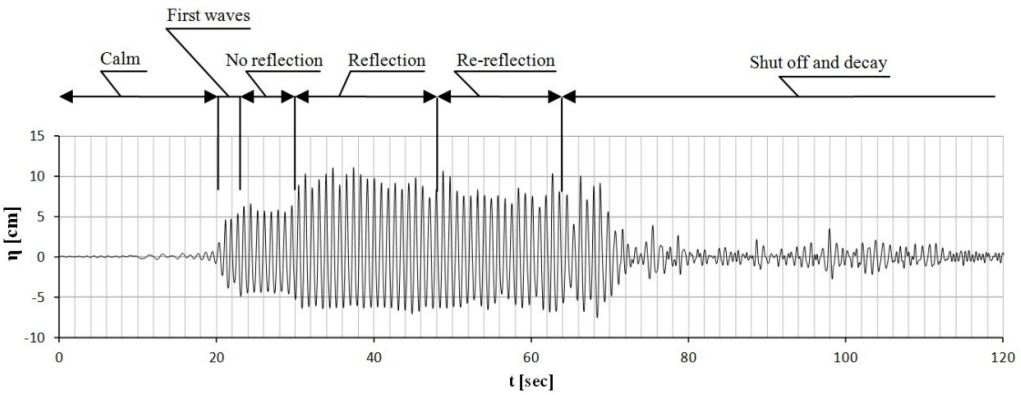


**Figure 4.9 :** A sample water surface elevation-time series showing wave evolution (Config. C1, Test No. 28, WG1).

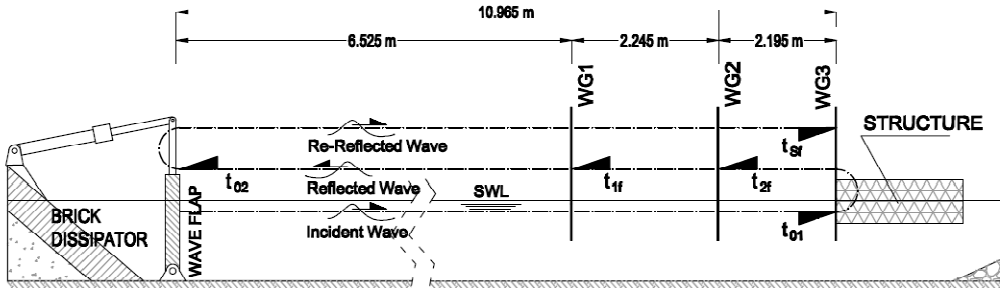


**Figure 4.10 :** A schematic display of wave travel durations.

Waves generated at the wave paddle need a travel time to reach the structure model. Upon interacting with the structure, wave reflection takes place, and the reflected waves travel back to the wave paddle. Upon arriving the wave paddle, re-reflection occurs, which disturbs the properties of incident wave series. Thus, the sampling of test data has to be finished before the effect of re-reflection is introduced.

To simplify the problem, let us use the notation given in Figure 4.10, where $x_{ij}$ denotes any distance between two special points i and j. The values of i and j are given as 0 for the wave paddle, 1 for WG1, 2 for WG2, 3 for WG3 and S for the structure, respectively. Remaining on the safe side, let us assume perfect reflection on both the wave paddle and the structure. In a similar way, let us define the travel durations $t_{ij}$ between two special points with the same definition of subindexes as given for the distances.

Now, by using Figure 4.10 and the notation mentioned above, let us check the sampling interval for any structural measurement. Such a sampling should initiate at the arrival of the first wave, which has to travel the distance $x_{0S}$ to arrive to the structure, and should finish at the arrival of re-reflection, which is equal to three times the distance $x_{0S}$. Thus, by using the terms $t_{iS}$ as the initiation time and $t_{fS}$ as the finishing time of the record, the maximum sampling duration $t_S$ for the structure can be achieved as:

$$\begin{aligned} t_S &= t_{fS} - t_{iS} \\ &= t(3x_{0S}) - t(x_{0S}) \\ &= t(2x_{0S}) \end{aligned} \qquad \textbf{(4.3)}$$

Now let us evaluate the sampling duration for the n-th wave gauge. Here, the sampling interval should start at the arrival of the first wave to the gauge n, which has to travel a distance of $x_{0n}$. The finish of the sampling duration should be at the

time of the arrival of the first wave reflected from the structure, which has to travel the distance $x_{nS}$ between the wave gauge and structure twice to initiate reflection at the probes location. Consequently, by using the terms $t_n$ for the sampling duration, $t_{in}$ as the start time and $t_{fn}$ as the end time of the sampling at the n-th wave gauge,

$$\begin{aligned} t_n &= t_{fn} - t_{in} \\ &= t(x_{0n} + 2x_{nS}) - t(x_{0n}) \\ &= t(2x_{nS}) \end{aligned} \tag{4.4}$$

Since the $x_{ij}$ distances between the measurement points are known, the travel times have to be calculated for each particular wave series. This has been achieved by using the following procedure:

i. Wave periods belonging to each wave series are known from the pilot tests. A further check of the test waves by applying zero-downcrossing analysis only to the first six waves has indicated that the period values agree very well with the pilot tests. Thus, wave travel velocities can be calculated by using the wave period data and water depth.

ii. As known, the travel speed of a wave can be given by its group velocity $c_g$, defined as

$$c_g = nc = n\frac{L_h}{T} \tag{4.5}$$

Here, n is given by Eq. 2.41, $L_h$ is the wavelength at the depth h and T is the wave period. The values of $L_h$ have been calculated by assuming linear wave theory valid and by using the linear dispersion relationship, leading to the well known wavelength formula

$$L_h = L_0 \tanh\frac{2\pi h}{L_h} \tag{4.6}$$

$L_0$ is the deepwater wavelength defined as

$$L_0 = \frac{gT^2}{2\pi} \tag{4.7}$$

By using Eq. 4.5 - 4.7 and by solving Eq. 4.6 with an iterative code, wave celerities belonging to each test have been calculated.

iii. Travel times belonging to each particular value of $x_{ij}$ have been calculated by

$$t_{ij} = \frac{x_{ij}}{c_g} \quad \textbf{(4.8)}$$

iv. Sampling durations and their initiation and finish times have been calculated by using Eq. 4.3 for the structure and Eq. 4.4 for the wave probes WG1 and WG2, respectively. Since wave reflection starts at the location of WG3, the sampling duration for this wave gauge becomes zero if only incident waves are to be calculated. Thus, records at WG3 are omitted for the calculation of wave characteristics. Travel times and sampling durations for WG1, WG2 and the structure are given in Table A.2.

**Calculation of incident wave properties by applying zero-downcrossing method**

The properties of the test waves have been calculated by applying zero-downcrossing analysis to the time series. For this purpose, a fraction of the time series has been analyzed, taken between the time intervals given in Table A.2 in order to hinder the effects of secondary reflections. The mean water surface elevations at each probe location have been calculated next prior to the zero-crossing analysis.

In zero-downcrossing analysis, a wave is defined as the sum of a crest and trough remaining between two consecutive points, where the water surface elevation curve crosses the zero elevation axis downward, i.e. from positive to negative.

In order to have a larger sampling time, test data acquired from WG1 has been used for the calculation of wave characteristics. The calculated characteristics for each test are summarized in Table A.3 and A.4.

#### 4.2.4.2 Overtopping rates

The water surface elevation data measured at the wave probe WG4 located in the reservoir has been used to calculate the overtopping rates. As expected due to the nature of regular waves, the water surface elevation - time series diagram yields a linear relationship with minor fluctuations caused by wave generation in the collector tank due to falling mass of water arriving from the duct at each wave cycle.

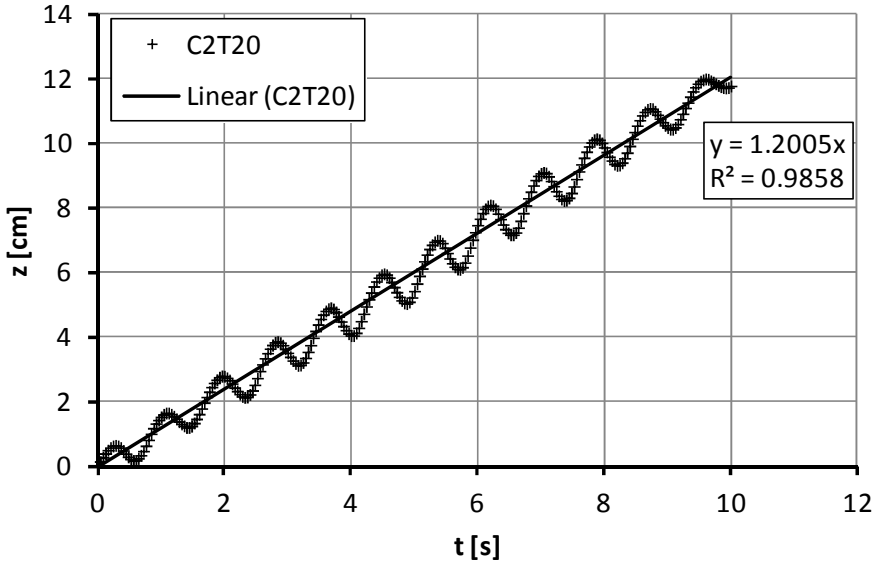


**Figure 4.11 :** A sample water surface elevation - time series record from WG4.

The water surface elevation vs. time curve for WG4 gives the elevation of the water collected in the reservoir (Figure 4.11). In order to calculate the actual $q_{1m}$ unit discharge values, the acquired water surface elevations first have to be converted to water volumes by multiplying the height values *z(t)* with the base area $A_B$ of the reservoir and dividing the result to the total width of sampling channel $b_{ch}$:

$$V_{1m}(t) = \frac{A_B}{b_{ch}} z(t) \qquad \textbf{(4.9)}$$

Substituting actual values ($A_B$ = 0.23x0.47 = 0.1081 m$^2$ and $b_{ch}$ = 0.20 m) yields

$$V_{1m}(t) = 0.5405 z(t) \qquad \textbf{(4.10)}$$

Since discharge rate is defined as the volume of flow per unit time, the slope $\varphi$ of the best fit line shown in Figure 4.11 gives the unit discharge rate:

$$q_{1m} = \frac{dV_{1m}(t)}{dt} = \tan\varphi \qquad \textbf{(4.11)}$$

By using Eq. 4.9 - 4.11 and by taking the total permissible test durations stated above, the mean unit discharge rates for the tested configurations have been calculated. The results are presented in Table A.4.

#### 4.2.4.3 Surface profile measurements of the overtopped volume

Data recorded from the two ultrasonic sensors US1 and US2 directly gives the distance $z_v$ of the sensor to the adjacent reflector, which is either the duct base wall for the no overtopping case, or the free surface of the fluid in existence of overtopping. Thus, the conversion of the achieved time series to the water surface elevation time series consists of a simple subtraction of the measured distance values $z_v(t)$ from the distance between the sensor and the duct base $z_S$:

$$z(t) = z_S - z_v(t) \tag{4.12}$$

Water surface elevation time series achieved for the overtopping volumes by applying Eq. 4.12 to the dataset have been plotted. A typical series showing the profiles at both US1 and US2 sensors simultaneously is shown in Figure 4.12. As seen, the shape of the overtopping volume profile is subject to change as it propagates along the duct. The reshaping is caused primarily by dispersion, and the motion represents the motion of water particles after a dam breaking event.

Two primary parameters have been searched in the records, which are the maximum and minimum heights of each overtopping volume. The process applied to the data for the estimation of maximum and minimum points has been explained in detail in Chapter 5.2.

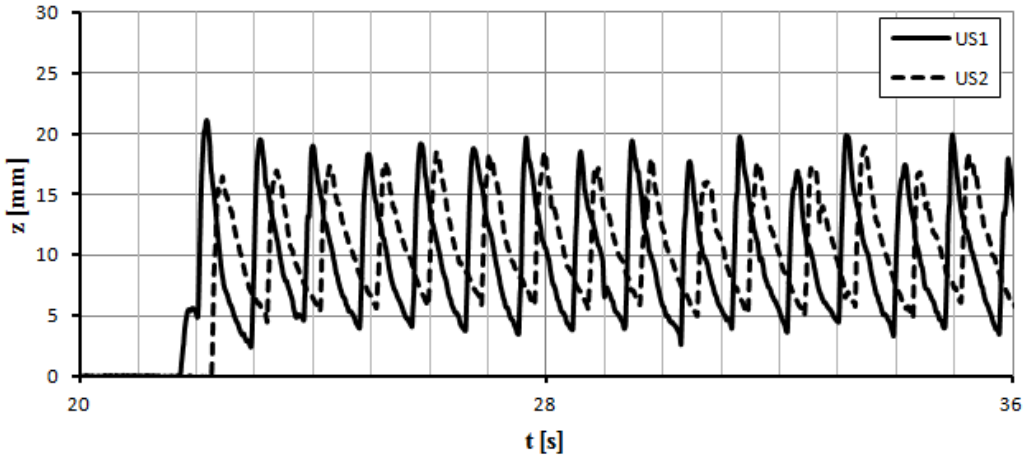


**Figure 4.12 :** A typical view of the overtopping volume profiles.

### 4.3 Performance of a Trimaran Floating Pipe Breakwater

#### 4.3.1 Model setup

##### 4.3.1.1 Wave flume

The flume used for the overtopping tests has been used for the floating breakwater tests, for which the details are given in Chapter 4.2.1.1. While the main elements in the flume such as wave dissipators are left the same, a jig consisting of two steel rails (Figure 4.13) has been attached to the bottom of the flume, over which brass reels are installed with spacings specially set to accomodate the mooring lines of the floating breakwater models to be tested. Thus, the submergence of the structure and the pretension in the mooring lines could be controlled from outside of the flume by adjusting the length of the mooring lines.

##### 4.3.1.2 Breakwater model

The floating breakwater models have been constructed of three 125 mm PVC pipe segments, stiffly connected to each other with plywood end plates. The pipe segments are sealed watertight by rubber and sillicone seals and timber plugs at both ends. Watertightness has been tested before conducting model tests. Plan and profile views and dimensions of the breakwater models are given in Figure 4.15.


**Figure 4.13 :** A bottom rail with reels attached prior to installation.

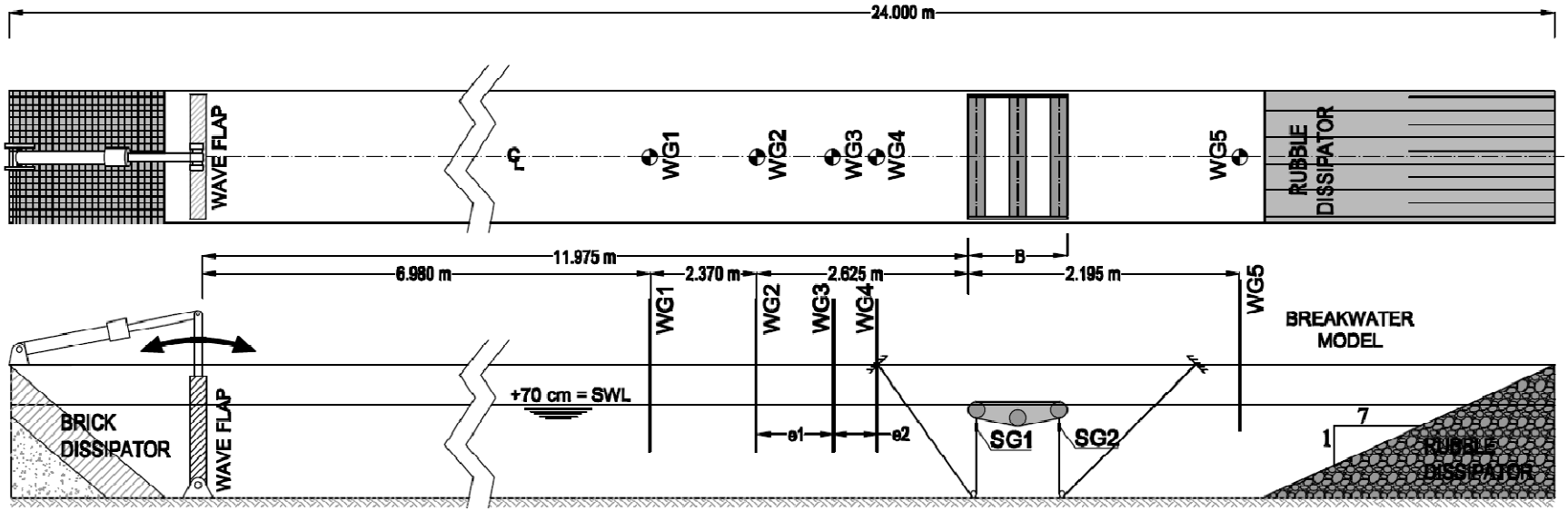


**Figure 4.14 :** Plan and profile drawings of the wave flume with the FBW model installed.

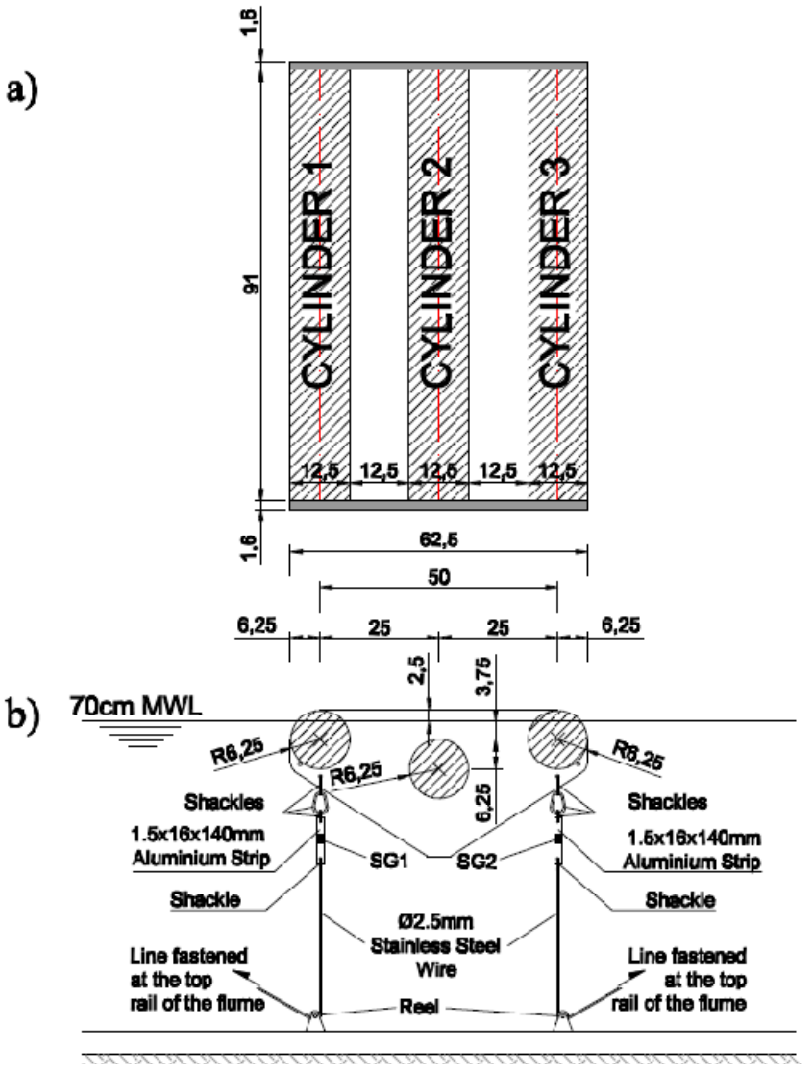


**Figure 4.15 :** Plan (a) and profile (b) drawings of the floating breakwater model and moorings. Measurements are based on configuration FB1.

Dimensions and physical properties of the tested floating breakwater models have been summarized in Table 4.3.

#### 4.3.1.3 Moorings

The mooring system has been arranged as vertical cables extending from the breakwater model down until the bottom of the flume, where they are winded over brass reels upwards and fixed at clamps mounted to the top rail of the flume. This arrangement enabled the adjustment of the floating breakwater model and the mooring line tensions. Mooring lines are composed of chrome-coated steel wire with 3mm diameter.

**Table 4.3 :** Physical properties of the tested floating breakwater configurations.

| Property | Notation | Unit | Conf. FB1 | Conf. FB2 | Conf. FB3 |
|---|---|---|---|---|---|
| Total width | B | [cm] | 62.50 | 75.00 | 87.50 |
| Pipe diameter | D | [cm] | 12.50 | 12.50 | 12.50 |
| Gap width | a | [cm] | 12.50 | 18.75 | 25.00 |
| Draft | d | [cm] | 16.25 | 16.25 | 16.25 |
| Weight | W | [N] | 74.51 | 77.74 | 80.86 |
| Total uplift force | $F_U$ | [N] | 316.99 | 320.79 | 324.59 |
| Excess buoyancy | $F_B$ | [N] | 242.48 | 243.05 | 243.73 |
| Centre of gravity | $z_G$ | [cm] | 4.98 | 5.15 | 5.27 |

### 4.3.2 Instrumentation and software

#### 4.3.2.1 Wave measurements

Measurement of water surface profiles has been achieved by using five resistance type wave gauges. Four of the gauges (WG1-WG4) are installed into the offshore side of the structure for the measurement of incident and reflected waves. The fifth probe (WG5) has been installed to the shore side of the structure to measure transmitted waves (Figure 4.14). Acquisition of the water surface profile data has been supplied over a connection of the probes with a wave monitor/amplifier made by HR Wallingford and an A/D card manufactured by Native Instruments. A sampling rate of 40 Hz has been used during all tests.

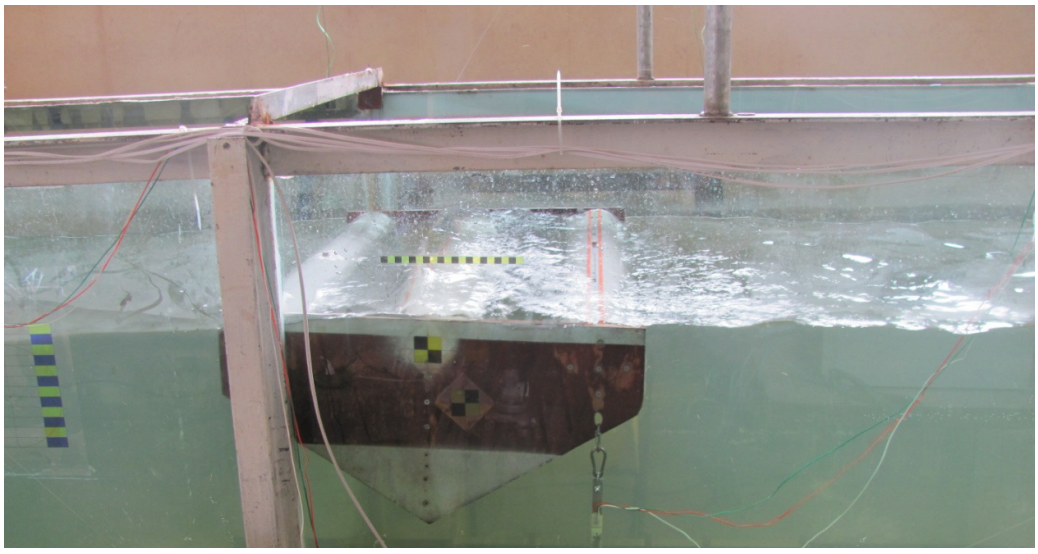

**Figure 4.16 :** A view of the model FB1 during the tests.

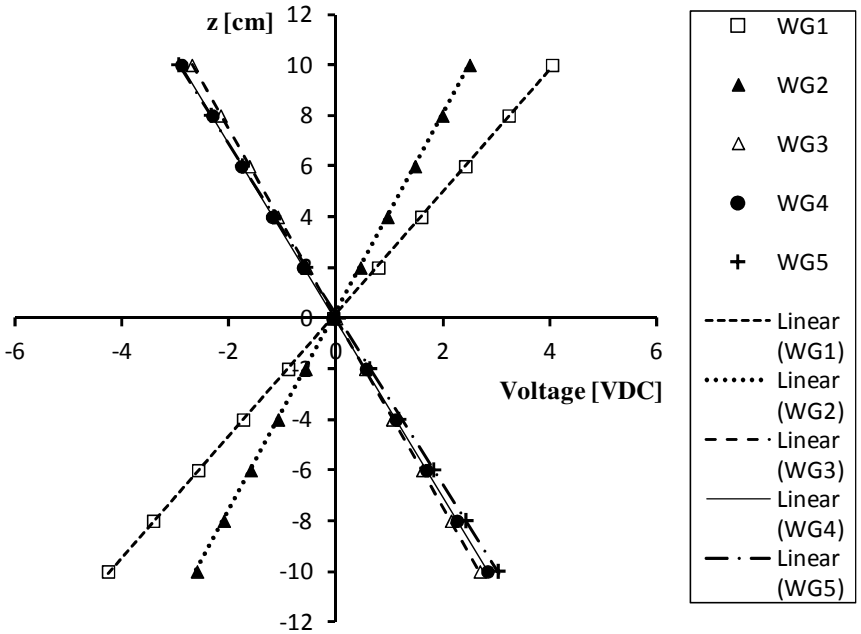


**Figure 4.17 :** Calibration curves for the wave probes (Config. C1).

Calibration of the wave probes has been conducted prior to each configuration in order to ensure the reliability of the records. Figure 4.17 shows the calibration equations of the wave gauges obtained before starting the tests on Configuration 1. The calibration equation for this type of probes is expected as a linear relationship between the measured voltage value and water surface elevation such as

$$y = mx + c \tag{4.13}$$

The values m and c of Eq. 4.13, together with corresponding correlation coefficients evaluated for Configuration C1 are given in Table 4.4. A typical profile of the incident wave (WG1) and transmitted wave (WG5) is shown in Figure 4.17. The variation of the wave heights at the start of the series is caused by the transient waves occuring at the startup of the test.

**Table 4.4 :** Calibration coefficients and corresponding $R^2$ values for the wave gauges.

| Probe No. | m | c | $R^2$ |
|---|---|---|---|
| WG1 | 2.4017 | 0.1917 | 0.9999 |
| WG2 | 3.9112 | 0.2282 | 1.0000 |
| WG3 | -3.7067 | -0.0222 | 1.0000 |
| WG4 | -3.4809 | -0.1246 | 0.9999 |
| WG5 | -3.3508 | 0.1318 | 0.9999 |

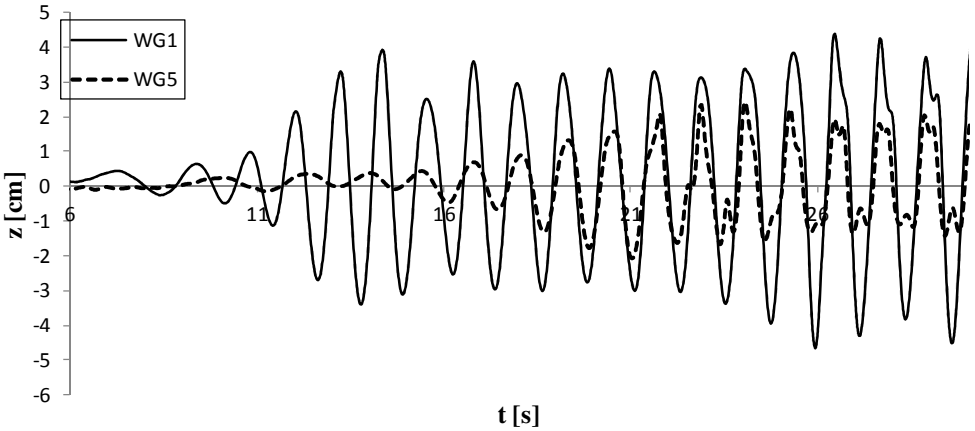


**Figure 4.18 :** A sample water surface elevation - time series record from WG1 and WG5.

#### 4.3.2.2 Mooring forces

The forces at the mooring lines of the floating breakwater models have been measured by using two strain gauges. One of the gauges (SG1) has been attached to the port fore mooring line, and the second (SG2) is installed on the port aft mooring line.

In order to measure the forces at the mooring lines, two strain gauges have been used. Two jigs made from aluminium strips of 120mmx15mmx1.5mm size have been used to mount the strain gauges. Dummy aluminium strips of same size have been attached to the starboard side of the structure to provide homogeneity.

Since the strain gauges should expand and retract combined with the carrier units, the interconnection between the gauges and the carriers is very important. In order to provide a good adherence, the surface of the carriers are first roughened by #300 sandpaper and blasted to carry away any metal residue. The gauges are fixed to the carriers by applying a special CA glue and are covered with an insulation material to provide additional watertightness. A TestBox 2010 data logger has been used to collect the data from the strain gauges at a sampling rate of 250 Hz.

### 4.3.3 Test matrix and procedure

Regular wave series have been used for the tests. For each configuration, the test matrix consists of 30 regular wave series with different wave height and wave period values. As made for the overtopping measurements, the series have been pre-tested

in a blank channel to obtain their wave characteristics. The properties of the test waves are given in Table 4.3.

### 4.3.4 Evaluation of test data

The evaluation of the test data consists of different steps. The first step is the evaluation of wave characteristics, where the target is the estimation of transmission and reflection coefficients. The analysis of the mooring line forces has been executed in the following step.

#### 4.3.4.1 Wave characteristics

In order to evaluate the wave characteristics from the test records, time domain analysis has been used. As carried out in the overtopping tests, the first step in the calculations is the estimation of the permissible record times. The same procedure conducted during the overtopping tests has been applied here, with a small difference for the estimation of the reflection coefficients. Here, it has been assumed that the reflection introduced by the rubble dissipator at the end of the wave flume is zero. The calculated durations are given in Appendix B. Zero crossing method to the test data has been applied as explained in Chapter 4.2.3.

#### 4.3.4.2 Mooring forces

The calibration of the strain gauges has been carried out in the wave flume to maintain the fluid media, in which they will be stationed during actual measurements. To achieve the calibration curves, different weights have been suspended to the free end of the mooring cable, and the elongation values measured under each weight are noted. The calibration curves for the configuration C1 are shown in Figure 4.19.

Since the cables are pretensioned at the start of each test because of excess buoyancy, the measurements on the strain gauges are used to align the structure properly, i.e. to provide an equal share of tension for the free structure. The weight of the mooring line, shackles and strain gauge mounts has been deducted from the total value to achieve the undisturbed excess floatation tensions.

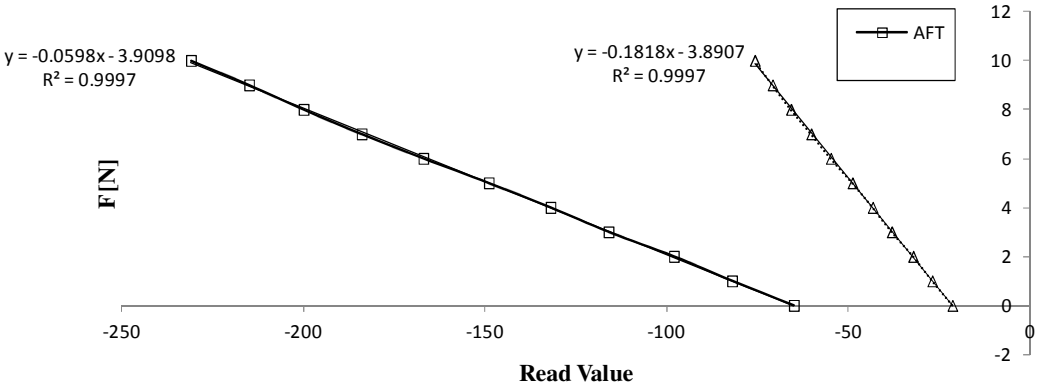


**Figure 4.19 :** Calibration curves for the strain gauges.

During the analysis of the mooring line forces, a procedure similar to the zero-crossing method has been applied. Here, the initial pretension value has been assumed as a zero reference, which has been subtracted from the total tensile force values. The resulting time series, as expected, represents a harmonic curve, where the positive peaks indicate the increase and the negative peaks indicate the decrease in the tensile forces.

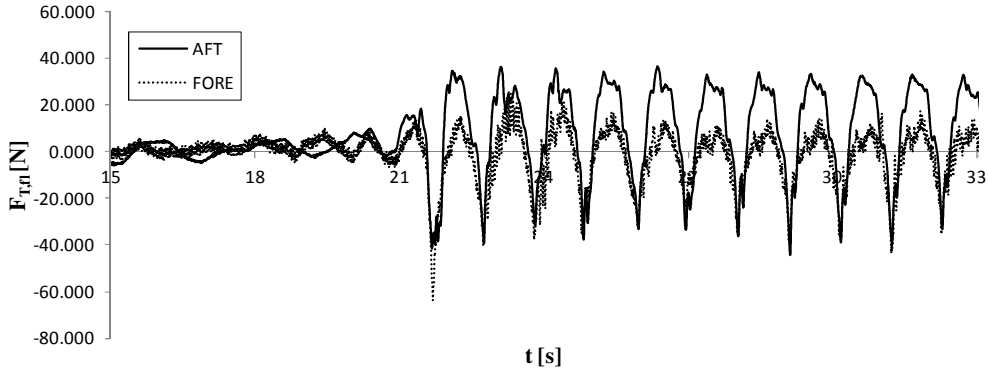


**Figure 4.20 :** A typical mooring force time series showing the cyclic component.

# 5. EVALUATION OF TEST RESULTS

The results obtained from physical model studies are inspected here in more detail in order to evaluate some empirical relationships between the governing paramters and the researched physical quantities. The following section explains the analysis made on the data of the overtopping tests, and the next section is based on the assessment of the floating breakwater model tests.

## 5.1 Quantification of Overtopping Rates over a Partially Immersed Fixed Horizontal Circular Cylinder

In this section, results acquired from wave overtopping tests have been evaluated in order to develop overtopping prediction formulae for the case considered. As first step, the variation of overtopping rate with fundamental governing parameters mentioned in Section 2.4 are assessed. In the following, some of the existing overtopping models given in Table 2.2 have been applied to test results. Further introduction of new parameters and recommendation of a method usable for wave energy converters is explained and discussed in the following section.

### 5.1.1 Identifying the case of zero discharge

In most of the existing overtopping-based studies, overtopping rates are related to wave runup and type of wave breaking. Since no runup measurements are made along the boundary of the cylinder, a simpler method has been adopted here, where the test results are classified according to the occurrence of overtopping. In fact, cases of no overtopping are observed only for the configurations C5 and C6, where the freeboard is highest. Consequently, a criterion for the onset of overtopping is searched for these both cases. The dominant parameters are chosen as the relative freeboard and the wave steepness, in a similar way to the conventional wave runup formulae. A plot of the test data depicting the cases of overtopping and no overtopping for both configurations is given in Figure 5.1, where the abscissa is the deepwater wave steepness and the ordinate is the dimensionless freeboard.

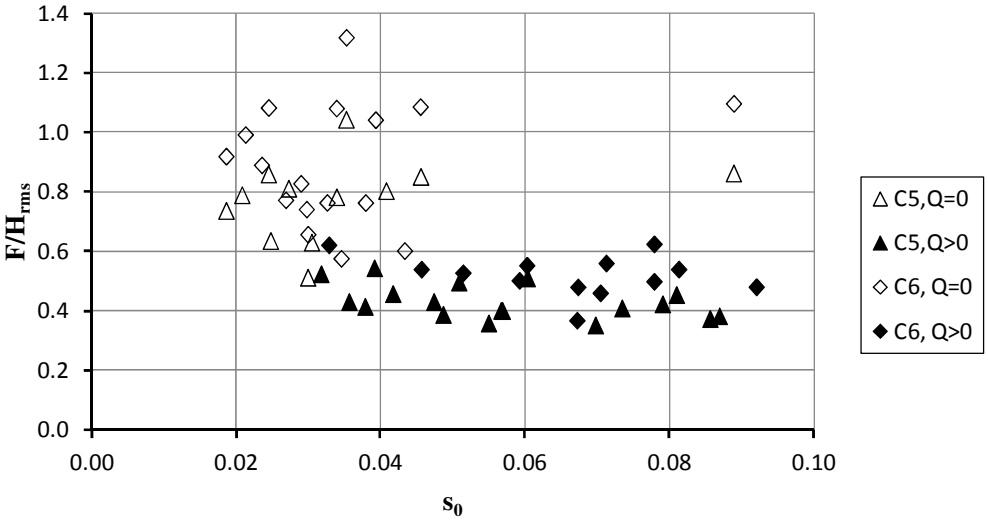


**Figure 5.1 :** Onset of overtopping.

It can be seen from Figure 5.1 that for both configurations a limit on dimensionless freeboard exist between the cases with overtopping and cases without overtopping. Due to the limited number of data however, it is hard to define an exact trendline. Consequently, let us make a rough estimation, where we shall set the overtopping limit only with respect to the dimensionless freeboard and restricted to the test data. In order to achieve this, let us take the highest relative freeboard values for the cases with overtopping and set them as a limit line. Assessing the problem this way, we can achieve $F/H_{rms} < 0.6$ for the configuration C6 and $F/H_{rms} < 0.5$ for the configuration C5, respectively. We can type the overtopping limits in the following way:

$$min(H_{rms}) > n_1 F \tag{5.1}$$

Here, $n_1$ is a coefficient, and its values are given as 2.00 for configuration C6 and 1.67 for configuration C5. At the first sight, this achievement might seems confusing, but if we rewrite F in terms of pipe diameter, we shall get

$$H_{rms} > 1.67F = 1.67(0.4D) = 0.67D \tag{5.2}$$

For the configuration C6, we shall similarly obtain

$$H_{rms} > 2.00F = 2.00(0.5D) = D \tag{5.3}$$

As it can be seen from Eq. 5.2 - 5.3, the wave height needed to start overtopping reduces with reducing freeboard, and its rate of reduction is larger than the reduction rate of the freeboard. This is expected to be a result of the decrease of the circular boundaries local slope at the MWL, but the data is limited to carry out a more detailed study.

### 5.1.2 Variation of unit discharge rates with governing parameters

As mentioned in Chapter 2.4, the main governing parameters on overtopping rates can be counted as the freeboard of the structure, the incident wave properties and the draft of the structure for a floating structure. In this section, we shall assess the variation of overtopping rates with these fundamental parameters.

#### 5.1.2.1 Effect of freeboard

The most important parameter governing the magnitude of wave overtopping rate is the freeboard of the structure. Let us make the first assessment by using the relative freeboard parameter, defined as the ratio of the freeboard to the diameter of the cylinder. A general view of the relation between overtopping rates and relative freeboard is shown in Figure 5.2, where all the dataset has been plotted.

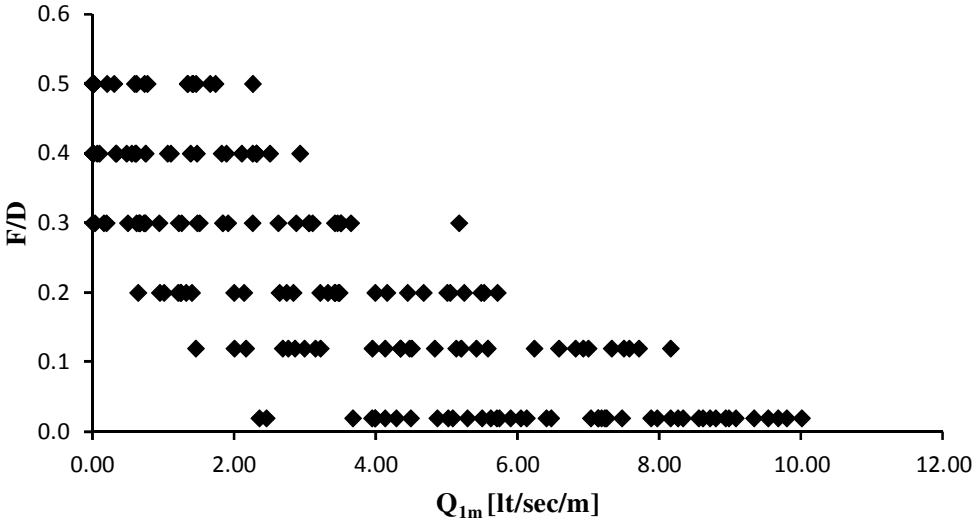


**Figure 5.2 :** Effect of relative freeboard on overtopping rates.

By keeping in mind that the plotted data for each relative freeboard value contains the same waves, an initial judge can be drawn out from Figure 5.2 as expected: Flow rates decrease with increasing freeboard.

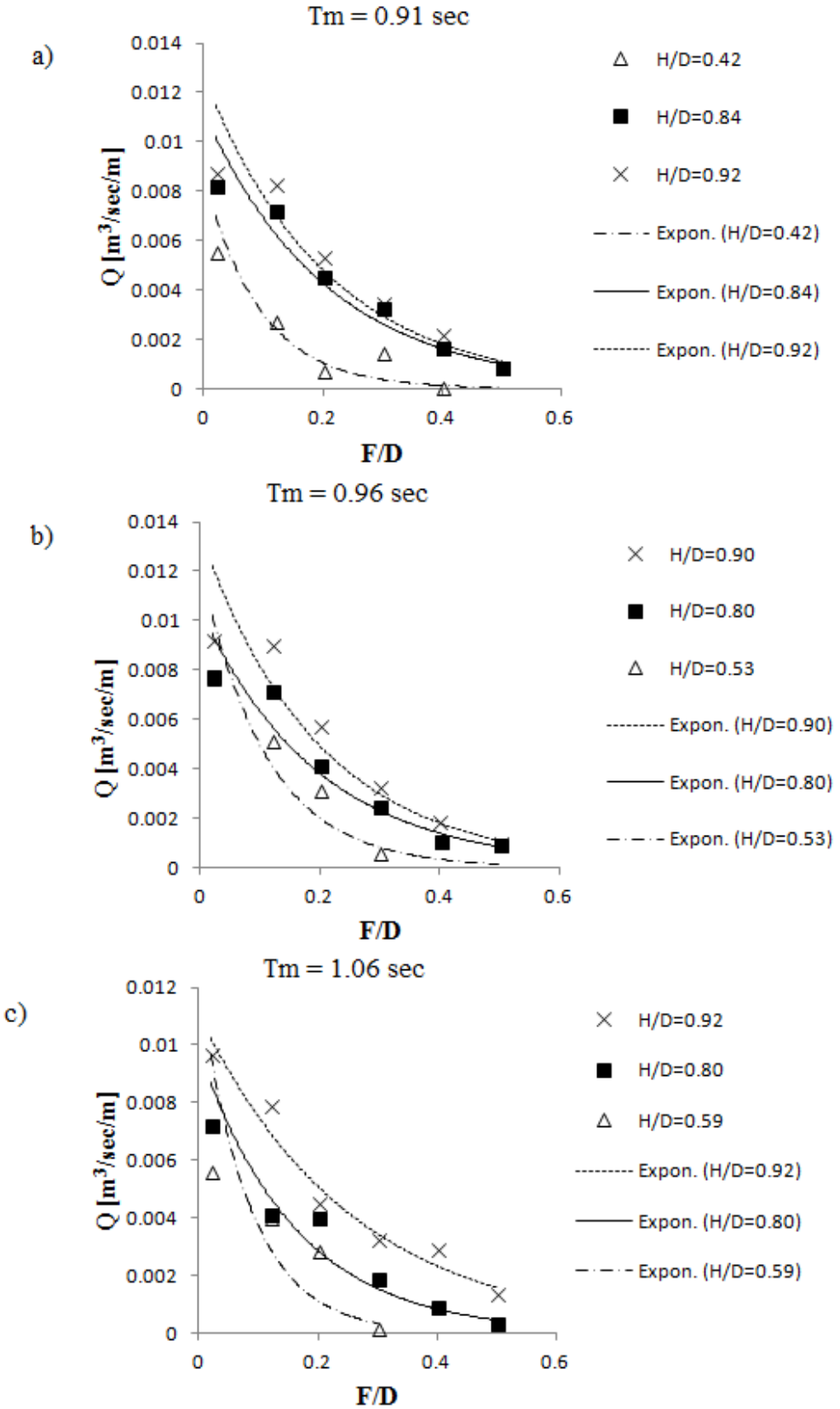


**Figure 5.3 :** Variation of overtopping rates with relative freeboard for fixed wave characteristics.

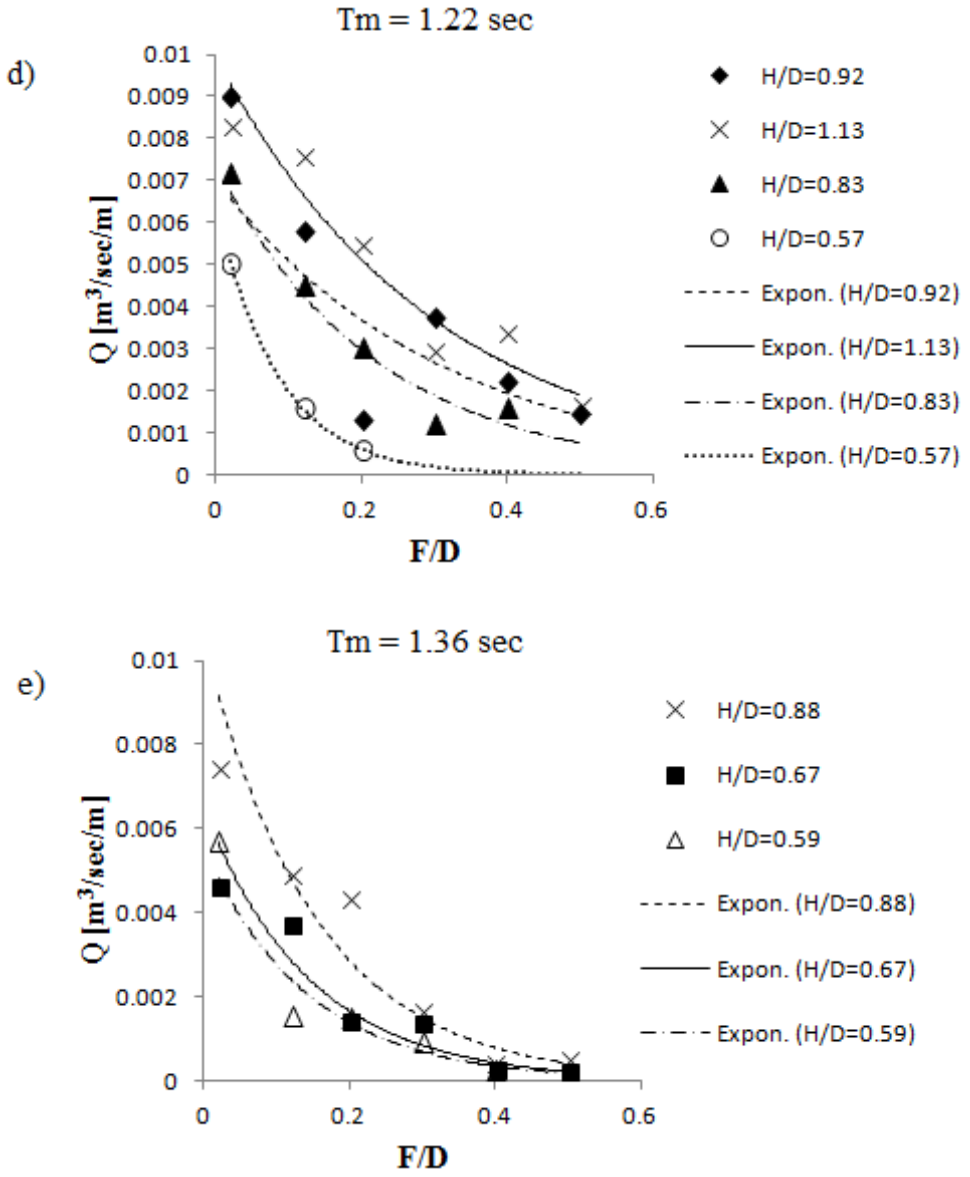


**Figure 5.3 (continued) :** Variation of overtopping rates with relative freeboard for fixed wave conditions.

Now let us check the variation of overtopping rates with relative freeboard under fixed wave characteristics. For this purpose, Figure 5.3 has been plotted, where the curves have been plotted by using incident waves having the same characteristics. The diagrams are initially separated by keeping the wave period fixed, with the wave height brought into a non-dimensional form by taking its ratio to the cylinder diameter. The curves are given for five different wave periods composing multiple wave height values. The diagrams clearly indicate that there is an exponential relationship between the overtopping rate and the relative freeboard with slight

scattering observed, expected to be caused by the small variations in the incident wave height deviating from the $H_{rms}/D$ group mean values.

Now let us assess the variation by introducing the dimensionless freeboard parameter, given in Figure 5.4. In this case, a corrected freeboard value $F_d$ has been used as explained below. The variation of the overtopping rates with the dimensionless freeboard indicates that a general equation can be written between these two parameters, either in an exponential form or in a linear form, which is hard to predict due to the scattering of the data.

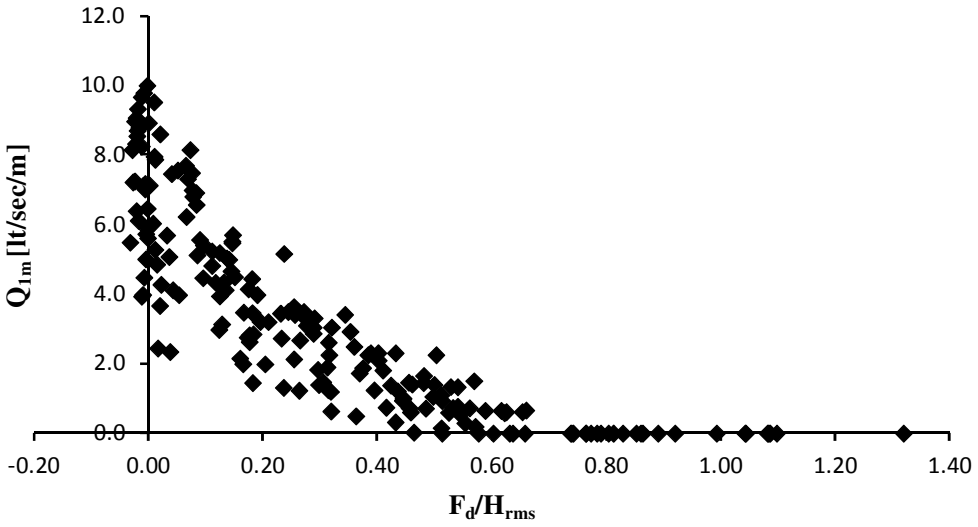


**Figure 5.4 :** Variation of overtopping rates with dimensionless freeboard.

Another plot of the data shown in Figure 5.4 has been given in Figure 5.5, where the ordinate has been plotted in a logarithmical scale. Furthermore, the data containing zero overtopping discharges have been removed. For this case, it is obvious that a linear trendline has a good fit to define the relationship with a high correlation coefficient ($R^2 = 0.7969$), however, there is still a fair amount of scattering evident in the diagram. Figure 5.4 and Figure 5.5 clearly indicate that the dimensionless freeboard alone is not sufficient to define a good relationship for the prediction of the overtopping rates. This outcome is based on two reasons. First, for the cases with zero freeboard, the dimensionless freeboard parameter approaches zero, leading to an accumulation of data nearby the y-axis. Second, there is a significant amount of scattering, indicating that a second parameter, or maybe more, should be introduced to achieve a better fit for the equation.

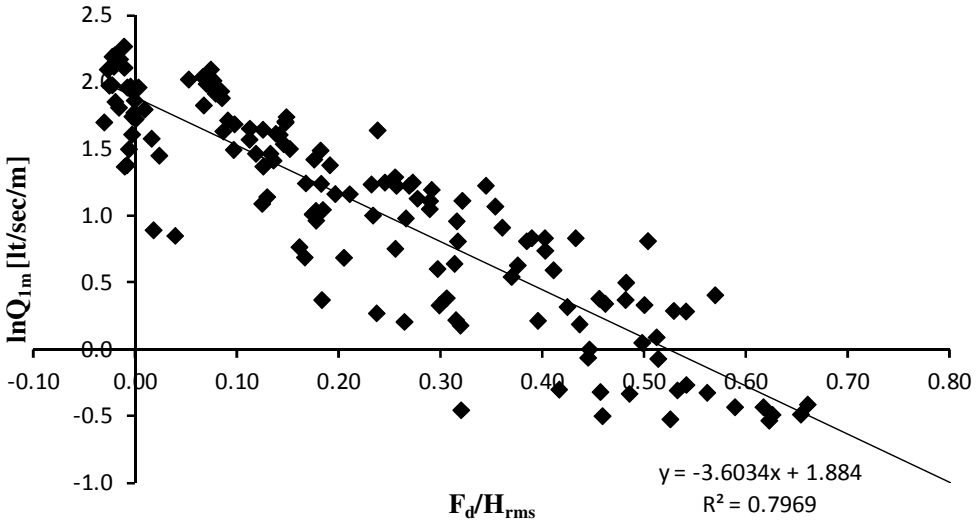


**Figure 5.5 :** Logarithmic plot of dimensionless freeboard vs. wave overtopping rate.

#### 5.1.2.2 Effect of wave height

To inspect the effect of wave height on overtopping rates, tests of equal period values with different wave heights are sorted out and grouped for each configuration. The groups are plotted on diagrams with the vertical axis showing the unit discharge $q_{1m}$ and the abscissa showing the RMS wave height $H_{rms}$. The diagrams are shown in Figure 5.6, clearly indicating that the unit discharge values $q_{1m}$ increase with increasing wave height for any fixed relative freeboard value and fixed wave period. The arrangement of the points indicate the existence of an exponential or linear type relationship between the wave height and wave period, but the number of the points is fairly few to make an absolute conclusion.

#### 5.1.2.3 Effect of wave period

To assess the effect of wave period on unit discharge rates, tests with close RMS wave height values and different wave periods under each configuration have been grouped. The groups are plotted as diagrams with the unit discharge rate $q_{1m}$ as the ordinate and the mean wave period $T_m$ as abscissa. Three diagrams are plotted with their difference being the constant relative height value of the incident waves, defined as the ratio of the incident RMS wave height $H_{rms}$ to the diameter of the cylinder D. On each diagram, different relative freeboards are separated. Shown in Figure 5.7 a-c, the diagrams indicate that under fixed relative freeboard and fixed wave height, unit discharges decrease with increasing wave period.

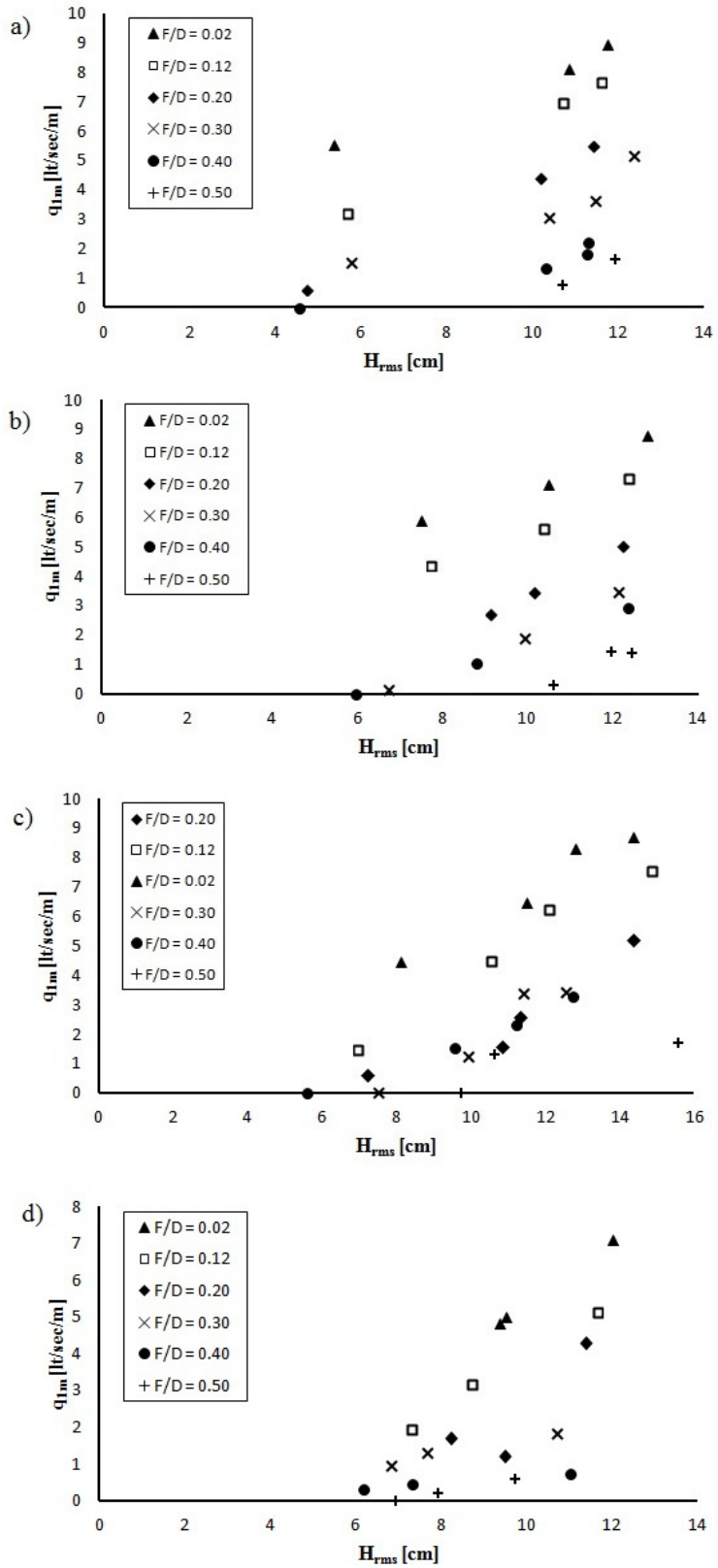


**Figure 5.6 :** Effect of wave height on unit discharges for fixed wave periods of (a) $T_m$ = 0.91s, (b) $T_m$ = 1.06s, (c) $T_m$ = 1.21s and (d) $T_m$ = 1.36s.

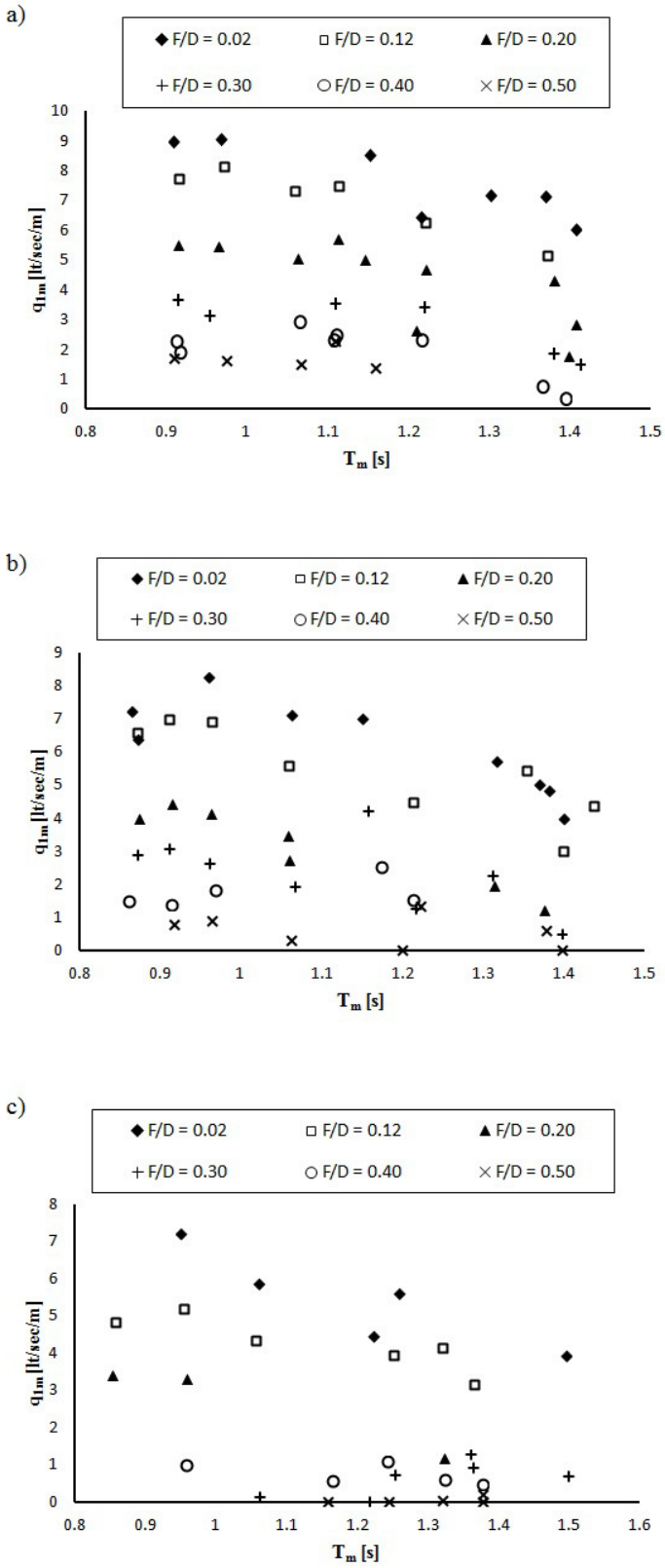


**Figure 5.7 :** Effect of wave period on unit discharges for fixed relative wave heights of (a) $H_{rms}/D = 0.90$, (b) $H_{rms}/D = 0.80$, (c) $H_{rms}/D = 0.60$.

#### 5.1.2.4 Effect of wave steepness

The effect of wave steepness on overtopping rates has been shown in Figure 5.8, separated for each different relative freeboard value. It has been observed that a logarithmic line fits the data well excluding the cases with relative freeboard values higher than 0.3.

The degrade in the goodness-of-fit of the logarithmic line can be assumed acceptable due to the finding of van der Meer and Janssen as cited in Section 2.4, who state that the effect of wave steepness loses its importance for the case of steep and/or vertical structures. This outcome is connected to the idea that if a local slope parameter is to be defined for a cylinder with its immersion depth as a variable, evaluated with respect to the cylinders tangent at the MWL, the slope should increase if one reduces the depth of immersion.

By obtaining the diagrams, two different wave steepness values have been tested, the deepwater wave steepness $s_0$ and the wave steepness at the structure depth $s_h$, respectively. It has been observed that structure depth gives better correlation values, but the increase is in the range of 2% - 4%.

### 5.1.3 Development of an overtopping model

Based on primary inspections carried on test results, and also verified by the findings in the literature review, the configurations have been classified as the emergent and zero-freeboard cases and assessed separately.

#### 5.1.3.1 Emergent cylinder

Let us first inspect the case of an emergent cylinder. Thus, the dataset is reduced to the configurations C2-C6 with the cases excluded where no overtopping has been observed. Based on the investigations carried out for the effect of governing parameters in Chapter 5.3.1, it is expected that a prediction formula can be written as a function of the dimensionless freeboard and wave steepness:

$$Q = f\left(\frac{F}{H}; s_h\right) \tag{5.4}$$

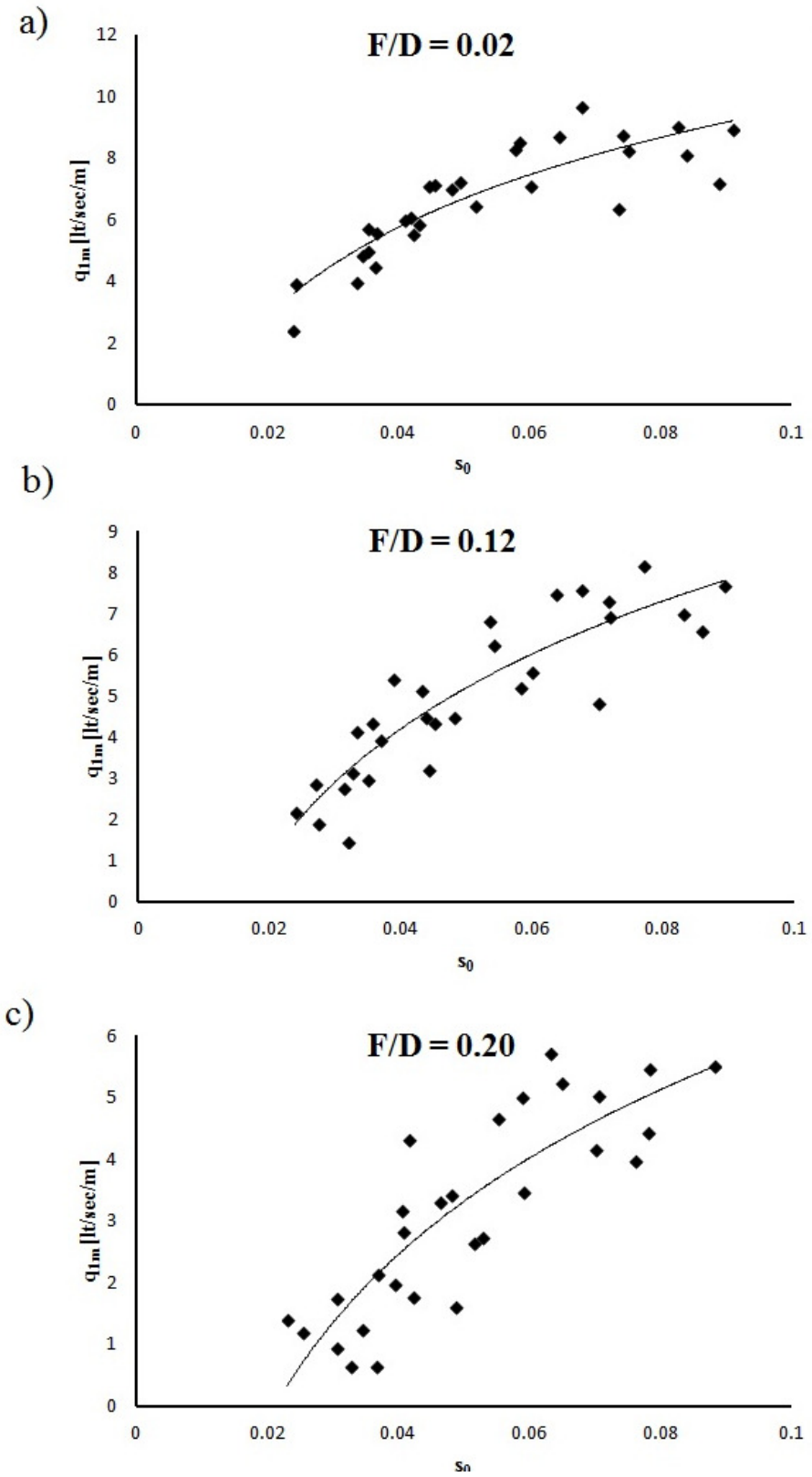


**Figure 5.8 :** Effect of wave steepness on unit discharges for fixed relative immersion depths.

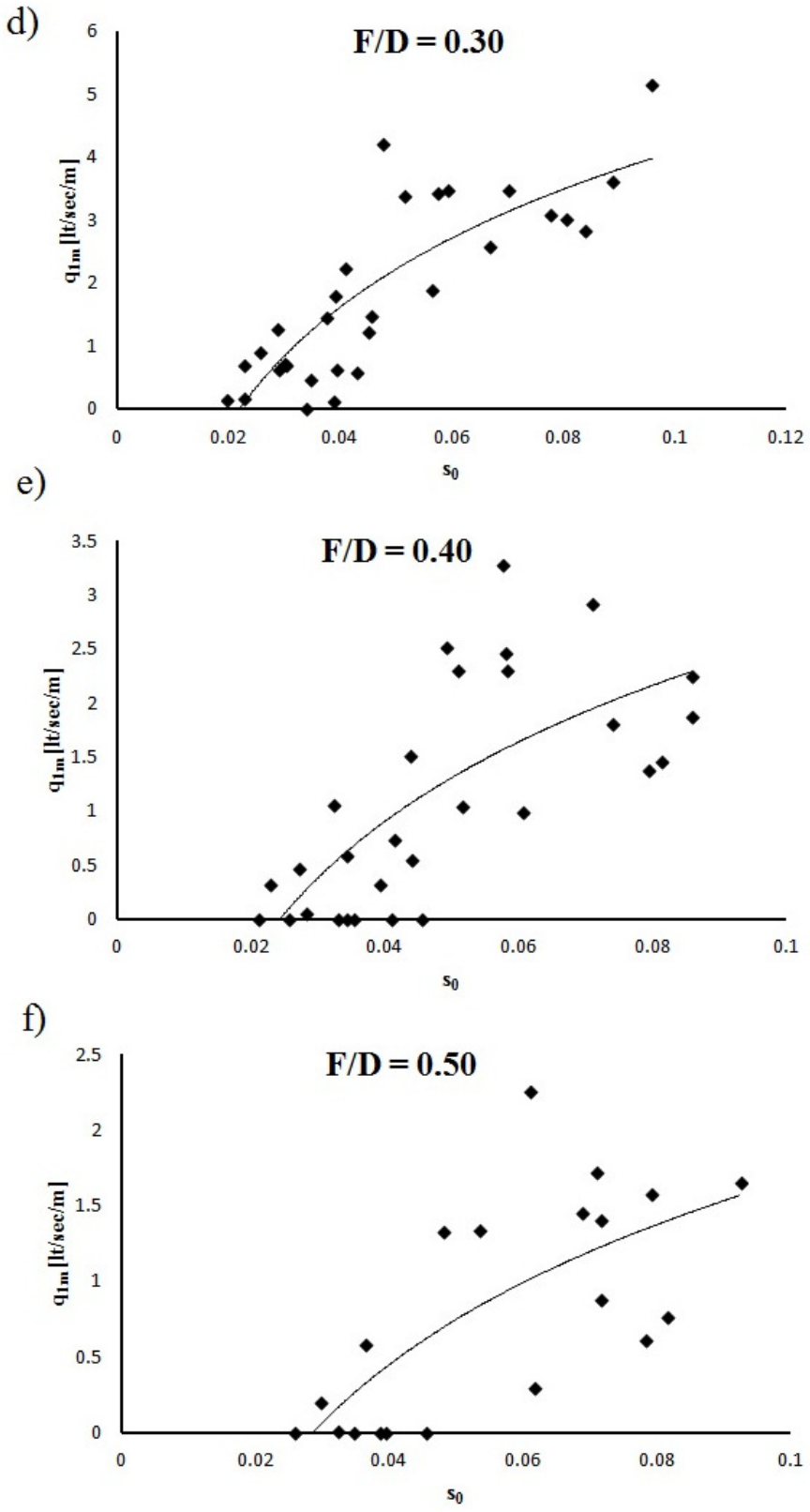


**Figure 5.8 (continued) :** Effect of wave steepness on unit discharges for fixed relative immersion depths.

In order to evaluate the formula, a nonlinear regression analysis have been carried out by using the parameters given in Eq. 5.4. First, an analysis has been carried out with the dimensionless discharge defined by the weir analysis and the dependent variables assigned as the wave steepness $s_h$ and the dimensionless freeboard $F_d/H_{rms}$. The resulted equation yields

$$\frac{Q_{1m}}{\sqrt{gH_{rms}^3}} = 0.059exp\left(-3.45\frac{F_d}{H_{rms}} + 0.31s_h\right) \quad \textbf{(5.5)}$$

Different combinations have been researched, of which the equations and corresponding correlation coefficients have been summarized in Table A.4. A model, based on the definition of a new dimensionless discharge rate, has given the best fit. The dimensionless discharge rate for this case has been defined as the ratio of the overtopping volume per one wave cycle to the cross section area of the cylinder:

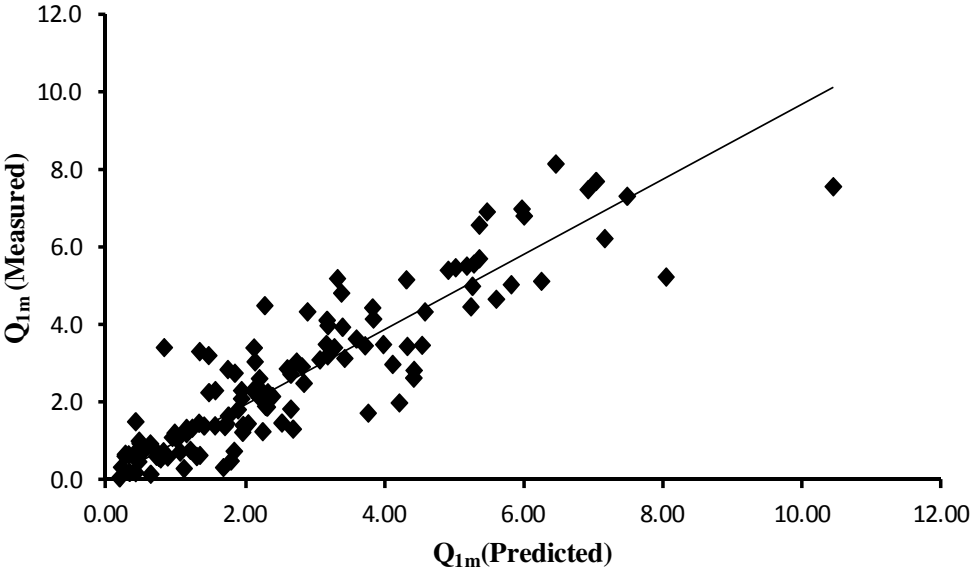


**Figure 5.9 :** Measured and predicted overtopping rates for Eq. 5.5.

$$Q_A = \frac{q_{1m}T_m}{0.25\pi D^2} \quad \textbf{(5.6)}$$

By using the dimensionless discharge defined by Eq. 5.6, following equation has been developed:

$$\frac{Q_{1m}T}{0.25\pi D^2} = 0.441exp\left(-4.542\frac{F_d}{H_{rms}} + 1.166s_h\right) \quad \textbf{(5.7)}$$

The plot of Eq. 5.6 is given in Figure 5.9 as the comparison of measured and predicted overtopping rates. It is obvious that there is still a fair amount of scattering. The plot of Eq. 5.7 is given in Figure 5.10. In this case, the scattering is less than the plot of Eq. 5.6. Checking the $R_M$ multiple correlation coefficients, Eq. 5.6 has a multiple correlation coefficient of 0.854 whereas Eq. 5.7 yields a value of 0.977. Thus, use of Eq. 5.7 may be recommended for the inspected range.

By taking the still-on-going situation about the improvement of overtopping rate models carried out by a vast number of experienced researchers, these equations are not to be refined further here.

In order to reduce the scattering for the estimation of overtopping rates for the configurations where the wave energy converter is planned to be deployed, two further equations have been developed by adopting Eq. 5.7 to a smaller database corresponding to the interested relative depth. For a relative depth of F/D = 0.12, one may use following equation ($R_M$ = 0.935; $\varepsilon_{a0}$ = 0.043; $\varepsilon_{r0}$ = 0.101)::

$$\frac{Q_{1m}T}{0.25\pi D^2} = 0.95\sqrt{s_h}^{-0.11} exp\left(-8.37\frac{F_d}{H_{rms}}\right) \quad \textbf{(5.8)}$$

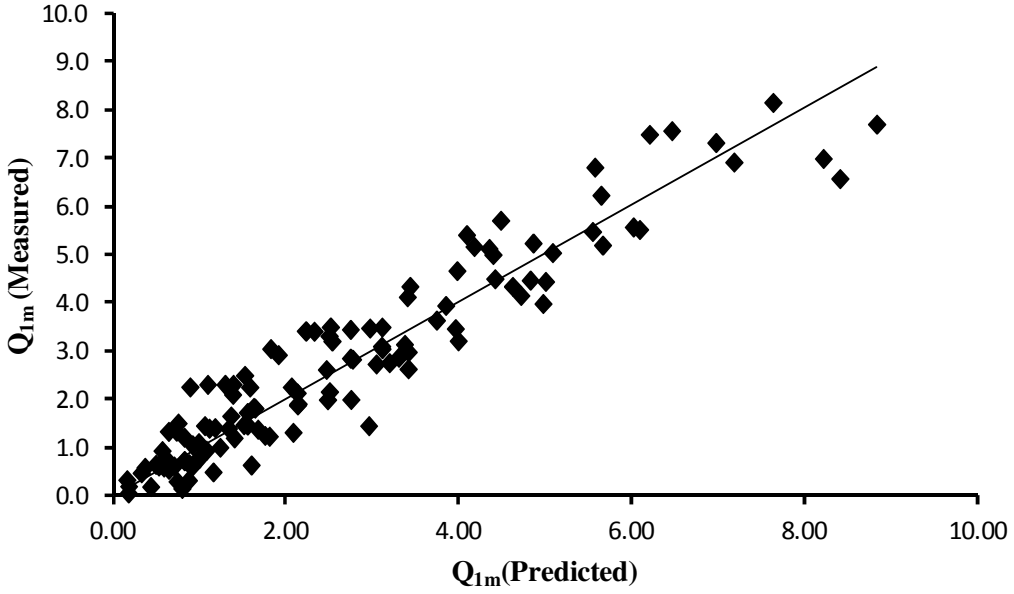


**Figure 5.10 :** Measured and predicted dimensionless discharge values (Eq. 5.7).

In case of a relative depth of F/D = 0.20, following equation has been fitted to the data ($R_M$ = 0.922; $\varepsilon_{a0}$ = 0.035; $\varepsilon_{r0}$ = 0.122):

$$\frac{Q_{1m}T}{0.25\pi D^2} = 1.35\sqrt{s_h}^{0.28} exp\left(-5.41\frac{F_d}{H_{rms}}\right) \quad \textbf{(5.9)}$$

The measured and predicted values of dimensionless discharges by using Eq. 5.8 have been plotted in Figure 5.10. As seen, the amount of scattering is relatively small. A similar plot for Eq. 5.9 has been given in Figure 5.11, indicating a reasonable agreement between the measured and predicted dimensionless overtopping rates.

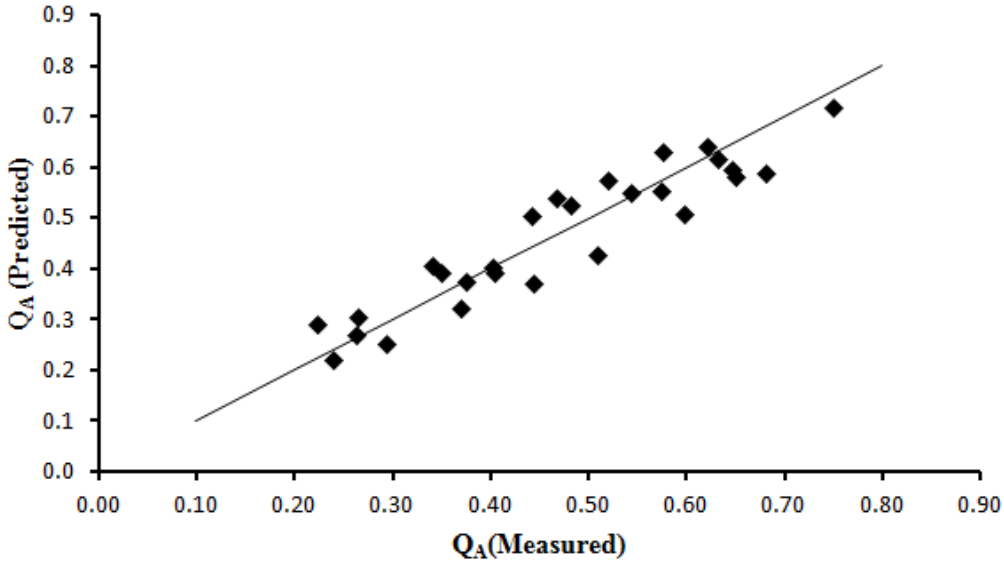


**Figure 5.11 :** Measured and predicted dimensionless discharge values (Eq. 5.8).

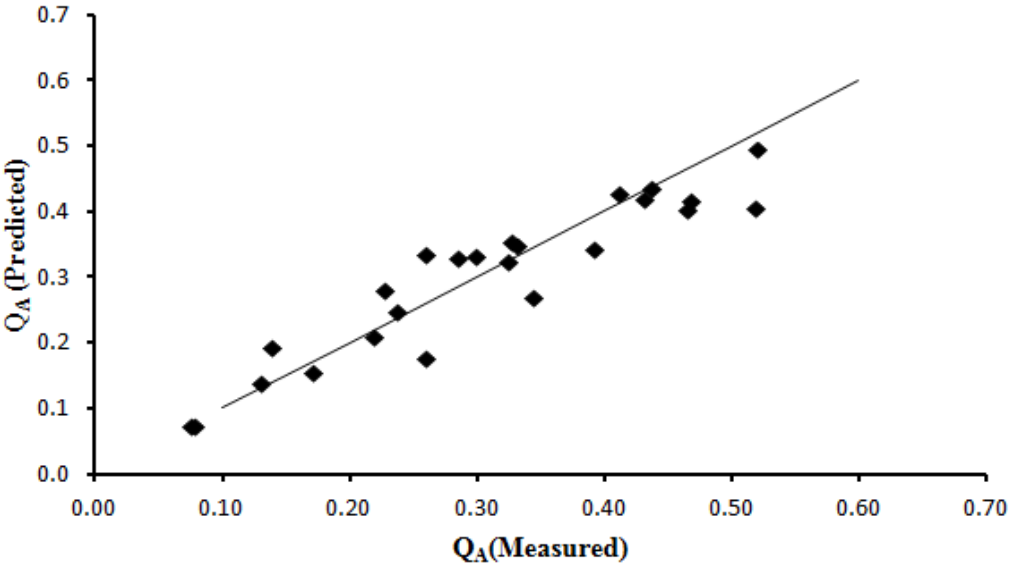


**Figure 5.12 :** Measured and predicted dimensionless discharge values for Eq. 5.9.

### 5.1.3.2 Cylinder with zero freeboard

Regarding the case of zero freeboard, it has been pointed by many researchers that the dimensionless freeboard is not an efficient parameter. Thus, the wave steepness has been inspected as one of the governing parameters. By using overtopping rates achieved from configurations C1 and C7, Figure 5.13 has been plotted. Though being dimensional, it is obvious that the overtopping rate can be expressed as a function of wave steepness.

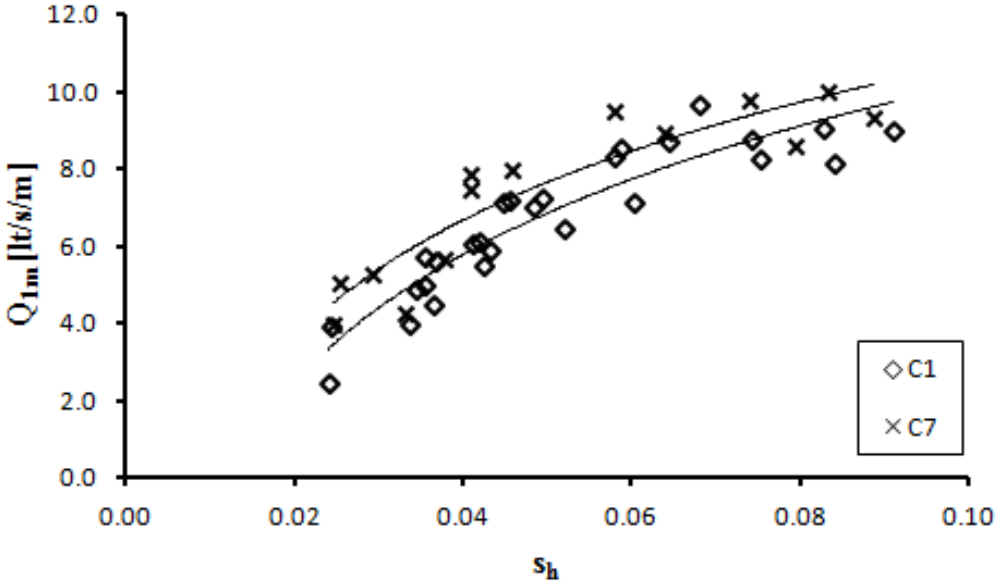


**Figure 5.13 :** Variation of overtopping rates with wave steepness for zero freeboard.

Following equation has been fitted for configuration C1 ($R^2$=0.866):

$$Q_{1m} = 4.809 \ln(s_h) - 21.250 \quad \textbf{(5.10)}$$

For configuration C7, a similar expression has been fitted ($R^2$=0.843):

$$Q_{1m} = 4.415 \ln(s_h) - 20.870 \quad \textbf{(5.11)}$$

Plotting the variation of dimensionless discharge calculated by weir approach with the wave steepness (Figure 5.14) gives a similar view to the output of Smid (2001) with a dimensionless discharge fluctuating along a fixed value. This value has been calculated as 0.06 for configuration C1 and 0.09 for configuration C7.

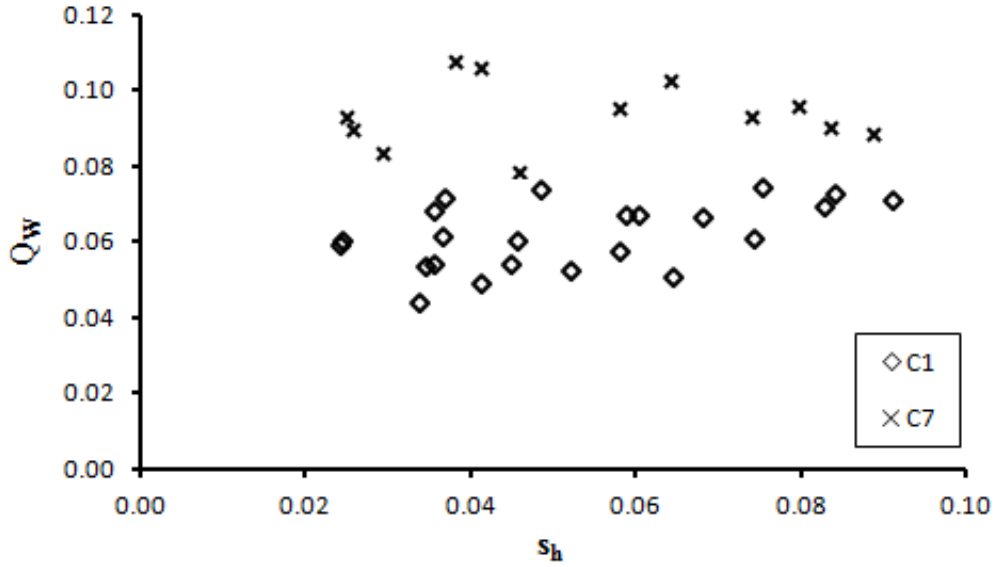


**Figure 5.14 :** Variation of overtopping rates with wave steepness for zero freeboard.

### 5.1.4 Correction parameters

#### 5.1.4.1 Partial setup correction

During the experiments, it has been observed that an increase in mean water level at the front of the structure takes place. This effect leads to a change in freeboard height when incident waves are present, which is found to affect the goodness-of-fit of the proposed relationships.

The reasons for the partial setup can be counted as in the following:

i. Upon interacting of the incident waves with the cylinder, runup and rundown events take place at the fore face of the cylinder, leading to generation of reflected waves with phase differences. The interaction of incident and reflected waves lead to an increase in mean water level in front of the structure, building a partial setup. While this phenomena is most evident for vertical and sloped coastal structures, a similar reason is expected for the case of a near-surface structure due to similarity in triggering events.

ii. The nonlinearity of the test waves may induce an increase in mean water level, which has been checked in Table A.7.

iii. The formation of a closed space in the wave flume during the tests may leads to the induction of currents to counter the mass transport caused by incident waves. These currents are expected to have a direction from the shore side back to the wave

paddle, increasing the MWL at the shoreward side of the flume to generate a driving head.

Based on the reasons mentioned above, a second correction factor has introduced to balance the effect of the partial setup. However, factors creating partial setup mentioned above are hard to interpret and to separate from each other. As a consequence, following algorithm has been applied to make the correction, where the water surface elevation time series at WG3 have been used to evaluate partial setup values:

i. The initial (i.e. calm) water level $z_0$ at WG3 is noted.

ii. The mean water levels during wave attack , $\bar{z}_\eta$ are calculated by taking the permissible test durations and a discrete number of waves into account for each test by averaging the water surface elevation time series along the sampling duration.

iii. The partial setup values $\delta_p$ are calculated as the difference of the mean water level $\bar{z}_\eta$ and the initial water level $z_0$:

$$\delta_p = z_0 - \bar{z}_\eta \tag{5.12}$$

The correction has been carried out by making following substitutions:

$$\begin{aligned} F_\delta &= F - \delta_p \\ d_\delta &= d + \delta_p \end{aligned} \tag{5.12}$$

By using the substitution given in Eq. 5.12, the modified dimensionless freeboard $R_D$ has been defined as:

$$R_D = \frac{F_\delta}{H_{rms}} \tag{5.13}$$

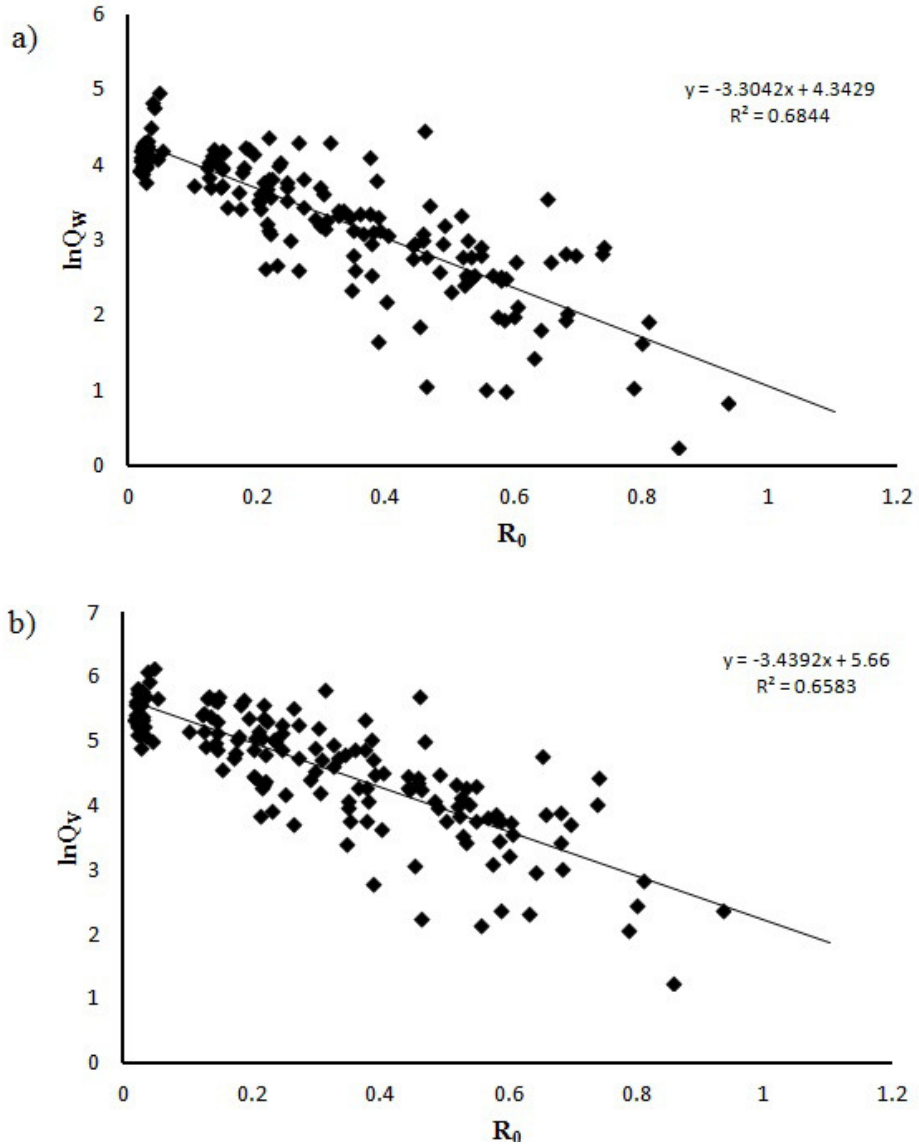


**Figure 5.15 :** Variation of $Q_W$ and $Q_V$ with $R_0$ "calm" dimensionless freeboard.

Diagrams showing the variation between $Q_W$ or $Q_V$ and the unmodified and modified dimensionless freeboard $R_D$ are given in Figure 5.15 and Figure 5.16, respectively. Compared with the initial dimensionless freeboard values, this correction introduces an increase in the goodness-of-fit at a magnitude of 4%. Since the data naturally contains some scattering as encountered in all overtopping studies, such an increase in correlation clearly indicates the importance of mean water level variation in front of the structure. Thus, all dimensionless freeboard values have been modified as mentioned above to include the effect of partial setup taking place in front of the cylinder.

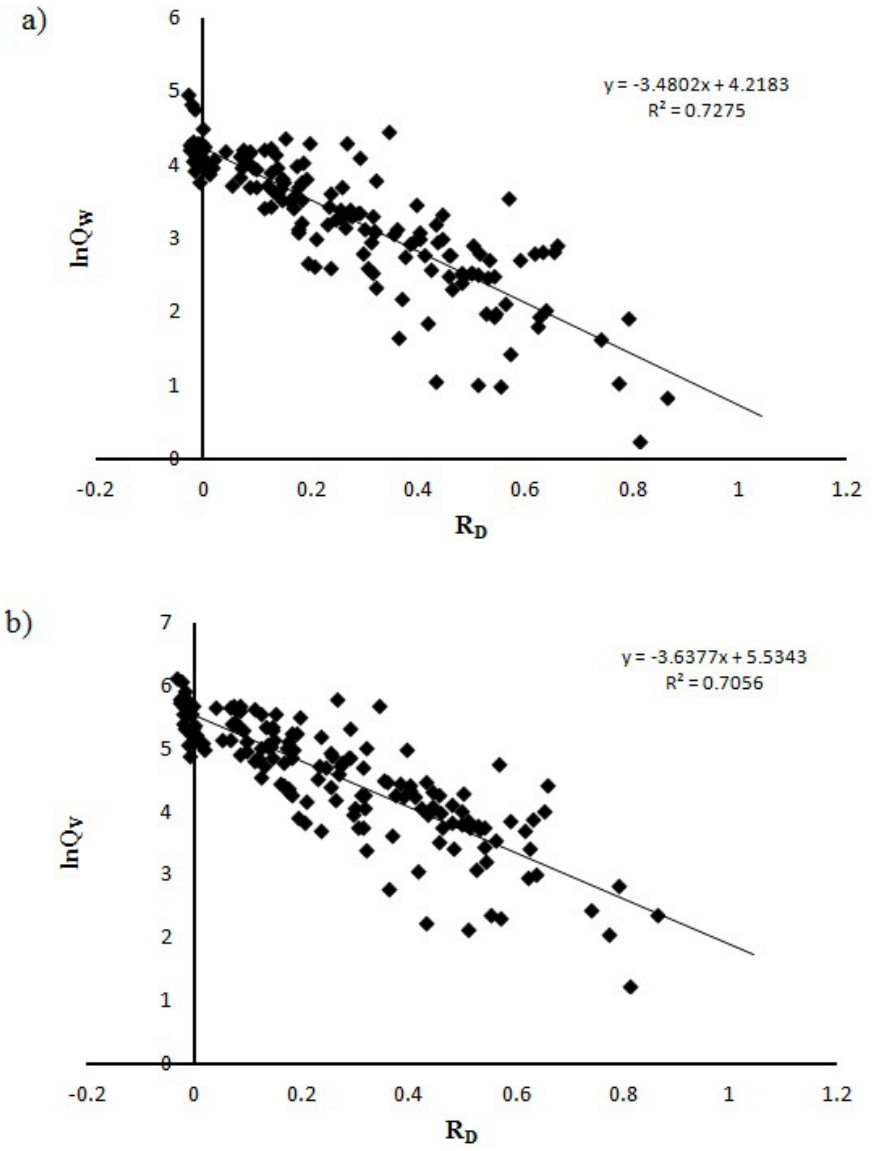


**Figure 5.16 :** Variation of $Q_W$ and $Q_V$ with $R_D$ modified dimensionless freeboard.

### 5.1.4.2 Limited draft correction

In all of the tested configurations test cylinders have a limited draft, which enables wave transmission between the sea floor and the bottom line of the cylinder. Since a cylinder with a fixed radius is used, the height of the free zone below the structure changes for each configuration. This phenomena is expected to affect wave transmission and hence wave overtopping.

In order to take the limited draft effect into account, the correction factor recommended by Kofoed (2002) has been taken into account (Eq. 2.41), which is based on the ratio of power transmission taking place along the draft of the structure

and along the whole depth. The factor κ has been calculated by searching the best-fit for the whole dataset, which gives a value of 0.5.

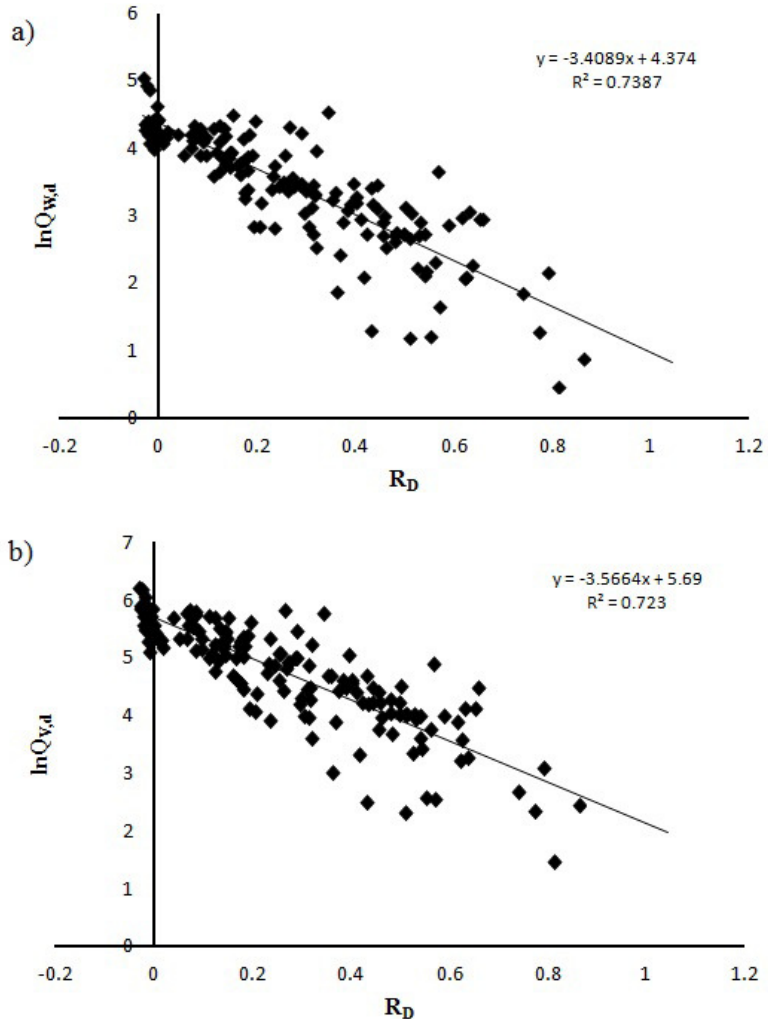


**Figure 5.17 :** Variation of depth-corrected dimensionless discharges $Q_{W,d}$ and $Q_{V,d}$ with dimensionless freeboard $R_D$.

As a second correction, let us apply the limited draft factor $\gamma_d$. In order to apply this factor, the dimensionless discharge values $Q_W$ and $Q_V$ are divided to $\gamma_d$. The results of this correction are shown in Figure 5.17. As seen from the figure, an increase in the correlation coefficients is evident again, but its magnitude is small, approx. 2%. The limitation of the improvement is based on the small difference between the configuration with the maximum draft and the configuration with the minimum draft. In configuration C1, where the cylinder is 98% submerged, 82% of the depth is unoccupied, whereas this value increases to only 91% for configuration C6 with 50% of the cylinder submerged.

As seen from Figs. 5.15 - 5.17, the improvement on the goodness-of-fit of the general model by involving depth- and partial setup corrections is obvious. Thus, depth-corrected dimensionless discharge values and corrected dimensionless freeboard values shall be used during the rest of this study.

### 5.1.5 Comparison with planar slopes

A comparative study of the tested system has been executed by using the overtopping rate equation recommended by Kofoed (2002) for the Wave Dragon WEC given as Eq. 2.65.

Measured overtopping rates on the cylinder body $Q_{CYL}$ and overtopping rates expected to take place on a linear 30-degree slope with the same draft and freeboard characteristics and under the same incident waves have been compared in Figure 5.18. As seen from Figure 5.18, a cylindrical overtopping ramp acts in a very close order to a linear ramp in the dimensionless freeboard range higher than 0.3. While for larger dimensionless freeboard values the performance of the system is weaker than a linear slope, a cylindrical ramp becomes more effective for smaller dimensionless freeboard values.

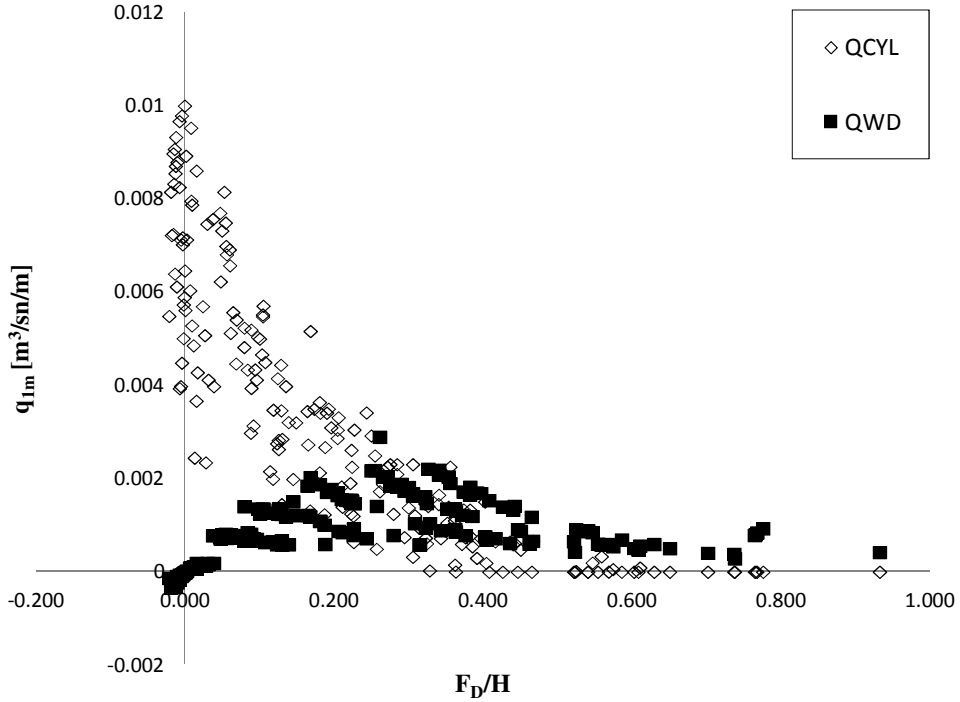


**Figure 5.18 :** Comparison of overtopping rates over the cylinder ($Q_{CYL}$) and a linear 30-degree slope ($Q_{WD}$).

## 5.2 Energy and power of the overtopped water mass

In this chapter, an assessment of the systems hydraulic efficiency based on wave energy capture has been carried out. For this purpose, the energy carried by the overtopping water volume has been derived under some assumptions explained below, and it is compared to the incident wave energy to obtain the energy capture ratio, which should give the hydraulic efficiency of the system. The initial step in energy and power calculations is the evolution of the hydrokinetic properties of the overtopping volume, given in detail in the following chapter.

### 5.2.1 Calculation of the hydrokinetic quantities

The energy carried by the volume of water overtopping the cylinder consists of two components, the potential energy of the water mass and the kinetic energy of the water particles, respectively.

In order to carry out a calculation for the total energy, both potential and kinetical energy values have been assessed separately. With respect to the definitions used in Chapter 2.3, the potential energy of the water mass can be expressed as the product of the water volumes weight and the elevation of its center of gravity with respect to a reference level. The kinetic energy, on the other hand, can be achieved as the sum of each individual water particles mass times half of their total velocity.

To evaluate the energy of the overtopped water volume, the data achieved by the ultrasonic sensors US1 and US2 has been used. The series obtained from these sensors yield the time vs. elevation curves for the overtopping volumes. It is known that overtopping rates can be achieved from these measurements by using the mean propagation velocity as:

$$Q(t) = z(t)v(t) \tag{5.14}$$

With respect to the data measured, the known parameters in Eq. 5.14 is the mean overtopping rate $Q_{1m}$ and the water surface elevation vs. time curve, i.e. z(t). Thus, the velocity distribution should be researched. This has been achieved by using the mean propagation velocity of the crest and trough points of each individual water mass caused by the overtopping of each singular wave in the time series record.

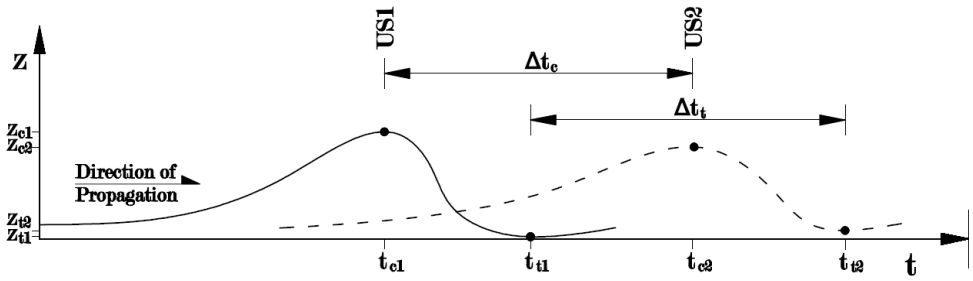


**Figure 5.19 :** Calculation of hydrokinetic quantities. Definition of terms used.

A sketch for the procession of data achieved from the US1 and US2 sensors as a plot of elevation vs. time series for a single overtopping volume is given in Figure 5.19, with the definition of key parameters used in the process mentioned here. The duration required for the propagation of the water mass from section US1 to section US2 has been measured both at the crest and the trough of the water mass, denoted as $\Delta t_c$ and $\Delta t_t$, respectively. In order to calculate $\Delta t_c$ and $\Delta t_t$, the crest and trough points on the water mass have to be captured with their elevation and time values, denoted by $z_{ci}$ and $z_{ti}$ for the elevation values and $t_{ci}$ and $t_{ti}$ for the time values, respectively. Here, the index i identifies the measurement location, i.e. 1 for US1 and 2 for US2.

It has been assumed that each trough point $z_t$ in a time series retrieved from a gauge indicate a separation between the water volumes of consecutive waves. By using a maxima - minima capture code, the time and elevation properties of crest and trough points have been extracted for each elevation-time series. Durations of the time series have been determined by using the optimum record times mentioned in Ch. 4.2. Mean and standard deviations of the properties $t_{ci}$, $t_{ti}$, $z_{ci}$ and $z_{ti}$ have been calculated by using their corresponding values for each individual wave in the analyzed time series record. Results indicate that the values are close for each individual overtopping volume under the same test (Table A.6), so a mean-value approach has been applied.

The crest and trough propagation velocities $v_c$ and $v_t$ have been calculated between sections US1 and US2 as the ratio of the distance between the sections to the travel duration needed for an overtopping volume to travel from section US1 to section US2. A comparative view of the calculated velocities is given in Figure 5.20.

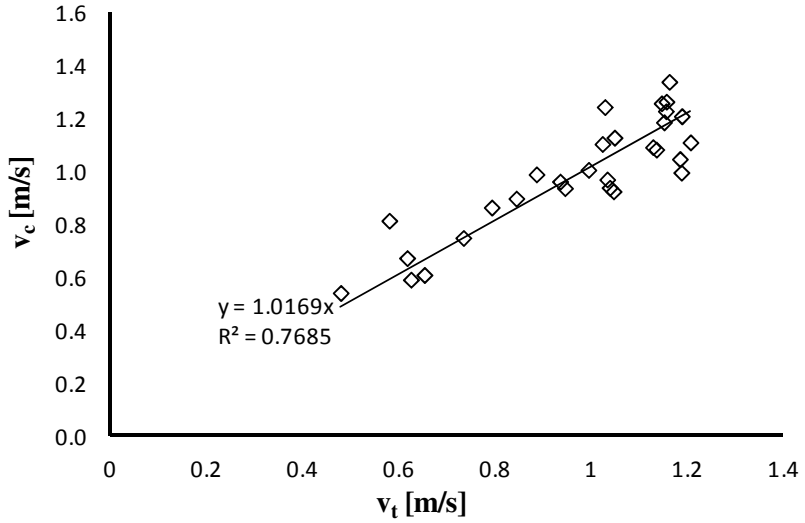


**Figure 5.20 :** Comparison of crest ($v_c$) and trough ($v_t$) propagation velocities.

Though there are differences between both crest and trough propagation velocities, their magnitude is not very large with a crest-to-trough velocity ratio remaining between 0.8 and 1.2 in all cases. Furthermore, while assumptions may be made such as a linear or exponential horizontal variation, there is no exact knowledge on the particle velocity distribution along the x-axis for any overtopping volume. Consequently, it has been assumed that the overtopping volume propagates with an average velocity v, calculated as the mean of crest- and trough velocities, equal along the whole x-axis of the volume. This assumption doubtlessly shall introduce some error to the values calculated, but a second improvement shall be carried out as explained below.

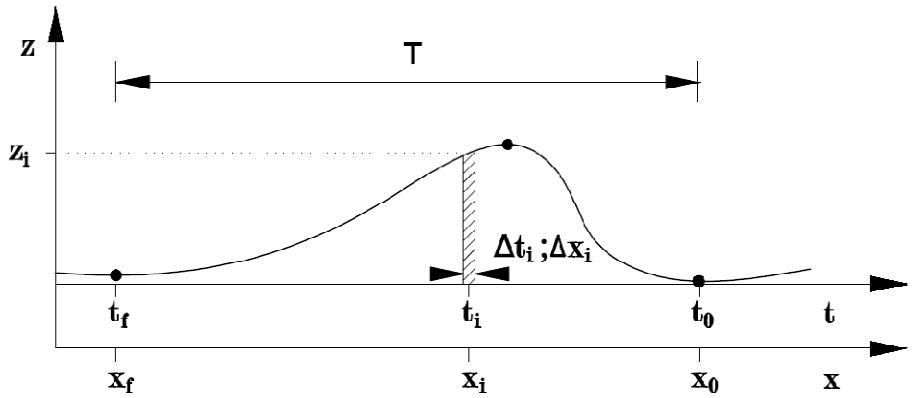


**Figure 5.21 :** Parameters used in the partial sum conversion.

By assuming an uniform propagation velocity along the whole overtopping volume, the time increment t of the time series can be converted to a distance-equivalent

value. Thus, the volume under the elevation-base width curve can be calculated. Theoretically this volume should yield the value of the mean overtopping rate achieved for the mentioned test. Rewriting Eq. 5.14 for the overtopping volume caused by one wave $Q_{1W}$ necessitates the evaluation of the following integral between the initiation time $t_0$ and finish time $t_f$:

$$Q_{1W} = \int_{t_0}^{t_f} z(t)v(t)dt \tag{5.15}$$

Since discrete data is present, we have to rewrite Eq. 5.15 in the partial sum form. For this case, an overtopping volume consists of N parts, where N is the number of measurements taken for the volume and is equal to the ratio of the wave period T to the sampling rate Δt (Fig. 5.21):

$$N = \frac{T}{\Delta t} \tag{5.16}$$

Thus, Eq. 5.15 becomes

$$Q_{1W} = \sum_{i=1}^{N} z_i \mathrm{v_i} \Delta t_i \tag{5.17}$$

Eq. 5.17, with this form, can be used for an accurate representation of the overtopping volume if velocity time series are known. For the current case, since a constant propagation velocity $\bar{v}$ assumption has been made and since the sampling intervals $\Delta t_i$ are constant, the base length for each part can be written as

$$\Delta x_i = v_i \Delta t_i = \bar{v} \Delta t \tag{5.18}$$

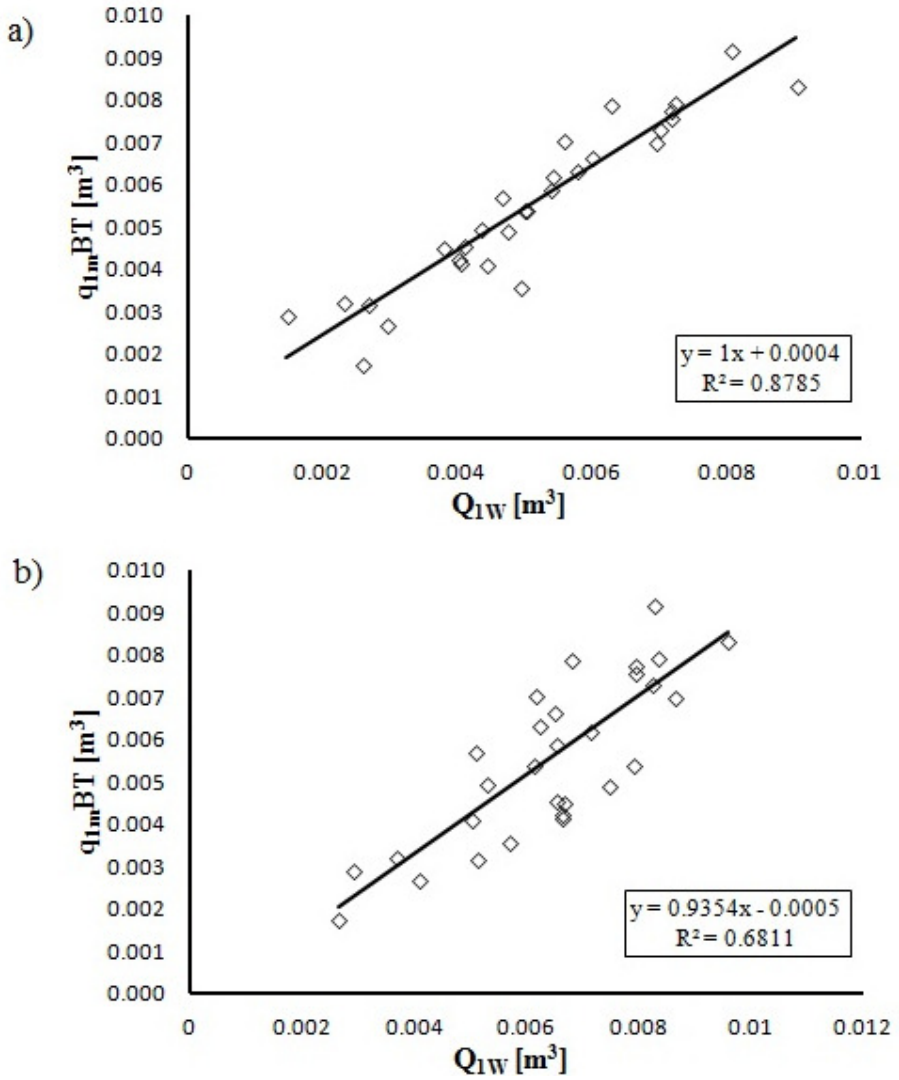


**Figure 5.22 :** Relation between overtopping volumes retrieved from mean overtopping rates ($q_{1m}BT$) and area-based calculation ($Q_{1W}$: s. Eq.5.19).

By substituting Eq. 5.18, Eq. 5.17 can be simplified further to

$$Q_{1W} = \Delta x_i \sum_{i=1}^{N} z_i \qquad \textbf{(5.19)}$$

By using Eq. 5.19, the measured elevation - time series have been converted to the elevation - base length series at both sections. Achieved results have been compared with the calculated mean overtopping rates. Shown in Fig. 5.22, the results indicate a fairly good agreement for the measurement location at US1 (Fig. 5.22(a)), whereas there is a fair amount of scattering at the measurement location US2 (Fig. 5.22(b)).

However, in order to take the effect of reshaping of the overtopping volume into account, an improvement has been carried out. For this purpose, the centroids of both

overtopping volumes measured at sections US1 and US2 have been used. The coordinates of the centroids ($x_G$; $z_G$) have been calculated by taking the statical moments of the overtopping volumes at both x- and z- axis, defined by the following equation set:

$$z_G = \frac{\sum z_i x_i \left(\frac{z_i}{2}\right)}{\sum z_i \Delta x_i}$$
$$x_G = \frac{\sum z_i \Delta x_i (x_i)}{\sum z_i \Delta x_i} \qquad \textbf{(5.22)}$$

Having used Eq. 5.22 for both locations US1 and US2, the coordinates of the centroid for each overtopping volume have been evaluated. The shift in the centroid location has been used to define a "corrected travel distance" $\Delta x_G$ (Figure 5.23). Propagation velocities hence have been recalculated by using the value of " $\Delta x_G$ and the corresponding time interval $\Delta t_G$.

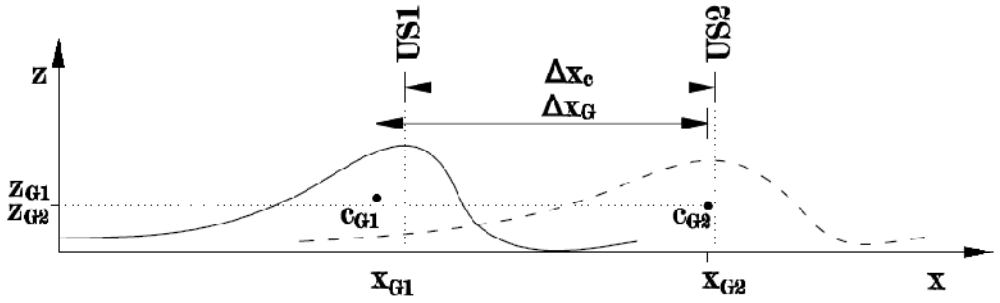


**Figure 5.23 :** Change of travel distance by introducing the centroids.

The comparison of the $Q_{1W}$ volumes calculated by using centroid displacements and the overtopping volumes retrieved from mean overtopping rates is given in Figure 5.24. As seen, the correlation has increased following this modification.

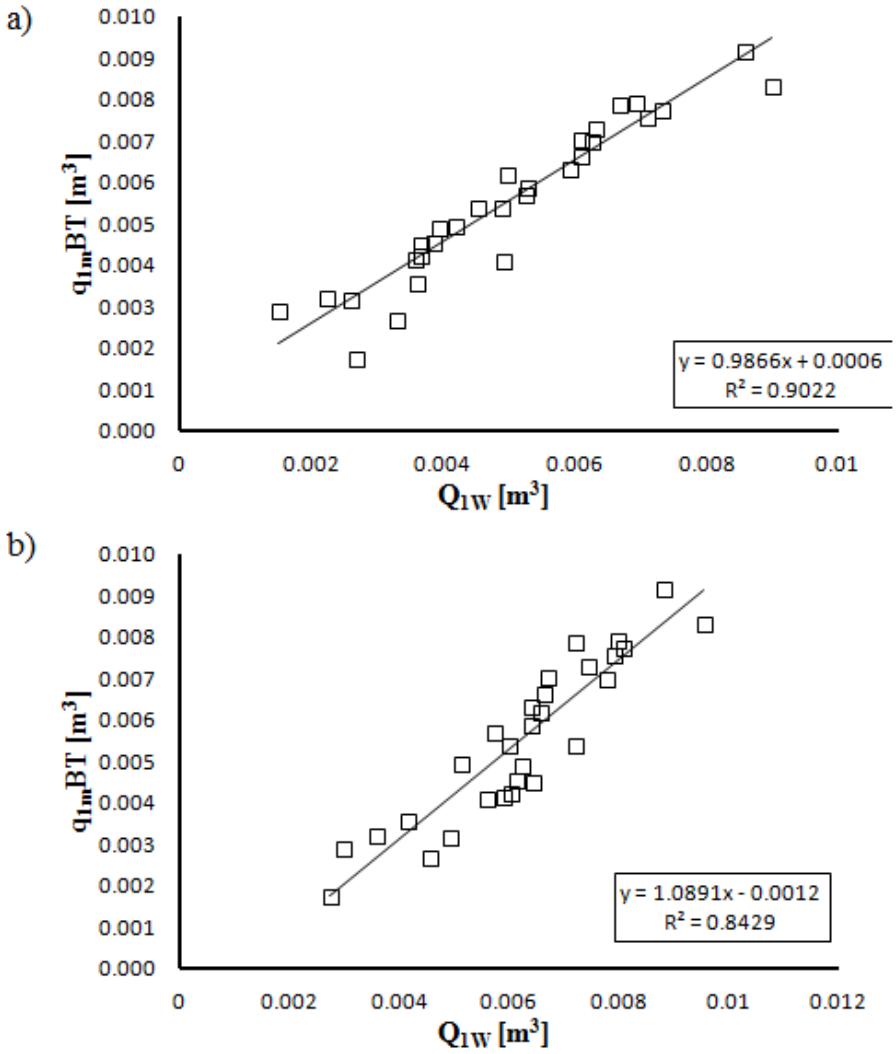


**Figure 5.24 :** Comparison of overtopping volumes after the centroid displacement correction, (a) US1, (b) US2.

### 5.2.2 Calculation of potential energy

The calculation of the potential energy necessitates the spatial distribution data of the overtopping volume, which has been assessed in the previous section. The values henceforth are calculated by using the section US1 and by assuming previous assumptions valid. For this case, the potential energy $E_P$ has been calculated in a similar way as it had been shown for a sine wave in Section 2.3.

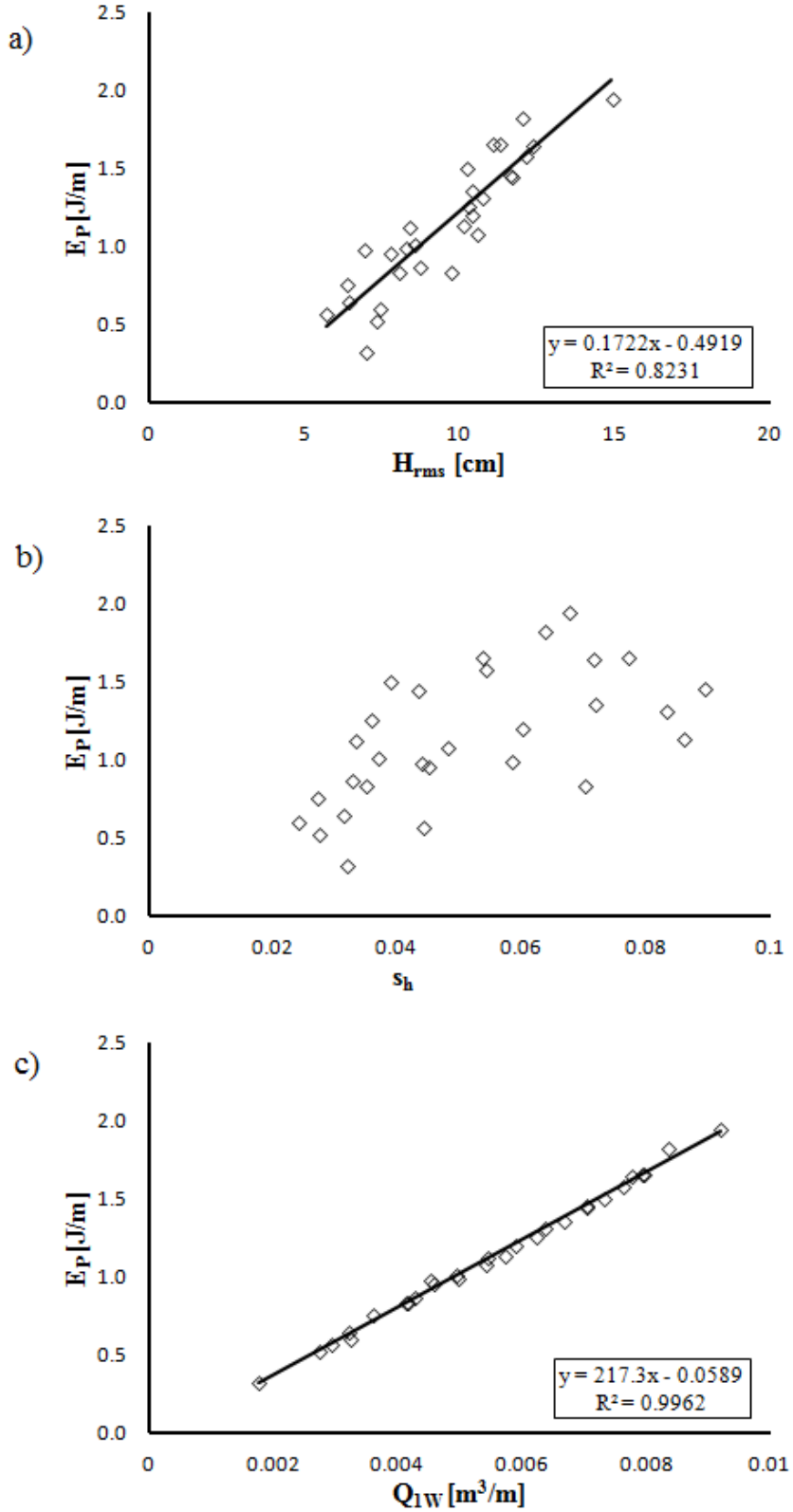


**Figure 5.25 :** Variation of potential energy per wave $E_P$ with (a) RMS wave height, (b) wave steepness and (c) overtopping volume per wave.

Potential energy values have been calculated with respect to the mean water level. Rewriting Eq. 2.22 with respect to MWL reference level for this case yields

$$E_P = \rho g \sum_{i=1}^{N} z_i \Delta x_i \left(\frac{z_i}{2} + F\right) \quad \textbf{(5.23)}$$

Since the location of the centroid $c_G$ is known, Eq. 5.23 further simplifies to

$$E_P = \rho g A_Q z_G \left(\frac{z_G}{2} + F\right) \quad \textbf{(5.24)}$$

Here, $A_Q$ is the cross section area of the overtopping volume for one incident wave. It should be noted that the calculated values belong to a one-wave duration.

The variation of potential energy carried per wave cycle with wave height is given in Figure 5.25(a). As seen, potential energy increases with increasing wave height, and a linear relationship may be defined. In Fig. 5.25(b), the variation of potential energy with wave steepness is given. Disregarding the scattering, it can be stated that potential energy intrusion increases with increasing wave steepness. However, there is a decrease for very steep waves, which should be caused due to the nonlinearity and fast dispersion reducing the maximum elevation in the overtopping volume. The variation of potential energy with overtopping volume per wave cycle is shown in Fig. 5.25(c), indicating a perfect linear relationship. It can also be argued from Fig. 5.25(c) that the variation of the centroids vertical coordinate may be omitted.

### 5.2.3 Calculation of kinetic energy

A similar approach has been used in the calculation of the kinetic energy $E_K$ rather than using the whole integrals along the overtopping volume, based on the uniform velocity assumption. Thus, kinetic energy for the overtopping volume has been expressed as:

$$E_K = \frac{1}{2} \rho A_Q v_G^2 \quad \textbf{(5.25)}$$

The variation of total kinetic energy contained in the overtopping volume per wave ($E_K$) with incident RMS wave height is shown in Figure 5.26(a). Again, kinetic energy increases with increasing wave height to be described either in a linear or an exponential trend.

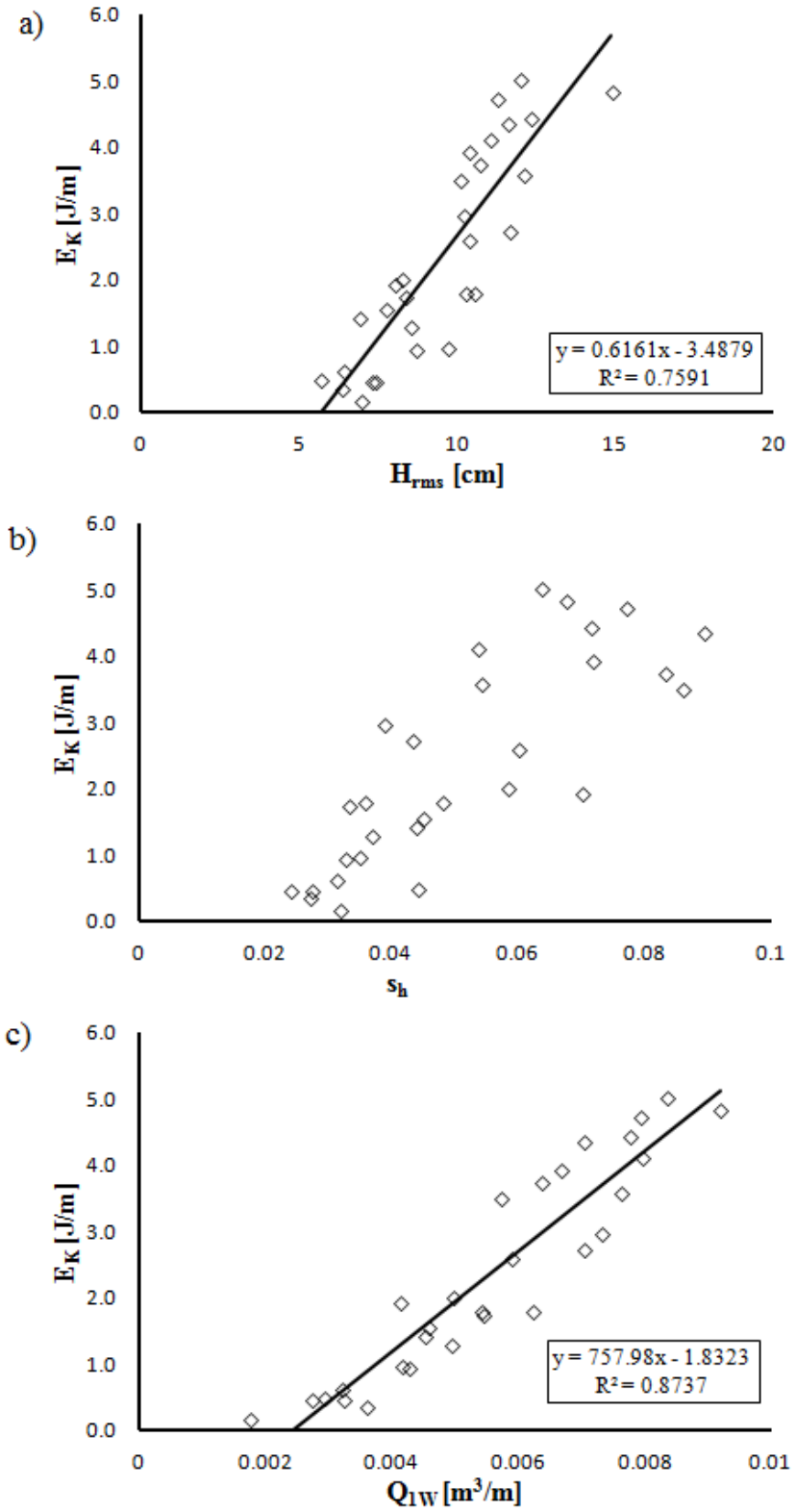


**Figure 5.26 :** Variation of kinetic energy per wave $E_K$ with (a) RMS wave height, (b) wave steepness and (c) overtopping volume per wave.

Fig. 5.26(b) shows the variation of kinetic energy with wave steepness. There is an increase with increasing wave steepness, but a significant amount of scattering is observed. The variation of kinetic energy with the overtopping volume per one wave cycle is given in Fig. 5.26(c), again showing a close-to-linear fit. The refinement of the given curves can be made by assuming a bi-linear or an exponential trend, but more data is needed for small overtopping volumes.

### 5.2.4 Calculation of power captured

Power captured by the system has been calculated as the mean power retrieved from both energy components calculated in the previous sections. This has been achieved by dividing the energy values contained in each wave cycle to the mean wave period values:

$$P_K = \frac{E_K}{T_m};\ P_P = \frac{E_P}{T_m} \tag{5.26}$$

The variation of mean captured power due to the potential energy $P_P$ of the overtopping volume with the RMS wave height is given in Figure 5.27(a). Again, it can be observed that $P_P$ increases with increasing wave height, but there is a large amount of scattering. The variation of $P_P$ with wave steepness (Fig. 5.27(b)) also shows a linear trend, but this curve can also be expressed as a bilinear or logarithmical curve if the point at 0.072, 0.908 is excluded. Conclusively, variation of $P_P$ with the mean overtopping rate (Fig. 5.27(c)) is plotted, showing a perfect linear trend as expected.

The variation of the mean captured power due to kinetic energy $P_K$ of the overtopping volume with governing parameters is given in Figure 5.28. From Fig. 5.28 it is observed that the effects of wave height, wave steepness and mean overtopping rate on kinetic energy based power component are similar to the case for the potential energy based power.

### 5.2.5 Hydraulic efficiency

In order to calculate the hydraulic efficiency of the system, the power values calculated in Chapter 5.2.4 have been divided to the incident wave power, calculated by Eq. 2.41. The results are given in Figure 5.29.

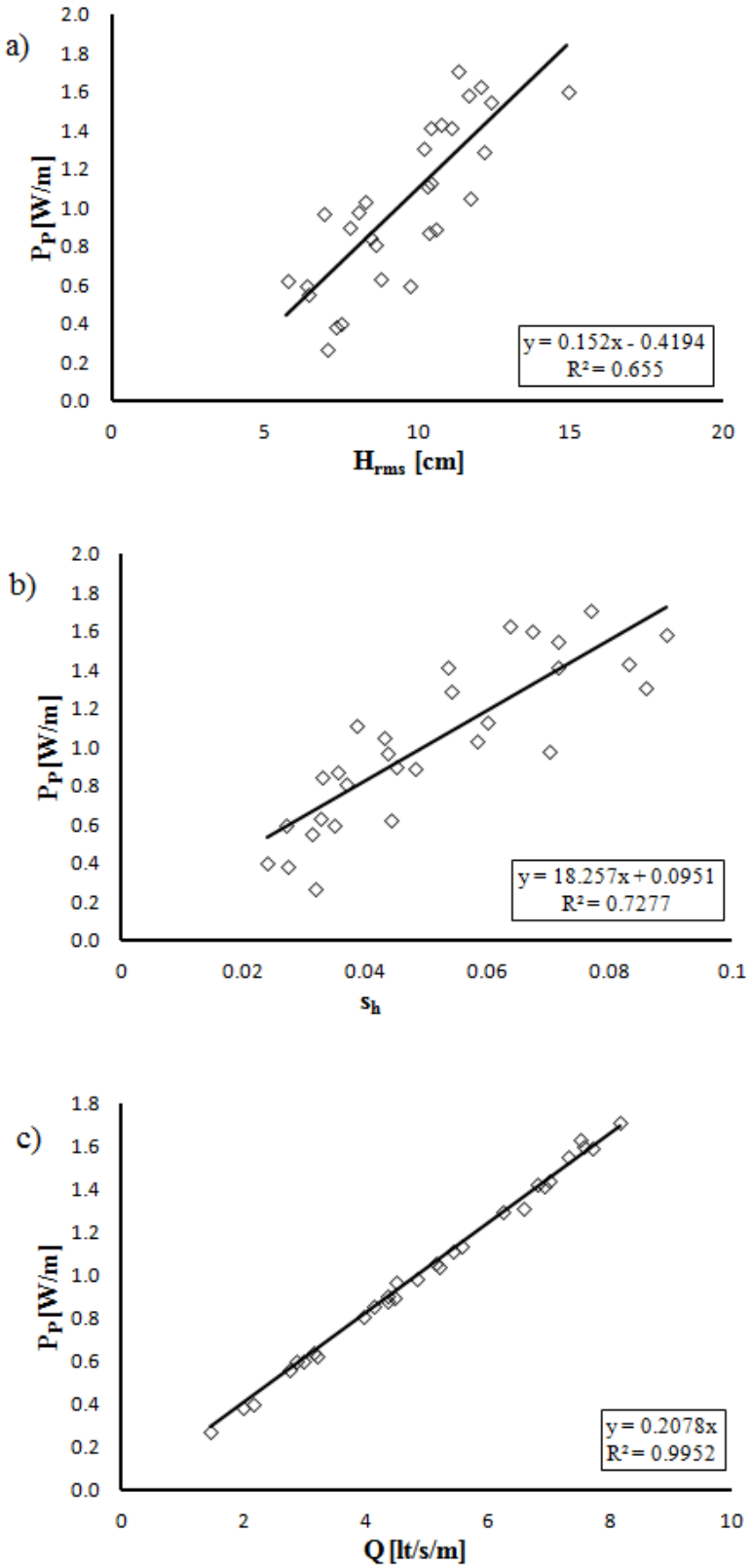


**Figure 5.27 :** Variation of mean power captured due to potential energy $P_P$ with (a) RMS wave height, (b) wave steepness and (c) mean overtopping rate.

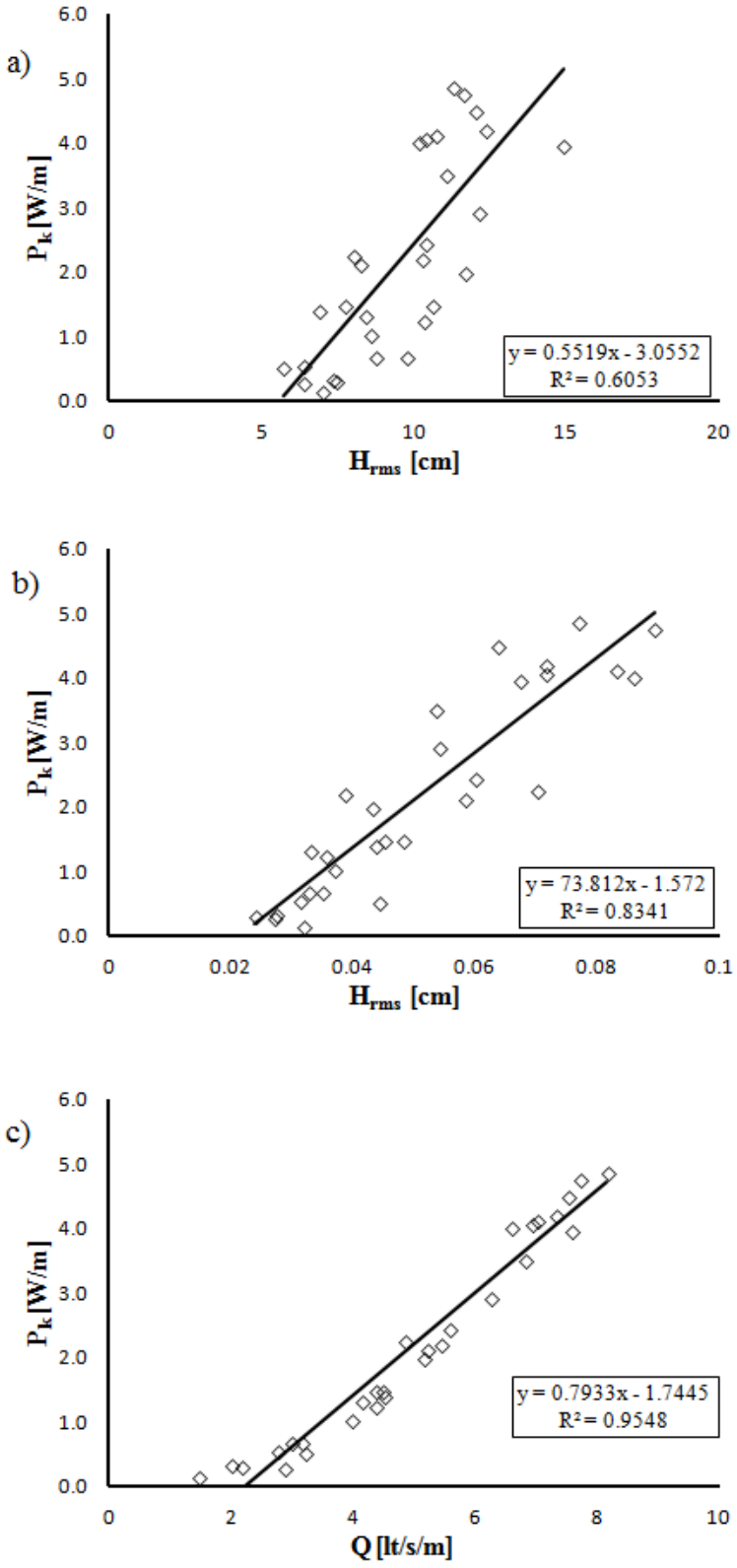


**Figure 5.28 :** Variation of mean power captured due to kinetic energy $P_K$ with (a) RMS wave height, (b) wave steepness and (c) mean overtopping rate.

Hydraulic efficiency has been defined by three different approaches. In the first one, the total efficiency has been calculated by taking the sum of the mean powers calculated with respect to the potential and kinetic energy components. A second definition has been given as the hydraulic efficiency calculated by taking only the kinetic energy component into account, and a third definition is based on the potential energy component.

By using the total efficiency, the variation of hydraulic efficiency has been plotted by sorting the data into groups with equal relative wave heights. The effect of wave steepness on hydraulic efficiency is shown in Figure 5.29(a), clearly indicating that the efficiency of the system increases with increasing wave steepness. Another plot, obtained by using the relative width parameter (i.e. diffraction parameter) defined as the ratio of the cylinder diameter to the wavelength (Figure 5.29(b)) indicates the same trend. The variation of hydraulic efficiency with the mean overtopping rate has been plotted in Figure 5.29(c). A power or exponential trend can be observed on this diagram. A last diagram (Figure 5.29(d)), showing the variation of hydraulic efficiency has been plotted against the volumetric dimensionless discharge $Q_V$. This diagram clearly shows a best-fit, which has been inspected further to derive an empirical formula for the prediction of hydraulic efficiency.

The result mentioned above is quite interesting if one inspects the meaning of the volumetric dimensionless discharge. The volumetric dimensionless discharge $Q_V$ is the ratio of the overtopped water volume per wave to the volume of water carried in the crest of a wave. Thus, the parameter itself can be classified as a sort of efficiency parameter for the overtopping rates. In other words, we can state that the power efficiency of an overtopping device is directly related to its overtopping efficiency.

An empirical relationship between the hydraulic efficiency and volumetric dimensionless discharge has been researched. It has been found out that an exponential equation fits the data well. Thus, following equation has been developed for the total efficiency $\chi_T$:

$$\chi_T = 0.0289 exp(9.776 Q_V) \qquad \textbf{(5.27)}$$

Eq. 5.27 showed a very good fit to the dataset with an average relative error of $\varepsilon_{r,0} = 0.8\%$ and a correlation coefficient of $R^2 = 0.9779$.

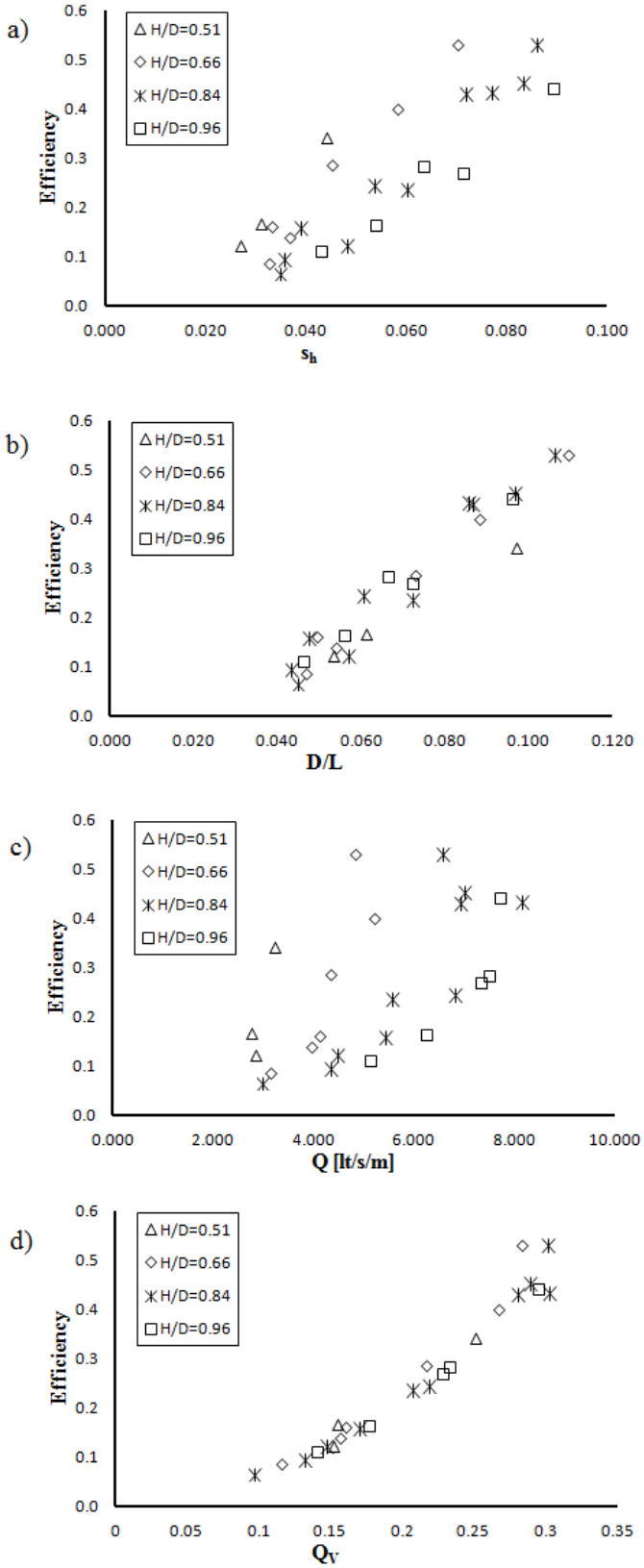


**Figure 5.29 :** Variation of efficiency with (a) wave steepness, (b) relative width,(c) mean overtopping and (d) dimensionless volumetric discharge.

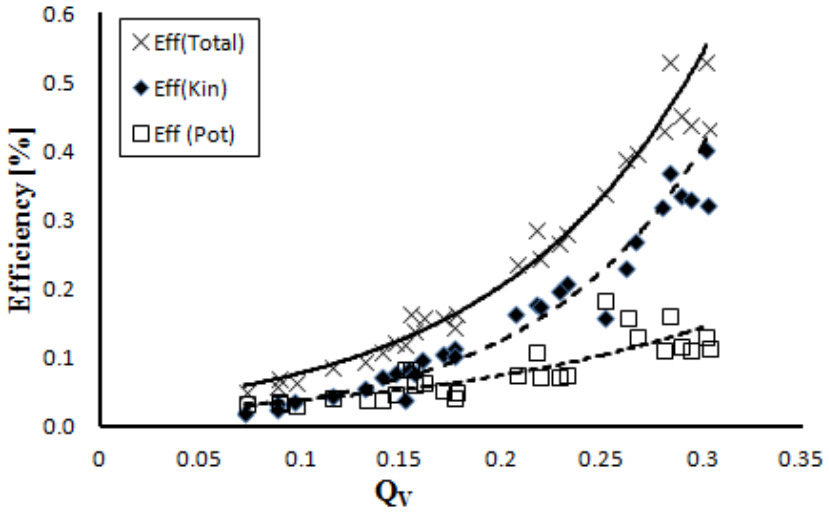


**Figure 5.30 :** Efficiency as a function of volumetric dimensionless discharge.

The variation of hydraulic efficiency with the dimensionless volumetric discharge rate has been plotted in Figure 5.30. The three curves given belong to the efficiency ratios calculated for the total, kinetic and potential energy amounts, respectively. From Figure 5.30 it can be concluded that the hydraulic efficiency of the system can reach values of 50% for volumetric dimensionless discharge rates over 25%. The contribution of kinetic energy to hydraulic efficiency also increases with increasing values of $Q_V$.

## 5.3 Performance of a Tethered Trimaran Floating Pipe Breakwater

### 5.3.1 Wave transmission

#### 5.3.1.1 Performance comparison for configurations FB1, FB2 and FB3

The values of the transmission coefficients calculated by applying zero-crossing analysis were given in Table B.6. Now let us check the variation of the transmission coefficients with governing parameters and the variations between the three configurations.

The variation of the transmission coefficient with the relative width parameter is given in Figure 5.31(a) for all three configurations. From Figure 5.31(a) it can clearly be observed that wave transmission decreases with increasing relative width. A very interesting point is the rate of decrease observed on the three configurations, which

clearly indicates that configuration FB1 has a higher wave attenuation performance. At first sight, this might be counted as an unexpected outcome, however, the result is closely related to the interaction between the cylinders. As one may expect from general hydrodynamics, reducing the distance between individual pipes increases the size of the section working together, i.e. the flow in the wake of a cylinder is affected due to the presence of the adjacent cylinder. Increasing the distance between the cylinders however tends to let each cylinder act as independent units. Thus, by searching an optimum distance between the cylinders, the interaction effect should be considered.

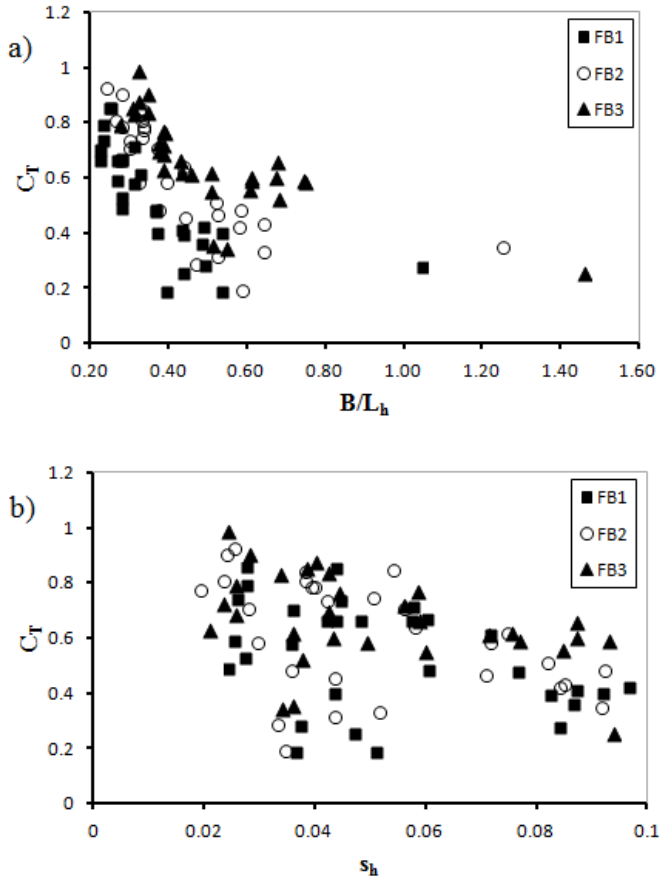


**Figure 5.31 :** Variation of transmission coefficient with wave height for fixed relative width for (a) FB1, (b) FB2 and (c) FB3.

Figure 5.31(b) shows the variation of the transmission coefficients with the incident wave steepness. A decrease of the transmission coefficient with increasing wave steepness is observed, while a depression zone is evident around $s_h = 0.05$. Points in this zone, also present on Figure 5.31(a), constitute the narrow range, where the natural frequency of the floating breakwater collides with the wave frequency, thus

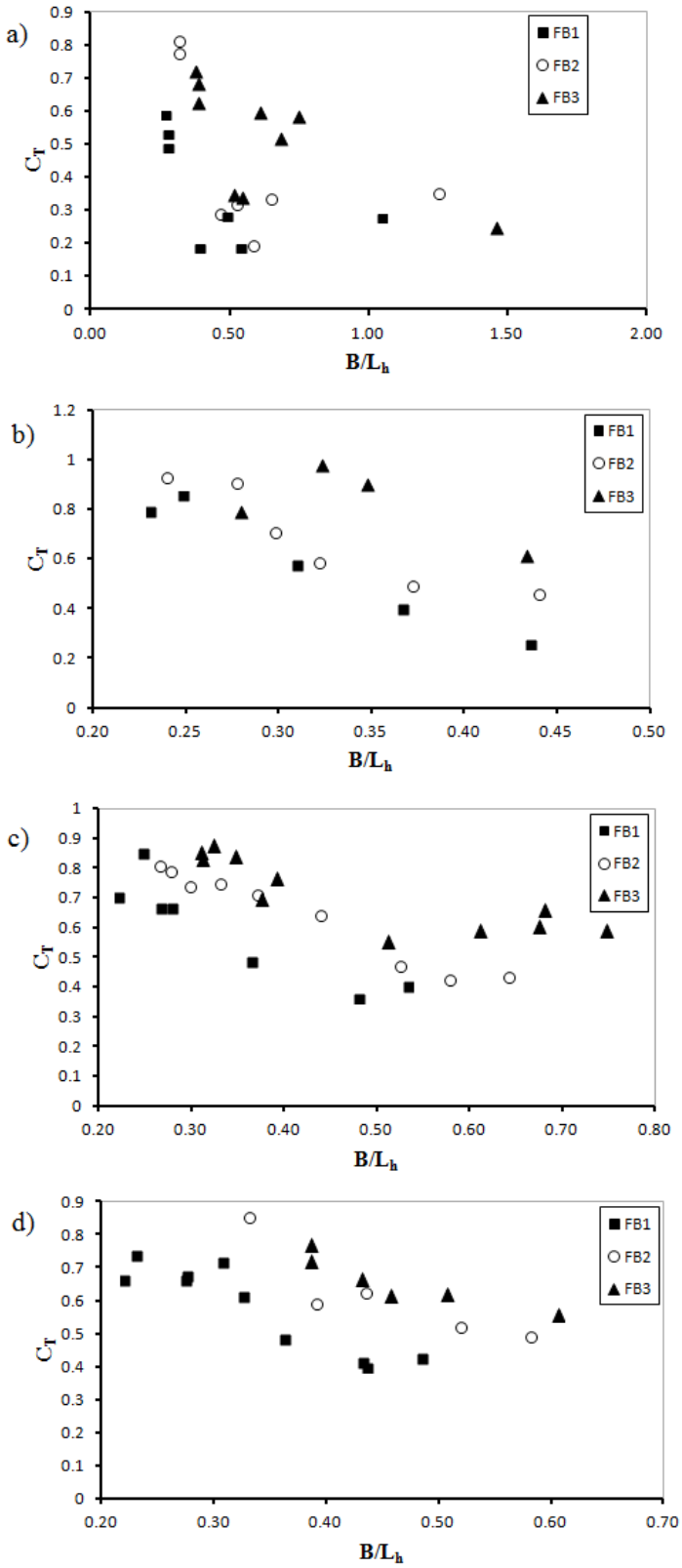


**Figure 5.32 :** Comparison of transmission coefficients. Variation with relative width for (a) H/D=0.45, (b) H/D=0.55, (c) H/D=0.82 and (d) H/D=1.02.

the structure generated radiation waves neutralize the transmitted and incident wave trains.

Both diagrams on Figure 5.31 indicate that FB1 shows a higher wave attenuation performance. In order to take a closer view, the data has been divided into subgroups of waves of equal height, classified according to the relative wave height, defined as the ratio of the incident wave height to the diameter of the cylinder. By using sorted data, Figs. 5.32-5.34 have been plotted.

In Figure 5.32, the variation of transmission coefficients with relative width is given under fixed relative wave height values. The wave height values conseutively increase from Fig. 5.32(a) to (d), bearing values of $H_{rms}/D$=0.45, 0.57, 0.85 and 1.01, respectively. Figure 5.32 indicates that transmission coefficients decrease with increasing values of relative width for all relative wave heights. Figure 5.32 clearly indicates that the performance of configuration FB1 is higher compared to configurations FB2 and FB3. The regions of performance stated by Gaythwaite (2004) are also clearly visible in the diagrams with transmission coefficients showing a high increase rate for the values of B/L smaller than 0.50 for waves with a relative height of H/D = 0.45. In a similar way, transmission coefficients for all configurations are seen below 0.4 for relative width values higher than 1.00 at the same relative wave height level. An increase in relative wave height to H/D=0.55 indicates that even at smaller values of B/L such as 0.35, the transmission coefficient is around 0.40 for configuration FB1, increasing to 0.50 for FB2 and approx. 0.65 for FB3. In case of larger wave amplitudes such as H/D=0.82, the relative width value of B/L=0.50 indicates a change in wave transmission with transmission coefficients being larger than 0.40 for smaller relative width values for configuration FB1 and 0.60 for FB3, respectively and remaining along these values for higher relative width values. It has been observed that increasing the relative wave height further to 1.02 has minor effect on transmission coefficients, since Figure 5.32(d) shows a similar trend to Figure 5.32(c).

It is obvious that in Figure 5.32 the breakwater width, calculated as the distance between the vertial tangents at the outer boundaries of the fore and aft cylinders, affects the trends. In order to give a refined diagram can be given by taking a second relative width parameter into account, defined as the ratio of the cylinder diameter to the incident wavelength. Thus, performance can be inspected as a function of the

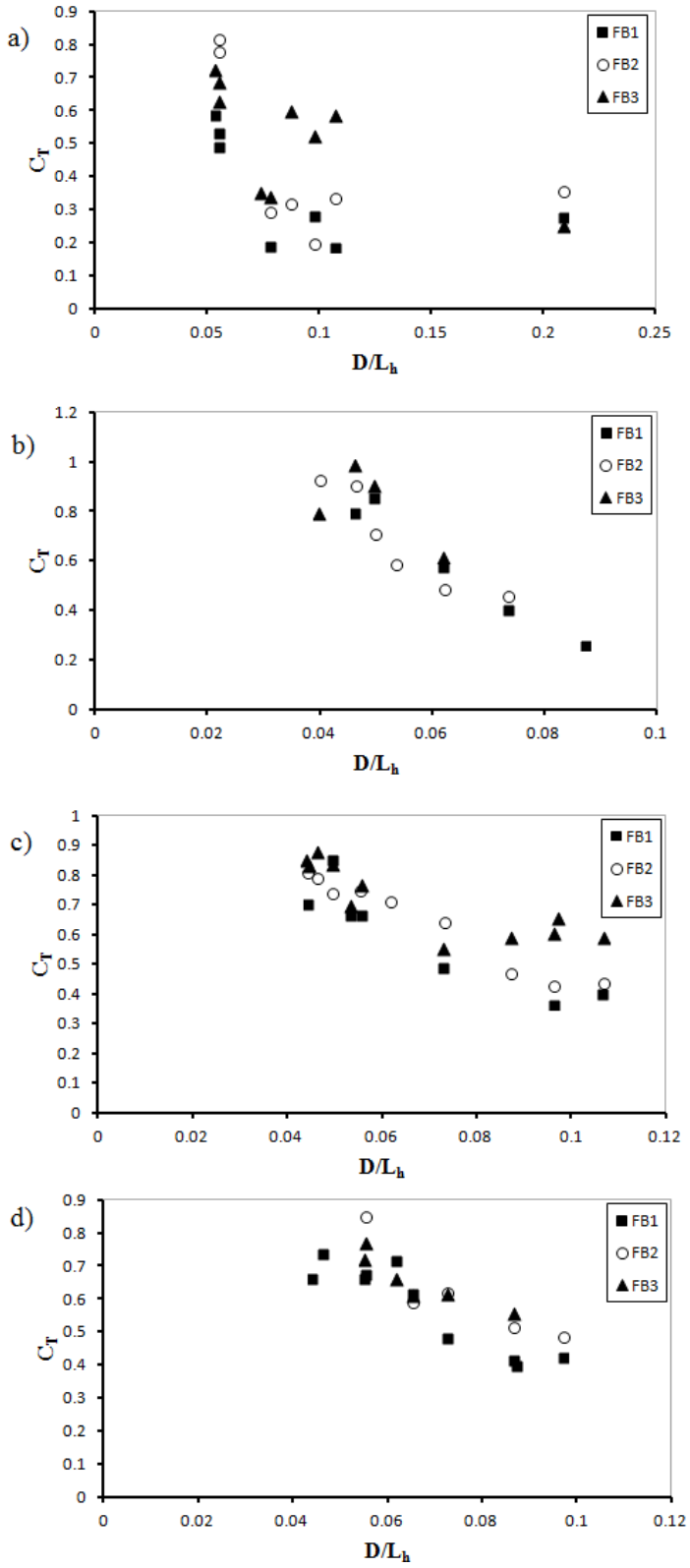


**Figure 5.33 :** Comparison of transmission coefficients. Variation with diffraction parameter for (a) H/D=0.45, (b) H/D=0.55, (c) H/D=0.82 and (d) H/D=1.02.

wavelength, disqualifying the width parameter varying for each configuration. Such a plot of the diagrams given in Figure 5.33. As seen in the figure, the performance of all configurations decreases with increasing wavelength, and the wave attenuation capacity of configuration FB1 is higher for all relative wave heights.

Figure 5.34 shows the variation of transmission coefficients with incident wave steepness $s_h$ calculated at the depth of the structure. In all relative wave height ratios it is obvious that increasing wave steepness leads to a decrease in transmitted waves. However, a drop in the decrease rate is observed as the relative wave height increases from $H_{rms}/D = 0.55$ to $H_{rms}/D = 0.82$.

A different group of diagrams has been prepared by keeping the relative width values constant and plotting the variation of transmission coefficients with respect to incident wave height. Shown in Figure 5.35, it is obvious that the wave transmission increases with increasing wave height for all cases with a threshold value, over which the transmission coefficient remains almost constant. This is expected to be caused by wave instability and triggering of wave breaking due to very high wave steepness values. For very small B/L values, the wave transmission is almost constant and independent from wave height, indicating the inefficiency of the structure as expected.

Checking all three diagrams in Figure 5.35, it is evident that configuration FB1 has a higher performance in all the compared relative widths. As a consequence, further research on wave transmission and mooring forces has been carried out for the configuration FB1 only.

By keeping the relative wave height values fixed, the variation of transmission coefficients with relative width is given for configuration FB1 in Figure 5.36 as a complement to Figure 5.35(a). It is shown that for all relative wave height values, the transmission coefficient decreases with increasing relative width, with its value increasing as the relative wave height value increases for a fixed relative width.

Based on the output received in this section, empirical formulae to predict wave transmission coefficients for configuration FB1 have been developed in the following section.

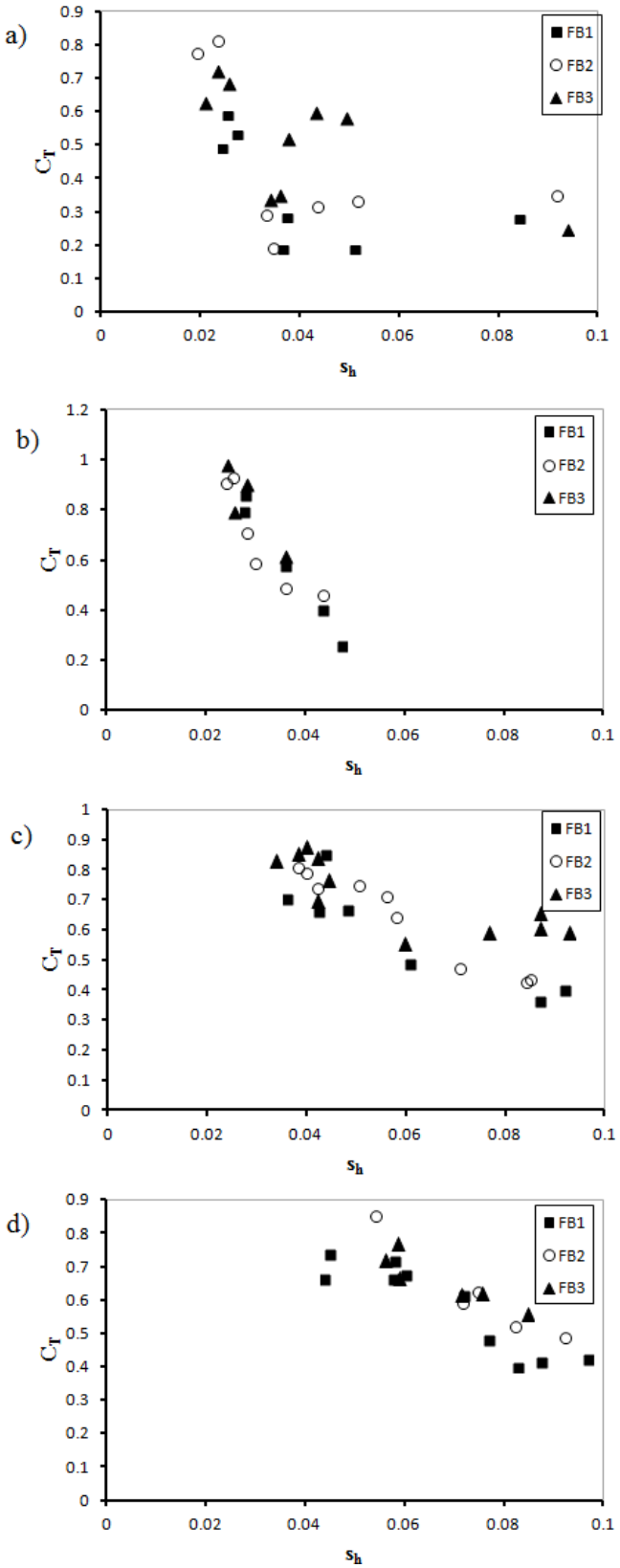


**Figure 5.34 :** Comparison of transmission coefficients. Variation with wave steepness for (a) H/D=0.45, (b) H/D=0.55, (c) H/D=0.82 and (d) H/D=1.02.

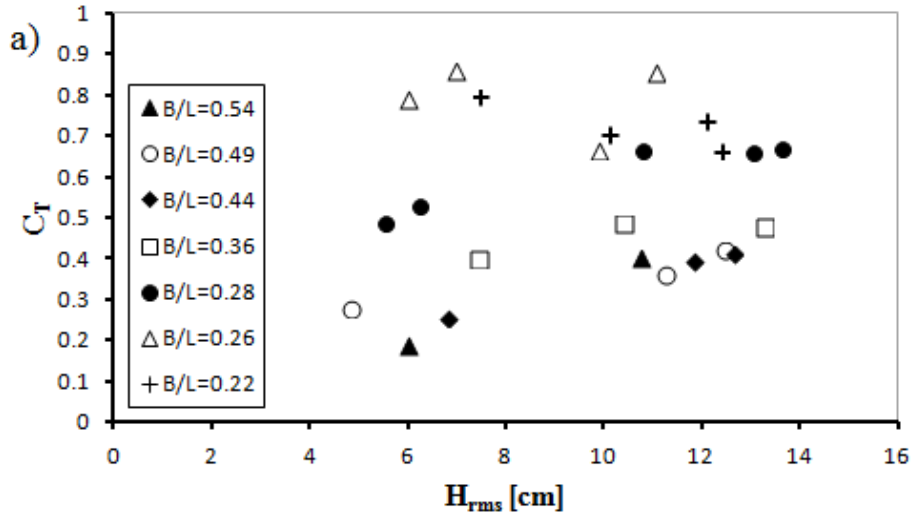


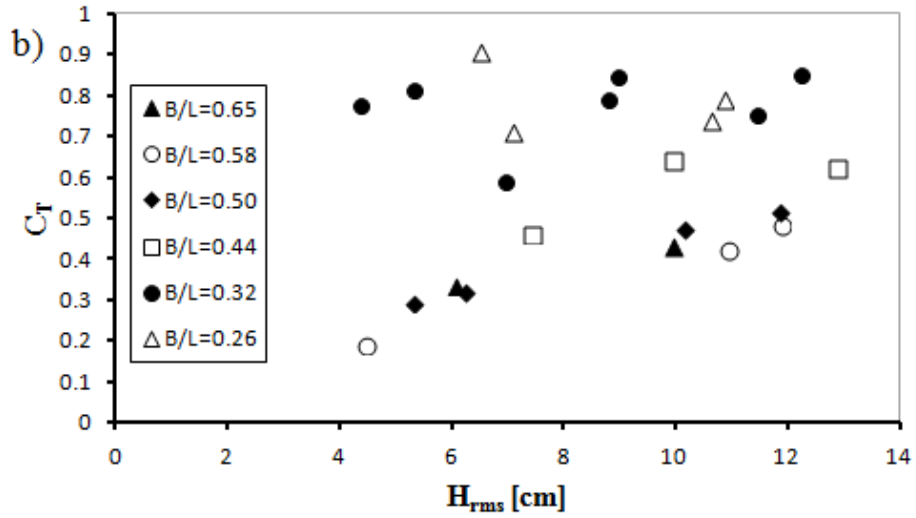


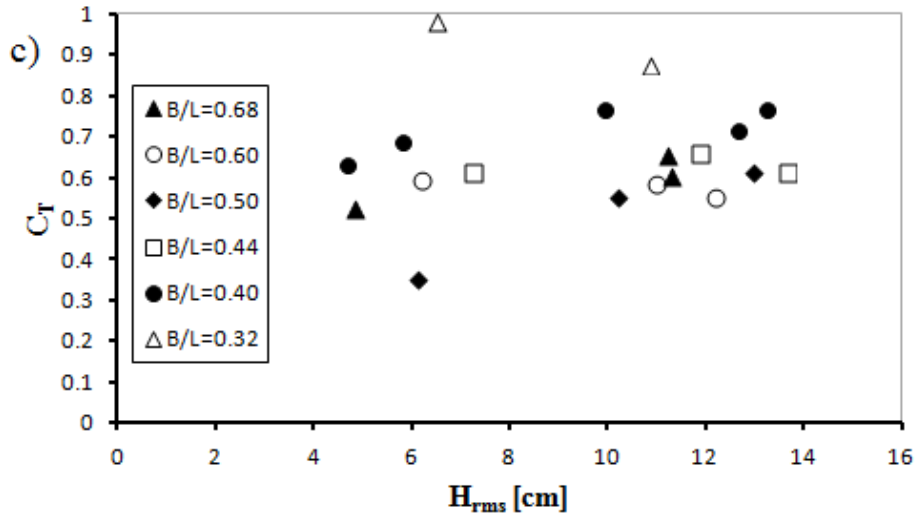


**Figure 5.35 :** Variation of transmission coefficient with wave height for fixed relative width for (a) FB1, (b) FB2 and (c) FB3.

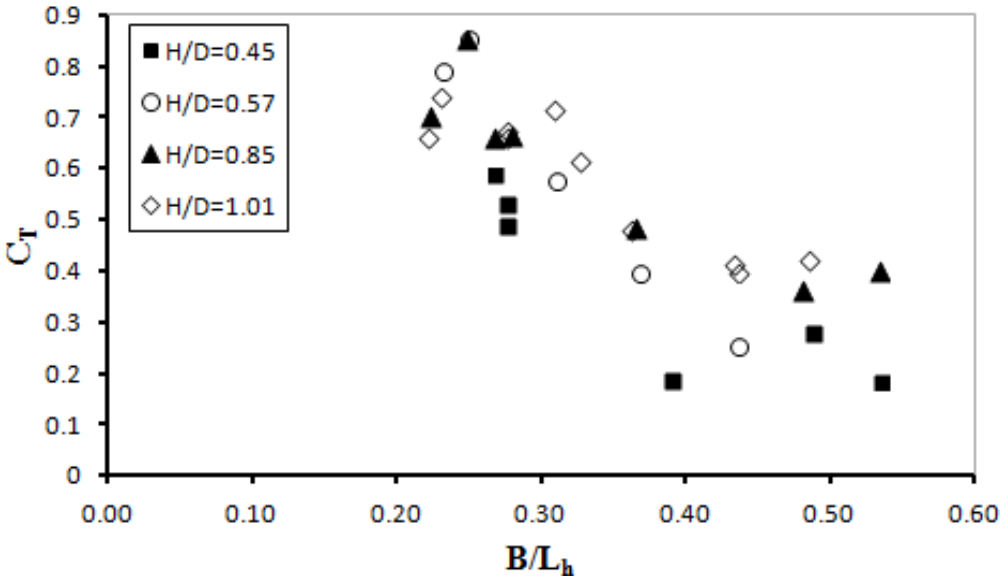


**Figure 5.36 :** Variation of transmission coefficient with relative width for fixed relative wave heights. Configuration FB1.

#### 5.3.1.2 Development of empirical transmission formula

In order to simplify the comparative study to be carried out during the efficiency assessment of the hybrid device, development of an empirical formula for the prediction of wave transmission has been found useful. In a previous study (Akgul and Kabdasli, 2012), it has been observed that a power function can be written between the transmission coefficient and governing parameters such as the relative width and wave steepness to predict the wave transmission. Here, an exponential expression has been searched to predict wave transmission, and the drop zone for the transmission coefficient around the wave period of T=0.91s has been ignored, remaining on the safe side.

Different combinations have been studied with the variables taken as the relative width $B/L_h$, wave steepness $s_h$ and relative wave height $H_{rms}/D$. The best-fit curve has been obtained for the expression given below ($R_M^2 = 0.903$; $\varepsilon_{a,0} = 0.061$; $\varepsilon_{r,0} = 13\%$):

$$C_T = 1.506 exp\left(9.24 s_h - 4.647 \frac{B}{L_h}\right) \quad \textbf{(5.28)}$$

Though one may anticipate the effect of wave steepness given in Eq. 5.28 as increasing the transmission coefficient values. However, since the equation already contains the relative width parameter, the effect of wave steepness parameter acts as a dimensionless writing of the wave height effect.

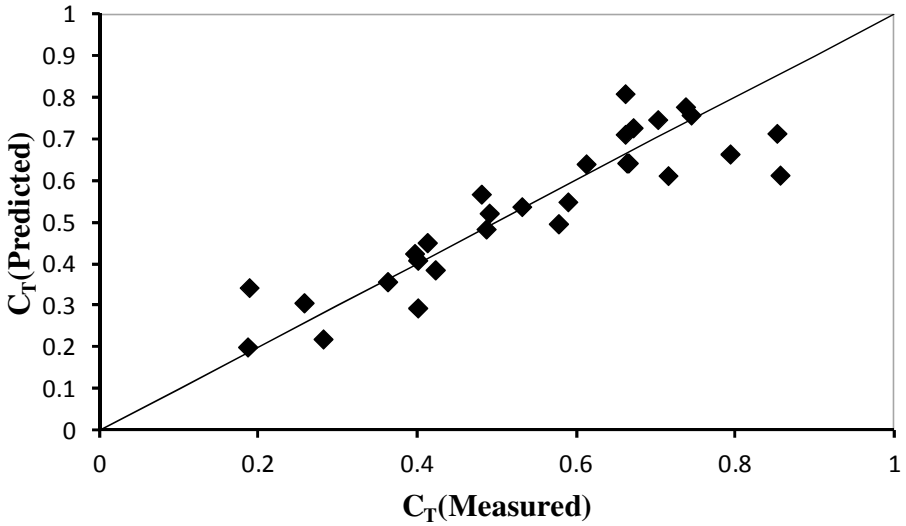


**Figure 5.37 :** Comparison of measured and predicted transmission coefficients.

The goodness-of-fit of Eq. 5.28 has been shown in Figure 5.37. While the formula seems sufficient to predict wave transmission for a wide range of data, it overpredicts for waves with high transmission property.

Another similar formula with the variables chosen as the relative width $B/L_h$ and the relative wave height $H_{rms}/D$ is as follows ($R_M^2$=0.887; $\varepsilon_{a,0}$ = 0.066; $\varepsilon_{r,0}$ = 14%):

$$C_T = 0.96exp\left(0.60\frac{H_{rms}}{D} - 3.28\frac{B}{L_h}\right) \quad \textbf{(5.29)}$$

Measured and predicted transmission coefficients by using Eq. 5.29 have been plotted in Figure 5.38.

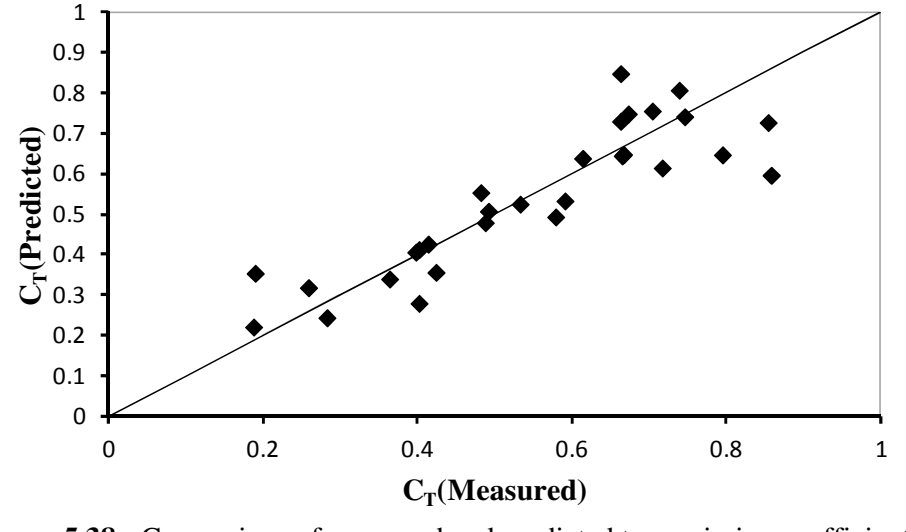


**Figure 5.38 :** Comparison of measured and predicted transmission coefficients.

#### 5.3.1.3 Application of Macagno's formula

As a second approach, the formulation (Eq. 2.10) of Macagno (1953) has been applied to all three configuration with an aim to inspect the effective width and draft values. As an initial attempt, actual width and draft values of the configurations have been written to the equation. In the following, a solution has been searched, giving the smallest mean relative error by changing the width of the structure. This way, an equivalent structure width has been defined for a comparison with an equivalent rectangular structure. The results have been evaluated by using the mean draft value for the cylinders (i.e. d=135mm). It is interesting to note that for this draft value, the exact width of configuration FB1 yielded the best fit (Figure 5.39).

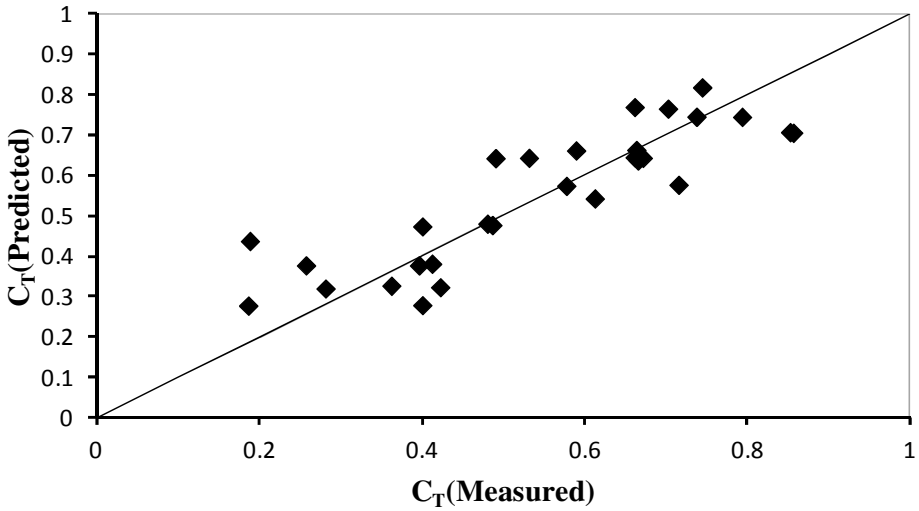


**Figure 5.39 :** Goodness-of-fit of Macagno's equation (Eq. 2.10) for config. FB1.

The equivalent rectangular width values $B_{eff,r}$ calculated for configurations FB2 and FB3 according to Eq. 2.10 are however much smaller than their actual widths. An efficiency loss ratio $\lambda_B$ has been defined as the ratio of the actual width to the ratio of the effective width for these configurations, indicating that the effective width drops to 67% for Configuration FB2 and 53% for Configuration FB3. Details are given in Table B.7.

### 5.3.2 Mooring forces

The mooring forces have been calculated for the configuration FB1 only. First, a theoretical inspection has been carried out to identify the hydrodynamic flow regime. For this purpose, water particle velocities and accelerations at the center of the cylinders have been calculated by assuming linear wave theory valid. Keulegan-

Carpenter Number (KC), Reynolds number ($N_{RE}$) and diffraction parameter (kr) have been evaluated in the following by using the cylinder diameter as the reference width. As known, KC number is the ratio of the maximum horizontal amplitude of a water particle oscillating under wave motion to the characteristic dimension of the obstacle. In the existing case, the obstacle has been defined as one cylinder, hence the diameter of the cylinder D has been used during the calculation of KC numbers as stated below:

$$KC = \frac{u_m T_m}{D} \tag{5.30}$$

Reynolds number for the cylinder has been calculated by Eq. 5.31:

$$N_{RE} = \frac{u_m D}{\nu} \tag{5.31}$$

Values of the KC number, Reynolds number and diffraction parameter calculated for the wave series tested are given in Table B.8. As seen, in all cases, the value of KC remains between 0.85 and 3.23 and Reynolds numbers vary between $1.6 \times 10^4$ and $4.4 \times 10^4$. Inspecting this range for the oscillatory flow case, one can conclude that the forces are inertia-dominated (Sumer and Fredsoe, 2006). The range of KC number also indicate that while flow separation takes place in all tests excluding Test 04 (Lower threshold given as 1.1), the size of the cylinder is large enough to prevent vortex shedding.

Inspecting the variation of the diffraction parameter kr, ranging between 0.66 and 0.14, coupled with the accompanying KC number for each test, it can be concluded that in most of the cases, the force acting on the cylinder is neither dominated by flow separation nor by diffraction; it is inertial (Sarpkaya and Isaacson, 1981).

Since no vortex shedding is evident, no lift forces are expected to be exerted on the structure due to vortex shedding. However, investigating the mooring line force-time series shows scatterings and fluctuations at the peaks. This phenomena can be explained by the free surface effect.

The recorded maximum and minimum mooring line forces have been summarized in Table B.9 and B.10. The cyclic component has been extracted from the time series and has been analyzed. In Figure 5.40, the variation of the amplitude of the cyclic component with incident RMS wave height has been plotted. From Figure 5.40, one

can conclude that both mooring line forces increase with increasing wave height. The plotted series belong to a particular wave period, and a general trend is observed as an increase of the slope of the curve as the wave period decreases. Thus, it can be concluded that decreasing the wave period leads to increase in mooring forces under the same wave height value.

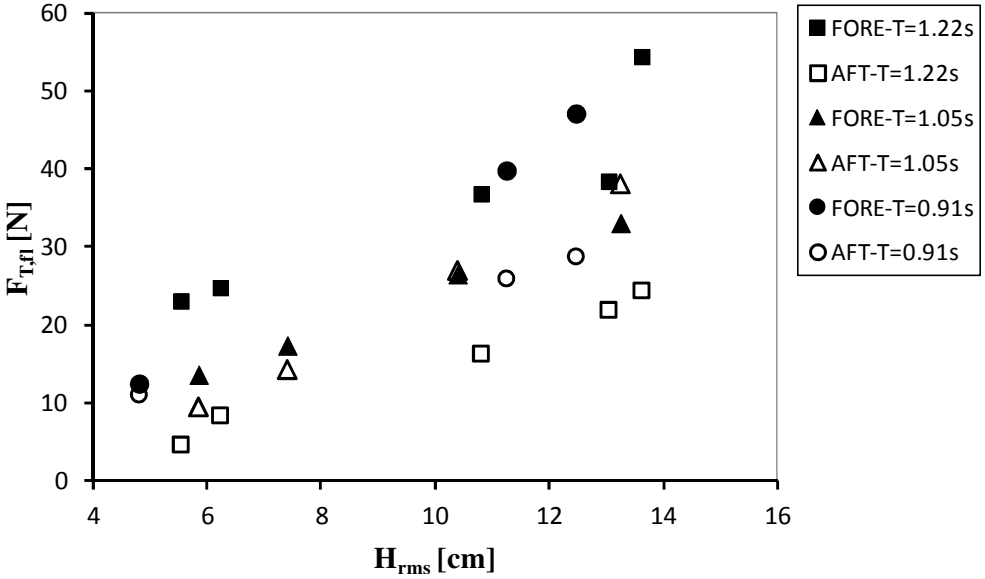


**Figure 5.40 :** Variation of the cyclic tension amplitude with wave height.

# 6. SYNTHESIS

The results achieved from the physical model tests explained in Chapter 4 and and analyzed in Chapter 5 are used here for the assessment of the hybrid system.

First, the performance intervals of both structures are matched in the following subchapter, and an optimum performance range based on incident wave properties is defined.

## 6.1 Coupled Assessment of Test Results

The performance of the structure, due to its hybrid property, can be given by two independent parameters, which are namely the overtopping rates and the transmission coefficients. Thus, comments on performance can be made only by inspecting both features at the same diagrams.

The most important assumption made here is that the effect of structural motions has been omitted. It is known that the motions of the structure can lead to a reduction of 50% in performance for some cases (Kofoed, 2002), but reducing structural motions is based on the design of the mooring system, and a proper mooring system can only be designed under a given wave climate. Thus, effect of structural motions can only be assessed in case a mooring system has been selected for a defined wave climate.

Under these circumstances, Figure 6.1 has been plotted by using the data achieved from the physical model tests. Two different groups of curves are given in Figure 6.1, one for the transmission coefficient and the other for the unit discharges, respectively. Figure 6.1 clearly indicates that as the relative width value increases, the effectiveness of the system as a wave attenuator device increases, evident due to the drop in transmission coefficients. Hydraulic efficiency, on the other hand, increases in the same circumstances with increasing relative width value.

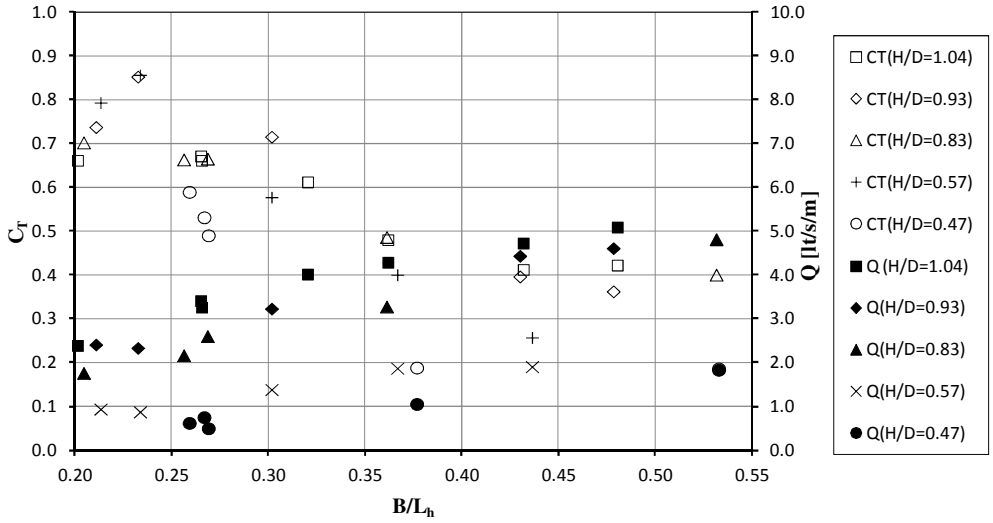


**Figure 6.1 :** Combined efficiency of the hybrid system.

Figure 6.2 shows the variation of transmission coefficients and hydraulic efficiency with wave steepness. It can be concluded that efficiency increases with increasing wave steepness while wave transmission decreases, indicating again that the performance of the structure increases for steeper waves. Regarding conventional sea states with common wave steepness values remaining between 0.030 and 0.045, it can be stated that hydraulic efficiency is in a range of 10%-20% with transmission coefficients varying between 0.74 and 0.20 and both increase with increasing relative wave height.

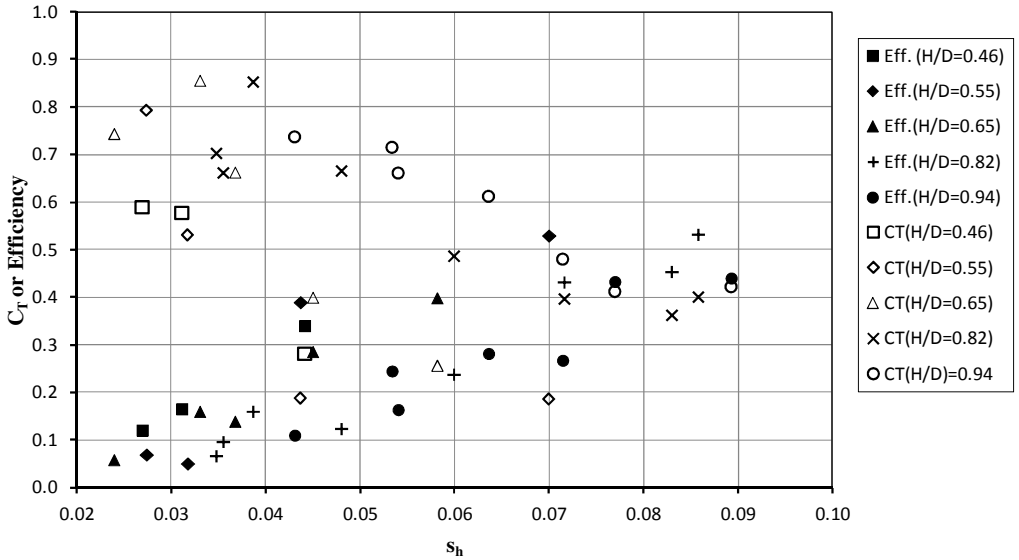


**Figure 6.2 :** Combined efficiency of the hybrid system.

Concerning steeper seas remaining between 0.045 and 0.060, which is a common case for fetch-limited environments, the efficiency reaches values up to 40% and wave transmission remains between 30% and 70%, varying according to the incident wave height.

The dataset achieved from the physical model tests has been rearranged and sorted according to equal relative width values. The variation of hydraulic efficiency and transmission coefficients with relative wave height has been plotted in Figure 6.3. As seen in the figure, increasing the wave height under the same relative width value increases transmission coefficients and also efficiency. As for relative width, transmission coefficients decrease with increasing relative width and efficiency is increasing.

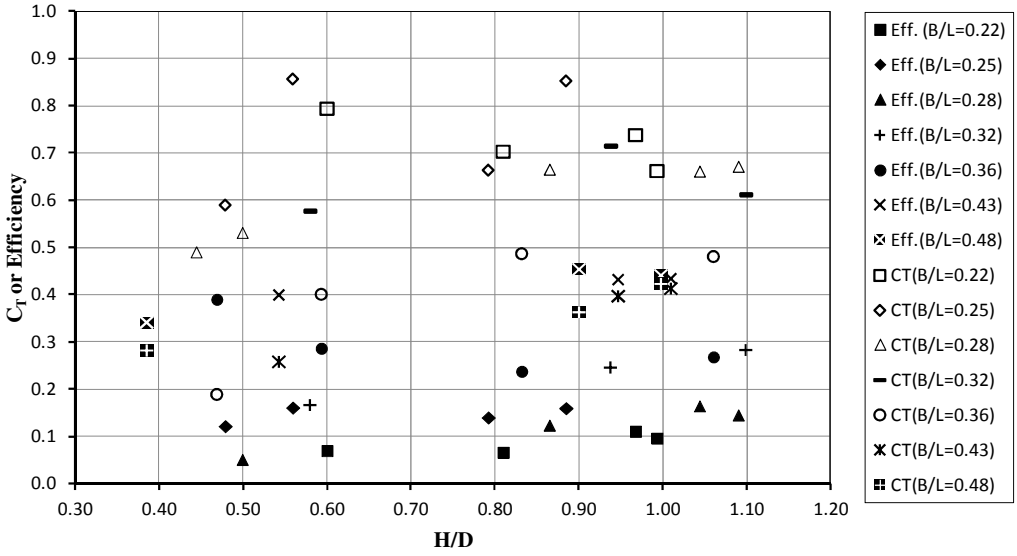


**Figure 6.3 :** Combined efficiency of the hybrid system.

# 7. CONCLUSION

## 7.1 Output of the Study

### 7.1.1 Wave overtopping over a circular cylinder

In order to measure the overtopping rates over a circular cylinder, two dimensional laboratory tests have been carried out in a wave flume in the ITU Hydraulics Laboratory. Seven different configurations with six different depths of immersion have been tested under regular wave series, and overtopping rates have been measured over a 20 cm wide control section located at the center of the flume.

Different arrangements of the governing parameters have been tested to establish an empirical relationship for the prediction of overtopping rates. The variation of overtopping rates with governing parameters has been studied. It has been found out that while the dominant parameter is the freeboard of the structure, the wave steepness also dominates especially for low freeboard values. In general, it has been concluded that keeping other variables constant, increasing wave heights leads to an increase in overtopping rates, whereas the effect of wave period is the opposite, i.e. overtopping rates decrease with increasing wave periods. An equation for the prediction of overtopping rates, Eq. 5.5, has been developed by carrying out a nonlinear regression analysis:

A comparison of the measured and predicted overtopping rates by Eq. 5.5 indicates that the conventional weir-based overtopping equation, while applicable, does not yield satisfying results, generating a fair amount of scattering. A reason for the failure of the conventional weir equation is expected as the change in the reflection coefficient of the cylinder with varying immersion depth. This topic, however, necessitates further research in order to reach more stable results.

It has been found out that the mean water level in front of the cylinder during wave attack has a significant effect on overtopping rates. The reason for this outcome may be the variation of wave reflection and the mean water level in front of the structure with changing depth of immersion, affecting the theoretical hydraulic head. Equations using different parameters have been tested. A new dimensionless discharge definition, given as the ratio of the overtopping volume per wave to the cross section area of the obstacle, has been developed. Using this definition, Eq. 5.7

has been written, providing the most accurate prediction results. Further equations, Eq. 5.8 and Eq. 5.9 have been presented to be used directly for the configurations with relative freeboard values of F/D = 0.12 and F/D = 0.20, respectively, in order to be used more reliably during the assessment of the WEC device.

Since the dimensionless freeboard term diminishes for the zero freeboard cases, two different formulae, varying according to the diameter of the cylinder, Eq. 5.10 and Eq. 5.11, have been given for the zero freeboard discharges, based on the variation of wave steepness and verifying the results of Smid (2001).

### 7.1.2 Hydraulic efficiency for the OWEC device

In order to develop the hydraulic efficiency, mean power contained in each overtopping volume has been calculated from its potential and kinetic energy components. These components have been derived by using the propagation velocities of the overtopping volume. It has been found out that the propagation velocity show minor changes between the crest and trough of the overtopping volume, but the profile of the volume changes due to dispersion. Thus, at first, uniform velocity distribution has been assumed valid along the whole volume, and a correction has been introduced later by calculating the velocity with respect to the displacement of the centroid of the overtopping volume. The energy components indicate that the major amount of energy is stored as kinetic.

Conversion from energy per overtopping volume to power per overtopping volume has been carried out by taking the time-averaged mean power, calculated as the ratio of the total captured energy to the mean wave period. Variation of mean captured power with various parameters has been inspected.

The hydraulic efficiency of the system has been calculated as the ratio of the captured wave power to the incident wave power. It has been found out that an empirical exponential formula (Eq. 5.27) as a function of volumetric overtopping discharge fits the data very well, to be used for the prediction of hydraulic efficiency.

### 7.1.3 Performance of a tethered trimaran floating breakwater

In order to assess the performance of a tethered trimaran floating breakwater, a second model setup has been prepared in the wave flume. Three different spacings

have been used to inspect the effect of pipe spacing on the performance of the tested breakwater model. It has been found out that increasing the distance between the cylinders leads to a reduction in wave attenuation, and the configuration with horizontal gap spacings equal to the pipe diameter is most effective. For this configuration, wave transmission has been formulated by using an exponential function of relative width and wave steepness (Eq. 5.28) or relative width and relative wave height (Eq. 5.29). Furthermore, the theoretical formula given by Macagno (1953) has been applied to the structure. An effective equivalent rectangular width parameter has been defined as the width to fulfill the best fit for the Macagno equation. It has been found out that Beff,r decreases with increase in pipe spacing, and it is equal to the actual structure width for a spacing to diameter ratio of 1 (i.e. Configuration FB1), if the draft of the structure is written as the average draft of the cylinders.

Obtained transmission results indicate that even for smaller B/L values between 0.35 and 0.50, the proposed floating breakwater model can act as a moderate wave attenuator device. The performance of the structure increases in case of waves with higher steepness and for relative width values exceeding 0.50.

Mooring forces of the system have been calculated and inspected. It has been found out that the forces do not act symmetrical on both mooring lines with a lag taking places between the maximum or minimum values of the mooring forces measured at fore and aft lines. This feature may be caused due to free surface effect, leading to changes in hydrostatic pressures under wave attack along the beam of the structure.

### 7.2 Hybrid System

A coupled assessment of the structures performance has been carried out in Section 6 by combining results achieved from both floating breakwater and circular overtopping ramp tests. The given diagrams, Fig. 6.1-6.3, clearly indicate that the effectiveness of the hybrid design increases with increasing wave steepness. Concerning conventional sea states with wave steepness values ranging between 0.03-0.045, it can be observed that the hydraulic efficiency of the system is in the range of 10%-20% and the transmission coefficients remain in the range of 0.20-0.74. While acceptable, both performances increase with increasing wave steepness values, indicating that the system may be applicable as a micro-scale wave energy

converter in fetch-limited zones, which falls together with the common application range of floating breakwaters as well.

As one may expect, the addition of the wave energy converter system to the floating breakwater shall also increase the blockage effect of the structure. As a result, a further drop in transmitted wave heights can be expected. On the other hand, the platform of the overtopping ramp shall also act as a load carrying unit, transferring the weight of the overtopping volume to the structure. From this point of view, and coupled with the randomness of the realistic sea waves, a problem to be solved is the possible snap loading on the mooring lines, which may exist due to cancellation of excess buoyancy by the weight of the overtopped volume.

### 7.3 Comments on Further Research

Following topics have been found interesting for further research:

- Performance of both systems and the hybrid device can be assessed for the case of irregular waves. While algorithms for the prediction of overtopping rates in case of random waves have been developed, the mooring forces and motion responses of the structure should be assessed in a more realistic marine environment. Though it is known that irregular waves could be generated in the wave flume used, the limited length of the channel restricts the total number of waves to 20-25, eliminating the accuracy of irregular wave results due to the very small size of the sample. Thus, these tests have not been carried out.
- Design and development of high-efficiency hydrokinetic power take-off systems can be studied. It is expected that evaluating such systems is a crucial step in development of micro-scale overtopping type wave energy converters.
- A hull form for the overtopping ramp and platform can be developed to improve efficiency and focus the overtopping volume at the turbine inlet. The design of this hull is also important to reduce the slamming forces exerting at the bottom of the platform due to impact of free surface.
- Design and implementation of a mooring system to minimize structural motions can be researched. A second alternative is the effect of a pivoted

mooring system, enabling the structure to take the incident waves always head-on.

- Effect of oblique waves can be studied in a three-dimensional wave basin.

It has been aimed to interpret the efficiency of a circular overtopping ramp with the focus held on the evaluation of overtopping rates and prediction of hydraulic efficiency in this study. A second work has been carried out on a floating breakwater unit utilizing horizontal pipe segments as main floats. It is believed that this work is a participation for the global research carried out on overtopping type wave energy converters and floating pipe breakwaters, and the action items given above may extend it further to a competitive functional device.

## REFERENCES


**Adee, B., Richey, E.P. and Christensen, D.R.** (1976). Floating Breakwater Field Assessment Program, Friday Harbor, Washington, *US Army Coastal Engineering Research Center Technical Report,* TR-76-7, Fort Belvoir, VA.

**Ahrens, J.P.** (1977). Prediction of Irregular Wave Overtopping, *US Army Corps of Engineers Coastal Engineering Research Center Coastal Engineering Technical Aid* CETA 77-7, Fort Belvoir, VA.

**Ahrens, J.P. and Heimbaugh, M.S.** (1988). Seawall overtopping model, *Proceedings of the 21st International Coastal Engineering Conference*, ASCE, Vol. 1, pp. 795-806.

**Akgul, M.A.** (2008). Experimental investigation of horizontal cylinder-type floating breakwaters with a circular cross section, *MSc Thesis*, ITU, Istanbul.

**Akgul, M.A. and Kabdasli, M.S.** (2012). Experimental study about the wave attenuation performance of a horizontal interconnected triple-pipe floating breakwater, *Proc. of the 22nd International Offshore and Polar Engineering Conference*, ISOPE, Rhodos, Greece, June 17-22.

**Akgul, M.A. and Kabdasli, M.S.** (2013). On the design of floating breakwater-wave energy converter hybrid systems, *Proc. of the IXth Clean Energy Symposium, UTES'13*, Konya, Turkey, December 25-28, pp. 784-793 (in Turkish).

**Aminti, P. and Franco, L.** (1988). Wave overtopping on rubble mound breakwaters, *Proceedings of the 21st International Coastal Engineering Conference*, ASCE, Vol. 1, pp. 770-781.

**Battjes, J.A.** (1974). Surf similarity. *Proceedings of the 14th International Coastal Engineering Conference*, ASCE, Vol. 1, pp. 476-480.

**Bradbury, A.P., Allsop, N.W. and Stephens, R.V.** (1988). Hydraulic Performance of Breakwater Crown Walls. *Hydraulic Research Wallingford Report No.* **SR146**, Wallingford, UK.

**Bayram, A.** (2000). Experimental study of a sloping float breakwater, *Ocean Engineering*, *27,* pp. 445-453.

**Brebner, A. and Ofuya, A.O.** (1968). Floating breakwaters, *Proceedings of the 11th International Conference on Coastal Engineering*, ASCE, Vol. 2, pp. 1055-1094.

**Briggs, M., Ye, W. and Demirbilek, Z.** (2002). Field and numerical comparisons of the RIBS floating breakwater, *Journal of Hydraulic Research*, *Vol. 40* (3), pp. 289-301.

**Carr, J.H.** (1951). Mobile breakwaters, *Proceedings of the 2nd International Coastal Engineering Conference*, ASCE, pp. 281-294.

**Carver, R.D.** (1979). Floating Breakwater Wave-Attenuation Tests for East Bay Marina, Olympia Harbor, Washington, *US Army Engineer Waterways Experiment Station Technical Report* HL 79-13, Vicksburg, Miss.

**CEM** (2003). Coastal Engineering Manual, *US Army Corps of Engineers Coastal Engineering Research Center*, Engineering Manual EM-1110-2-1100, Fort Belvoir, VA.

**Chakrabarti, S.K.** (1987). *Hydrodynamics of Offshore Structures*, Springer Verlag, Heidelberg.

**Chen, K. and Wiegel, R.L.** (1970). Floating breakwaters for reservoir marinas, *12nd International Conference on Coastal Engineering*, ASCE, Vol. 2, pp. 1647-1666.

**Cruz, J.** (2008). *Ocean Wave Energy: Current Status and Future Perspectives*, Springer Verlag, Netherlands.

**Davidson, D.D.** (1971). Wave Transmission and Mooring Force Tests of Floating Breakwater, Oak Harbor, Washington. *US Army Engineer Waterways Experiment Station Technical Report* TR 71-3, Vickburg, Miss.

**De Rouck, J., Van de Walle, B., Geeraerts, J., Troch, P., Van Damme, L., Kortenhaus, A. and Medina, J.** (2003). Full scale wave overtopping measurements, *Proc. of the Coastal Structures 2003*, ASCE, pp. 494-506.

**De Waal, J.P. and Van der Meer, J.W.** (1992). Wave runup and overtopping on coastal structures, *Proc. of the 23rd International Conference on Coastal Engineering,* ASCE, Vol. 2, pp. 1758-1771.

**De Wit, M. and Hovhanessian, G.** (2008). Monitoring the 352 meter long Monaco floating pier, in: Tailor Made Concrete Structures, Walraven and Stoelhorst (eds), Taylor and Francis Group, London, pp. 219-222.

**Dean, R.G. and Dalrymple, R.A.** (1991). *Water Wave Mechanics for Engineers and Scientists*, World Scientific, Singapore.

**Diamantoulaki, I. and Angelides, D.C.** (2010). Analysis of performance of hinged floating breakwaters, *Engineering Structures*, *32*, pp. 2407-2434.

**Dodd, N.** (1998). Numerical model of wave run-up, overtopping, and regeneration, *Journal of Waterway, Port, Coastal and Ocean Engineering*, *Vol. 124 (2)*, pp. 73-81.

**Drew, B., Plumer, A.R. and Sahinkaya, M.N.** (2009). A review of wave energy converter technology, *Proc. of IMechE Vol. 223 Part A: J. of Power and Energy,* pp. 887-901.

**Drimer, N., Agnon, Y. and Stiassnie, M.** (1992). A simplified analytical model for a floating breakwater in water of finite depth, *Applied Ocean Research*, *14*, pp. 33-41.

**EurOtop** (2007). European Manual for the Assessment of Wave Overtopping. Ed. Pullen, T., Allsop N.W.H., Bruce, T., Kortenhaus, A., Schüttrumpf, H. and Van der Meer, J.W. Retrieved 04.12.2013 from url: http://www.overtopping-manual.com.

**Evans, D.V., Jeffrey, D.C., Salter, S.H. and Taylor, J.R.M.** (1979). Submerged cylinder wave energy device: Theory and experiment, *Applied Ocean Research*, *1*, pp. 1-12.

**Evans, D.V. and Linton, C.M.** (1991). Submerged floating breakwaters, *Journal of Offshore Mechanics and Arctic Engineering*, *113*, pp. 205-210.

**Franco, L., de Gerloni, M. and Van der Meer, J.W.** (1994). Wave overtopping on vertical and composite breakwaters, *Proc. of the 24th International Coastal Engineering Conference,* ASCE, Vol.1, pp. 1030-1045.

**Franco, L., Briganti, R., Bellotti, G., De Rouck, J. and Geeraerts, J.** (2003). Full-scale measurement of wave overtopping at Ostia-Rome yacht harbour breakwater, *Proc. of Coastal Structures 2003,* ASCE, pp. 507-519.

**Fugazza, M. and Natale, L.** (1988). Energy losses and floating breakwater response, *Journal of Waterway, Port, Coastal and Ocean Engineering, Vol. 114 (2)*, pp. 191-205.

**Gaythwaite, J.W.** (2004). *Design of Marine Facilities for the Berthing, Mooring and Repair of Vessels*, ASCE Publishing, Virginia, US.

**Geeraerts, J., Troch, P., De Rouck, J., Van Damme, L. and Pullen, T.** (2003). Hazards resulting from wave overtopping - full scale measurements, *Proc. of Coastal Structures 2003,* ASCE, pp. 481-493.

**Goda, Y.** (1985). *Random Seas and Design of Maritime Structures*, World Scientific Publishing, Singapore.

**Grantham, K.N.** (1953). Wave run-up on sloping structures, *Trans. of the American Geophysical Union*, *Vol. 34*, No. 5, pp. 720-724.

**Hagerman, G.** (1992). Economics of wave power, in: Ocean Energy-The State of the Art, Seymour, R.J. (ed), ASCE Publishing, .

**Hales, L.Z.** (1981). Floating Breakwater: State-of-the-Art Literature Review, *US Army Coastal Engineering Research Center Technical Report*, **TR-81-1**, Fort Belvoir, VA.

**Harms, V.W.** (1979). Design criteria for floating tire breakwaters. *Journal of Waterway, Port, Coastal and Ocean Engineering*, Vol. 105 (2), pp. 149-170.

**Headland, J.R. and Vallianos, L.** (1990). Dynamic analysis of floating breakwater mooring systems, *Proceedings of 22nd International Conference on Coastal Engineering*, ASCE, Vol. 2, pp. 1320-1333.

**Hebsgaard, M., Sloth, P. and Juhl, J.** (1998). Wave overtopping of rubble mound breakwaters, *Proceedings of the 26th International Conference on Coastal Engineering*, ASCE, Vol. 2, pp. 2235-2248.

**Hedge, A.V., Kamath, K. and Magadum, A.S.** (2007). Performance characteristics of horizontal interlaced multilayer moored floating pipe breakwater. *Journal of Waterway, Port, Coastal and Ocean Engineering*, *Vol. 133 (4)*, pp. 275-285.

**Hedge, A.V., Kamath, K. and Deepak, J.C.** (2008). Mooring forces in horizontal interlaced moored floating pipe breakwater with three layers. *Ocean Engineering, 35*, pp. 165-173.

**Isaacson, M. and Bhat, S.** (1996). Dynamic analysis of twin-pontoon floating breakwaters. In Chwang, Lee and Leung (Ed.), *Hydrodynamics*, Balkema, Rotterdam. ISBN: 90 5410 860 6

**Jackson, R.A.** (1964). Twin-Log Floating Breakwater, Small Boat Basin No. 2, Juneau, Alaska. *US Army Engineer Waterways Experiment Station* Miscallenous Paper No. 2-648, Vicksburg, Miss.

**Juhl, J. and Sloth, P.** (1994). Wave overtopping of breakwaters under oblique waves, *Proceedings of the 24th International Coastal Engineering Conference*, ASCE, Vol. 1, pp. 1182-1196.

**Kabdasli, S.** (1992). *Kiyi muhendisligi*. ITU Publishing, Istanbul.

**Kee, S.T. and Kim, M.H.** (1997). Flexible membrane wave barrier II: Floating/Submerged buoy-membrane system, *Journal of Waterway, Port, Coastal and Ocean Engineering*, *Vol. 123 (2)*, pp. 82-90.

**Kikkawa, H., Shi-Igai, H. and Kono, F.** (1968). Basic study on wave overtopping on sea wall, *Proc. of the 14th Conference on Coastal Engineering in Japan*, pp. 118-122 (in Japanese).

**Kinsman, B.** (1965). *Wind waves: Their Generation and Propagation on the Ocean Surface*, Prentice Hall Inc, Englewood Cliffs, N.J.

**Kobayashi, N., Otta, A.K. and Roy, I.** (1987). Wave reflection and run-up on rough slopes, *Journal of Waterway, Port, Coastal and Ocean Engineering*, *Vol. 113 (3)*, pp. 282-298.

**Kobayashi, N. and Raichle, A.W.** (1994) Irregular wave overtopping of revetments in surf zones, *Journal of Waterway, Port, Coastal and Ocean Engineering*, *Vol. 120 (1)*, pp. 56-73.

**Kobayashi, N. and Wurjanto, A.** (1989). Wave overtopping on coastal structures, *Journal of Waterway, Port, Coastal and Ocean Engineering*, *Vol. 115 (2)*, pp.235-251.

**Kofoed, J.P.** (2002). Wave overtopping of marine structures - Utilization of wave energy, *PhD Thesis*, Hydraulics & Coastal Engineering Laboratory, Department of Civil Engineering, Aalborg University, Aalborg.

**Kofoed, J.P., Frigaard, P., Friis-Madsen, E., Sorensen, H.C.** (2006). Prototype testing of the wave energy converter wave dragon, *Renewable Energy*, *31*, pp. 181-189.

**Koftis, T. and Pinos, P.** (2006). Experimental study on wave overtopping of floating breakwaters, *Proceedings of the 1st International Conference on the Application of Physical Modelling to Port and Coastal Protection, (COASTLAB'06),* IAHR, pp. 351-362.

**Kortenhaus, A., Pearson, J., Bruce, T., Allsop, N.W.H. and van der Meer, J.W.** (2003). Influence of parapets and recurves on wave overtopping and wave loading of complex vertical walls, *Proc. Coastal Structures 2003*, ASCE, pp. 203-216.

**Leach, P.A., McDougal, W.G. and Sollitt, C.K.** (1985). Hinged floating breakwater, *Journal of Waterway, Port, Coastal and Ocean Engineering*, *Vol. 111 (5)*, pp. 895-909.

**Lee, J. and Cho, W.** (2002). Effects of mean wave drift force on mooring tension and performance of a moored floating breakwater, *KSCE Journal of Civil Engineering*, *Vol. 6 (2)*, pp. 193-201.

**Lo, E.Y.M.** (1998). Flexible dual membrane wave barrier, *Journal of Waterway, Port, Coastal and Ocean Engineering*, *Vol. 124 (5)*, pp. 264-271.

**Lorenzo, A.B.M., Van der Meer, J.W. and Hawkes, P.J.** (2000). Effects of bi-modal waves on overtopping: Application of UK and Dutch prediction methods, *Proc. of Coastal Structures 2000*, pp. 2114- 2127.

**Losada, I., Zanuttigh, B., Koca, K., Kortenhaus, A., Angelelli, E., Kirca, O., Bas, B. and Elginoz, N.** (2013). Wave Energy Converters. *EU-FP7 MERMAID Project Report***,** Deliverable: D 3.3.2, December 2013.

**Loukogeorgaki, E. and Angelides, D.C.** (2005). Stiffness of mooring lines and performance of floating breakwater in three dimensions, *Applied Ocean Research*, *27*, pp. 187-208.

**Macagno, E.O.** (1953). Fluid mechanics - experimental study of the effects of the passage of a wave beneath an obstacle, *Proceedings of the Academic des Sciences,* Paris, France, February 1953.

**Mani, J.S.** (1991). Design of Y-Frame floating breakwater, *Journal of Waterway, Port, Coastal and Ocean Engineering*, *Vol. 117 (2)*, pp. 105-119.

**Mays, T., Plaut, R.H. and Liapis, S.I.** (1999). Three-dimensional analysis of submerged, moored, horizontal, rigid cylinders used as breakwaters, *Ocean Engineering 26*, pp. 1311-1333.

**Martinelli, L., Ruol, P. and Zanuttigh, B.** (2009). Impulsive loads on interconnected floating bodies, *Proceedings of the 28th International Conference on Ocean, Offshore and Arctic Engineering*, ASME, Honolulu, Hawaii, May 21-June 5.

**McCartney, B.** (1985). Floating breakwater design. *Journal of Waterway, Port, Coastal and Ocean Engineering*, *Vol. 111 (2)*, pp. 304-318.

**Murali, K. and Mani, J.S.** (1997). Performance of cage floating breakwater, *Journal of Waterway, Port, Coastal and Ocean Engineering*, *Vol. 123 (4)*, pp. 172-179.

**Mynett, A.E., Serman, D.D. and Mei, C.C.** (1979). Characteristics of Salter's cam for extracting energy from ocean waves, *Applied Ocean Research, 1*, pp. 13-20.

**Nagai, S. and Takada, A. (**1972). Relations between the run-up and overtopping of waves, *Proceedings of the 12th International Coastal Engineering Conference*, ASCE, Vol. 2, pp. 1975-1992.

**Ofuya, A.O.** (1968). On floating breakwaters. *Queen's University,* Research Report No. CE-60*,* Kingston, Ontario, Canada, November 1968.

**Oliver, J.G., Aristaghes, P., Cederwall, K., Davidson, D.D., de Graaf, F.F.M., Thackery, M. and Torum, A.** (1994). Floating breakwaters - A practical guide for design and construction, *Report of Permanent International Association of Navigation Congresses Working Group No. 13*, Supplement to Bulletin No. 85, (PIANC), Brussels.

**Owen, M.W.** (1980). Design of Sea Walls Allowing for Wave Overtopping. Report No. EX 924, *HR Wallingford*,

**Ozdamar, A.** (2000). Dalga enerjisinden elektrik enerjisi elde edilmesi uzerine bir arastirma: Cesme ornegi. *Su Urunleri Dergisi*, *Vol. 17,* pp. 1-12.

**Ozeren, Y., Wren, D.G. and Alonso, C.V.** (2008). Development of floating wave barriers for cost-effective protection og irrigation pond levees, *Transactions of the ASABE*, *Vol. 51 (5)*, pp. 1599-1612.

**Ozeren, Y., Wren, D.G., Altinakar, M. and Work, P.A.** (2011). Experimental investigation of cylindrical floating breakwater performance with various mooring configurations, *Journal of Waterway, Port, Coastal and Ocean Engineering*, *Vol. 137 (6)*, pp. 300-309.

**Paape, A.** (1960). Experimental data on the overtopping of seawalls by waves, *Proceedings of the 7th International Coastal Engineering Conference*, ASCE, Vol. 1, pp. 674-681.

**Pearson, J., Bruce, T., Allsop, W., Kortenhaus, A. and van der Meer, J.W.** (2004). Effectiveness of recurve walls in reducing wave overtopping on seawalls and breakwaters. *Proceedings of the 29th International Coastal Engineering Conference,* ASCE, Vol. 3, pp. 4404-4416.

**Pedersen, J. and Burcharth, H.F.** (1992). Wave forces on crown walls, *Proceedings of the 23rd International Coastal Engineering Conference*, ASCE, Vol. 2, pp. 1489-1502.

**Peňa, E., Ferreras, J. and Sanchez-Tembleque, F.** (2011). Experimental study on wave transmission coefficient, mooring lines and module connector forces with different designs of floating breakwaters, *Ocean Engineering*, *38*, pp. 1150-1160.

**Plaut, R.H., Archilla, J.C. and Mays, T.W.** (2000). Snap loads in mooring lines during large three-dimensional motions of a cylinder, *Nonlinear Dynamics, 23*, pp. 271-284.

**Rahman, M.A., Mizutani, N. and Kawasaki, K.** (2006). Numerical modeling of dynamic responses and mooring forces of submerged floating breakwater, *Coastal Engineering*, *53*, pp. 799-815.

**Ruol, P., Zanuttigh, B., Martinelli, L., Kofoed, J.P. and Frigaard, P.** (2010). Near-shore floating wave energy converters: Applications for coastal protection, *Proceedings of the 32nd International Coastal Engineering Conference*, ASCE, 1:32 [Online].

**Salter, S.H.** (1974). Wave power, *Nature*, *249(5459)*, pp. 720-724.

**Sarpkaya, T. and Isaacson, M.** (1981). *Mechanics of Wave Forces on Offshore Structures*. Van Nostrand Reinhold Co., New York.

**Saville, T., JR. and Caldwell, J.M.** (1953). Experimental study of wave overtopping on shore structures, *Proc. of the Minnesota International Hydraulics Convention*, IAHR, Minneapolis, 1953.

**Saville, T., JR.** (1955). Laboratory Data on Wave Runup and Overtopping on Shore Structures, Technical Manual TM 64, *US Army Corps of Engineers Beach Erosion Board*, Washington, D.C.

**Sawaragi, T., Deguchi, I. and Park, S.** (1988). Reduction of wave overtopping rate by the use of artificial reefs, *Proceedings of the 21st International Coastal Engineering Conference,* ASCE, Vol. 1, pp. 335-349.

**Schüttrumpf, H.F.R.** (2001). Wellenueberlaufstroemung bei Seedeichen - Experimentelle und theoretische Untersuchungen, *PhD Thesis*, Leichtweiss-Institut für Wasserbau, TU Braunschweig, Braunschweig.

**Shield, W.** (1910). *Principles and Practice of Harbour Construction*, Longman's Civil Engineering Series, Longmans, Green and Co., London.

**Shi-Igai, H. and Kono, T.** (1970). Analytical approach on wave overtopping on levees, *Proceedings of the 10th International Coastal Engineering Conference*, ASCE, Vol. 1, pp. 563-573.

**Sibul, O.** (1955). Flow over reefs and structures by wave action, *Trans. of the American Geophysical Union*, *Vol. 36 (1)*, pp. 61-69.

**Smid, R.** (2001). Untersuchungen zur Ermittlung der mittleren Wellenüberlaufrate an einer senkrechten Wand und einer 1:1,5 geneigten Böschung für Versuche mit und ohne Freibord. *Entwurf am Leichtweiss-Institut für Wasserbau, Fachbereich Bauingenieurwesen,* TU Braunschweig, Braunschweig, Germany, 26 S.

**SPM** (1984). Shore Protection Manual, 4th ed. *US Army Corps of Engineers, Coastal Engineering Research Center, US Government Printing Office*, Washington, D.C.

**Stiassnie, M.** (1982). A simple mathematical model of a floating breakwater, *Applied Ocean Research*, *2*, pp. 107-111.

**Sumer, B.M. and Fredsøe, J.** (2006) *Hydrodynamics Around Cylindrical Structures*, World Scientific, Singapore.

**Sundar, V., Sundaravadivelu, R. and Purusotham, S.** (2003). Hydrodynamic characteristics of moored floating pipe breakwaters in random waves, *Proc. of Instn. Mech. Engrs*, Vol 217 (M): J. Engineering for the Maritime Environment, pp. 95-110.

**Sundar, V., Sundaravadivelu, R., Kalyani, M**. (2005). Forces due to oblique waves on a submerged open moored cylinder in deep waters, *Ocean Engineering*, *32*, pp. 651-666.

**TAW (Technical Advisory Committee for Flood Defence in the Netherlands)** (2002). Wave Run-Up and Wave Overtopping at Dikes, *Delft Hydraulics,* Delft, Netherlands.

**Thorpe, T.W.** (1999). A Brief Review of Wave Energy - A Report Produced for the UK Department of Trade and Industry, Report No. R120, *ETSU*, May 1999, Oxfordsire, UK.

**Tsuruta, S. and Goda, Y.** (1968). Expected discharge of irregular wave overtopping, *Proceedings of the 11th International Coastal Engineering Conference*, ASCE, Vol.2, pp. 833-852.

**Tuan, T.Q. and Oumeraci, H.** (2010). A numerical model of wave overtopping on seadikes, *Coastal Engineering*, *57*, pp. 757-772.

**Umeyama, M.** (1993). Wave overtopping on vertical boundary and water-surface displacement, *Journal of Waterway, Port, Coastal and Ocean Engineering*, *Vol. 119, No. 3*, pp. 243-260.

**Umeyama, M.** (1994). Wave deformation in front of vertical wall due to wave overtopping, *Journal of Waterway, Port, Coastal and Ocean Engineering*, *Vol. 120, No. 5*, pp. 490-498.

**Url-1** <*http://www.wavedragon.net*>, date retrieved 21.08.2012.

**Url-2** <*http://www.waveplane.com/*>, date retrieved 08.04.2013.

**Url-3 <***http://www.clash.ugent.be/***>**, date retrieved 23.09.2013.

**Url-4** <*http://www.mermaidproject.eu/*>, date retrieved 25.07.2013.

**Url-5** <*http://www.troposplatform.eu/*>, date retrieved 25.07.2013.

**Ursell, R.** (1950). Surface waves on deep water in the presence of a submerged circular cylinder, I, *Proceedings of the Cambridge Philosophical Society*, *Vol. 46*, pp. 141-152.

**Van Gent, M.R.A.** (2002). Wave overtopping at dikes, *Proceedings of the 28th International Coastal Engineering Conference*, Cardiff, United Kingdom, pp. 2203-2215.

**Van der Meer, J.W. and Janssen, J.P.F.M.** (1994). Wave Run-Up and Wave Overtopping at Dikes and Revetments, Publication No. 485, *Delft Hydraulics*, Delft, Netherlands.

**Van der Meer, J.W., Bruce, T., Allsop, W., Franco, L., Kortenhaus, A., Pullen, T. and Schüttrumpf, H.** (2013). EurOtop revisited. Part 1: sloping structures, *Proc. of the Coasts, Marine Structures and Breakwaters Conference,* ICE, Edinburgh, United Kingdom, pp. 132-141.

**Victor, L., Troch, P. and Kofoed, J.P.** (2009). Prediction of the individual wave overtopping volumes of a wave energy converter using experimental testing and first numerical model results, *Proceedings of the 8th European Wave and Tidal Energy Conference,* Uppsala, Sweden, pp. 999-1008.

**Weggel, J.R.** (1976). Wave overtopping equation, *Proceedings of the 15th International Coastal Engineering Conference*, ASCE, Vol. 2, pp. 2737-2755.

**Williams, A.N., Geiger, P.T. and McDougal, W.G.** (1991). Flexible floating breakwater, *Journal of Waterway, Port, Coastal and Ocean Engineering*, *Vol. 117 (5)*, pp. 429-450.

**Williams, A.N. and McDougal, W.G.** (1996). A dynamic submerged breakwater, *Journal of Waterway, Port, Coastal and Ocean Engineering*, *Vol. 122 (6*), pp. 288-296.

**Williams, A.N.** (1996). Floating membrane breakwater, *Journal of Offshore Mechanics and Arctic Engineering*, *Vol. 118*, pp. 46-52.

**Williams, A.N. and Abul-Azm, A.G.** (1997). Dual pontoon floating breakwater, *Ocean Engineering*, *24*, pp. 465-478.

**Williams, A.N., Lee, H.S. and Huang, Z.** (2000). Floating pontoon breakwaters, *Ocean Engineering*, *27*, pp. 221-240.

**Yamamoto, T., Yoshida, A. and Ijima, T.** (1980). Dynamics of elastically moored floating objects, *Applied Ocean Research*, *2*, pp. 79-95.

**Yamamoto, T.** (1981). Moored floating breakwater response to regular and irregular waves, *Applied Ocean Research*, *3*, pp. 27-36.

**APPENDICES**

**APPENDIX A:** Analysis of wave data for the overtopping tests.
**APPENDIX B:** Results of floating breakwater tests.

## APPENDIX A: ANALYSIS OF WAVE DATA FOR OVERTOPPING TESTS

**Table A.1 :** Wave characteristics achieved from the pilot tests.

| Test No. | Series No. | $H_{rms}$ [cm] | $T_m$ [sec] | $L_0$ [m] | $s_0$ [-] | $L_h$ [m] | $s_h$ | $h/gT^2$ | $H/gT^2$ |
|---|---|---|---|---|---|---|---|---|---|
| 1 | 063 | 9.79 | 1.511 | 3.562 | 0.027 | 3.146 | 0.024 | 0.0317 | 0.0034 |
| 2 | 061 | 11.82 | 1.405 | 3.079 | 0.038 | 2.816 | 0.041 | 0.0357 | 0.0059 |
| 3 | 021 | 9.92 | 1.408 | 3.093 | 0.032 | 2.826 | 0.034 | 0.0361 | 0.0049 |
| 4 | 060 | 11.86 | 1.360 | 2.885 | 0.041 | 2.675 | 0.045 | 0.0377 | 0.0065 |
| 5 | 120 | 9.83 | 1.367 | 2.915 | 0.034 | 2.698 | 0.035 | 0.0371 | 0.0050 |
| 6 | 220 | 6.99 | 1.363 | 2.898 | 0.024 | 2.681 | 0.035 | 0.0377 | 0.0052 |
| 7 | 019 | 12.08 | 1.315 | 2.698 | 0.045 | 2.534 | 0.045 | 0.0418 | 0.0068 |
| 8 | 219 | 7.63 | 1.316 | 2.702 | 0.028 | 2.537 | 0.035 | 0.0410 | 0.0050 |
| 9 | 218 | 9.76 | 1.261 | 2.481 | 0.039 | 2.361 | 0.037 | 0.0447 | 0.0055 |
| 10 | 418 | 5.86 | 1.257 | 2.465 | 0.024 | 2.352 | 0.024 | 0.0457 | 0.0037 |
| 11 | 057 | 12.28 | 1.224 | 2.337 | 0.053 | 2.268 | 0.064 | 0.0475 | 0.0098 |
| 12 | 017 | 11.59 | 1.226 | 2.345 | 0.049 | 2.276 | 0.058 | 0.0478 | 0.0088 |
| 13 | 217 | 10.33 | 1.213 | 2.295 | 0.045 | 2.210 | 0.052 | 0.0479 | 0.0079 |
| 14 | 417 | 7.88 | 1.222 | 2.330 | 0.034 | 2.255 | 0.036 | 0.0474 | 0.0055 |
| 15 | 216 | 12.20 | 1.154 | 2.077 | 0.059 | 2.026 | 0.059 | 0.0533 | 0.0090 |
| 16 | 416 | 7.88 | 1.152 | 2.070 | 0.038 | 2.019 | 0.048 | 0.0535 | 0.0075 |
| 17 | 215 | 12.43 | 1.117 | 1.946 | 0.064 | 1.902 | 0.068 | 0.0573 | 0.0106 |
| 18 | 214 | 12.89 | 1.059 | 1.750 | 0.074 | 1.728 | 0.074 | 0.0632 | 0.0116 |
| 19 | 414 | 10.28 | 1.056 | 1.740 | 0.059 | 1.719 | 0.060 | 0.0627 | 0.0095 |
| 20 | 514 | 9.46 | 1.052 | 1.726 | 0.055 | 1.701 | 0.043 | 0.0630 | 0.0068 |
| 21 | 613 | 5.00 | 1.015 | 1.607 | 0.031 | 1.591 | 0.042 | 0.0712 | 0.0066 |
| 22 | 412 | 11.99 | 0.967 | 1.459 | 0.082 | 1.452 | 0.083 | 0.0756 | 0.0131 |
| 23 | 512 | 10.56 | 0.965 | 1.453 | 0.073 | 1.447 | 0.075 | 0.0768 | 0.0119 |
| 24 | 612 | 6.70 | 0.952 | 1.414 | 0.047 | 1.409 | 0.049 | 0.0783 | 0.0078 |
| 25 | 411 | 12.32 | 0.910 | 1.292 | 0.095 | 1.290 | 0.091 | 0.0855 | 0.0144 |
| 26 | 511 | 10.83 | 0.912 | 1.298 | 0.083 | 1.294 | 0.084 | 0.0852 | 0.0133 |
| 27 | 711 | 5.14 | 0.902 | 1.269 | 0.040 | 1.266 | 0.042 | 0.0896 | 0.0069 |
| 28 | 610 | 10.53 | 0.869 | 1.178 | 0.089 | 1.180 | 0.089 | 0.0944 | 0.0142 |
| 29 | 710 | 6.34 | 0.847 | 1.119 | 0.057 | 1.118 | 0.074 | 0.0929 | 0.0119 |
| 30 | 805 | 6.172 | 0.620 | 0.600 | 0.103 | 0.600 | 0.078 | 0.1797 | 0.0125 |

**Table A.2 :** Travel durations between measurement points (s. Figure 4.10).

| Test No. | Series No. | $T_m$ [cm] | $c_h$ [m/sec] | $t_{01}$ [sec] | $t_{1f}$ [sec] | $t_{2f}$ [sec] | $t_{Sf}$ [sec] |
|---|---|---|---|---|---|---|---|
| 1 | 063 | 1.511 | 2.074 | 15.612 | 24.378 | 55.603 | 31.224 |
| 2 | 061 | 1.405 | 2.005 | 7.984 | 12.468 | 28.437 | 15.969 |
| 3 | 021 | 1.408 | 2.007 | 8.007 | 12.503 | 28.516 | 16.013 |
| 4 | 060 | 1.360 | 1.967 | 7.293 | 11.388 | 25.974 | 14.586 |
| 5 | 120 | 1.367 | 1.973 | 7.192 | 11.230 | 25.614 | 14.384 |
| 6 | 220 | 1.363 | 1.970 | 7.249 | 11.319 | 25.817 | 14.498 |
| 7 | 019 | 1.315 | 1.926 | 6.503 | 10.155 | 23.162 | 13.007 |
| 8 | 219 | 1.316 | 1.927 | 6.503 | 10.155 | 23.162 | 13.007 |
| 9 | 218 | 1.261 | 1.873 | 6.453 | 10.076 | 22.981 | 12.905 |
| 10 | 418 | 1.257 | 1.869 | 5.802 | 9.059 | 20.663 | 11.604 |
| 11 | 057 | 1.224 | 1.832 | 5.431 | 8.480 | 19.341 | 10.861 |
| 12 | 017 | 1.226 | 1.838 | 5.395 | 8.425 | 19.215 | 10.790 |
| 13 | 217 | 1.213 | 1.822 | 5.363 | 8.735 | 19.102 | 10.727 |
| 14 | 417 | 1.222 | 1.834 | 4.788 | 7.476 | 17.051 | 9.575 |
| 15 | 216 | 1.154 | 1.755 | 4.552 | 7.062 | 16.107 | 9.045 |
| 16 | 416 | 1.152 | 1.751 | 4.500 | 7.027 | 16.026 | 9.000 |
| 17 | 215 | 1.117 | 1.710 | 3.975 | 6.206 | 14.155 | 7.949 |
| 18 | 214 | 1.059 | 1.631 | 3.969 | 6.198 | 14.137 | 7.939 |
| 19 | 414 | 1.056 | 1.628 | 4.017 | 6.273 | 14.307 | 8.034 |
| 20 | 514 | 1.052 | 1.620 | 3.956 | 6.177 | 14.089 | 7.912 |
| 21 | 613 | 1.015 | 1.571 | 3.969 | 6.198 | 14.137 | 7.939 |
| 22 | 412 | 0.967 | 1.507 | 3.828 | 5.977 | 13.633 | 7.656 |
| 23 | 512 | 0.965 | 1.492 | 3.819 | 5.964 | 13.603 | 7.639 |
| 24 | 612 | 0.952 | 1.477 | 3.498 | 5.462 | 12.458 | 6.996 |
| 25 | 411 | 0.910 | 1.418 | 3.488 | 5.446 | 12.422 | 6.976 |
| 26 | 511 | 0.912 | 1.418 | 3.203 | 5.001 | 11.406 | 6.405 |
| 27 | 711 | 0.902 | 1.402 | 3.199 | 4.996 | 11.395 | 6.399 |
| 28 | 610 | 0.869 | 1.357 | 3.050 | 4.763 | 10.863 | 6.100 |
| 29 | 710 | 0.847 | 1.326 | 3.020 | 4.716 | 10.756 | 6.040 |
| 30 | 805 | 0.620 | 0.968 | 2.646 | 4.132 | 9.424 | 5.292 |

**Table A.3 :** $H_{rms}$ root mean squared wave heights achieved by zero-crossing method, mean values and standard deviations (All values in centimeters).

| Test No. | Series No. | Conf. C1 | Conf. C2 | Conf. C3 | Conf. C4 | Conf. C5 | Conf. C6 | Conf. C7 | σ | υ |
|---|---|---|---|---|---|---|---|---|---|---|
| 1 | 063 | 12.29 | 12.10 | 12.79 | 11.44 | 11.23 | 10.65 | - | 11.75 | 0.78 |
| 2 | 061 | 9.92 | 10.23 | 11.25 | 10.24 | 8.68 | 8.08 | - | 9.73 | 1.16 |
| 3 | 021 | 11.78 | 9.72 | 9.37 | 9.65 | 9.15 | 9.15 | 9.26 | 9.73 | 0.93 |
| 4 | 060 | 14.37 | 14.88 | 14.37 | 12.58 | 12.76 | 15.56 | - | 14.09 | 1.18 |
| 5 | 120 | 11.37 | 11.67 | 12.00 | 10.71 | 11.00 | 9.73 | - | 11.08 | 0.81 |
| 6 | 220 | 11.44 | 10.28 | 11.53 | 10.60 | 10.79 | 10.52 | - | 10.86 | 0.51 |
| 7 | 019 | 7.16 | 7.44 | 7.52 | 7.03 | 6.46 | 6.46 | - | 7.01 | 0.46 |
| 8 | 219 | 9.46 | 8.72 | 9.37 | 7.67 | 7.31 | 7.94 | - | 8.41 | 0.91 |
| 9 | 218 | 12.22 | 12.36 | 12.77 | 12.14 | 12.34 | 12.43 | - | 12.38 | 0.22 |
| 10 | 418 | 11.92 | 11.99 | 12.84 | 11.17 | 10.90 | 11.38 | - | 11.70 | 0.70 |
| 11 | 057 | 11.64 | 11.05 | 11.76 | 9.72 | 10.18 | 10.79 | - | 10.85 | 0.80 |
| 12 | 017 | 11.32 | 10.56 | 11.48 | 9.94 | 9.58 | 9.73 | 10.12 | 10.39 | 0.76 |
| 13 | 217 | 8.62 | 8.54 | 8.54 | 7.09 | 7.33 | 7.87 | - | 8.00 | 0.67 |
| 14 | 417 | 6.54 | 8.39 | 8.94 | 5.93 | 6.77 | 5.93 | 7.39 | 7.13 | 1.17 |
| 15 | 216 | 8.19 | 7.30 | 9.51 | 6.82 | 6.17 | 6.94 | 6.86 | 7.40 | 1.11 |
| 16 | 416 | 11.40 | 11.60 | 11.73 | 11.44 | 11.28 | 11.89 | - | 11.56 | 0.23 |
| 17 | 215 | 11.25 | 11.26 | 12.02 | 10.91 | 10.77 | 11.58 | - | 11.30 | 0.46 |
| 18 | 214 | 10.13 | 10.37 | 10.46 | 9.91 | 8.81 | 10.60 | 10.04 | 10.05 | 0.60 |
| 19 | 414 | 8.40 | 6.39 | 9.67 | 6.21 | 5.84 | 7.92 | 8.24 | 7.52 | 1.41 |
| 20 | 514 | 7.21 | 6.97 | 8.11 | 7.53 | 5.60 | 5.60 | - | 6.84 | 1.03 |
| 21 | 613 | 5.94 | 6.34 | 5.55 | 4.68 | 5.34 | 5.76 | 5.71 | 5.62 | 0.52 |
| 22 | 412 | 10.16 | 10.72 | 10.83 | 10.37 | 10.30 | 10.68 | 10.77 | 10.55 | 0.27 |
| 23 | 512 | 10.09 | 10.36 | 10.74 | 9.62 | 8.63 | 10.33 | 10.37 | 10.02 | 0.70 |
| 24 | 612 | 9.14 | 7.73 | 7.48 | 6.73 | 5.96 | 5.70 | 6.56 | 7.04 | 1.18 |
| 25 | 411 | 9.19 | 10.12 | 10.44 | 10.00 | 9.37 | 9.16 | 10.41 | 9.81 | 0.56 |
| 26 | 511 | 6.63 | 8.24 | 6.93 | 5.70 | 5.84 | 6.32 | 9.15 | 6.97 | 1.28 |
| 27 | 711 | 4.81 | 6.89 | 6.47 | 5.37 | 6.22 | 5.37 | 6.34 | 5.93 | 0.75 |
| 28 | 610 | 5.43 | 8.01 | 8.91 | 5.08 | 5.34 | 5.34 | 9.33 | 6.78 | 1.89 |
| 29 | 710 | 4.72 | 5.69 | 5.34 | 5.75 | 4.54 | 4.54 | 5.41 | 5.14 | 0.53 |
| 30 | 805 | 5.34 | 4.78 | 4.85 | 5.06 | 5.35 | 5.35 | 4.53 | 5.04 | 0.33 |

**Table A.4 :** $T_m$ mean wave period values achieved by zero-crossing method, mean values and standard deviations (All values in centimeters).

| Test No. | Series No. | Conf. C1 | Conf. C2 | Conf. C3 | Conf. C4 | Conf. C5 | Conf. C6 | Conf. C7 | σ | υ |
|---|---|---|---|---|---|---|---|---|---|---|
| 1 | 063 | 1.22 | 1.22 | 1.22 | 1.22 | 1.22 | 1.22 | | 1.22 | 0.00 |
| 2 | 061 | 1.31 | 1.35 | 1.30 | 1.31 | 1.33 | 1.32 | | 1.32 | 0.02 |
| 3 | 021 | 1.40 | 1.40 | 1.40 | 1.40 | 1.40 | 1.40 | 1.40 | 1.40 | 0.00 |
| 4 | 060 | 1.22 | 1.22 | 1.22 | 1.21 | 1.22 | 1.22 | | 1.22 | 0.00 |
| 5 | 120 | 1.38 | 1.37 | 1.37 | 1.38 | 1.37 | 1.38 | | 1.37 | 0.01 |
| 6 | 220 | 1.41 | 1.44 | 1.41 | 1.41 | 1.39 | 1.40 | | 1.41 | 0.02 |
| 7 | 019 | 1.50 | 1.50 | 1.49 | 1.50 | 1.49 | 1.50 | | 1.50 | 0.00 |
| 8 | 219 | 1.38 | 1.37 | 1.38 | 1.36 | 1.38 | 1.38 | | 1.37 | 0.01 |
| 9 | 218 | 1.06 | 1.06 | 1.06 | 1.07 | 1.06 | 1.06 | | 1.06 | 0.00 |
| 10 | 418 | 1.11 | 1.11 | 1.11 | 1.11 | 1.11 | 1.11 | | 1.11 | 0.00 |
| 11 | 057 | 1.15 | 1.17 | 1.15 | 1.16 | 1.17 | 1.16 | | 1.16 | 0.01 |
| 12 | 017 | 1.21 | 1.21 | 1.22 | 1.22 | 1.21 | 1.20 | 1.22 | 1.21 | 0.01 |
| 13 | 217 | 1.26 | 1.25 | 1.26 | 1.25 | 1.24 | 1.25 | | 1.25 | 0.01 |
| 14 | 417 | 1.32 | 1.32 | 1.32 | 1.34 | 1.34 | 1.34 | 1.31 | 1.33 | 0.01 |
| 15 | 216 | 1.36 | 1.37 | 1.37 | 1.36 | 1.38 | 1.38 | 1.37 | 1.37 | 0.01 |
| 16 | 416 | 0.91 | 0.92 | 0.91 | 0.91 | 0.91 | 0.91 | | 0.91 | 0.00 |
| 17 | 215 | 0.96 | 0.97 | 0.97 | 0.95 | 0.97 | 0.98 | | 0.97 | 0.01 |
| 18 | 214 | 1.06 | 1.06 | 1.06 | 1.07 | 1.05 | 1.06 | 1.06 | 1.06 | 0.00 |
| 19 | 414 | 1.17 | 1.17 | 1.15 | 1.17 | 1.17 | 1.16 | 1.15 | 1.16 | 0.01 |
| 20 | 514 | 1.21 | 1.21 | 1.22 | 1.22 | 1.21 | 1.21 | | 1.22 | 0.00 |
| 21 | 613 | 1.26 | 1.26 | 1.24 | 1.26 | 1.25 | 1.25 | 1.23 | 1.25 | 0.01 |
| 22 | 412 | 0.91 | 0.91 | 0.91 | 0.91 | 0.91 | 0.92 | 0.92 | 0.91 | 0.00 |
| 23 | 512 | 0.96 | 0.96 | 0.96 | 0.96 | 0.96 | 0.96 | 0.96 | 0.96 | 0.00 |
| 24 | 612 | 1.06 | 1.06 | 1.06 | 1.06 | 1.06 | 0.97 | 1.06 | 1.05 | 0.04 |
| 25 | 411 | 0.87 | 0.87 | 0.87 | 0.87 | 0.86 | 0.87 | 0.87 | 0.87 | 0.00 |
| 26 | 511 | 0.96 | 0.95 | 0.95 | 0.96 | 0.96 | 0.96 | 0.97 | 0.96 | 0.01 |
| 27 | 711 | 1.01 | 1.01 | 1.00 | 1.01 | 1.00 | 1.01 | 1.00 | 1.01 | 0.00 |
| 28 | 610 | 0.85 | 0.86 | 0.87 | 0.87 | 0.87 | 0.87 | 0.88 | 0.87 | 0.01 |
| 29 | 710 | 0.91 | 0.91 | 0.89 | 0.90 | 0.91 | 0.91 | 0.91 | 0.91 | 0.01 |
| 30 | 805 | 0.62 | 0.61 | 0.63 | 0.61 | 0.62 | 0.62 | 0.60 | 0.62 | 0.01 |

**Table A.5 :** $q_{1m}$ unit discharge values [lt/s/m].

| Test No. | Series No. | Conf. C1 | Conf. C2 | Conf. C3 | Conf. C4 | Conf. C5 | Conf. C6 | Conf. C7 |
|---|---|---|---|---|---|---|---|---|
| 1 | 063 | 3.936 | 2.156 | 1.393 | 0.719 | 0.000 | 0.000 | - |
| 2 | 061 | 6.036 | 4.336 | 2.827 | 1.471 | 0.322 | 0.000 | - |
| 3 | 021 | 3.982 | 2.981 | 1.990 | 0.492 | 0.004 | 0.000 | 4.277 |
| 4 | 060 | 7.126 | 5.123 | 3.475 | 1.830 | 0.742 | 0.588 | - |
| 5 | 120 | 4.856 | 3.136 | 1.314 | 1.210 | 0.473 | 0.197 | - |
| 6 | 220 | 5.008 | 1.994 | 1.232 | 0.934 | 0.330 | 0.000 | 5.074 |
| 7 | 019 | 7.173 | 5.408 | 3.204 | 2.251 | 0.595 | 0.015 | - |
| 8 | 219 | 5.731 | 4.119 | 1.181 | 0.190 | 0.000 | 0.000 | 5.283 |
| 9 | 218 | 5.611 | 3.941 | 2.131 | 0.729 | 0.000 | 0.000 | - |
| 10 | 418 | 2.447 | 2.850 | 0.000 | 0.000 | 0.000 | 0.000 | 3.978 |
| 11 | 057 | 8.705 | 7.564 | 5.234 | 3.446 | 2.495 | 1.726 | - |
| 12 | 017 | 8.322 | 6.226 | 4.662 | 3.411 | 2.306 | 1.333 | - |
| 13 | 217 | 6.462 | 4.466 | 2.630 | 1.249 | 0.609 | 0.000 | 7.958 |
| 14 | 417 | 4.483 | 1.451 | 0.636 | 0.029 | 0.000 | 0.000 | - |
| 15 | 216 | 8.545 | 6.807 | 4.997 | 3.048 | 2.306 | 1.337 | - |
| 16 | 416 | 7.022 | 2.755 | 3.409 | 0.738 | 0.057 | 0.000 | 7.873 |
| 17 | 215 | 9.666 | 7.488 | 5.706 | 3.497 | 2.097 | 2.254 | - |
| 18 | 214 | 8.786 | 7.317 | 5.036 | 3.494 | 2.921 | 1.411 | - |
| 19 | 414 | 7.123 | 5.568 | 3.463 | 1.904 | 1.053 | 0.297 | 9.523 |
| 20 | 514 | 5.889 | 4.338 | 2.730 | 0.151 | 0.000 | 0.000 | 5.695 |
| 21 | 613 | 6.117 | 4.496 | 0.942 | 0.651 | 0.000 | 0.000 | 7.462 |
| 22 | 412 | 9.067 | 8.149 | 5.474 | 3.098 | 1.814 | 1.398 | - |
| 23 | 512 | 8.250 | 6.914 | 4.150 | 2.614 | 1.098 | 0.725 | 9.786 |
| 24 | 612 | 7.245 | 5.193 | 3.312 | 0.651 | 0.002 | 0.000 | 8.922 |
| 25 | 411 | 8.971 | 7.699 | 5.517 | 3.638 | 2.253 | 1.653 | - |
| 26 | 511 | 8.149 | 6.987 | 4.439 | 3.046 | 1.378 | 0.769 | 9.997 |
| 27 | 711 | 5.487 | 3.209 | 1.003 | 1.504 | 0.000 | 0.000 | 4.119 |
| 28 | 610 | 7.220 | 6.572 | 3.982 | 2.867 | 1.465 | 0.615 | 9.324 |
| 29 | 710 | 6.395 | 4.819 | 3.415 | 0.616 | 0.000 | 0.000 | 8.604 |
| 30 | 805 | 2.346 | 2.675 | 1.242 | 0.664 | 0.089 | 0.000 | 3.667 |

**Table A.6 :** Appropriate higher order wave theories for the test waves.

| Test No. | Series No. | $h/(gT^2)$ | $H/(gT^2)$ | Appropriate Wave Theory |
|---|---|---|---|---|
| 1 | 063 | 0.0317 | 0.0034 | STOKES 4 |
| 2 | 061 | 0.0357 | 0.0059 | STOKES 2 |
| 3 | 021 | 0.0361 | 0.0049 | STOKES 2 |
| 4 | 060 | 0.0377 | 0.0065 | STOKES 2 |
| 5 | 120 | 0.0371 | 0.0050 | STOKES 2 |
| 6 | 220 | 0.0377 | 0.0052 | STOKES 2 |
| 7 | 019 | 0.0418 | 0.0068 | STOKES 2 |
| 8 | 219 | 0.0408 | 0.0053 | STOKES 2 |
| 9 | 218 | 0.0447 | 0.0055 | STOKES 2 |
| 10 | 418 | 0.0457 | 0.0037 | STOKES 2 |
| 11 | 057 | 0.0475 | 0.0098 | STOKES 3 |
| 12 | 017 | 0.0478 | 0.0088 | STOKES 3 |
| 13 | 217 | 0.0479 | 0.0079 | STOKES 3 |
| 14 | 417 | 0.0474 | 0.0055 | STOKES 2 |
| 15 | 216 | 0.0533 | 0.0090 | STOKES 3 |
| 16 | 416 | 0.0535 | 0.0075 | STOKES 3 |
| 17 | 215 | 0.0573 | 0.0106 | STOKES 3 |
| 18 | 214 | 0.0632 | 0.0116 | STOKES 3 |
| 19 | 414 | 0.0627 | 0.0095 | STOKES 3 |
| 20 | 514 | 0.0630 | 0.0068 | STOKES 2 |
| 21 | 613 | 0.0712 | 0.0066 | STOKES 2 |
| 22 | 412 | 0.0756 | 0.0131 | STOKES 3 |
| 23 | 512 | 0.0768 | 0.0119 | STOKES 3 |
| 24 | 612 | 0.0783 | 0.0078 | STOKES 3 |
| 25 | 411 | 0.0855 | 0.0144 | STOKES 3 |
| 26 | 511 | 0.0852 | 0.0133 | STOKES 3 |
| 27 | 711 | 0.0896 | 0.0069 | STOKES 2 |
| 28 | 610 | 0.0944 | 0.0142 | STOKES 3 |
| 29 | 710 | 0.0929 | 0.0119 | STOKES 3 |
| 30 | 805 | 0.1797 | 0.0125 | STOKES 3 |

## APPENDIX B: RESULTS OF FLOATING BREAKWATER TESTS

**Table B.1 :** Wave characteristics for the floating breakwater tests.

| Test No. | Series No. | $H_{rms}$ [cm] | $T_0$ [s] | $L_0$ [m] | $L_h$ [m] | $s_0$ | $s_h$ | $c_h$ [m/s] |
|---|---|---|---|---|---|---|---|---|
| 1 | 805 | 5.384 | 0.620 | 0.599 | 0.599 | 0.087 | 0.087 | 0.967 |
| 2 | 610 | 10.532 | 0.866 | 1.171 | 1.171 | 0.091 | 0.092 | 1.351 |
| 3 | 710 | 5.928 | 0.865 | 1.168 | 1.168 | 0.051 | 0.051 | 1.349 |
| 4 | 711 | 4.688 | 0.907 | 1.282 | 1.280 | 0.038 | 0.038 | 1.412 |
| 5 | 511 | 11.173 | 0.913 | 1.300 | 1.298 | 0.086 | 0.087 | 1.422 |
| 6 | 411 | 11.854 | 0.909 | 1.290 | 1.288 | 0.096 | 0.097 | 1.417 |
| 7 | 612 | 6.404 | 0.960 | 1.438 | 1.433 | 0.047 | 0.047 | 1.492 |
| 8 | 512 | 11.020 | 0.960 | 1.438 | 1.433 | 0.081 | 0.083 | 1.492 |
| 9 | 412 | 12.229 | 0.964 | 1.449 | 1.444 | 0.087 | 0.087 | 1.498 |
| 10 | 613 | 5.531 | 1.016 | 1.613 | 1.600 | 0.035 | 0.037 | 1.574 |
| 11 | 514 | 6.763 | 1.051 | 1.722 | 1.704 | 0.044 | 0.044 | 1.622 |
| 12 | 414 | 10.191 | 1.054 | 1.733 | 1.714 | 0.060 | 0.061 | 1.626 |
| 13 | 214 | 13.039 | 1.057 | 1.743 | 1.724 | 0.077 | 0.077 | 1.631 |
| 14 | 215 | 13.695 | 1.119 | 1.953 | 1.915 | 0.070 | 0.072 | 1.712 |
| 15 | 416 | 7.242 | 1.151 | 2.067 | 2.017 | 0.035 | 0.036 | 1.752 |
| 16 | 216 | 11.664 | 1.154 | 2.078 | 2.026 | 0.057 | 0.058 | 1.756 |
| 17 | 517 | 4.865 | 1.228 | 2.352 | 2.260 | 0.024 | 0.025 | 1.841 |
| 18 | 417 | 5.788 | 1.229 | 2.357 | 2.263 | 0.027 | 0.028 | 1.842 |
| 19 | 217 | 9.846 | 1.222 | 2.329 | 2.240 | 0.046 | 0.048 | 1.833 |
| 20 | 017 | 12.387 | 1.231 | 2.366 | 2.269 | 0.055 | 0.057 | 1.844 |
| 21 | 057 | 13.033 | 1.229 | 2.357 | 2.263 | 0.058 | 0.060 | 1.841 |
| 22 | 418 | 6.132 | 1.251 | 2.445 | 2.334 | 0.025 | 0.026 | 1.865 |
| 23 | 218 | 9.578 | 1.253 | 2.450 | 2.339 | 0.041 | 0.042 | 1.867 |
| 24 | 219 | 7.034 | 1.309 | 2.675 | 2.518 | 0.026 | 0.028 | 1.923 |
| 25 | 019 | 10.843 | 1.311 | 2.683 | 2.524 | 0.042 | 0.044 | 1.925 |
| 26 | 220 | 6.996 | 1.368 | 2.922 | 2.704 | 0.026 | 0.028 | 1.977 |
| 27 | 060 | 11.472 | 1.369 | 2.925 | 2.706 | 0.041 | 0.044 | 1.977 |
| 28 | 021 | 9.801 | 1.402 | 3.068 | 2.811 | 0.033 | 0.036 | 2.005 |
| 29 | 061 | 11.631 | 1.409 | 3.099 | 2.833 | 0.040 | 0.044 | 2.011 |
| 30 | 063 | 8.082 | 1.505 | 3.536 | 3.134 | 0.022 | 0.026 | 2.082 |

**Table B.2 :** Sampling durations for the wave probes WG1 and WG5.

| Test No. | Series No. | $t_{01}$ [s] | $t_{1f}$ [s] | $\Delta T_1$ [s] | $t_{05}$ [s] | $t_{5f}$ [s] | $\Delta T_5$ [s] |
|---|---|---|---|---|---|---|---|
| 1 | 805 | 11.655 | 28.336 | 16.681 | 23.660 | 63.651 | 39.991 |
| 2 | 610 | 5.961 | 14.492 | 8.531 | 12.101 | 32.353 | 20.452 |
| 3 | 710 | 5.977 | 14.532 | 8.555 | 12.134 | 32.643 | 20.509 |
| 4 | 711 | 5.444 | 13.236 | 7.792 | 11.052 | 29.733 | 18.681 |
| 5 | 511 | 5.369 | 13.053 | 7.684 | 10.899 | 29.321 | 18.422 |
| 6 | 411 | 5.411 | 13.157 | 7.745 | 10.986 | 29.554 | 18.568 |
| 7 | 612 | 4.855 | 11.804 | 6.949 | 9.856 | 26.515 | 16.659 |
| 8 | 512 | 4.855 | 11.804 | 6.949 | 9.856 | 26.515 | 16.659 |
| 9 | 412 | 4.817 | 11.711 | 6.894 | 9.779 | 26.308 | 16.529 |
| 10 | 613 | 4.331 | 10.530 | 6.199 | 8.793 | 23.654 | 14.861 |
| 11 | 514 | 4.054 | 9.856 | 5.802 | 8.230 | 22.141 | 13.911 |
| 12 | 414 | 4.028 | 9.792 | 5.764 | 8.176 | 21.996 | 13.820 |
| 13 | 214 | 4.004 | 9.735 | 5.731 | 8.128 | 21.867 | 13.739 |
| 14 | 215 | 3.574 | 8.689 | 5.115 | 7.256 | 19.519 | 12.263 |
| 15 | 416 | 3.376 | 8.208 | 4.832 | 6.854 | 18.438 | 11.584 |
| 16 | 216 | 3.359 | 8.167 | 4.808 | 6.820 | 18.346 | 11.526 |
| 17 | 517 | 2.967 | 7.214 | 4.247 | 6.023 | 16.204 | 10.181 |
| 18 | 417 | 2.963 | 7.204 | 4.241 | 6.016 | 16.183 | 10.168 |
| 19 | 217 | 2.999 | 7.291 | 4.292 | 6.088 | 16.377 | 10.290 |
| 20 | 017 | 2.953 | 7.180 | 4.227 | 5.995 | 16.128 | 10.132 |
| 21 | 057 | 2.963 | 7.204 | 4.241 | 6.016 | 16.183 | 10.168 |
| 22 | 418 | 2.858 | 6.948 | 4.090 | 5.801 | 15.606 | 9.805 |
| 23 | 218 | 2.851 | 6.932 | 4.081 | 5.788 | 15.572 | 9.783 |
| 24 | 219 | 2.611 | 6.349 | 3.737 | 5.301 | 14.261 | 8.960 |
| 25 | 019 | 2.604 | 6.330 | 3.727 | 5.256 | 14.220 | 8.934 |
| 26 | 220 | 2.391 | 5.813 | 3.422 | 4.854 | 13.057 | 8.204 |
| 27 | 060 | 2.389 | 5.807 | 3.419 | 4.849 | 13.045 | 8.196 |
| 28 | 021 | 2.277 | 5.536 | 3.259 | 4.623 | 12.436 | 7.813 |
| 29 | 061 | 2.254 | 5.481 | 3.227 | 4.577 | 12.312 | 7.736 |
| 30 | 063 | 1.975 | 4.803 | 2.828 | 4.010 | 10.788 | 6.778 |

**Table B.3 :** RMS Wave heights with the average and standard deviation values for FB1, FB2 and FB3.

| Test No. | Series No. | FB1 $H_{rms}$ [cm] | FB2 $H_{rms}$ [cm] | FB3 $H_{rms}$ [cm] | Average $H_{rms}$ [cm] | St. Dev. [cm] |
|---|---|---|---|---|---|---|
| 1 | 805 | 5.05 | 5.493 | 5.609 | 5.384 | 0.295 |
| 2 | 610 | 10.767 | 9.949 | 10.867 | 10.528 | 0.504 |
| 3 | 710 | 5.987 | 6.048 | 5.75 | 5.928 | 0.157 |
| 4 | 711 | 4.814 | 4.449 | 4.801 | 4.688 | 0.207 |
| 5 | 511 | 11.253 | 10.95 | 11.293 | 11.165 | 0.188 |
| 6 | 411 | 12.472 | 11.88 | 11.204 | 11.852 | 0.634 |
| 7 | 612 | 6.783 | 6.248 | 6.182 | 6.404 | 0.330 |
| 8 | 512 | 11.836 | 10.146 | 11.005 | 10.996 | 0.845 |
| 9 | 412 | 12.621 | 11.861 | 12.206 | 12.229 | 0.381 |
| 10 | 613 | 5.858 | 5.308 | 5.426 | 5.531 | 0.290 |
| 11 | 514 | 7.414 | 7.414 | 6.111 | 6.980 | 0.752 |
| 12 | 414 | 10.398 | 9.949 | 10.227 | 10.191 | 0.227 |
| 13 | 214 | 13.253 | 12.882 | 12.982 | 13.039 | 0.192 |
| 14 | 215 | 13.733 | 13.733 | 13.657 | 13.708 | 0.044 |
| 15 | 416 | 7.245 | 7.245 | 7.238 | 7.243 | 0.004 |
| 16 | 216 | 11.721 | 11.372 | 11.899 | 11.664 | 0.268 |
| 17 | 517 | 5.549 | 4.377 | 4.669 | 4.865 | 0.610 |
| 18 | 417 | 6.237 | 5.331 | 5.797 | 5.788 | 0.453 |
| 19 | 217 | 10.809 | 8.803 | 9.927 | 9.846 | 1.005 |
| 20 | 17 | 13.044 | 11.456 | 12.662 | 12.387 | 0.829 |
| 21 | 57 | 13.623 | 12.241 | 13.236 | 13.033 | 0.713 |
| 22 | 418 | 5.983 | 6.952 | 5.462 | 6.132 | 0.756 |
| 23 | 218 | 9.9 | 8.97 | 9.864 | 9.578 | 0.527 |
| 24 | 219 | 6.988 | 7.08 | 7.08 | 7.049 | 0.053 |
| 25 | 19 | 11.056 | 10.63 | 10.63 | 10.772 | 0.246 |
| 26 | 220 | 7.499 | 6.493 | 6.493 | 6.828 | 0.581 |
| 27 | 60 | 12.092 | 10.852 | 10.852 | 11.265 | 0.716 |
| 28 | 21 | 10.123 | 9.479 | 9.479 | 9.694 | 0.372 |
| 29 | 61 | 12.412 | 10.85 | 10.85 | 11.371 | 0.902 |
| 30 | 63 | 8.174 | 7.99 | 7.99 | 8.051 | 0.106 |

**Table B.4 :** Mean wave periods and average vs. standard deviation values for FB1, FB2 and FB3.

| Test No. | Series No. | FB1 $T_m$ [s] | FB2 $T_m$ [s] | FB3 $T_m$ [s] | Average $T_m$ [s] | St. Dev. [s] |
|---|---|---|---|---|---|---|
| 1 | 805 | 0.608 | 0.620 | 0.620 | 0.616 | 0.007 |
| 2 | 610 | 0.868 | 0.863 | 0.870 | 0.867 | 0.004 |
| 3 | 710 | 0.867 | 0.863 | 0.867 | 0.866 | 0.002 |
| 4 | 711 | 0.907 | 0.907 | 0.908 | 0.907 | 0.001 |
| 5 | 511 | 0.915 | 0.914 | 0.913 | 0.914 | 0.001 |
| 6 | 411 | 0.913 | 0.913 | 0.903 | 0.910 | 0.006 |
| 7 | 612 | 0.958 | 0.96 | 0.953 | 0.957 | 0.004 |
| 8 | 512 | 0.965 | 0.959 | 0.967 | 0.964 | 0.004 |
| 9 | 412 | 0.963 | 0.966 | 0.964 | 0.964 | 0.002 |
| 10 | 613 | 1.031 | 1.018 | 1.016 | 1.022 | 0.008 |
| 11 | 514 | 1.045 | 1.045 | 1.049 | 1.046 | 0.002 |
| 12 | 414 | 1.053 | 1.053 | 1.054 | 1.053 | 0.001 |
| 13 | 214 | 1.052 | 1.056 | 1.061 | 1.056 | 0.005 |
| 14 | 215 | 1.118 | 1.118 | 1.120 | 1.119 | 0.001 |
| 15 | 416 | 1.152 | 1.152 | 1.139 | 1.148 | 0.008 |
| 16 | 216 | 1.152 | 1.153 | 1.154 | 1.153 | 0.001 |
| 17 | 517 | 1.220 | 1.234 | 1.234 | 1.229 | 0.008 |
| 18 | 417 | 1.225 | 1.234 | 1.227 | 1.229 | 0.005 |
| 19 | 217 | 1.221 | 1.224 | 1.218 | 1.221 | 0.003 |
| 20 | 17 | 1.228 | 1.237 | 1.232 | 1.232 | 0.005 |
| 21 | 57 | 1.229 | 1.229 | 1.233 | 1.230 | 0.002 |
| 22 | 418 | 1.243 | 1.259 | 1.251 | 1.251 | 0.008 |
| 23 | 218 | 1.250 | 1.259 | 1.257 | 1.255 | 0.005 |
| 24 | 219 | 1.309 | 1.313 | 1.313 | 1.312 | 0.002 |
| 25 | 19 | 1.312 | 1.305 | 1.305 | 1.307 | 0.004 |
| 26 | 220 | 1.370 | 1.369 | 1.369 | 1.369 | 0.001 |
| 27 | 60 | 1.378 | 1.368 | 1.368 | 1.371 | 0.006 |
| 28 | 21 | 1.399 | 1.415 | 1.415 | 1.410 | 0.009 |
| 29 | 61 | 1.410 | 1.415 | 1.415 | 1.413 | 0.003 |
| 30 | 63 | 1.511 | 1.505 | 1.505 | 1.507 | 0.003 |

**Table B.5 :** Transmission coefficients calculated for FB1, FB2 and FB3.

| Test No. | Series No. | $H_{rms}$ [cm] | $T_m$ [s] | FB1 $C_T$ | FB2 $C_T$ | FB3 $C_T$ |
|---|---|---|---|---|---|---|
| 1 | 805 | 5.38 | 0.62 | 0.189 | 0.353 | 0.251 |
| 2 | 610 | 10.53 | 0.87 | 0.401 | 0.436 | 0.591 |
| 3 | 710 | 5.93 | 0.87 | 0.187 | 0.336 | 0.586 |
| 4 | 711 | 4.69 | 0.91 | 0.282 | 0.194 | 0.523 |
| 5 | 511 | 11.17 | 0.91 | 0.363 | 0.427 | 0.603 |
| 6 | 411 | 11.85 | 0.91 | 0.423 | 0.488 | 0.657 |
| 7 | 612 | 6.40 | 0.96 | 0.258 | 0.319 | 0.600 |
| 8 | 512 | 11.00 | 0.96 | 0.397 | 0.473 | 0.590 |
| 9 | 412 | 12.23 | 0.96 | 0.413 | 0.518 | 0.554 |
| 10 | 613 | 5.53 | 1.02 | 0.189 | 0.292 | 0.341 |
| 11 | 514 | 6.98 | 1.05 | 0.401 | 0.460 | 0.352 |
| 12 | 414 | 10.19 | 1.05 | 0.487 | 0.644 | 0.552 |
| 13 | 214 | 13.04 | 1.06 | 0.481 | 0.623 | 0.616 |
| 14 | 215 | 13.71 | 1.12 | 0.613 | 0.590 | 0.612 |
| 15 | 416 | 7.24 | 1.15 | 0.578 | 0.490 | 0.615 |
| 16 | 216 | 11.66 | 1.15 | 0.716 | 0.714 | 0.662 |
| 17 | 517 | 4.87 | 1.23 | 0.491 | 0.777 | 0.630 |
| 18 | 417 | 5.79 | 1.23 | 0.532 | 0.815 | 0.687 |
| 19 | 217 | 9.85 | 1.22 | 0.666 | 0.791 | 0.765 |
| 20 | 017 | 12.39 | 1.23 | 0.662 | 0.751 | 0.718 |
| 21 | 057 | 13.03 | 1.23 | 0.672 | 0.851 | 0.767 |
| 22 | 418 | 6.13 | 1.25 | 0.590 | 0.588 | 0.723 |
| 23 | 218 | 9.58 | 1.26 | 0.664 | 0.847 | 0.695 |
| 24 | 219 | 7.05 | 1.31 | 0.857 | 0.710 | 0.902 |
| 25 | 019 | 10.77 | 1.31 | 0.853 | 0.740 | 0.838 |
| 26 | 220 | 6.83 | 1.37 | 0.794 | 0.910 | 0.984 |
| 27 | 060 | 11.27 | 1.37 | 0.738 | 0.790 | 0.876 |
| 28 | 021 | 9.69 | 1.41 | 0.703 | 0.852 | 0.831 |
| 29 | 061 | 11.37 | 1.41 | 0.662 | 0.810 | 0.851 |
| 30 | 063 | 8.05 | 1.51 | 0.745 | 0.930 | 0.791 |

**Table B.6 :** Transmission coefficients calculated for FB1, FB2 and FB3.

| Test No. | Series No. | $H_{rms}$ [cm] | $T_m$ [s] | FB1 $C_T$ | FB2 $C_T$ | FB3 $C_T$ |
|---|---|---|---|---|---|---|
| 1 | 805 | 5.38 | 0.62 | 0.189 | 0.353 | 0.251 |
| 2 | 610 | 10.53 | 0.87 | 0.401 | 0.436 | 0.591 |
| 3 | 710 | 5.93 | 0.87 | 0.187 | 0.336 | 0.586 |
| 4 | 711 | 4.69 | 0.91 | 0.282 | 0.194 | 0.523 |
| 5 | 511 | 11.17 | 0.91 | 0.363 | 0.427 | 0.603 |
| 6 | 411 | 11.85 | 0.91 | 0.423 | 0.488 | 0.657 |
| 7 | 612 | 6.40 | 0.96 | 0.258 | 0.319 | 0.600 |
| 8 | 512 | 11.00 | 0.96 | 0.397 | 0.473 | 0.590 |
| 9 | 412 | 12.23 | 0.96 | 0.413 | 0.518 | 0.554 |
| 10 | 613 | 5.53 | 1.02 | 0.189 | 0.292 | 0.341 |
| 11 | 514 | 6.98 | 1.05 | 0.401 | 0.460 | 0.352 |
| 12 | 414 | 10.19 | 1.05 | 0.487 | 0.644 | 0.552 |
| 13 | 214 | 13.04 | 1.06 | 0.481 | 0.623 | 0.616 |
| 14 | 215 | 13.71 | 1.12 | 0.613 | 0.590 | 0.612 |
| 15 | 416 | 7.24 | 1.15 | 0.578 | 0.490 | 0.615 |
| 16 | 216 | 11.66 | 1.15 | 0.716 | 0.714 | 0.662 |
| 17 | 517 | 4.87 | 1.23 | 0.491 | 0.777 | 0.630 |
| 18 | 417 | 5.79 | 1.23 | 0.532 | 0.815 | 0.687 |
| 19 | 217 | 9.85 | 1.22 | 0.666 | 0.791 | 0.765 |
| 20 | 017 | 12.39 | 1.23 | 0.662 | 0.751 | 0.718 |
| 21 | 057 | 13.03 | 1.23 | 0.672 | 0.851 | 0.767 |
| 22 | 418 | 6.13 | 1.25 | 0.590 | 0.588 | 0.723 |
| 23 | 218 | 9.58 | 1.26 | 0.664 | 0.847 | 0.695 |
| 24 | 219 | 7.05 | 1.31 | 0.857 | 0.710 | 0.902 |
| 25 | 019 | 10.77 | 1.31 | 0.853 | 0.740 | 0.838 |
| 26 | 220 | 6.83 | 1.37 | 0.794 | 0.910 | 0.984 |
| 27 | 060 | 11.27 | 1.37 | 0.738 | 0.790 | 0.876 |
| 28 | 021 | 9.69 | 1.41 | 0.703 | 0.852 | 0.831 |
| 29 | 061 | 11.37 | 1.41 | 0.662 | 0.810 | 0.851 |
| 30 | 063 | 8.05 | 1.51 | 0.745 | 0.930 | 0.791 |

**Table B.7 :** Predicted and measured $C_T$ values and amount of absolute and relative error in the predictions for Eq. 5.28.

| Test No. | Series No. | Predicted $C_T$ | Measured $C_T$ | $\varepsilon_a$ | $\varepsilon_r$ |
|---|---|---|---|---|---|
| 2 | 610 | 0.295 | 0.401 | 0.106 | 0.265 |
| 3 | 710 | 0.201 | 0.187 | 0.014 | 0.076 |
| 4 | 711 | 0.220 | 0.282 | 0.062 | 0.218 |
| 5 | 511 | 0.358 | 0.363 | 0.005 | 0.014 |
| 6 | 411 | 0.386 | 0.423 | 0.037 | 0.087 |
| 7 | 612 | 0.307 | 0.258 | 0.049 | 0.191 |
| 8 | 512 | 0.426 | 0.397 | 0.029 | 0.072 |
| 9 | 412 | 0.452 | 0.413 | 0.039 | 0.094 |
| 10 | 613 | 0.344 | 0.189 | 0.155 | 0.819 |
| 11 | 514 | 0.409 | 0.401 | 0.008 | 0.021 |
| 12 | 414 | 0.484 | 0.487 | 0.003 | 0.005 |
| 13 | 214 | 0.568 | 0.481 | 0.087 | 0.181 |
| 14 | 215 | 0.641 | 0.613 | 0.028 | 0.046 |
| 15 | 416 | 0.497 | 0.578 | 0.081 | 0.140 |
| 16 | 216 | 0.613 | 0.716 | 0.103 | 0.144 |
| 17 | 517 | 0.523 | 0.491 | 0.032 | 0.064 |
| 18 | 417 | 0.538 | 0.532 | 0.006 | 0.012 |
| 19 | 217 | 0.643 | 0.666 | 0.023 | 0.034 |
| 20 | 017 | 0.712 | 0.662 | 0.050 | 0.076 |
| 21 | 057 | 0.728 | 0.672 | 0.056 | 0.083 |
| 22 | 418 | 0.550 | 0.590 | 0.040 | 0.068 |
| 23 | 218 | 0.643 | 0.664 | 0.021 | 0.031 |
| 24 | 219 | 0.614 | 0.857 | 0.243 | 0.284 |
| 25 | 019 | 0.714 | 0.853 | 0.139 | 0.163 |
| 26 | 220 | 0.665 | 0.794 | 0.129 | 0.163 |
| 27 | 060 | 0.778 | 0.738 | 0.040 | 0.054 |
| 28 | 021 | 0.747 | 0.703 | 0.044 | 0.063 |
| 29 | 061 | 0.810 | 0.662 | 0.148 | 0.223 |
| 30 | 063 | 0.758 | 0.745 | 0.013 | 0.018 |
| | | | AVERAGE: | 0.061 | 0.128 |

**Table B.8 :** Predicted and measured $C_T$ values and amount of absolute and relative error in the predictions for Eq. 5.29.

| Test No. | Series No. | Predicted $C_T$ | Measured $C_T$ | $\varepsilon_a$ | $\varepsilon_r$ |
|---|---|---|---|---|---|
| 2 | 610 | 0.281 | 0.401 | 0.120 | 0.300 |
| 3 | 710 | 0.222 | 0.187 | 0.035 | 0.189 |
| 4 | 711 | 0.245 | 0.282 | 0.037 | 0.131 |
| 5 | 511 | 0.341 | 0.363 | 0.022 | 0.060 |
| 6 | 411 | 0.357 | 0.423 | 0.066 | 0.155 |
| 7 | 612 | 0.320 | 0.258 | 0.062 | 0.238 |
| 8 | 512 | 0.407 | 0.397 | 0.010 | 0.025 |
| 9 | 412 | 0.427 | 0.413 | 0.014 | 0.035 |
| 10 | 613 | 0.355 | 0.189 | 0.166 | 0.878 |
| 11 | 514 | 0.413 | 0.401 | 0.012 | 0.031 |
| 12 | 414 | 0.480 | 0.487 | 0.007 | 0.014 |
| 13 | 214 | 0.555 | 0.481 | 0.074 | 0.153 |
| 14 | 215 | 0.639 | 0.613 | 0.026 | 0.042 |
| 15 | 416 | 0.494 | 0.578 | 0.084 | 0.145 |
| 16 | 216 | 0.615 | 0.716 | 0.101 | 0.141 |
| 17 | 517 | 0.508 | 0.491 | 0.017 | 0.035 |
| 18 | 417 | 0.526 | 0.532 | 0.006 | 0.011 |
| 19 | 217 | 0.649 | 0.666 | 0.017 | 0.026 |
| 20 | 017 | 0.730 | 0.662 | 0.068 | 0.103 |
| 21 | 057 | 0.749 | 0.672 | 0.077 | 0.115 |
| 22 | 418 | 0.534 | 0.590 | 0.056 | 0.095 |
| 23 | 218 | 0.646 | 0.664 | 0.018 | 0.028 |
| 24 | 219 | 0.598 | 0.857 | 0.259 | 0.303 |
| 25 | 019 | 0.728 | 0.853 | 0.125 | 0.147 |
| 26 | 220 | 0.648 | 0.794 | 0.146 | 0.184 |
| 27 | 060 | 0.807 | 0.738 | 0.069 | 0.094 |
| 28 | 021 | 0.756 | 0.703 | 0.053 | 0.075 |
| 29 | 061 | 0.848 | 0.662 | 0.186 | 0.281 |
| 30 | 063 | 0.742 | 0.745 | 0.003 | 0.004 |
| | | | AVERAGE: | 0.066 | 0.139 |

**Table B.9 :** Application of Macagno's equation to the dataset. Equivalent widths.

| Config. No | B [cm] | $B_{eff,r}$ [cm] | $\lambda_B$ | $\varepsilon_{r,0}$ |
|---|---|---|---|---|
| FB1 | 62.5 | 62.5 | 1.00 | 0.179 |
| FB2 | 75.0 | 50.6 | 0.67 | 0.178 |
| FB3 | 87.5 | 46.7 | 0.53 | 0.165 |

**Table B.10 :** Fore mooring line forces. Maximum, minimum and cyclic amplitude.

| Test No. | Series No. | Pretension [N] | Maximum [N] | Minimum [N] | Cyclic Amplitude [N] |
|---|---|---|---|---|---|
| 4 | 711 | -69.55 | -79.88 | -54.99 | 12.45 |
| 5 | 517 | -65.35 | -77.64 | -31.53 | 23.05 |
| 6 | 613 | -85.51 | -95.75 | -68.57 | 13.59 |
| 7 | 418 | -67.81 | -79.72 | -43.03 | 18.34 |
| 8 | 710 | -71.59 | -84.86 | -33.26 | 25.80 |
| 9 | 417 | -88.84 | -99.00 | -49.48 | 24.76 |
| 10 | 612 | -81.18 | -92.91 | -64.88 | 14.02 |
| 11 | 219 | -41.11 | -78.67 | -15.74 | 31.47 |
| 12 | 416 | -46.18 | -67.04 | -21.80 | 22.62 |
| 13 | 514 | -72.80 | -95.33 | -60.67 | 17.33 |
| 14 | 220 | -37.74 | -86.94 | -9.19 | 38.87 |
| 15 | 63 | -52.40 | -114.47 | 0.00 | 71.67 |
| 16 | 218 | -51.00 | -79.47 | -13.13 | 33.17 |
| 17 | 21 | -33.36 | -111.31 | 0.00 | 64.53 |
| 18 | 414 | -88.38 | -108.73 | -55.77 | 26.48 |
| 19 | 610 | -74.77 | -116.78 | -42.53 | 37.13 |
| 20 | 217 | -54.67 | -92.61 | -19.00 | 36.80 |
| 21 | 19 | -62.09 | -132.34 | -16.25 | 58.04 |
| 22 | 511 | -98.08 | -132.11 | -52.53 | 39.79 |
| 23 | 216 | -52.44 | -99.67 | -8.95 | 45.36 |
| 24 | 512 | -75.34 | -115.46 | -41.70 | 36.88 |
| 25 | 60 | -39.40 | -140.42 | 0.00 | 71.06 |
| 26 | 61 | -20.04 | -124.98 | 0.00 | 71.15 |
| 27 | 411 | -48.46 | -101.67 | -7.46 | 47.10 |
| 28 | 412 | -68.87 | -131.44 | -28.45 | 51.50 |
| 29 | 17 | -62.31 | -114.29 | -37.46 | 38.41 |
| 30 | 214 | -86.07 | -126.10 | -60.02 | 33.04 |
| 31 | 57 | -43.53 | -112.04 | -3.20 | 54.42 |
| 32 | 215 | -49.03 | -101.04 | 0.00 | 51.34 |

**Table B.11 :** Aft mooring line forces. Maximum, minimum and cyclic amplitude.

| Test No. | Series No. | Pretension [N] | Maximum [N] | Minimum [N] | Cyclic Amplitude [N] |
|---|---|---|---|---|---|
| 4 | 711 | -80.56 | -90.70 | -68.67 | 11.02 |
| 5 | 517 | -68.08 | -72.10 | -62.90 | 4.60 |
| 6 | 613 | -72.83 | -77.44 | -58.60 | 9.42 |
| 7 | 418 | -76.17 | -82.15 | -55.14 | 13.51 |
| 8 | 710 | -70.59 | -80.27 | -60.59 | 9.84 |
| 9 | 417 | -54.63 | -60.16 | -43.46 | 8.35 |
| 10 | 612 | -71.18 | -83.80 | -57.53 | 13.13 |
| 11 | 219 | -67.69 | -75.49 | -43.18 | 16.15 |
| 12 | 416 | -75.49 | -82.10 | -55.01 | 13.55 |
| 13 | 514 | -68.10 | -79.53 | -51.09 | 14.22 |
| 14 | 220 | -69.32 | -73.83 | -43.35 | 15.24 |
| 15 | 63 | -74.09 | -77.52 | -48.54 | 14.49 |
| 16 | 218 | -70.50 | -78.17 | -45.40 | 16.39 |
| 17 | 21 | -71.31 | -78.55 | -42.74 | 17.91 |
| 18 | 414 | -67.81 | -93.22 | -39.35 | 26.94 |
| 19 | 610 | -71.18 | -74.61 | -44.08 | 15.27 |
| 20 | 217 | -57.79 | -70.53 | -37.98 | 16.28 |
| 21 | 19 | -70.89 | -91.46 | -35.85 | 27.81 |
| 22 | 511 | -81.82 | -102.80 | -50.97 | 25.92 |
| 23 | 216 | -74.34 | -100.97 | -43.92 | 28.52 |
| 24 | 512 | -71.27 | -88.82 | -43.83 | 22.49 |
| 25 | 60 | -73.77 | -95.50 | -37.64 | 28.93 |
| 26 | 61 | -65.38 | -87.21 | -42.22 | 22.49 |
| 27 | 411 | -72.67 | -101.48 | -43.99 | 28.75 |
| 28 | 412 | -79.48 | -116.60 | -46.41 | 35.09 |
| 29 | 17 | -63.29 | -84.14 | -40.38 | 21.88 |
| 30 | 214 | -73.98 | -113.39 | -37.30 | 38.05 |
| 31 | 57 | -62.29 | -86.62 | -37.87 | 24.38 |
| 32 | 215 | -72.93 | -108.47 | -40.77 | 33.85 |

**Table B.12 :** Values of KC number, Reynolds number and diffraction parameter.

| Test No. | Series No. | $H_{rms}$ [cm] | $T_m$ [s] | u [m/s] | a [$m/s^2$] | KC | $N_{RE}$ | $k_r$ |
|---|---|---|---|---|---|---|---|---|
| 4 | 805 | 5.050 | 0.608 | 0.176 | 1.106 | 0.856 | 22010 | 0.656 |
| 5 | 610 | 10.767 | 0.868 | 0.319 | 2.005 | 2.216 | 39888 | 0.335 |
| 6 | 710 | 5.987 | 0.867 | 0.178 | 1.116 | 1.231 | 22193 | 0.336 |
| 7 | 711 | 4.814 | 0.907 | 0.139 | 0.874 | 1.009 | 17383 | 0.307 |
| 8 | 511 | 11.253 | 0.915 | 0.323 | 2.030 | 2.365 | 40390 | 0.303 |
| 9 | 411 | 12.472 | 0.913 | 0.358 | 2.252 | 2.617 | 44794 | 0.305 |
| 10 | 612 | 6.783 | 0.958 | 0.190 | 1.192 | 1.454 | 23711 | 0.274 |
| 11 | 512 | 11.836 | 0.965 | 0.329 | 2.065 | 2.537 | 41074 | 0.274 |
| 12 | 412 | 12.621 | 0.963 | 0.352 | 2.209 | 2.709 | 43955 | 0.272 |
| 13 | 613 | 5.858 | 1.031 | 0.156 | 0.977 | 1.283 | 19443 | 0.245 |
| 14 | 514 | 7.414 | 1.045 | 0.197 | 1.236 | 1.644 | 24587 | 0.230 |
| 15 | 414 | 10.398 | 1.053 | 0.274 | 1.722 | 2.309 | 34262 | 0.229 |
| 16 | 214 | 13.253 | 1.052 | 0.350 | 2.200 | 2.947 | 43763 | 0.228 |
| 17 | 215 | 13.733 | 1.118 | 0.349 | 2.194 | 3.123 | 43646 | 0.205 |
| 18 | 416 | 7.245 | 1.152 | 0.181 | 1.137 | 1.668 | 22617 | 0.195 |
| 19 | 216 | 11.721 | 1.152 | 0.293 | 1.841 | 2.701 | 36629 | 0.194 |
| 20 | 517 | 5.549 | 1.220 | 0.135 | 0.847 | 1.315 | 16841 | 0.174 |
| 21 | 417 | 6.237 | 1.225 | 0.151 | 0.948 | 1.479 | 18859 | 0.174 |
| 22 | 217 | 10.809 | 1.221 | 0.262 | 1.644 | 2.555 | 32698 | 0.175 |
| 23 | 17 | 13.044 | 1.228 | 0.315 | 1.979 | 3.094 | 39373 | 0.173 |
| 24 | 57 | 13.623 | 1.229 | 0.328 | 2.064 | 3.229 | 41057 | 0.174 |
| 25 | 418 | 5.983 | 1.243 | 0.144 | 0.904 | 1.431 | 17985 | 0.168 |
| 26 | 218 | 9.900 | 1.250 | 0.237 | 1.488 | 2.369 | 29611 | 0.168 |
| 27 | 219 | 6.988 | 1.309 | 0.163 | 1.026 | 1.710 | 20411 | 0.156 |
| 28 | 19 | 11.056 | 1.312 | 0.258 | 1.621 | 2.708 | 32244 | 0.156 |
| 29 | 220 | 7.499 | 1.370 | 0.171 | 1.078 | 1.880 | 21437 | 0.145 |
| 30 | 60 | 12.092 | 1.378 | 0.275 | 1.728 | 3.032 | 34374 | 0.145 |
| 31 | 21 | 10.123 | 1.399 | 0.230 | 1.445 | 2.573 | 28740 | 0.140 |
| 32 | 61 | 12.412 | 1.410 | 0.281 | 1.763 | 3.164 | 35066 | 0.139 |
| 33 | 63 | 8.174 | 1.511 | 0.180 | 1.128 | 2.170 | 22444 | 0.125 |

**CURRICULUM VITAE**


| | |
|---|---|
| **Name Surname:** | Mehmet Adil AKGUL |
| **Place and Date of Birth:** | Istanbul, TURKEY, 18.08.1981 |
| **Address:** | Forsa Str. Aydinalp Apt. 27/6 34742 Kadikoy, Istanbul, TURKEY |
| **E-Mail:** | akgulme@itu.edu.tr, adil.akgul@gmail.com |
| **B.Sc.:** | Civil Engineer, ITU Civil Engineering Faculty 2005 |
| **M.Sc.:** | Coastal Engineer, ITU Institute of Science and Technology, Department of Coastal Sciences and Engineering, 2008 |


**Professional Experience and Rewards:**

**Project engineer:** ITU Hydraulics Laboratory Water and Marine Sciences R&D Center, January 2005-present.

**Research engineer:** Design and development of 3D underground shaking table design, National Project funded by Turkish Republic Ministry of Development, 2005-2012.

**Research assistant:** ITU Civil Engineering Faculty Hydraulics Department, May 2007-present.

**Researcher:** "Innovative Multi-Purpose Off-Shore Platforms: Planning, Design and Operation (MERMAID)", EU-FP7 Project, January 2012-present.

**Academic visitor:** University of Strathclyde, Department of Naval Architecture and Marine Engineering, Glasgow, UK, April 2013-September 2013.

**List of Publications and Patents:**

**International Journal Papers:**

- **Akgul, M.A.**, Yilmazer, D., Oguz, E., Yagci, O., Kabdasli, M.S., 2013. The Effect of an Emergent Vegetation (i.e. Phragmistes Australis) on Wave Attenuation and Wave Kinematics, *Journal of Coastal Research*, Special Issue 65, pp. 147-152.
- Loukogeorgaki, E., Acanal, L., Yagci, O., Kirca, V.S.O., **Akgul, M.A.** 2013. Performance of an Inclined Thin Plate in Wave Attenuation, *Journal of Coastal Research*, Special Issue 65, pp. 141-146.

**International Conference Papers:**

- Oguz, E., **Akgul, M.A.**, Incecik, A. (2013). "Offshore Wind Farms: Potential and Applicability in the Southern Marmara Region, Turkey", 15th Congress of Intl. Maritime Assoc. of Mediterranean, IMAM 2013, A Coruna, Spain, 14-17 Oct. 2013.
- **Akgul, M.A.**, Kabdasli, M.S. (2012). *"Experimental Study about the Wave Attenuation Performance of a Horizontal Interconnected Triple-Pipe Floating Breakwater"*, The 22nd International Ocean and Polar Engineering Conference (ISOPE 2012), 17-22 June 2012, Rhodes, Greece.
- Bagci, T., Elginoz, N., Bas, B., Oguz, E., **Akgul**, **M.A.**, Yuce, A., Kabdasli, M.S. (2009) "*An experimental study on geotextile usage for protection of scour under submarine pipelines*" 13th Congress of Intl. Maritime Assoc. of Mediterranean, IMAM 2009, İstanbul, Turkey, 12-15 Oct. 2009.

**National Conference Papers**

- **Akgul, M.A.**, 2013. Offshore Ports, *Proc. of the 1st National Congress on Ports of Turkey*, 1-2 November 2013, Izmir, Turkey, pp. 217-232 (*in Turkish*).
- **Akgul, M.A.** (2013), On a Low-Reflective Caisson Design with Open Rubble-Covered Front Face, *Proc. of the 1st National Congress on Ports of Turkey*, 1-2 November 2013, Izmir, Turkey, pp. 201-216 (*in Turkish*).
- Kabdasli, M.S. and **Akgul, M.A.**, 2012. Ecological Marina Design. *Proc. of the 9th National Conference on Coasts of Turkey*, 14-17 November 2012, Hatay, Turkey, pp. 881-888 (*in Turkish*).
- Oguz, E., Kabdasli, M.S. and **Akgul, M.A.**, 2012. An Experimental Study about the Effect of Emergent Vegetation on Wave Transformation, *Proc. of the 9th National Conference on Coasts of Turkey*, 14-17 November 2012, Hatay, Turkey, pp. 1029-1036 (*in Turkish*).
- **Akgul, M.A.**, Kabdasli, M.S. and Ayhan, N., 2011. An Experimental Study about the Usage of Light Crest Armor on High-Crested Superstructured Rubble Mound Breakwaters, *Proc. of the 7th National Coastal Engineering Symposium*, UCTEA Chamber of Civil Engineers, 21-23 November 2011, Trabzon, Turkey (*in Turkish*).
- Kabdasli, M.S., **Akgul, M.A.** (2010), *"An Assessment of the Development of In-City Maritime Transportation in Istanbul"*, 8th National Conference on Coasts of Turkey, 27 April 27-May 1, 2010, Trabzon, Turkey, pp. 845-856 (*in Turkish*).
- Kabdasli, M.S., **Akgul, M.A.**, Elginoz, N. (2010), *"History of Coastal Engineering in Turkey"*, 8th National Conference on Coasts of Turkey, 27 April 27-May 1, 2010, Trabzon, Turkey, pp. 1151-1160 (*in Turkish*).
- Kirca, V.S.O., Kabdasli, M.S., Seker, D.Z., Celikoyan, M., **Akgul, M.A.** *"An Experimental Study about the Displacement of a Caisson Breakwater Protected by Antifer Blocks"*, UCTEA Chamber of Civil Engineers, 6th National Coastal Engineering Symposium, 25-28 October 2007, Izmir, Turkey, pp. 419-426 (*in Turkish*).

**PUBLICATIONS/PRESENTATIONS ON THE THESIS**

- **Akgul, M.A.**, Kabdasli, M.S. (2014), "On a Wave Energy Converter - Floating Breakwater Hybrid", *Energy, Education, Science and Technology Part A. Energy Science and Research*, **32(1)**; pp. 509-520.
- **Akgul, M.A.**, Kabdasli, M.S. (2014), "Dairesel Yüzeyli Aşma Tipi Bir Dalga Enerjisi Dönüştürücüde Hidrolik Verimin Deneysel İncelenmesi", *Gazi Üniversitesi Mimarlık Mühendislik Fakültesi Dergisi* (in Turkish; *Article in Review*.)
- **Akgul, M.A.**, Kabdasli, M.S. (2013), "*A Study of a Circular Overtopping Ramp for Overtopping Type Wave Energy Converters*", Proc. of the IX$^{th}$ Clean Energy Symposium, December 25-28 2013, Konya, Turkey, pp. 794-803 (*in Turkish*).
- **Akgul, M.A.**, Kabdasli, M.S. (2013), "*On the Design of a Floating Breakwater-Wave Energy Converter Hybrid System*", Proc. of the IX$^{th}$ Clean Energy Symposium, December 25-28 2013, Konya, Turkey, pp. 784-793 (*in Turkish*).